Energy-Efficient Digital Signal Processing for Multi-carrier and Multi-antenna Systems

Rafik Zayani

CONSERVATOIRE NATIONAL DES ARTS ET MÉTIERS

le cnam

ED SMI - Sciences des Métiers de l'Ingénieur

CEDRIC EA4629 Laboratory

Habilitation à Diriger des Recherches

Presented by

Rafik ZAYANI

Energy-Efficient Digital Signal Processing for Multi-carrier and Multi-antenna Systems

Defended on November 27th, 2020.

Committee :

Reviewers

Prof. Marie-Laure BOUCHERET, ENSEEIHT/INPT, Toulouse, France
Prof. Maryline HELARD, INSA of Rennes, France
Prof. Jurgen PEISSIG, Hanovre Leibniz University, Germany

Examiners

Prof. Geneviève BAUDOIN, ESIEE Paris, France
Prof. Ridha BOUALLEGUE, Sup'Com, Carthage University, Tunis, Tunisia
Prof. Yves LOUET, CentraleSupelec, Rennes, France
Prof. Markku RENFORS, Tampere University of Technology, Finland

HDR Guarantor

Prof. Daniel ROVIRAS, CNAM Paris, France

Acknowledgements

I would like to thank the three reviewers - Marie-Laure BOUCHERET (ENSEEIHT/INPT, Toulouse), Maryline HELARD (INSA of Rennes) and Jurgen PEISSIG (Hanovre Leibniz University)- and the members of the jury - Geneviève BAUDOIN (ESIEE Paris), Ridha BOUALLEGUE (Sup'Com/Carthage University, Tunis), Yves LOUET (CentraleSupelec of Rennes), Markku RENFORS (Tampere University of Technology) and Daniel ROVIRAS (CNAM Paris) - for kindly accepting the invitation to my HDR and honoring me with their participation, leading to a very interesting and rich scientific discussion.

Being a part of Innov'COM/Sup'Com (since 2005) and CEDRIC/CNAM (since 2010) has been a great and fruitful academic experience. I would like to thank my Innov'COM and CEDRIC/LAETITIA teammates (Ali, Hmaied, Iness, Maher, Moez, Mondher, Yahia, ...) for sharing the ups and downs, the laughters and the encouragements.

Daniel, I would like to thank you so much for your amazing support and for all the opportunities you have so generously provided to me from the start. I learned from you much dynamism and enthusiasm in advising students. M. Bouallegue, my PhD advisor, thank you for the support and for the confidence in me. The members of LAETITIA team (Christophe, Didier, Michel, Mylène, Pascal, Tarek, ...), our interactions shape me not only as a researcher but also as a person. In particular, I have been so lucky to work closely with Michel over the last years, thank you for our enriching, lively exchanges and scientific discussions. To my students: Hanen, Hayfa, Maha, Meryem, Mounira, Oussema, Raida, Wafa, Xinying, ... thank you for your dedication and for your hard work.

I would like to dedicate this HDR thesis to my parents, my wife and my dear children (Adam et Skander); all my kindest thoughts are addressed for you, thank you for all your love and support.

Foreword

In this manuscript, I summarize my career path since I have been recruited as Associate Professor at ISI/Tunis ElManar University in 2009 and my research contributions in wireless/green communications at Innov'COM (Sup'Com of Carthage University, Tunisia) and CEDRIC/LAETITIA (CNAM University, France) laboratories. This dissertation is submitted to Conservatoire National des Arts et Métiers (CNAM) in partial fulfillment of the requirements for the degree of Habilitation à Diriger des Recherches.

The researches have been done depending on several factors, like accepted projects, industrial collaborations and opportunities for instance. Thus, I have been doing my best for seeking collaborations and projects that help to lead fruitful environment. As far as I am concerned, I have had the opportunity to conduct my researches where I wanted to, thanks to the inspiring environment.

This document does not exhaustively present all my contributions, but I have tried to make this dissertation the most self-content as possible. Indeed, I selected the most interesting results obtained via several collaborations, research projects and co-supervision (01 postdoc, 09 PhD and 12 MSc students). For each contribution, I give the problem addressed, the related works and the main achievements with theoretical and/or simulation results.

This dissertation is divided into two parts. The first one, professional career, summarizes my teaching and research activities as Associate Professor. This part contains three chapters; the first one is my curriculum vitae, with an exhaustive publication list at this time. The second chapter focuses on my teaching activities and provides the description of the courses I have taught, with some quantified data on my teaching service and the third chapter summarizes my research activities. First, my contributions during my PhD thesis are briefly reported and the main research paths I have been investigating since 2009 are presented. The second part of the manuscript is dedicated to my scientific contributions and is divided in five chapters. The first one summarizes my contributions on the design of multicarrier waveforms towards asynchronous/heteregenous wireless communication systems. The second chapter focuses on the improvement of the network energy-efficiency related to the power consumption, through optimization methods and machine learning tools. The third chapter is dedicated to work on Massive MIMO systems, where new and interesting findings are presented. The fourth chapter comes a bit aside from the previous studies and deals with indoor localization, but where expertise on mathematical optimization and machine learning have been re-used. The last chapter is dedicated to the research perspectives I intended to follow for short, mid and long-term researches.

Contents

List of Figures

List of Tables

Nomenclature

Abbreviations and Acronyms

ACE	Active Constellation Extension
ACI	Adjacent channel interference
ACPR	Adjacent channel power ratio
Adagrad	Adaptive Gradient
ADAM	Adaptive Moment Estimation
ADC	analog to digital converters
AWC	adaptive waveform communications
AWGN	Additive White Gaussian Noise
BER	Bit Error Rate
BF-OFDM	Block-Filtered OFDM
BPSK	Binary Phase Shift Keying.
CC	Clipping and control
CFO	Carrier frequency offset
CP	Cyclic Prefix
CNN	Convolutional neural network
CSI	Channel State Information
DAC	Digital to analog converters
DFE	Decision Feedback Equalization
DL	Downlink
DPD	Digital predistortion
DVB	Digital Video Broadcasting
DFT	Discrete Fourier Transform
EDM	Euclidean distance matrix
EE	Energy efficiency
EGF	Extended Gaussian Function
eMBB	enhanced mobile broadband
ET	Envelope tracking
EVM	Error vector magnitude

FBMC	Filter Bank based MultiCarrier
FFT	Fast Fourier Transform
FMT	filtered multi-tone
FLOPS	Number of floating point operations
FIR	Finite Impulse Response
f-OFDM	Filtered-OFDM
FRESH	FREquency SHift
FPGA	field programmable gate array
FSE	fractionally spaced
GD	Gradient descent
GFDM	Generalized frequency division multiplexing
GMP	generalized memory polynomial
IBO	input back-off
IC	Interference Cancellation
ICI	Inter-Carrier-Interference
IDFT	Inverse Discrete Fourier Transform
IEEE	Institute of Electrical and Electronics Engineers
IFFT	Inverse Fast Fourier Transform
IIC	Iterative Interference Cancellation
i.i.d.	independent and identically distributed
INI	Inter-numerology interference
IOTA	Isotropic Orthogonal Transfer Algorithm
ISI	Inter-Symbol-Interference
KPI	key performance indicators
LLR	Log Likelihood Ratio
LM	Levenberg-Marquardt
LSA	Least-square approximation
LTE	Long Term Evolution
MGF	moment-generating function
mMTC	massive machine type communications
MC	Multicarrier
MLP	multi-layer perceptron
MIMO	Multiple-Input Multiple-Output
MISO	Multiple-Input Single-Output
ML	Maximum Likelihood
MLD	Maximum Likelihood Detection
MMSE	Minimum Mean Square Error
MP	Memory polynomial
MRC	Maximum Ratio Combining.
MSE	Mean Square Error
MUI	Multi user interference
MWF	Multicarrier waveform
NAG	Nesterov accelerated gradient
NLD	Nonlinear distortion

NN	Neural Network
NR	New Radio
NSOC	non second order circular
OBO	Output back-off
OFDM	Orthogonal Frequency Division Multiplexing
OOB	Out-of-band
OQAM	Offset Quadrature Amplitude Modulation
P2JO	Ping-Pong Joint Optimization
PA	Power amplifier
PACE	Pilot Aided Channel estimation
PAM	Pulse Amplitude Modulation
PAPR	Peak-to-average power ratio
PCS	Peak-canceling signals
PDF	Probability Density Function
PHYDYAS	PHYsical layer for DYnamic spectrum AccesSand cognitive radio
POCS	Projection onto convex sets
POPS	Ping-pong Optimized Pulse Shaping
PPN	PolyPhase Network
PRT	Peak reduction tones
PSD	Power Spectral Density
PTS	Partial Transmit Sequence
QAM	Quadrature Amplitude Modulation
QCQP	Quadratically constrained quadratic programs
QPSK	Quadrature Phase Shift Keying
QR	quasi-rectilinear
RB	Resource block
RF	Radio frequency
RMSProp	Root Mean Square Propagation
RRC	Root raised-cosine
RSSI	Receive signal strength indicator
RZF	Regularized zero-forcing
SCS	Subcarrier spacing
SDR	software defined radio
SE	Spectral efficiency
SER	Symbol error rate
SIC	Successive Interference Cancellation
SINR	Signal-to-Interference-plus-Noise Ratio
SIR	Signal-to-Interference Ratio
SISO	Single-Input Single-Output
SIMO	Single-Input Multiple-Output
SLM	Selective Mapping
SM	Spatial Multiplexing
SNR	Signal-to-Noise Ratio
SNOI	Signal of non interest

SO	secondary order
SOI	Signal of interest
SRRC	Square Root Raised Cosine
SSE	symbol spaced
SSPA	Solid state power amplifier
STBC	Space Time Block Coding
TI	Tone Injection
TO	Timing offset
TR	Tone Reservation
TWTA	(Traveling wave tube amplifier
WOLA	Weighted Overlap and Add
UFMC	Universal filtered multicarrier
UL	Uplink
UNOI	user of non interest
UOI	User of interest
URLLC	Ultra-reliable and low latency communications
USRP	Universal software radio peripherals
UT	User terminal
WL	widely linear
ZF	Zero Forcing
ZP	Zero padding

Notations

Vectors and matrices are denoted by bold letters (e.g. $\mathbf{X}$). Other notational conventions are summarized as follows:

$\mathbb{C}^n$, $\mathbb{R}^n$	The sets of vectors of length n, with complex and real elements.
$\mathbb{C}^{p\times n}$, $\mathbb{R}^{p\times n}$	The set of matrices with p rows and n columns, with complex and real elements.
$\mathbb{N}$	The set of positive integer elements.
$\log(\cdot)$	The natural logarithm.
$\log_2(\cdot)$	The base 2 logarithm.
x^*	Complex conjugate of the complex value x.
$\lvert x\rvert$	The absolute value of a scalar.
$\lfloor x\rfloor$	The floor operator, i.e. the smallest integer less than x.
$\lceil x\rceil$	The ceil operator, i.e. the smallest integer greater than or equal to x.
$\lvert\Omega\rvert$	The cardinality of the set Ω, i.e. the number of elements in the finite set Ω.
$\cap$	The intersection operator.
$\cup$	The union operator.
$\mathbb{E}\{\cdot\}$	The expectation operator.
$[\cdot]^T$	The transpose operator.
$[\cdot]^H$	The complex conjugate (Hermitian) transpose operator.
$\mathbf{X}^{-1}$	The inverse of matrix $\mathbf{X}$.
$\mathbf{I}_n$	The identity matrix of size n.
$\mathbf{0}_n$	The square zero matrix of size n.
$\mathbf{0}_{n\times m}$	The zero matrix of size $n_r \times n_t$.
$\lVert\mathbf{v}\rVert$	Euclidean norm of vector $\mathbf{v}$.
$\lVert\mathbf{v}\rVert_*$	Nuclear norm of vector $\mathbf{v}$.
$\lVert\mathbf{v}\rVert_F$	Frobenius norm of vector $\mathbf{v}$.
$\mathfrak{Re}\{x\}$	Real part of the complex value x.
$\mathfrak{Im}\{x\}$	Imaginary part of the complex value x.
$*$	Convolution operator.
$\odot$	Point-to-point multiplication operator.

Part I

Professional Career

Chapter 1

Extended curriculum vitae

1.1 Civil status

Rafik ZAYANI
Ass. Professor (Maître de conférences HDR, CNU 61)
Research: Innov'COM lab (LR-11/TIC-03), Sup'Com, University of Carthage, Tunisia.
Teaching: Institut Supérieur d'Informatique (ISI), University of Tunis ElManar, Tunisia.

Present Position: H2020 Marie Sklodowska-Curie IF fellow
CEDRIC-EA4629, CNAM-Paris, France.

E-mail: rafik.zayani@cnam.fr and/or rafik.zayani@supcom.tn
Phone: +33140272994
Web site: http://cedric.cnam.fr/lab/en/author/zayani/
Marital status: Married, 02 children

1.2 Education

2005-2009 **PhD in Telecommunications**, ENIT (Ecole Nationale d'Ingénieurs de Tunis)/University of Tunis ElManar, Tunisia.
My PhD was done in collaboration between the Innov'COM laboratory of Sup'Com school in Tunisia and the Signal and Communications group of IRIT (Institut de Recherche en Informatique de Toulouse) in France.
Title : Adaptive pre-distortions for HPA nonlinearities compensation using neural networks.

Committee :
President
Prof. T. AGUILLI, Professor, ENIT/University of Tunis ElManar, Tunisia
Reviewers
Prof. S. BELGUITH, Professor, ESTI/University of Carthage, Tunisia
Prof. R. KOSAI, Professor, ENSIM/Le Mans University, France
Examiners
Prof. A. BOUALLEGUE, Professor, ENIT/University of Tunis ElManar, Tunisia
Supervisors
Prof. D. ROVIRAS, Professor, CEDRIC/CNAM, France
Prof. R. BOUALLEGUE, Sup'Com/Univeristy of Carthage, Tunisia

2004 **MSc in Communication Systems**, ENIT/University of Tunis ElManar, Tunisia.

2000-2003 **Engineer degree in Telecommunications**, ENIT/University of Tunis ElManar, Tunisia.

1998-2000 Preparatory classes for "Grandes Ecoles", Technology, Institut Preparatoire aux Etudes d'Ingenieurs de Monastir (IPEIM), Tunisia.
National rank : 11/251.

1998 High school graduation, Scientific section.

1.3 Professional experience

Since Nov. 2018 **H2020 Marie Sklodowska-Curie IF fellow: CNAM-Paris, CEDRIC laboratory. Granted by H2020 MSCA ADAM5 project**
Research: Massive MIMO Systems: Spectral, Energy and Hardware Efficiency
Teaching: Digital communications, Radiocommunications and Information theory.
EiCNAM-Paris

Since 2009 **Ass. Professor (Maître de conférences, CNU 61): ISI/University of Tunis ElManar, Tunis.**
Teaching: Digital communications, wireless communications and networking.

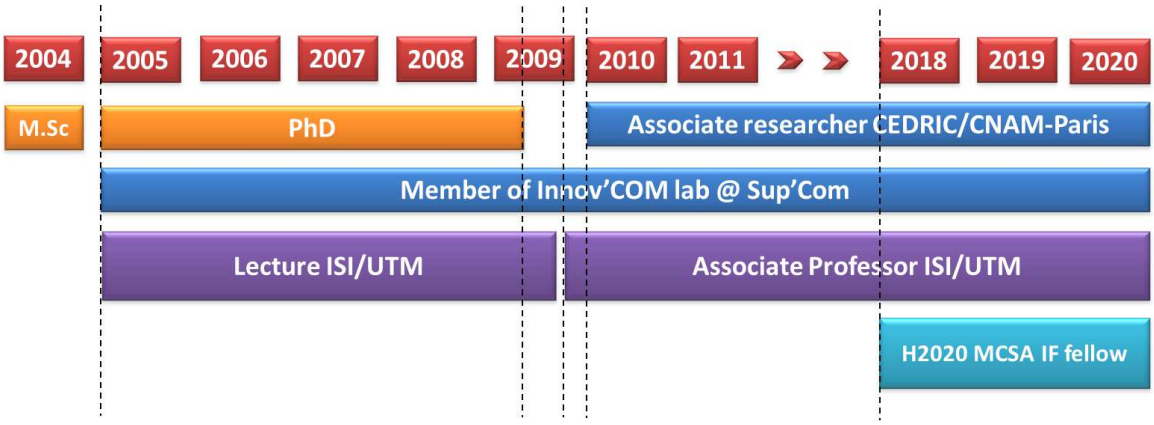

Figure 1.1: Professional experience.

Since 2005 **Member : Innov'Com laboratory, Sup'Com/University of Carthage, Tunis.**
Research: Energy-Efficient Multicarrier waveforms based systems: From PA linearity-efficiency trade-off optimization to machine learning.

Since 2010 **Associate researcher : CEDRIC laboratory/CNAM-Paris**
Research: Energy-Efficient Multicarrier waveforms based systems: From PA linearity-efficiency trade-off optimization to machine learning.

2005-2009 **PhD in Telecommunications: ENIT/University of Tunis ElManar, Tunisia.**
Research: Machine learning for energy-efficient multi-carrier systems
Teaching: Digital communications and networking. **ISI/University of Tunis El-Manar, Tunis.**

2004 **M.Sc Internship: Sys'Com laboratory, ENIT/University of Tunis ElManar, Tunisia.**
Research: Study and development of a secure localization systems
Teaching: Signal transmission and networking. **ISI/University of Tunis ElManar, Tunis.**

1.4 Supervision

1.4.1 Postdocs

Yahia MEDJAHDI
Title: Comparative Study of Physical Layer in MTC Context
Date: 2016-2017
Supervision: 33%
Funding: ANR WONG5 project
Results: 3 journal papers, 5 conference papers

1.4.2 PhD students

Xinying Cheng
Title: Energy Efficiency enhancement for massive MIMO-OFDM systems with RF impairments
Date: 2018-2020 (in progress)
Supervision: 40%
Funding: Scholarship of Sorbonne University
Results: 2 journal papers

Meryem Benosman
Title: Investigating machine learning techniques to improve the energy-efficiency of multi-carrier waveforms based massive MIMO
Date: 2018-2020 (in progress)
Supervision: 40%
Funding: PHC-TASSILI ATOME5+ project

Hayfa Fhima
Title: Study and implementation of Widely Linear (WL) receiver for Filter-Bank based Multicarrier (FBMC-OQAM) modulations
Date: 2015-2019 (defended in December 2019)
Supervision: 40%
Funding: Co-tutelle Sup'Com and CNAM
Results: 1 journal papers, 4 conference papers

Wafa Njima	**Title:** Indoor localization for IoT-sensor systems **Date:** 2015-2019 (defended in December 2019) **Supervision:** 40% **Funding:** Co-tutelle Sup'Com and CNAM **Results:** 2 journal papers, 3 conference papers
Hanen Bouhadda	**Title:** Theoretical BER performance analysis of non-linearly amplified FBMC-OQAM systems **Date:** 2012-2016 (defended in Mars 2019) **Supervision:** 40% **Funding:** PHC-Utique C3 project **Results:** 1 journal papers, 5 conference papers
Raida Zouari	**Title:** Wireless localization using artificial neural networks **Date:** 2013-2017 (defended in may 2017) **Supervision:** 60% **Funding:** Innov'COM, Sup'Com **Results:** 3 conference papers and 01 journal
Mounira Laabidi	**Title:** PAPR reduction for FBMC-OQAM systems **Date:** 2012-2016 (defended in July 2019) **Supervision:** 60% **Funding:** Innov'COM, Sup'Com **Results:** 4 conference papers
Oussama Belhadj Belkacem	**Title:** Receiver techniques for Power Amplifier nonlinear cancellation in MIMO-OFDM systems **Date:** 2011-2015 (defended in March 2015) **Supervision:** 45% **Funding:** Innov'COM, ENIT **Results:** 2 journal papers, 4 conference papers
Maha Dakhli	**Title:** Theoretical Analysis and compensation of HPA nonlinearity in MIMO-OFDM systems **Date:** 2010-2014 (defended in January 2014) **Supervision:** 60% **Funding:** Innov'COM, ENIT **Results:** 2 journal papers, 4 conference papers

1.4.3 Master students

Samar Chebbi
Title: Machine learning for channel estimation in massive MIMO with hardware impairments
Date: Spring semester 2020
Supervision: 50%
Funding: CEDRIC laboratory

Xinying Cheng
Title: Development of experimental testbed to evaluate the performance of 5G multicarrier waveforms
Date: Spring semester 2018
Supervision: 50%
Funding: ANR WONG5 project

Xtina Fu
Title: Experimental testbed for the evaluation of PAPR reduction methods for 5G multicarrier waveforms
Date: Spring semester 2018
Supervision: 50%
Funding: ANR WONG5 project

Aime Kielys
Title: Configuration of USRP based SDR to evaluate the impact of HPA nonlinearities on post-OFDM waveforms
Date: Spring semester 2017
Supervision: 30%
Funding: ANR WONG5 project

Yasmine Ben Afia
Title: Joint approach for PAPR reduction and PA linearization for post-OFDM multicarrier waveforms
Date: Spring semester 2017
Supervision: 50%
Funding: CEDRIC laboratory

Ikram Marzougui
Title: Design and simulation of small-cells based heterogeneous wireless networks
Date: Spring semester 2016
Supervision: 100%
Funding: Innov'COM, Sup'Com

Hela Hizaoui
Title: Estimation and cancellation of nonlinear distortions caused by HPA for cooperative systems
Date: Spring semester 2012
Supervision: 100%
Funding: Innov'COM, Sup'Com

Hanen Bouhadda
Title: Memory Crossover Neural Network Predistortion for the joint compensation of crosstalk and HPA nonlinearities in STBC-OFDM systems
Date: Spring semester 2011
Supervision: 100%
Funding: Innov'COM, Sup'Com

Mounira Laabidi	**Title:** PAPR reduction for MIMO-OFDM systems using the polyphase inversion and interleaving (PII) method **Date:** Spring semester 2011 **Supervision:** 100% **Funding:** Innov'COM, Sup'Com
Rym Moncer	**Title:** Implementation of digital pre-distortion algorithms on TMS320DSK plateforme: Application pour la 4G **Date:** Spring semester 2008 **Supervision:** 50% **Funding:** Innov'COM, ENIT
Souad Zid	**Title:** Power amplifier effect analysis for OFDM systems **Date:** Spring semester 2005 **Supervision:** 50% **Funding:** Innov'COM, ENIT

1.5 Research projects

H2020-MSCA-IF ADAM5 project	**Title:** ADvanced multicarrier wAveforms based Massive MIMO with full-duplex capability for green 5G and beyond **Funding:** Marie Sklodowska-Curie Individual European Fellowship Actions, Seal of Excellence of Horizon 2020 **Dates:** 2018-2020 (ongoing project) **Role:** Principal Investigator **Partners:** CEDRIC/CNAM-Paris and CEA-Leti Grenoble **Goal:** Propose new digital signal processing based solutions coping with the expected 5G requirements, with a particular focus on mitigating RF impairments and reducing energy consumption of wireless devices, through a set of new algorithms and advanced techniques.
ANR WONG5 project	**Title:** Waveforms MOdels for Machine Types CommuNication inteGrating 5G Networks **Funding:** Research national agency (ANR) **Dates:** 2016-2020 **Role:** in charge of the design of post-OFDM waveforms and their energy-efficiency improvement + developement of the WONG5 experimental testbed **Partners:** CEDRIC/CNAM-Paris, THATLES, CentraleSupélec and CEA Leti **Goal:** Study and propose the most appropriate post-OFDM waveform that is adapted to critical machine type communications (MTC).

PHC-TASSILI ATOME5+	**Title:** Energy-Efficiency improvement for multi-carrier waveforms based massive MIMO **Funding:** CMCU PHC-TASSILI **Dates:** 2019-2022 **Role:** Supervision of PhD students **Partners:** CEDRIC/CNAM-Paris, France and LTT, University of TLEMCEN, Algeria **Goal:** Study new communication techniques to enhance the energy-efficiency of multi-carrier waveforms based massive MIMO.
PHC-Utique C3 project	**Title:** Cooperative and Cognitive Communications in wireless Adhoc networks **Funding:** CMCU PHC-Utique **Dates:** 2011-2014 **Role:** Coordinator for Sup'Com Tunis **Partners:** Innov'Com lab, Sup'com, Sys'Com lab, ENIT, Tunisia and CEDRIC/CNAM-Paris, L2S, SUPELEC, France **Goal:** Investigating a joint approach for the radio access, resource allocation and routing in Adhoc networks.
FP7 EMPhAtiC project	**Title:** Enhanced Multicarrier Techniques for Professional Ad-Hoc and Cell-Based Communications **Funding:** FP7 EC ICT **Dates:** 2012-2015 **Role:** in charge of Nonlinear distortion mitigation techniques for multi-carrier waveforms. **Partners:** CTTC Spain, CEDRIC/CNAM-Paris, TUT Finland, TUM Germany, UCL Belgium, DIOPHANTUS Greece, ILMENAU Germany, SINTEF Norway, NOVI SAD Serbia, CASSIDIAN France, BITGEAR Serbia, MAGISTER, Finland **Goal:** Develop, evaluate and demonstrate the capability of enhanced multi-carrier techniques to make better use of the existing radio frequency bands in providing broadband data services in coexistence with narrow-band legacy services.

1.6 Scientific interactions, scientific community organization and awards

1.6.1 Collaborations

Visiting researcher CEDRIC laboratory/CNAM-Paris, Since Nov. 2018 I have been granted by the Marie Sklodowska-Curie Individual European Fellowship Actions, Seal of Excellence of Horizon 2020, in 2018, for the ADAM5 project dealing with energy-efficiency of the massive MIMO systems. Moreover, I am participating in the supervision of the PhDs of Xinying Cheng and Meryem Benosman.

Collaboration with the VERTIGO team of CEDRIC laboratory I have been interested in ma-

chine learning based energy-efficient massive MIMO with very low computational complexity. In this regard, I am interacting with Dr. Marin Ferecatu and Dr. Nicolas Audebert, specialist in data science and machine learning, via the supervision of the Samar Chebbi's MSc internship.

Collaboration with the LTT laboratory, University of TLEMCEN I am currently collaborating with Prof. Tarek Bendimerad via the PHC-Utique ATOME5+ project on the supervision of the Meryem Benosman's PhD.

Visiting Researcher CEDRIC laboratory/CNAM-Paris, Jan. - Oct. 2018 I have been interested in the development of an experimental testbed to study the capability of the most promising multi-carrier waveforms to accommodate the requirements of the futures wireless communications. In this visit, which was granted by the ANR WONG5 project, I collaborated with Prof. Daniel Roviras, Dr. Hmaied Shaiek and Dr. Cristophe Alexandre. In addition, my collaboration with Prof. Michel Terre took place with the supervision of Wafa Njima's PhD. Following this visit, we have been granted by CMCU PHC-TASSILI for the project ATOME5+.

Visiting Researcher CEDRIC laboratory/CNAM-Paris, May - Sep. 2016 I have had the opportunity to collaborate with Prof. Daniel Roviras's team to investigate new multi-carrier waveform design addressing the major limitations of the traditional CP-OFDM in challenging new spectrum use scenarios. During this visit, which was granted by the ANR WONG5 project, I participated with Prof. Daniel Roviras and Dr. Hmaied Shaiek in the supervision of Dr. Yahia Medjahdi's postdoc.

Invited professor CNAM-Paris, Feb. - Apr. 2016 In the department of Electronique, Electrotechnique, Automatique, Mesures (EPN03) of the CNAM school, I have been invited for three months. During this visit, I have jointly worked with Prof. Daniel Roviras and Dr. Hmaied Shaiek on widely linear equalization for FBMC-OQAM systems via the supervision of Hayfa Fhima's PhD. Moreover, I participated, with Prof. Michel Terre, in the supervision of Wafa Njima's PhD.

Collaboration with CEA-Leti, Grenoble In 2016, I was studying the WOLA-OFDM waveform. I collaborated with the Jean-baptiste Dore's team to investigate and compare the performance of the WOLA-OFDM waveform and the one proposed by CEA-Leti, the BF-OFDM. Our collaboration is pursuing, in 2020, with Dr. Dore and Dr. Benoit Miscopin on the study of new outphasing techniques to enhance the efficiency-linearity tradeoff of RF transmitters.

Collaboration with the CentraleSupélec, Renne with Prof. Yves Louet on (1) the evaluation of global power amplifier efficiency with PAPR reduction for post-OFDM MWFs and (2) Impact of selective channels on post-OFDM waveforms for 5G MTCs. These works were done in the framework of the ANR WONG5 project.

Collaboration with THALES Communications with Dr. Sylvain Traverso on carrying out some testbed experiments in order to convince evidences of some multicarrier waveforms feasibility using real-world environment imposing some RF imperfections: RF power amplifier nonlinearities, IQ imbalance and mirror-frequency interference and phase noise. I provided results concerning CP-OFDM, WOLA-OFDM and BF-OFDM, and Dr. Traverso provided filtered-OFDM's results.

Collaboration with MEDIATRON laboratory of Sup'Com school, Tunis with Prof. Mohamed Siala and Prof. Fatma Abdelkefi on the characterization of a new design of PHYDYAS waveforms, namely POPS-PHYDYAS, which is based on the mix of the POPS algorithm and the PHYDYAS waveform. this collaboration took place via the Zeineb Hraiech's PhD.

Invited professor CNAM-Paris, Mar. - Jun 2014 in the framework of the PHC-Utique C3 project, I participated in the supervision of Hanen Bouahadda's PhD. The scientific topic was the study of the performance of FBMC-OQAM systems in presence of PA nonlinearities.

Visiting Researcher CEDRIC/CNAM-Paris, Sep. - Nov. 2013 In the FP7 EMPHATIC project, the LAETITIA/CEDRIC team was interested in improving the energy-efficiency of FBMC-OQAM which was a good candidate to 5G. In this regard, I was invited in the LAETITIA team to investigate new signal processing solutions for PA linearization and PAPR reduction addressing the reduction of FBMC-OQAM systems power-consumption.

1.6.2 Scientific seminars and conferences

I participated in the organization of two special sessions in international conferences. Moreover, I was an invited speaker in a special session on 5G MWFs radio access technology. In 2016, I organized an international school on advanced MWFs and 5G networks. I have been also involved as Technical Program Committee member for the IEEE IWCMC 2019 Advances in 5G and Beyond Symposium. In addition, I gave two seminars in French laboratories.

Invited Speaker	**Title:** Special Session: Post-OFDM waveforms for 5G radio access technology **Event:** 14th International Symposium on Wireless Communication Systems (ISWCS), Bologna, Italy, 2017.
General Chair	**Title:** Winter school: International School on Advanced Waveforms for 5G Networks **Date and place:** 21-23 January 2016, Tunis, Tunisia. **Website:** http://www.supcom.mincom.tn/isw5g2016/.
Special Session Organizer	**Title:** PAPR reduction and power amplifier linearization for energy-efficient 5G waveforms **Event:** 13th International Symposium on Wireless Communication Systems (ISWCS), Poznan, Poland, 2016. **Title:** Post-OFDM waveforms for 5G radio access technology **Event:** 14th International Symposium on Wireless Communication Systems (ISWCS), Bologna, Italy, 2017.

Seminars

Title: Linear precoding for energy-efficient Massive MIMO downlink systems
Date and place: January 2020 at **ETIS, ENSEA**, Cergy-Pontoise university, France

Title: RF transmitters with high power efficiency and linearity ::digital predistortion and PAPR reduction::
Date and place: December 2019 at **CEA-Leti**, Grenoble, France.

Title: Experimental testbed for Multicarrier Waveforms performance evaluation
Date and place: June 2018 at **CentraleSupelec**, Renne, France.

1.6.3 Awards

I have been awarded a **H2020 Marie Sklodowska-Curie** Individual European grant for my ADAM5 project proposal.

1.7 Scientific Outreach

Participation to PhD defense committee
Krishna Bulusu: Performance Analysis and PAPR reduction techniques for filter-bank based multicarrier systems with nonlinear power amplifiers
Date and place: 29/04/2016, CNAM-Paris
Role: Examinator

Reviewer for International Journals (4 per year in average)
IEEE Communication letters
IEEE Wireless Communication letters
IEEE Transaction on Wireless Communications
IEEE transaction on Communications
EURASIP Journal on Advances on Signal Processing
EURASIP Journal on wireless Communications and Networking
Hindawi Wireless Communications and Mobile Computing

Reviewer for International Conferences
IEEE International Conference on Communications (ICC)
IEEE International Symposium on Wireless Communication Systems (ISWCS)
IEEE International Symposium on Signal, Image, Video and Communications (ISIVC)
IEEE International conference on Wireless Communications and Mobile Computing (IWCMC)

Technical Program Committee member for International Conferences
IEEE International conference on Wireless Communications and Mobile Computing (IWCMC 2019 Advances in 5G and Beyond Symposium).

Guest Editor for Special Issue in International Journals
Hindawi Wireless Communications and Mobile Computing, **Special Issue:** Interference Mitigation for Massive IoT Deployments

1.8 Committee Member

2012-2018	**General Secretary** of the Tunisian Association for Scientific Innovation and Technology (TASIT)
2013-present	**PhD Qualification Committee Member** at Innov'COM laboratory of Sup'Com school

1.9 Certifications

Artificial Intelligence Certification, CentraleSupelec, Paris, France, 2019.
CISCO CCNA Exploration Certification, Sup'Com, Tunisia, 2009.

1.10 Publications

1.10.1 Submitted international peer-reviewed journals

[SJ1] **R. Zayani** and D. Roviras, "Low-Complexity Linear Precoding for Low-PAPR Massive MU-MIMO-OFDM Downlink Systems", submitted to IEEE Open Journal of the Communications Systems (OJ-COMS), 2020.

1.10.2 Published international peer-reviewed journals

[J19] X. Cheng, **R. Zayani**, H. Shaiek and D. Roviras, **"Analysis and Cancellation of Mixed-Numerologies Interference for Massive MIMO-OFDM UL"**, in IEEE Wireless Communications Letters 2020.

[J18] H. Fhima, **R. Zayani**, H. Shaiek, D. Roviras, B. S. Chang and R; Bouallegue, "Comparison of Linear, Widely Linear and Fresh Equalizers for FBMC-OQAM systems with different Numerologies", submitted to Springer Wireless Personal Communications, 2020.

[J17] X. Cheng, **R. Zayani**, H. Shaiek and D. Roviras, **"Inter-Numerology Interference Analysis and Cancellation for Massive MIMO-OFDM Downlink Systems"**, in IEEE Access, vol. 7, pp. 177164-177176, 2019. doi: 10.1109/ACCESS.2019.2957194.

[J16] **R. Zayani**, H. Shaiek and D. Roviras, **"Efficient Precoding for Massive MIMO Downlink under PA Nonlinearities"**, in IEEE Communications Letters.
doi: 10.1109/LCOMM.2019.2924001.

[J15] **R. Zayani**, H. Shaiek, D. Roviras, **"PAPR-aware Massive MIMO-OFDM Downlink"**, IEEE Access 2019.

[J14] H. Shaiek, **R. Zayani**, Y. Medjahdi, D. Roviras, **"Analytical analysis of SER for beyond 5G post-OFDM Waveforms in presence of High Power Amplifiers"**, IEEE Access 2019.

[J13] W. Njima, **R. Zayani**, I. Ahriz, M. Terre, R. Bouallegue, **"Beyond Stochastic Gradient Descent for Matrix Completion Based Indoor Localization"**, Applied Sciences - Special Issue : IoT for Smart Cities: 2019, 9, 2414.

[J12] W. Njima, I. Ahriz, **R. Zayani**, M. Terre, R. Bouallegue, **"Deep CNN for Indoor Localization in IoT Sensors Systems"**, Sensors, 2019.

[J11] **R. Zayani**, H. Shaiek, D. Roviras. **"Ping-Pong Joint Optimization of PAPR Reduction and HPA Linearization in OFDM Systems"**, IEEE Transactions on Broadcasting, pp. 1 - 8, 2018, (doi:10.1109/TBC.2018.2855664).

[J10] **R. Zayani**, H. Shaiek, X. Cheng, X. Fu, C. Alexandre and D. Roviras, **"Experimental Testbed of post-OFDM Waveforms Toward Future Wireless Networks"**, IEEE Access 6: 67665-67680 (2018).

[J09] Yahia Medjahdi, Sylvain Traverso, Robin Gerzaguet, Hmaied Shaiek, **R. Zayani**, David Demmer, Rostom Zakaria, Jean-Baptiste Doré, Mouna Ben Mabrouk, Didier Le Ruyet, Yves Louet, Daniel Roviras, **"Comparative study of waveforms in MTC context"**, IEEE Access 2017.

[J08] **R. Zayani**, H. Shaiek, D. Roviras and Y. Medjhadi, **"BER analysis of FBMC-OQAM systems with Phase Estimation Error"**, IET Communications 10.1049/iet-com.2017.0646.

[J07] **R. Zayani**, H. Shaiek, D. Roviras and Y. Medjahdi, **"Closed-Form BER Expression for (QAM or OQAM)-Based OFDM System With HPA Nonlinearity Over Rayleigh Fading Channel"**, IEEE Wireless Communications Letters, (2015), Volume: 4, Issue: 1, Pages: 38 - 41, DOI: 10.1109/LWC.2014.2365023.

[J06] Maha Cherif Dakhli, **R. Zayani**, Ridha Bouallegue, **"BER Analysis and Compensation for the Effects of Polynomial HPA Non-linearity in MIMO OFDM Systems Over Fading Channel"**, Springer Wireless Personal Communications 81(1): 133-149 (2015).

[J05] H. Bouhadda, H. Shaiek, D. Roviras, **R. Zayani**, Y. Medjhadi and R. Bouallegue, **"Theoretical Analysis of BER performance of FBMC-OQAM signals in Nonlinear channel using Polynomials HPA Model"**, EURASIP Journal on Advances in Signal Processing 2014, 2014:60 - doi:10.1186/1687- 6180-2014-60.

[J04] M. Dakhli, **R. Zayani** and R. Bouallegue, **"Theoretical analysis and compensation for the joint effects of HPA nonlinearity and RF crosstalk in VBLAST MIMO-OFDM systems over Rayleigh fading channel"**, EURASIP Journal on Wireless Communications and Networking 2014, 2014:61 - doi:10.1186/1687-1499-2014-61.

[J03] O. B. Belkacem, M. L. Ammari, **R. Zayani**, R. Bouallegue, **"On the effect of neural network compensation on MIMO-STBC systems in the presence of HPA nonlinearity"**, Transactions on Emerging Telecommunications Technologies (2014) DOI: 10.1002/ett.2837.

Journals published during my PhD thesis

[J02] **R. Zayani**, R. Bouallegue and D. Roviras, **"Adaptive Pre-distortions based on Neural Networks associated with Levenberg-Marquardt algorithm for Satellite Downlinks"**, EURASIP Journal on Wireless Communications and Networking, Volume 2008 (2008), Article ID 132729, 15 pages - doi:10.1155/2008/132729.

[J01] **R. Zayani** and R. Bouallegue, **"Pre-Distortion for the compensation of HPA nonlinearity with neural networks: Application to satellite communications"**, IJCSNS International Journal of Computer Science and Network Security (2007) Vol. 7 No.3.

1.10.3 Patents

[P01] **R. Zayani**, H. Shaiek, D. Roviras, S. Bulusu, **"Procédé de mise en forme d'un signal en vue de son amplification, procédéd'amplification, dispositif de mise en forme, et dispositif d'amplification associés"**, November 2016, France, Réf : FR 1660518.

1.10.4 Book chapters

[B01] S. Bulusu, H. Shaiek, D. Roviras , **R. Zayani**. **"Power Amplifier Effects and Peak-to-Average Power Ratio Mitigation"**, Book Title: "Orthogonal Waveforms and Filter Banks for Future Communications Systems", pp. 1-20, 2017.

1.10.5 International peer-reviewed conferences with proceedings

[C42] W. Njima, M. Terré, I. Ahriz, **R. Zayani** and R. Bouallegue, **"Localization by inversion of the Taylor Expansion of the received power"**, 2019 IEEE 30th Annual International Symposium on Personal, Indoor and Mobile Radio Communications (PIMRC), Istanbul, Turkey, 2019, pp. 1-6.

[C41] **R. Zayani**, C. Alexandre, H. Shaiek, D. Roviras. **"A Testbed for experimental performance evaluation of Multicarrier Waveforms in presence of RF PA"**, ISWCS2018, August 2018, pp.1, Lisbon, Portugal.

[C40] Y. Medjahdi, Y. Louet, D. Roviras, S. Traverso, R. Gerzaguet , H. Shaiek, **R. Zayani**, D. Demmer, R. Zakaria, J. Doré, M. Ben Mabrouk, D. le Ruyet. **"Impact of selective channels on post-OFDM waveforms for 5G Machine Type Communications"**, IEEE ISWCS 2018, August 2018, pp.1-5, Portugal.

[C39] Y. Louet, D. Roviras, H. Shaiek, **R. Zayani**, **"Global power amplifier efficiency evaluation with PAPR reduction method for post-OFDM waveforms"**, IEEE ISWCS 2018, August

2018, pp.1-5, Portugal,

[C38] K. Tani, Y. Medjahdi, H. Shaiek, **R. Zayani**, D. Roviras, **"PAPR reduction of post-OFDM waveforms contenders for 5G and Beyond using SLM and TR algorithms"**, IEEE ICT 2018: 104-109.

[C37] H. Fhima, H. Shaiek, **R. Zayani**, D. Roviras, B. Sens Chang, R. Bouallegue. **"Analysis of Widely Linear Equalization over Frequency Selective Channels with Multiple Interferences"**, WiMOB 2018, October 2018, Limassol, Cyprus,

[C36] H. Fhima, B. S. Chang, **R. Zayani**, H. Shaiek, D. Roviras, R. Bouallegue, **"Performance of Linear and Widely Linear Equalizers for FBMC/OQAM modulation"**, ICT 2018: 605-609.

[C35] Z. Hraiech, F. Abdelkefi, M. Siala, **R. Zayani**, **"On the Performances of POPS-PHYDYAS Waveforms"**, VTC Spring 2018: 1-5.

[C34] Bruno S. Chang, Carlos A. F. da Rocha, Hayfa Fhima, **R. Zayani**, Hmaied Shaiek and Daniel Roviras, **"On the Performance of a Widely Linear SC-FDE System Under Multiple Independent Interferences"**, IEEE PIMRC 2017.

[C30] Hayfa Fhima, **R. Zayani**, Hmaied Shaiek, Daniel Roviras, Bruno Sens Chang and Ridha Bouallegue, **"Widely Linear equalizer performance with multiple independent interferences"**, IEEE ISCC 2017, Crete, Greece.

[C29] W. Njima, I. Ahriz, **R. Zayani**, M. Terre, R. Bouallegue, **"Comparison of Similarity Approaches for Indoor Localization"**, Wimob 2017, October 2017, pp.1-5, Rome, Italy,

[C28] W. Njima, I. Ahriz, **R. Zayani**, M. Terre, R. Bouallegue, **"Smart Probabilistic Approach with RSSI Fingerprinting for Indoor Localization"**, Softcom 2017, September 2017, pp.1-5, Split, Croatia,

[C27] I. Ahriz, W. Njima, **R. Zayani**, M. Terre, R. Bouallegue, **"Error Density for indoor localization based on RSSI fingerprint"**, ISWCS 2017, August 2017, pp.1-5, Bologna, Italy.

[C26] Y. Medjahdi, **R. Zayani**, H. Shaiek and D. Roviras, **"WOLA processing: a useful tool for windowed waveforms"**, IEEE ICC 2017, Paris, France.

[C25] R. Gerzaguet, Y. Medjahdi, D. Demmer, **R. Zayani**, J-B. Dore, H. Shaiek and D. Roviras, **"Comparison of promising candidate waveforms for 5G: WOLA-OFDM, UF-OFDM and BF-OFDM"**, in IEEE ISWCS 2017.

[C24] **R. Zayani**, Y. Medjhadi, H. Shaiek, D. Roviras, **"WOLA-OFDM: a potential candidate for asynchronous 5G"**, IEEE Globecom 2016, Washington, USA.

[C23] M. Laabidi, **R. Zayani**, R. Bouallegue: **"A Quick Convergence Active Constellation Extension Projection onto Convex Sets Algorithm for Reducing the PAPR of OFDM System"**, AINA Workshops 2016: 439-443

[C22] H. Bouhadda, **R. Zayani**, H. Shaiek, D. Roviras and R. Bouallegue, **"Receiver Technique for Detection and Correction of Nonlinear High Power Amplifier Distortion Errors in OFDM systems"**, IEEE VTC2015-Spring, 81th Vehicular Technology Conference, Glasgow, Scotland.

[C21] M. Laabidi, **R. Zayani**, D. Roviras and R. Bouallegue, **"PAPR Reduction in FBMC/OQAM systems Using Active Constellation Extension And Tone Reservation Approaches"**, IEEE ISCC 2015 - The Twentieth IEEE Symposium on Computers and Communications, 06-09 July 2015, Larnaca, Cyprus.

[C21b] M. Laabidi, **R. Zayani** and R. Bouallegue, "A new tone reservation scheme for PAPR reduction in FBMC/OQAM systems". IWCMC 2015: 862-867.

[C21c] M. Laabidi, **R. Zayani** and R. Bouallegue, "A novel multi-block selective mapping scheme for PAPR reduction in FBMC/OQAM systems". 2015 World Congress on Information Technology and Computer Applications (WCITCA).

[C20] R. Zouari, I. Ahriz, **R. Zayani**, A. Dziri and R. Bouallegue, **"Relevant CIR Parameters selection for Fingerprinting Based Location Algorithm"**, IEEE SoftCOM 2015, The 23rd International Conference on Software, Telecommunications and Computer Networks

[C19] **R. Zayani**, Y. Medjhadi, H. Bouhadda, H. Shaiek, D. Roviras and R. Bouallegue, **"Adaptive Predistortion techniques for non-linearly amplified FBMC-OQAM signals"**, IEEE VTC2014-Spring, 79th Vehicular Technology Conference, Seoul, South Korea.

[C18] H. Bouhadda, H. Shaiek, Y. Medjahdi, D. Roviras, **R. Zayani** and R. Bouallegue, **"Theoretical analysis of BER performance of non-linearly amplified FBMC-OFDM signals"**, IEEE ICC 2014, IEEE International Conference on Communication, Sydeny, Australia.

[C17] R. Zouari, **R. Zayani**, R. Bouallegue, **"Indoor localization based on feed-forward Neural Networks and CIR fingerprinting techniques"**, IEEE RWS 2014: Radio and Wireless Symposium, 271-273.

[C16] S. S. K. Chaitanya Bulusu, H. Shaiek, D. Roviras, **R. Zayani**, **"Reduction of PAPR for FBMC-OQAM systems using dispersive SLM technique"**. IEEE ISWCS 2014: the eleventh International Symposium on Wireless Communication Systems, August 2014, pp.1-5, Barcelona, Spain.

[C15] M. Dakhli, **R. Zayani** and R. Bouallegue, **"A Theoretical Characterization and Compensation of Nonlinear Distortion Effects and Performance analysis using Polynomial Model in MIMO OFDM Systems under Rayleigh fading channel"**, IEEE ISCC2013, The Eighteenth IEEE Symposium on Computers and Communications, July 7 - 10, 2013, Split, Croatia.

[C14] O. B. Belkacem, M. L. Ammari, **R. Zayani**, R. Bouallegue: **"Capacity Analysis of MIMO-STBC System in the Presence of Nonlinear Distortion and Neural Network Compensator"**. ISWCS 2013.

[C13] O. B. Belkacem, **R. Zayani**, M. L. Ammari, R. Bouallegue, D. Roviras, **"Neural Network equalization for Frequency-Selective Nonlinear MIMO Channels"**, IEEE ISCC2012, The Seventeenth IEEE Symposium on Computers and Communications (ISCC'12), July 1 - 4, 2012, Cappadocia, Turkey.

[C12] M. Dakhli, **R. Zayani** and R. Bouallegue, **"Compensation For Nonlinear Distortion IN MIMO OFDM Systems based on MMSE Receiver"**, IEEE ICCS'12, International IEEE Conference on Communication Systems, November 21st to 23rd, 2012, Singapore.

[C11] M. Dakhli, **R. Zayani** and R. Bouallegue, **"A compensation method based on NN at the transmitter and the receiver level for nonlinear distortion in MIMO OFDM systems using MMSE receiver"**, IEEE ISSPIT 2012, IEEE International Symposium on Signal Processing and Information Technology: December 12-15, 2012 - Ho Chi Minh City- Vietnam.

[C10] H. Bouhadda, **R. Zayani**, R. Bouallegue and D. Roviras, **"Memory CO-NNPD for the Compensation of Memory Crosstalk and HPA Nonlinearity"**, EUSIPCO 2011, 19th European Signal Processing Conference, August 29- September 2, 2011, Barcelone, Spain.

[C09] M. Dakhli, **R. Zayani** and R. Bouallegue, **"Neural Network compensator based MMSE receiver for HPA nonlinearity in MIMO OFDM systems"**, MMS2011, 11th Mediterranean Microwave Symposium (MMS), September 8-10, 2011, Hammamet, Tunisia.

[C08] **R. Zayani**, R. Bouallegue and D. Roviras, **"Crossover Neural Network Predistorter for the Compensation of Crosstalk and Nonlinearity in MIMO OFDM Systems"**, IEEE PIMRC 2010, 21st Annual IEEE Int. Symposium on Personal, Indoor and Mobile Radio Communications, September 26-29, 2010, Istanbul, Turkey.

[C07] M. Dakhli, **R. Zayani** and R. Bouallegue, **"On the effect of High Power Amplifier Nonlinearity on MIMO MC-CDMA systems"**, IEEE ISSPIT 2010, IEEE International Symposium on Signal Processing and Information Technology, December 15-18, 2010, Luxor, Egypt.

Communications published during my PhD thesis

[C06] **R. Zayani**, R. Bouallegue and D. Roviras, **"Levenberg-Marquardt learning Neural Network for Adaptive Pre-distortion for time-varying HPA with memory in OFDM systems"**, EUSIPCO 2008, 16th European Signal Processing Conference, August 25-29, 2008, Lausanne, Switzerland.

[C05] **R. Zayani**, R. Bouallegue and D. Roviras, **"An Adaptive Neural Network Pre-distorter**

for nonstationary HPA in OFDM systems", EUSIPCO 2007, 15th European Signal Processing Conference, September 3-7, 2007, Poznan, Poland.

[C04] **R. Zayani** and R. Bouallegue, **"A Neural Network Pre-Distorter for the Compensation of HPA Nonlinearity: Application to Satellite Communications"**, IEEE CCNC 2007, IEEE Consumer Communications and Networking Conference, January 11-13, 2007, Las Vegas, Nevada, USA.

[C03] **R. Zayani** and R. Bouallegue, **"A Novel Analog Pre-distorter of TWTA non-linearity in high power satellite transmitters"**, IEEE WASA2006, International Conference on Wireless Algorithms, Systems and Applications, August 15-18, 2006, XI'AN, CHINA.

[C02] **R. Zayani**, R. Guedria and R. Bouallegue, **"Compensation of the OFDM non-linear distortions by the inverse model method"**, IEEE ICACT 2006, 8th International Conference on Advanced Communication Technology, February 20-22, 2006, Phoenix Park, Gangwon Do, Korea.

[C01] **R. Zayani**, S. Zid et R. Bouallegue, **"Simulateur des non-linéarités HPA sur un systeme OFDM"**, OHD 2005, 18th Colloque International Optique Hertzienne et Diélectriques, September 6-8, 2005, Hammamet, Tunisie.

1.10.6 Technical project reports

[D06] Y. Medjahdi, S. Traverso, J-B. Dore, H. Shaiek, D. Roviras, R. Gerzaguet, **R. Zayani**, D. Demmer, P. Chevalier, Y. Louet, M. Ben Mabrouk, R. Zakaria, D. Le Ruyet, **"Critical and comparative study of waveforms in C-MTC context"**, Deliverable D2.1, ANR WONG5 project, 2017.

[D05] H. Shaiek, D. Roviras, Y. Medjahdi, **R. Zayani**, M. Ben Mabrouk, Y. Louet, **"Performance of the candidate waveforms in the presence of power amplifier"**, Deliverable D3.1, ANR WONG5 project, 2017.

[D04] Y. Louet, A. Nafkha, H. Shaiek, D. Roviras and **R. Zayani**, **"Overall power budget"**, Deliverable D3.3, ANR WONG5 project, 2018.

[D03] J-B. Dore, D. Roviras, H. Shaiek, **R. Zayani**, S. Traverso, **"Choice of the candidate Waveforms for the demonstrator"**, Deliverable D5.1, ANR WONG5 project, 2018.

[D02] S. Traverso, **R. Zayani**, H. Shaiek, C. Alexandre, D. Roviras and J-B. Dore, **"Waveforms MOdels for Machine Type CommuNication inteGrating 5G Networks"**, Deliverable D5.2, ANR WONG5 project, 2018.

[D01] **R.Zayani**, S. Traverso, H. Shaiek, D. Roviras, C. Alexandre, **"Experimental testbed of post-OFDM Waveforms"**, Deliverable D5.3, ANR WONG5 project, 2019.

1.10.7 Thesis

R. Zayani, **"Adaptive Predistortion of HPA nonlinearities using Neural Networks"**. Ph.D Dissertation, ENIT, March 2009.

Chapter 2

Teaching activities

2.1 Introduction

In this chapter, I describe my teaching activities that have been dedicated to a variety of students: classes at the undergraduate or graduate engineering level at ISI/University of Tunis ElManar, and also for alternating graduate engineering students (in partnership with industry) at CNAM-Paris during or after business hours. This has allowed me to work with students from a variety of backgrounds who were very diverse both culturally and linguistically. My courses are mainly concerned with digital communications, radio-communications and networking.

Section 2.2 summarizes the teaching classes I gave during my PhD while Section 2.3 and Section 2.4 detail my teaching activities since I have been Associate Professor.

The teaching activities[1] are separated in lectures (L), directed works (DW) and labworks (LW).

2.2 Teaching during PhD

Although I spent most of my time in preparing my PhD, I tried to maintain a teaching activity in order to pursue an academic career because of my interest in scientific research and my unmitigated passion for teaching. From 2005 to 2009, I was temporary lecturer at ISI/University of Tunis ElManar. The studies at ISI comprise two graduations, i.e. *Licence* and *Engineer*. The Licence level comprises 3 years denoted (L1, L2 and L3) and the Engineer level 3 years, i.e. ING1, M1 and M2. I had the opportunity to teach to undergraduate students (L1, L2 and L3) courses involving some fundamentals of telecommunications and networking. Indeed, I started teaching to students in undergraduate level the course *radiowave propagation* and *Introduction to telecommunications* for L1, *Digital data transmission* and *TCP/IP Networking* for L2 and *Computer networks administration* for L3. I taught a labwork for ING1 entitled *Communication systems*. My teaching time was about 190 HDW per year. It is worth to mention that I kept some of these fundamentals courses in my next statutory teaching period where some evolutions have been naturally appeared. Table 2.1 summarizes my teaching experience as temporary lecturer.

[1] The amount of hours are given in hour of directed works (HDW), i.e. 1 hour of lecture = 1.5 HDW and 1 HDW = 1 HLW.

Table 2.1: Teaching activities during PhD.

Period	Topic	Level	Volume (HDW)
2005-2009	Computer networks administration (L/DW/LW)	L3	168
2005-2009	TCP/IP Networking (L/DW/LW)	L2	336
2006-2009	Digital data transmission (L/DW)	L2	63
2007-2009	Introduction to telecommunications (L/DW)	L1	42
2005-2009	Radiowave propagation (L/DW)	L1	84
2006-2009	Communication systems (LW)	ING1	63
2005-2009	**Total in HDW**		**756**

Teaching description

(i) Computer networks administration

The purpose of this lecture is to give a sound understanding of computer network configuration, with a strong emphasis on the management and administration of the network. I taught interconnection, routing (RIP, OSPF and BGP), network access control (VLAN, ACL, Firewall), NAT, administration through SNMP and HPOpenView platform. Through networking labs, I gave students the opportunity of learning further configuration details and acquire practical knowledge. **I was in charge of these labworks and I built LW exercises using several tools for computer networks management and supervision.**

(ii) TCP/IP Networking

In this course, I taught to students the fundamentals of computer networking, with a strong emphasis on TCP/IP and the internet model. Indeed, I taught TCP/IP architecture, the internet protocol version 4 (IPv4), addressing and the transport layer (TCP and UDP). In the laboratory works, students exercise practical configurations, like setting up a network, packet captures and protocols analysis. **I was in charge of the labworks and I entirely produced their handout.**

(iii) Digital data transmission

I taught to undergraduate students the fundamentals of digital data transmission. I focussed on techniques of PHY and MAC layers. The contents of this course was: data transmission chain overview, baseband and passband modulations, channel coding, ...

(iv) Introduction to telecommunications

This course aimed at developing the fundamental principles of telecommunication systems and their recent technological innovations. Specifically, Its goal was just to give a synthetic panorama of the telecommunication sector by describing the main elements constituting such a system and the main techniques, in an introduction level.

(v) Radiowave propagation

This course gave the fundamentals of electromagnetic waves and prorogations. I taught Maxwell's equations, propagation, uniform plane waves and waveguide.

(vi) Communication Systems

In this labwork, I taught to students the design of transceiver chain through MATLAB or circuit hardware and real signals, gathering all their knowledge in analog modulaions. The transmission was accomplished through radio-frequency link. They implemented AM and FM modulator/demodulator using electronic

devices. Using MATLAB, they implemented channel encoder, digital mapping, multi-tone modulator, propagation channel and the whole receiver chain.

2.3 Statutory teaching at ISI/University of Tunis ElManar since 2009

Since 2009, I have taught undergraduate and graduate engineering courses at ISI/University of Tunis ElManar. I recall that the studies are divided into two main parts, 3 years in undergraduate level (Licence) and 3 years in a Telecommunications and Networking engineering speciality (1st year (ING1), 2sd year M1 and 3rd year M2). I have mainly taught in the department of Communication Systems and Networking (CSN), where I am committed to create a synergy between teaching and research considering that they are complementary activities continually supporting each other. Since creating such synergy requires a good background on telecommunications and networking fundamentals, I have kept some of the courses that I taught during my PhD with of course some evolutions. After a solid background on these fundamentals is formed, I devote a significant effort to combine research and teaching, whenever possible, by bringing research into the classroom by teaching recent results to students, especially for graduate level. For example in the courses *radiocommunications* and *advanced digital communications* that I teach for graduate engineering level (M1 and M2), I try to assign some creative projects to students, which permit them to implement the studied new algorithms and concepts.

My teaching time per year at ISI/University of Tunis ElManar averages 228 HDW. In 2015/2016, I was in sabbatical where I was released from my regular teaching and responsibilities to focus entirely on my research/scholarly interests. During this year, I spent time in organizing a winter school and visiting the CNAM school to participate in some research programmes. Teaching hours are illustrated in Table 2.2.

Table 2.2: Statutory teaching activities.

Period	Topic	Level	Volume (HDW)
Since 2009	Radiocommunications (L/DW)	M1	294
Since 2009	Digital communications (L/DW/LW)	M1	294
2009-2011	Wireless networks protocols (L/DW/LW)	M1	84
2009-2015	Computer networks administration (L/DW/LW)	L3	360
Since 2009	TCP/IP Networking (L/DW/LW)	L2	672
Since 2009	**Total in HDW**		**1704**

Teaching description

(i) Advanced digital communications

In 2014, **I introduced a lecture on advanced digital communication techniques** for the engineer students in last year. I have taught to the students advanced topics in digital communications. Students have been provided with up-to-date knowledge of the technologies studied for modern communication systems and the principles underlying their design. The course has covered two main areas, advanced multi-carrier waveforms and new MIMO technologies.

I teach 30 HDW, per year, of lectures.

(ii) Radiocommunications

In this course, students were given a system overview of how radiocommunication systems are built up. The main emphasis is on digital radiocommunication and the lowest layer, physical layers, and how the radio channel affects design choices. Advanced technologies, like OFDM and MIMO, were taught and their performance were studied under many radio channel models and in presence of hardware imperfections.

I am in charge of this course (30 HDW per year in average). I have produced the slides and 5 DWs. Concerning LW, I have entirely built labworks exercises on MATLAB.

(iii) Digital communications

The course gives a fundamental description to the principles and systems for digital transmission of information over channels with Gaussian noise, including detailed analysis of digital carrier modulation formats including assessment of signal-to-noise ratio, bit error rate, and power and bandwidth efficiency for amplitude-shift keying (ASK), phase-shift keying (PSK), frequency-shift keying (FSK), and Quadrature-Amplitude Modulation (QAM). Line codes (NRZ, RZ, AMI, Manchester) and PSD of line codes were addressed. Moreover, I taught matched filter receivers and receiver design, transmission bandwidth, Nyquist pulses, sampling and inter-symbol interference, Gaussian noise, and related error analysis in symbol detection, coding, convolutional codes, decoding,...

I am in charge of this course and I have produced slides. I teach (42 HDW per year). I produced the labworks in MATLAB.

(iv) Wireless networks protocols

This course described fundamental concepts and principles on wireless network technologies such as the IEEE 802.11 wireless LANs and Bluetooth wireless PANs. Concepts regarding WLAN and the IEEE 802.11.x protocols were taught in detail starting from the very basic data communication concepts up to the analysis of the MAC and routing protocols. Laboratory experiments include tools and techniques to monitor, measure, and characterize the performance of wireless LANs as well as the use of network simulation tools to model and evaluate the performance of IEEE 802.11.

(v) Computer networks administration

From 2009 to 2015, **I was in charge of this course**, which I taught during my PhD (see description in the previous section), and I have evolved the handout. In particular, I added chapters on traffic control via RMON and its corresponding labworks. I taught 2 groups for which 30 HDW per year.

(vi) TCP/IP Networking

This course is the evolution of the one I taught during my PhD. **I am in charge of this course**, where some chapters are added such as internet protocol version 6 (IPv6) and routing algorithms, link state and distance vector routing.

Works supervision experience

Up to now, over 80 highly qualified students in their project graduation. These projects concern undergraduate and graduate levels for different specialities. Specifically, they are related to hardware/software developments including transmission/reception to remote management of industrial and medical systems. These projects have adopted new technologies integration (GPS, RFID, CPL,....) and tele-informatics over communication networks. They have been very beneficial to my students who have gone on to secure highly sought-after positions in industry. At ISI/University of Tunis ElManar, undergraduate and graduate students are asked to perform an internship, most often in industry but it can be in an academic laboratory, in order to obtain their, respectively, Licence (L3) or Engineer degree (M2).

2.4 Teaching at CNAM-Paris

Since 2018, I have mainly taught graduate engineering students at CNAM-Paris. I teach LW in *Digital Communications 1*, *Digital Communications 2* and *Information theory* for alternating graduate students (M1) in the following specialities :
- Systemes Electroniques, Telecommunications et Informatique (SETI).
- Systemes Electroniques et Signalisation Ferroviaire (SESF).
In these LW for alternating students, I try to create a link between the theory studied in lecture and some of the practice aspects that students face in their work by giving them some labworks exercises in the design and evaluation of various components of a digital transceiver through MATLAB or circuit hardware and real signals.

Furthermore, I am handling, with colleagues (Prof. Daniel Roviras and Dr. Cristophe Alexandre), a labworks for alternating graduate students (M2, final year), as a practical application project, in radiocommunications where I teach to students hands-on experiences in the design, implementation and evaluation of some techniques deployed in recent generations of wireless communication systems through software defined radios (SDRs).
In the academic year 2018-2019, I taught lecture in *Basics of digital communications 2 (BDC-II)* to students in the International Master of CNAM. This course focused on passband digital communications. The concepts addressed in this course, which was taught in English, are: (1) Study the QAM, PSK, FSK and PSD of modulation formats, (2) Design an optimal coherent receiver for an arbitrary digital modulation format in Gaussian noise, (3) Analyze the bit, symbol, and frame error probabilities for any arbitrary digital modulation format and (4) Equalization techniques (ZF, MMSE) for frequency selective channels.

My teaching time at CNAM averages 150 HDW per year that are summarized in Table 2.3.

Table 2.3: Teaching activities at CNAM.

Period	**Topic**	**Level**	**Volume (HDW)**
Since 2018-2019	Basics of digital communications 2 (L/DW)	M1	42
Since 2018	Digital communications 1 (LW)	M1	98
Since 2018	Digital communications 2 (LW)	M1	52.5
Since 2018	Information theory (LW)	M1	35
Since 2018	Radiocommunications (Practical project)	M2	60
Since 2018	**Total in HDW**		**287.5**

2.5 Teaching Material

I have produced course material for multiple educational levels (a package with slides, tutorials and labworks):
- R. Zayani, *Digital communications*, M1 level, published locally at ISI/University of Tunis ElManar.
- R. Zayani, *Radiocommunications*, M1 level, published locally at ISI/University of Tunis ElManar.
- R. Zayani, *Basics of digital communications 2*, M1 level, published locally at CNAM-Paris.

- R. Zayani et al., *Computer networks administration*, L3 level, published locally at ISI/University of Tunis ElManar.
- R. Zayani et al., *TCP/IP Networking*, L2 level, published locally at ISI/UniversityTunis ElManar.
- R. Zayani et al., *Labworks on Networking*, L3 level, published locally at ISI/University of Tunis ElManar.
- D. Roviras, R. Zayani and C. Alexandre, *OFDM Project : Radiocommunications*, M2 level, published locally at CNAM-Paris.

2.6 Leadership in educational programmes

During all my teaching activity, I have been fully involved in order to further improve the educational programme at, especially, the ISI/University of Tunis ElManar where I have taught during my PhD and then in my tenured associate professorship.

"Atelier Réseaux"

In 2006, I initiated laboratory works in networking ('Atelier réseaux') for undergraduate students (L3 level). I tried to provide to students a global mastering in computer networks. These labs cover various practical experimentations, such as, setting up a computer network, installation, address configuration, troubleshooting, applicative protocol traffic analysis (FTP, Telnet, SSH, DHCP, ...), network security policies configuration (VLAN, ACL, Firewall, ...), network management and supervision (SNMP, RMON, HPOpenView) and system administration : Windows, Linux.

Laboratory equipment management

I have prepared the LW material containing a package with experimentation descriptions that have been dispatched between a group of teachers. The management of the laboratory and equipment was also in my charge.

Participation to ISI engineer curriculum committee

I was involved the ISI engineer curriculum committee for two times, in 2010 and 2016. These reforms aim at providing innovative training engineer programs with themes of excellence and to create the expertise adequate to the new digital world.

Participation to engineer degree projects committee

I have participated in many committees and have acted as an examiner on several undergraduate and graduate engineering's degree projects.

Chapter 3

Research activities

In this chapter, I summarize my research activities. Section 3.1 gives an overview of my research topics, a summary of my PhD is given in Section 3.2 and Section 3.3 summarizes my research interests and developed expertise since I have been Associate Professor.

3.1 Research topics

Green wireless communication technologies have received increasing attention due to concerns over the explosive increase in power-consumption in the information and communications technologies (ICT) sector and, correspondingly, increasing carbon dioxide (CO2) emissions. Indeed, ICT currently consumes 3% of the world-wide energy and generates about 2% of the world-wide CO2 emissions [3].

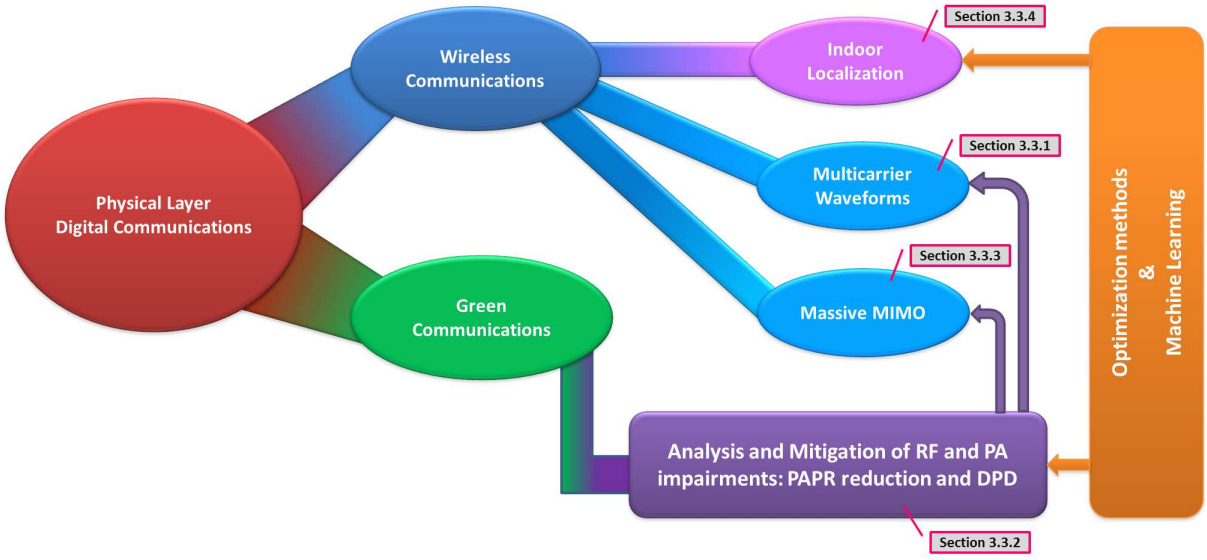

Figure 3.1: Research topics.

Therefore, energy efficiency in signal processing hardware has been in high demand in order to achieve this green goal, in particular to contribute to the reduction of both user equipment energy consumption

resulting in longer battery lifetime, and the base station energy consumption resulting in power saving and reduced environmental pollution.

Note that the most important part (50-80%) of the total power budget is actually consumed by the transmit power amplifier (PA) which has to be operated near its saturation region, generating however severe nonlinear amplitude-to-amplitude (AM-AM) and amplitude-to-phase (AM-PM) distortions. These undesirable impairments are very harmful, yielding in-band distortions and out-of-band (OOB) radiation, which cause signal distortion and adjacent channel interference, respectively.

In the lights of these facts, my research activities have focused, in one hand, on developing a deep understanding how the radio-frequency (RF) PA affects the performance of wireless communication systems. In another hand, I have been interested in developing new digital processing (DSP) based solutions aiming at mitigating RF PA impairments jointly with increasing energy-efficiency. In addition, it is important that these solutions are of low-complexity in order to enable real-time operation.

The different research topics, which are summarized in Figure 3.1, are described in the following.

Machine Learning for energy-efficient communications During my PhD (2005-2009), I was specially studying PA linearization techniques. Indeed, I started working on the development of digital predistortion (DPD) schemes based on neural network techniques to linearize RF transmitters using the cyclically prefixed-orthogonal frequency division multiplexing (CP-OFDM) technology. This latter, which has been largely adopted by physical layer (PHY) of today's long term evolution advanced (LTE-A), is very sensitive to PA nonlinear distortions since its time-domain signal has large peak-to-average power ratio (PAPR).

Advanced Multi-carrier Waveforms (MWFs) with high energy-efficiency for future WCSs The need for reducing the energy-consumption has been accentuated by the trends of accommodating, in addition to enhanced mobile broadband (eMBB), new service regimes that arise with new emerging applications like machine-type communications (mMTC) (also known as Internet of Things (IoT)), and ultra-reliable and low latency communications (URLLC). Indeed, future generations of wireless communications will have to cope with high degree of heterogeneity in terms of services and requirements. Regarding physical layer specifications, the major innovation with respect to former standards is to seek new multicarrier waveforms (MWFs) in order to address the major limitations of the traditional CP-OFDM in challenging new spectrum use scenarios, like asynchronous multiple access, as well as the support of mixed numerology. This latter refers to different parameter settings in the MWF such as subcarrier spacing (SCS), symbol duration and cyclic prefix (CP) length.

Besides this, the post-OFDM MWFs still suffer from high PAPR of the modulated signal that would lose their good property in presence of PA. Therefore, high power efficiency and PA with perfect linearity are of paramount importance when considering a wireless system with a massive number of low-cost and low-power MTC/URLLC devices, meaning that each device has to become more energy-efficient if not the total energy consumption shall increase.

As far as I am concerned, it is important to study the performance of wireless communication systems exploiting new MWFs with a particular attention to the energy consumption. Therefore, my research interests, in this topic, are in two folds: (1) Identifying the most suitable post-OFDM waveforms to the future wireless communications requirements by analyzing their performance in terms of spectral-efficiency, energy-efficiency, OOB radiation, user asynchronicity and complexity. (2) developing new DSP solutions, to mitigate RF impairments, that are more adequate to post-OFDM waveforms, through a set of algorithms and advanced techniques,

Massive MIMO systems : Energy-efficiency and Hardware-efficiency One of the most ul-

timate wireless communication technology is massive multiple-input multiple-output (MIMO), where the base stations (BSs) have to be equipped with hundreds of individually controllable RF chains. Here, energy-efficient hardware becomes indispensable to motivate corresponding energy and cost-efficient massive MIMO BS deployments. Therefore, my research activities have been widened to develop DSP solutions for massive MIMO enabling the use of low-end power amplifiers that are allowed to operate close to saturation. In particular, I have developed downlink transmission schemes to address the PAPR reduction problem and the mitigation of nonlinear PA distortions in massive MIMO based wireless communications. Furthermore, I have been interested in investigating advanced optimization approaches and machine learning tools in order to improve the energy and hardware efficiencies in massive MIMO systems.

In addition, the upcoming wireless communication systems are expected to support a wide range of services with diverse requirements. Therefore, multi-carrier WF based massive MIMO and mixed numerologies transmission are proposed as solutions. In this regard, I have been interested in studying the capability of massive MIMO to deal with the spatial multiplexing of users who are sharing the same bandwidth and are using different numerologies.

Indoor Localization: from matrix completion to deep learning Besides the above topics, I have been also involved in some works that aim at developing solutions for indoor localization. In fact, many applications in wireless sensor networks (WSN), such as surveillance, equipment monitoring and control, target tracking and health monitoring, require the location of sensor nodes. Here, we have considered the problem in which some unkown sensor nodes determine their own location (position) using the coordinates of a small number of sensors, called anchor nodes, whose positions are known (obtained by GPS or by installing them at points with known coordinates). In particular, we have adopted advanced approaches, such as matrix completion and machine learning, to develop accurate solutions for indoor localization with an important focus on reducing the computational complexity.

3.2 PhD thesis

3.2.1 Introduction and context

The aim of my PhD was the investigation of new linearization techniques applied to power amplifier for broadband radio-communications. In this context, we used feedforward neural networks (NN) based baseband adaptive predistortion techniques. Indeed, we have considered three power amplifier models. The first PA is a stationary memoryless travelling wave tube amplifier (TWTA), whose output signal can be expressed as

$$\mathbf{z} = F_a(\rho)\exp(jF_p(\rho)\exp(\phi)) \tag{3.1}$$

where ρ and ϕ are, respectively, the modulus and phase of the input signal. The memoryless TWTA can be modeled using Saleh's model [4] whose AM/AM and AM/PM characteristics can be represented as

$$F_a(\rho) = \frac{\alpha_a \rho}{1+\beta_a \rho^2} \qquad\qquad F_p(\rho) = \frac{\alpha_p \rho^2}{1+\beta_p \rho^2}, \tag{3.2}$$

where α_a and β_a are the parameters controlling the nonlinear level, and α_p and β_p are phase displacements. The second PA model is a nonstationary memoryless TWTA whose parameters (α_a, β_a, α_p and β_p) are time-varying. The third one is an amplifier with memory modeled, according to Hammerstein, by a memoryless amplifier followed by a linear filter [5] [6]. Indeed, we have presented new NN structures

which give the best performance for the three power amplifier models. Equally important, many NN training algorithms have been deployed and tested in order to identify the most adequate for adaptive predistortions. This comparison has been conducted through computer simulation for 64 carriers and 16-quadrature amplitude modulation (QAM) OFDM system. It is based on some quality measure (mean square error (MSE), symbol error rate (SER)), the required training time to reach a particular quality level, and computation complexity. The chosen adaptive predistortions (NN structures associated with an adaptive algorithm) have the fastest convergence toward the best performance while performing the lowest computational complexity.

3.2.2 Contributions of the thesis

Neural Network Predistortion for stationary memoryless TWTA The basic idea proposed is to identify the PA inverse transfer functions with a feed-forward neural network (see Figure 3.2). Therefore, by using the indirect learning structure, we aim at obtaining direct estimation of the inverse of the AM/AM and AM/PM nonlinearity characteristics. In order to do that, two processes, referred to as Training and Generalization, have to be performed. During the training process (Figure 3.2(a)), indirect learning architecture (ILA) is applied to obtain direct estimation of the inverse of the AM/AM and AM/PM nonlinearity characteristics. Using the ILA, the PA output signal is used as NN input while PA input signal is considered as desired signal. The error calculated between the NN input and output signals is sent to a learning algorithm that adjusts the NN coefficients to make the error getting lower at each iteration. It is worth mentioning that the training process can be performed offline since the PA is stationary. Concerning the generalization process, coefficients of the trained NN are recopied on the NNDPD that achieves the predistortion.

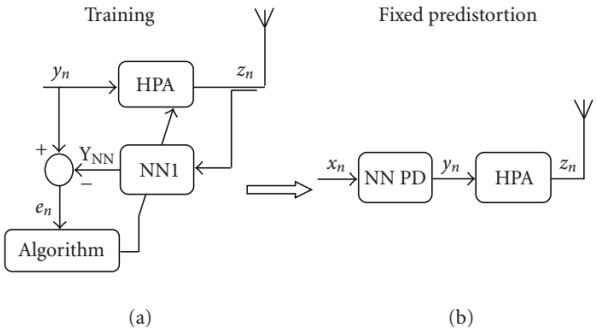

Figure 3.2: Block diagrams for training and generalization of DPD with PA.

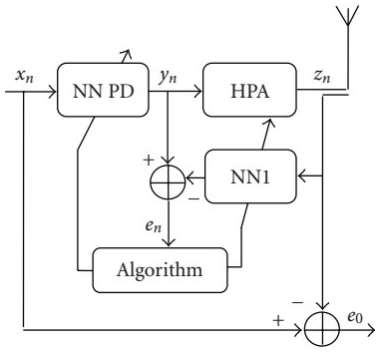

Figure 3.3: Simultaneous DPD updating.

The neural predistorter was a multi-layer perceptron, which has two inputs, namely the I and Q components of the input signal complex envelope. The NN has N_h hidden layers and an output layer with two neurones that are the predistorted signals I and Q. Different structures have been deployed and compared, starting by one hidden layer with 2 neurons, then increasing progressively the number of neurons, before testing a network with two hidden layers, and again increasing progressively the number of neurons on the two layers. Note that activation functions of hidden layers are hyperbolic tangent, while the ones of the output neurones are linear.

Symbol error rate (SER) metric is a typical performance measure to quantify the capability of the proposed predistortion structures to reduce HPA distortions. Then, Figure 3.8 shows the SER performance

versus signal to noise ratio (SNR) of many NNDDP's configurations for an OFDM system in presence of a stationary memoryless TWTA operated with an IBO of 8 dB. PD(2, x, 2) represents a NN with one hidden layer of x neurons, PD(2, x - y, 2) represents a NN with two hidden layers of x and y neurons, respectively. From these results, we note that all the NNDPDs can reduce the SER compared to the one without any predistorter. Moreover, a satisfactory performance can be obtained with a NN with one hidden layer of nine neurones, which is referred to as DPD(2,9,2).

Neural Network Predistortion for nonstationary memoryless TWTA Here, we assume that the PA parameters are time-varying requiring an improved DPD structure. In this regard, We have studied an adaptive predistortion architecture that performs simultaneously the estimation of the inverse PA characteristics in a postdistortion stage and in a simple predistortion one, as shown by Figure 3.3.

It is worth to mention that the initial DPD (i.e., NN coefficients) can be performed offline, and will be adapted online, regarding the variation of the PA characteristics, using an iterative algorithm. Therefore, this latter has to be selected with a very wise way because it should provide satisfactory performance with a reduced complexity. Thus, I have tested and implemented many advanced algorithms [7] with the NNDPD selected above. Among these algorithms, we find gradient descent (GD) back-propagation [8], GD with momentum (GDm) [9], conjugate gradient (CGF) [10], quasi-Newton (BFG) [11] and Levenberg-Marquardt (LM) [12].

Figure 3.4 shows, for all methods, the mean square error (MSE) versus the iterations number averaged over 100 simulations. One can note that the MSE in LM decreases much faster toward the best performance compared the other algorithms. It is important to study the computational complexity of the different algorithms.

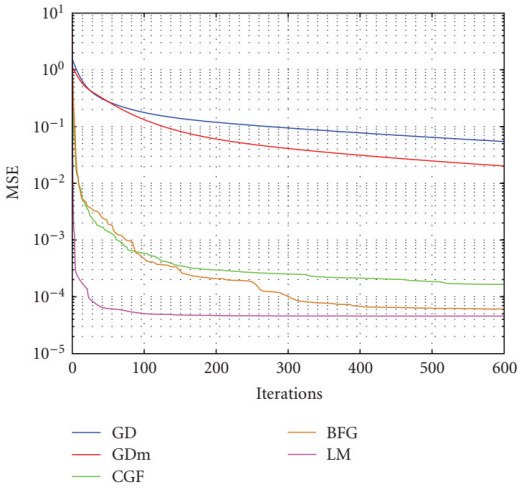

Figure 3.4: MSE vs. iterations number for the different studied algorithms.

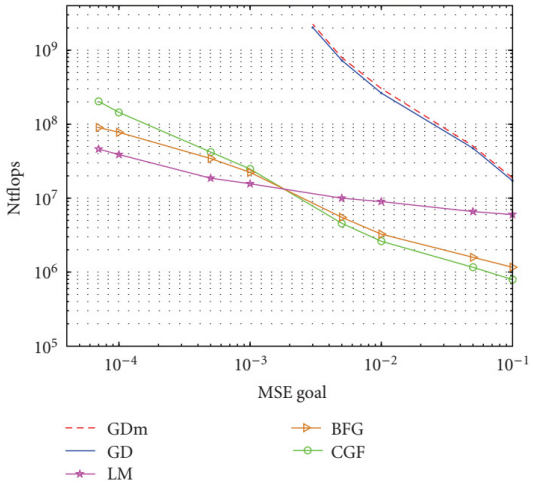

Figure 3.5: Computational complexity required vs. the MSE goal.

In Figure 3.5, we give the number of operations (Ntflops) required by each algorithm to reach the MSE convergence goal. Note that the number of floating operations, additions and subtractions are one flop if real and two if complex. Multiplications and divisions count one flop each if the result is real and six flops if it is complex.

We can observe, from these results, that LM algorithm performs better than all the other algorithms.

Although it requires the most significant number of computation per epoch (because of the Hessian approximation), it requires the lowest computational complexity (Ntflops) for a given MSE goal. Moreover, the gain performed by the LM algorithm gets higher as the error goal goes lower.

Neural Network Predistortion for PA with memory In new generations of wireless communications which use OFDM as modulation scheme, memory effects of PA can no longer be ignored due to the broadband input signal. Consequently, the NNDPD structure should be improved by adding a tap delay line to deal with this imperfection (memory effect). Indeed, we have introduced two NNDPD structures. They are the following: (1) A fully connected multi-layer NN (FCNN) predistorter with memory (see Figure 3.6). The tap delay input is connected to nine neurons in the hidden layer. The output neurons are real and imaginary parts. The fully connected NN aims at simultaneously mitigating memory and PA nonlinear effects. (2) A neural network mimetic structure (see Figure 3.7), which combines a linear network (LN) and a memoryless nonlinear neural network (NLN). The LN-NLN predistorter is composed of a linear filter followed by a memoryless neural network, with one hidden layer of nine neurons, and with two linear output neurons. Using this mimetic scheme (LN-NLN), we realize separately the memory predistortion with the linear network and the compensation of the memoryless PA nonlinearities with the nonlinear neural network. A comparative study of these two structures has been done in terms of performance and complexity. To ensure a good comparison between the different structures, we have chosen the same length of the tap delay line (4 memory cells). The LM algorithm, which has given the best performance with the lowest computational complexity, has been considered.

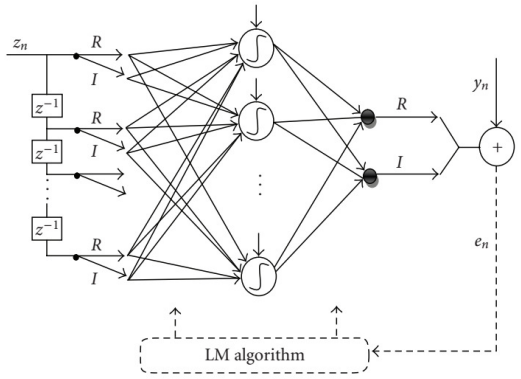

Figure 3.6: Fully connected NN predistorter structure.

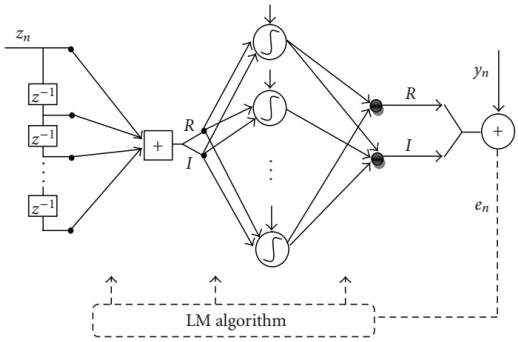

Figure 3.7: Linear network + nonlinear network predistorter structure.

Figure 3.9 shows the SER performance versus SNR in systems with a linear PA along with nonlinear memory PA without predistortion and a nonlinear memory PA with NN memoryless predistortion, FCNN predistortion, and LN-NLN predistortion.

The realistic level of memoryless nonlinear distortions is considered by operating the PA with an IBO of 7 dB. From these results, we note that the two memory NN structures (FCNN and LN-NLN) are able to reduce considerably the SER compared to the one without any predistortion. Moreover, one can note that the mimetic structure (LN-NLN) performs slightly better than the FCNN structure when they are both trained with LM. Figure 3.10 and 3.11 represent AM/AM curves of the amplified signal versus input signal without predistortion and predistorted signal versus input signal for two studied predistortions (memoryless NN PD and LN-NLN).

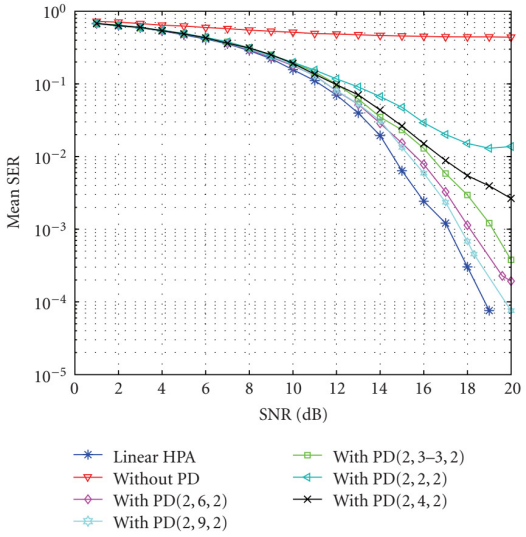

Figure 3.8: SER vs. SNR of OFDM system with predistorter: a 16-QAM modulation is used over 64 subcarriers and IBO=8dB.

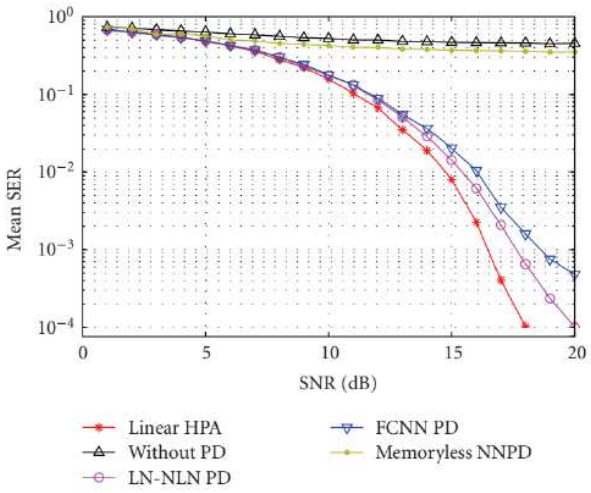

Figure 3.9: SER vs. SNR for 16-QAM OFDM with 64 subcarriers at IBO=7dB.

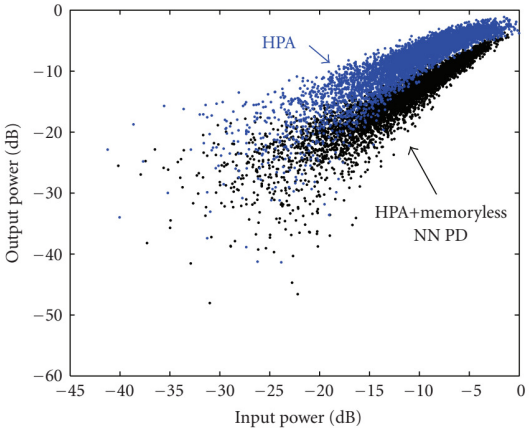

Figure 3.10: AM/AM curves for memoryless NNDPD.

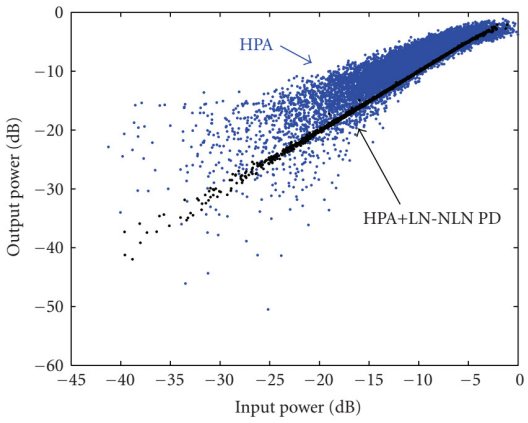

Figure 3.11: AM/AM curves for LN-NLN DPD.

Memory effects are not taken into account in the memoryless NN PD structure. Thus, we can see on Figure 3.10 that the AM/AM curve of the concatenated system (memoryless NN PD + HPA) is thicker than the resulting AM/AM curve of Figure 3.11 obtained with an LN-NLN PD.

Table 3.1 summarizes the results of the comparative study of the two-mentioned structures in terms of complexity. The variables *Nlearnflops* and *Nrunflops* are the number of floating operations that each structure requires to learn per epoch and to run, respectively, per OFDM sample.

We deduce from Table 2 that the computational complexity of the mimetic structure (LN-NLN) is much lower than the fully connected one (FCNN) with an approximate ratio of more than 80% in learning phase and nearly 40% in the generalization phase.

Table 3.1: Complexity comparison of NN predistorter structures.

Structure	Nlearnflops	LRatio	Nrunflops	RRatio
LN-NLN	LN 57 NLN 5059 Total 5116	1	LN 25 NLN 64 Total 89	1
FullyCNN	32981	6.45	145	1.63

3.3 Research interests since 2009

In this section, I summarize researches I have been leading since 2009. Most of my researches has been focused on energy-efficient digital signal processing techniques related to new PHY technologies based future generation of wireless communications (5G and beyond). Such promising technologies include enhanced multicarrier waveforms (MWFs) that enable a flexible accommodation of various applications/services with different requirements, and massive MIMO that employs linear precoding and combining schemes and offers significant gains in terms of spectral- and energy- efficiencies compared to the traditional MU-MIMO. In massive MU-MIMO, impairments such as fading, noise, and interference vanish for very large number of BS antennas. In order to introduce such technologies within 5G based heterogeneous

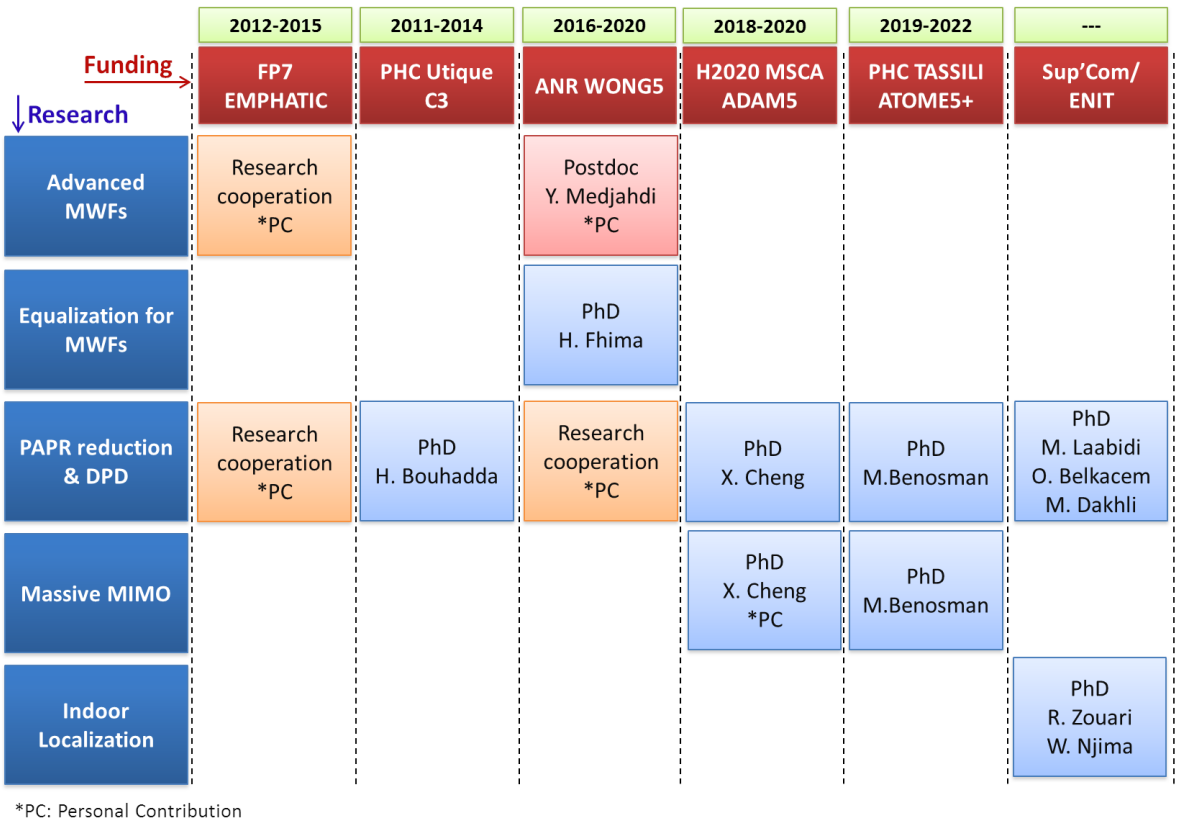

Figure 3.12: Research activities and their related funding.

and mass-market applications, a major issue in the design and implementation of radio equipment is the cost-efficiency in terms of implementation size, cost and power consumption. On one hand, the cost and size of individual radio equipment are strongly limited leading to various Dirty-RF impairments impacting the good properties of the above mentioned technologies. On another hand, facilitating very dense deployments of wireless communication links to connect over trillion wireless devices will result in increasing the power consumption of the ICT sector for more than 14% of estimated world-wide power consumption by 2020 causing 1.4 Giga ton CO2, nearly 2.7% of the global carbon footprint [13] [14].

Thus, I have been dealing with the promising 5G technologies, where low latency, good reliability and high data rate are of paramount importance while a particular attention has been given to the aspect of energy consumption. The main focus has been on the radio access network, in particular on the power amplifier, which is known for dominating energy consumption in the radio transmitter.

In the following, we present the different research activities, which are illustrated in Figure 3.12 with their related funding. The structure of the second part of this manuscript will follow the research axes presented here.

3.3.1 Advanced Multicarrier Waveform design solutions for 5G and Beyond

I have been interested in investigating advanced MWFs to address the major limitations of the traditional CP-OFDM in challenging new spectrum use scenarios, like asynchronous multiple access, as well as the support of mixed numerology which allows the service to choose between a set of supported subcarrier spacing (SCS) and symbol duration. Indeed, I have had major contributions in the ANR WONG5 project in which notable waveforms have been introduced. Post-OFDM MWFs are basically based on filtering or/and windowing processing in either time or frequency domain [15]. Indeed, a first class of these MWFs gathers the ones that adopt a per-subcarrier pulse-shaping to reduce out-of-band (OOB) radiation and increase relaxed synchronization requirements: offset quadrature amplitude modulation based filter-bank multicarrier (FBMC-OQAM) [16] [17] and filtered multi-tone (FMT) [18] have been heavily studied. Generalized frequency division multiplexing (GFDM) [19] employs a circular convolution [20] to directly apply the filtering operation on a time-frequency block [21]. Another class of sub-band filtering-based waveforms (i.e. apply filtering at sub-band level over single or multiple resource blocs (RBs)) has been investigated, where the universal filtered multicarrier (UFMC) [22], filtered-OFDM (f-OFDM) [23] and fast Fourier transform FBMC (FFT-FBMC) [24] and block-filtered OFDM (BF-OFDM) [25] are the most studied.

Time-domain windowing can also be a useful tool to achieve the desired enhancements, which permit to prevent steep changes between two OFDM symbols so as to confine OOB emission. In this regard, I have studied an advanced windowing based multicarrier approach called - weighted overlap and add based OFDM (WOLA-OFDM) [26], which has been introduced to the 5G-NR as a low-complexity candidate method (it has nearly computational complexity as the classical CP-OFDM). In addition, WOLA-OFDM allows transparent design where transmitter (Tx) and receiver (Rx) units use independent waveform processing techniques, which will comply with the 3GPP agreement [27]. **This work has been published in [C24]**.

Furthermore, some alternatives make the use of both filtering and windowing, such as windowed cyclic prefix-based circular-OQAM (WCP-COQAM) [28] where a circularly pulse shaping filter combined with a time-domain windowing is applied. In this regard, we have investigated a new MWF design that is based on the WOLA processing and the circular convolution approach [15] with the Post-doc of Dr.

Yahia Medjahdi that I co-supervised with Prof. Daniel Roviras. The proposed MWF called- WOLA based circular offset quadrature amplitude modulation (WOLA-COQAM) has shown better performance than the classical windowed based MWFs confirming the capability of WOLA processing in supporting asynchronous multi-user access. These works have been performed in the framework of the ANR WONG5 project and **published in [C26]**. These were my first contributions in the WONG5 project, in which I participated as an associate researcher at CEDRIC laboratory of CNAM University. Indeed, I acted as visiting researcher in many times. Consequently, I had the opportunity to collaborate with the WONG5's partners, such as THALES, CEA-Leti and CentraleSupelec. I have been interested to study the ability of these MWFs to address the different 5G requirements in challenging new spectrum use scenarios, like asynchronous multi-user access, as well as the support of mixed numerology. Indeed, an exhaustive analysis and objective comparison of several 5G MWFs in order to identify the most suitable waveform configuration to any C-MTC case according to its critical requirements have been carried out with the Yahia's Post-doc. For instance, several C-MTC key performance metrics such as spectral efficiency (SE), out-of-band (OOB) radiations end-to-end latency, robustness to asynchronous multi-user uplink transmission, PAPR, and transceiver complexity have been assessed in order to identify the most suitable waveform configuration to any C-MTC case according to its critical requirements. Note that classical CP-OFDM served as a reference basis. **This work has been published in [J09]**.

Through this exhaustive evaluation over all 5G MWFs, where pertinent and major discussions have been carried out with all WONG5's partners, we have shown that: (1) All the studied windowed or filtered MWFs can offer a satisfactory spectral localization (i.e., low OOB radiation) compared to the traditional CP-OFDM, especially when the guard band (GB), separating the useful and interfering signal is quite large. Nevertheless, the filtered WFs offer the best spectral localization, especially the ones that adopt a per-subcarrier filtering, thanks to the good spectral containment of the adopted prototype filters. (2) concerning spectral efficiency (SE), it depends on wether short or long packet sizes. Indeed, FBMC-OQAM and FMT provide the worst SE performance compared to all other MWFs due to the bad time-localization of their respective prototype filters. It is worth to mention that GFDM and WCP-COQAM offer better SE performance, despite their long prototype filters, due to the employed circular convolution. However, all the investigated MWFs provide the same SE performance when long sequences scenario (i.e., the filter impulse response length becomes negligible) is considered. (3) We move now to the latency, MWFs using a CP have higher latencies compared to other MWFs that do not consider adding a CP, such as FBMC-OQAM, GFDM and FMT, when for long packet sizes. However, when packet sizes are very short, OFDM based MWFs (CP-OFDM, WOLA-OFDM, UFMC, f-OFDM, N-continuous OFDM) have the lowest latencies compared to the other MWFs that are affected by the filtering-related ramp-up and ramp-down. (4) Most importantly, the robustness of these MWFs to time and frequency synchronization errors is studied. FBMC-OQAM and FMT, which have the best spectral localized transmit/receive filters, provide the best performance. Moreover, FFT-FBMC, f-OFDM and WOLA-OFDM can provide satisfactory performance compared to the classical CP-OFDM. Finally, BF-OFDM is more sensitive due to the fact that it uses a basic OFDM receiver. It is worth to point out that adding the WOLA processing at the receiver side with the BF-OFDM transmitter would perform excellent performance making them very attractive to C-MTC applications. (5) When coming to the complexity, WOLA-OFDM provides the lowest level, it is almost the same as CP-OFDM. However, the computational complexity required by N-continuous OFDM and UFMC is excessively high about 200 times the CP-OFDM/WOLA-OFDM complexity. The other WFs have tolerable computational complexity, compared to the CP-OFDM/WOLA-OFDM, it is approximately 2 times for BF-OFDM and

FFT-FBMC, 3 times for FBMC-OQAM and 9 times for GFDM. Finally, this objective comparison would be useful to identify the most suitable MWF to any C-MTC case according to its technical challenges.

As explained above, FBMC-OQAM offers the best spectral localization leading then to the best performance in supporting asynchronous and mixed numerology transmissions. Nevertheless, it does not fulfil the robustness requirements when a frequency selective channel is considered. Therefore, one of my research activities was oriented to study advanced equalization schemes, with Hayfa Fhima's PhD, to overcome this FBMC-OQAM's drawback. Since FBMC-OQAM is based on a non second order circular (NSOC) modulation and its signal is a cyclo-stationary one, it motivates the use of widely linear (WL) and Fresh processing. Then, three different MMSE equalizer schemes have been developed, referred to as linear (LE), widely linear (WLE) and widely linear Fresh (WL Fresh) equalizers. For the proposed equalizers, both symbol spaced (SSE) and fractionally spaced (FSE) processing have been evaluated, in synchronous DL/UL and asynchronous UL scenarios, with mixed numerologies transmissions. **These works have been published in [C36], [C34], [C30] and [J19]**. Through these studies, we have demonstrated that WL Fresh equalizer provides the best performance in synchronous and asynchronous scenarios, outperforming the classical Linear and WL equalizers.

3.3.2 Nonlinear distortion characterization and machine learning based mitigation techniques for energy-efficient 5G MWFs

Despite the mentioned MWFs advantages, all of them still suffer from the high PAPR of the modulated signal. This feature has a significant impact on the power-efficiency of the PA, which is an intrinsic nonlinear device. Indeed, the PAPR issue leads to the PA saturation and, consequently, output signal can be affected by in-band and out-of-band distortion effects [29]. Therefore, the outstanded MWFs lose rapidly their good frequency localization property when a RF PA is employed. To deal with the high power peaks of MWF signals and avoid the nonlinear and saturation operating regions of the PA, a large back-off can be considered, which results in reduced power-efficiency and a large amount of the consumed power is dissipated as heat, since the PA is operated far from its saturation point. Therefore, I have been interested in studying the performance of the future wireless communications exploiting MWFs in presence of RF PA impairment, especially when the power-efficiency is high, by using both analysis and evaluation through practical scenarios. Equally importantly, I have been interested in developing new and reliable digital signal processing based solutions coping with the expected 5G requirements, with a particular focus on mitigating RF PA impairments while reducing the power-consumption, through a set of new algorithms and advanced techniques. Since 2009, my contributions to researches regarding this topic have been performed in several research projects, such as the FP7 EMPHATIC, the CMCU-PHC-Utique C3, the PHC-TASSILI ATOME5+ and the ANR WONG5 projects. Some of these contributions have been achieved with the PhD students I have co-supervised (see Figure 3.12). In the following, I will give short description for each investigate issue.

- **Theoretical characterization of nonlinear distortion effects in MWFs based systems** A theoretical characterization of nonlinear distortion effects, in OFDM and FBMC transmission systems, has been addressed during the PhD of Hanen Bouhadda and with my personal contribution, supported in part by the C3 project and in part by EMPHATIC project, receiving fund by, respectively, the PHC-Utique and the FP7 EC ICT. In this investigation, we have adopted Bussgang's theorem showing that the in-band distortion effects on the decision variables can be characterized by means of a complex gain and an additive Gaussian term with zero-mean and

suitable variance. Then, we have introduced analytical expressions for the gain and the variance, where a new approach has been developed leading to performing these expressions for any simulated or measured PA model. Consequently, closed-form analytical expressions have been derived and illustrated to evaluate the bit-error-rate (BER) performance using OFDM with rectangular pulse shaping as well as well-localized filter-bank based multicarrier (FBMC) running under an additive white Gaussian noise (AWGN) or a frequency-flat fading Rayleigh channels. **These works have been, respectively, published in [J05] and [J07]**.

Then, in the framework of the WONG5 project, we focussed our attention on developing an universal approach to make this study feasible for any 5G MWF. In collaboration with Prof. Daniel Roviras, Dr. Hmaied Shaiek and Dr. Yahia Medjahdi, we have presented further discussions and comparisons on different waveforms: CP-OFDM, WOLA-OFDM, UFMC, f-OFDM and FBMC/OQAM and we have provided insights on the impact of in-band NLD caused by RF PA. **This investigation has been presented in [J14]** where simulation and theoretical results are shown to be in agreement for different MWFs and various IBO values.

- **Machine Learning for green communications: High PA Efficiency and Linearity**

  In order to improve PA linearity and efficiency, two complementary solutions have to be deployed in MWF based systems. These latter are grouped into two categories including PAPR reduction and PA linearization.

  Concerning PA linearization, digital predistortion (DPD) has drawn most of the attention among all the studied methods. Although its simplicity, it has proven to be effective providing a good trade-off between efficiency, linearity and implementation complexity and has been the main focus of my conducted works. My previous conducted studies on the field of DPD were limited to SISO-OFDM systems. We pursued my investigations on DPD based energy-efficiency solutions considering MIMO technology and post-OFDM MWFs. Furthermore, We have been interested in designing DPD using machine learning approaches. In particular, We have developed some low-complexity and highly-efficient neural network (NN) architectures to deal with DPD and its issues. A first issue encountered in DPD is that its efficiency can be affected by the RF crosstalk generated between transmission/reception paths when MIMO techniques are considered. To overcome this problem, **We introduced, in papers [C08] and [C10], crossover neural network predistorter (CO-NNPD) models** to compensate simultaneously for RF crosstalk and PA nonlinearities while taking into account the memory effect in MIMO-OFDM systems.

  Due to the similarity between OFDM and post-OFDM MWFs, it is natural to consider employing DPD to compensate amplitude and phase nonlinear distortions of MWF signals. However, some of the post-OFDM MWFs, like the FBMC-OQAM, have a different signal structure compared with OFDM. Therefore, directly applying the DPD schemes of OFDM systems to FBMC-OQAM systems may be not very effective. To deal with this issue, we considered the investigation of the PA nonlinearity effects mitigation in FBMC-OQAM systems. First, we showed that the classical DPD scheme performs worse with the FBMC-OQAM system when compared to the OFDM one. Such degradation can be explained by the fact that this DPD, which aims to compensate simultaneously the amplitude and phase nonlinearities, is not able to compensate perfectly the phase error. Indeed, AM/AM distortion can only be perfectly tackled when the PA is operated far from the saturation, otherwise the predistorted amplifier exhibits a residual AM/AM distortion that affects the correction of the AM/PM distortion. In the regard to get efficient DPD, my efforts were deployed to build

a new NN based DPD scheme around the concept of separating the compensation of the phase and amplitude distortions. By using the proposed scheme, it was shown that OFDM and FBMC-OQAM systems reach the same performance showing that a higher attention must be paid for phase correction in filtered MWFs like FBMC. **This work has been published in [C19]**.

On the other hand, the MCM techniques suffer from high PAPR which is one of the most crucial issues that need to be solved effectively with a reasonable complexity. Indeed, when a PA non-linearity is taken into account, the good frequency localization property provided by the post-OFDM MWFs is severely compromised due to the spectral regrowth, thereby hampering much of its attractive appeal to be promising candidate for future wireless communications. In order to advance this, we must opt for PAPR reduction techniques, in order to operate the PA more efficiently without damaging the performance of the MCM techniques. Hence, I have been interested in developing algorithms for PAPR reduction, which are based on probabilistic approach and adding signal methods. I have been first interested in reducing the PAPR of FBMC-OQAM signals with the Mounira Laabidi's PhD. Indeed, FBMC-OQAM has an overlapping structure and the classical methods applied for OFDM cannot be directly applied to FBMC-OQAM. Then, **we have introduced, in [C21b] and [C23], new overlapped tone reservation (TR) and active constellation (ACE)** by extending, respectively, the classical TR and ACE with taking into consideration the overlapping structure of FBMC-OQAM signals. **joint TR and ACE has been put-forward in [C21]**. Coming to the proposed probabilistic schemes, **we have introduced in [C21c] a novel multi-blocks selective mapping (MB-SLM)**, where it has been shown that the PAPR reduction performance achieved with FBMC-OQAM is similar to the one of OFDM, if the signal overlapping structure of the former is well exploited. More recently, I pursued this investigation, in the framework of the WONG5 project, to study new PAPR reduction schemes for other post-OFDM MWFs (**published in [C38]**), like WOLA-OFDM, UFMC and f-OFDM, that have been good promising candidates for the futures wireless systems. In addition, a global power amplifier efficiency evaluation with PAPR reduction **has been presented in [C39]** for post-OFDM MWFs.

- **Joint approach for PAPR reduction and PA linearization** In conventional systems, PAPR reduction and linearization techniques have been optimized separately and applied independently. I started focusing on their association aiming at avoiding mutual effects in order to enhance interoperability. I have introduced a joint approach for PAPR reduction and PA linearization that consists in a really synergistic combination of the two operations in order to improve power amplifier efficiency and linearity. Its key idea was to synthesize only one correction signal in a Ping-Pong manner between PAPR reduction and DPD. The proposed Ping-Pong joint optimization approach provides significant improvement, compared to conventional association schemes, in fulfilling OOB requirements and preserving low in-band distortion while preserving excellent energy-efficiency of the system. The proposed approach, which was a part of the ANR WONG5 project, **has been first patented [P01] and then published in [J11]**.

- **Experimental tesbed of post-OFDM Multi-carrier Waveforms toward 5G and beyond networks** It has been encouraged to concentrate on more careful and thoughtful design, evaluations, realizations and comparison of CP-OFDM waveform and its most promising enhancements, i.e., WOLA-OFDM and BF-OFDM especially in experimental testbed. In the framework of the ANR WONG5 project, I was in charge of the development of an experimental testbed to study

the capability of new multicarrier waveforms to accommodate 5G requirements. Testbed experiments were done with an implementation of CP-OFDM and its most promising enhancements, i.e., WOLA-OFDM and BF-OFDM, with configurable universal software radio peripherals (USRPs)-based software defined radio prototype. These experiments were done in a realistic laboratory-like environment, where capabilities of the selected waveforms to accommodate 5G requirements are evaluated while focusing on the optimization of the energy efficiency. On one hand, I have provided details and deign guidance to improve energy-efficiency and robustness of the studied waveforms through new approaches of DPD and PAPR reduction in the presence of real RF PA. In particular, I focused on the mitigation of in-band and OOB non-linear distortions and their effects on power spectrum density (PSD) and bit-error-rate (BER), respectively. It has been demonstrated that the combination of PAPR reduction and DPD allows the transmitter to significantly improve the spectrum localization without sacrificing the in-band and OOB waveform quality, while achieving high power-efficiency, thus operating the PA very close to its saturation region, as well. On another hand, I addressed the impact of the lack of synchronism between transmitters on the performance of the selected waveforms, which is of special relevance for future 5G MTC applications. Experimental results show that BF-OFDM and WOLA-OFDM would permit the accommodation of 5G requirements when RF PA issues are tackled. In some specific scenarios, ideal spectrum utilization can be realized by these waveforms, using only one tone as guard band while keeping good energy-efficiency. **This work was the subject of one conference paper [C41] and one peer-reviewed journal [J10]**.

3.3.3 Massive MIMO Networks: Energy and Hardware efficiency

Massive MIMO, also known as large-scale multi-user (MU) MIMO, has been recognized as the most promising technology for future generations of wireless communications because it is the most ultimate enablers of enhanced energy-efficiency (EE) and spectral-efficiency (SE). Within the H2020 MSCA ADAM5 project, I have been interested in two investigation issues related to massive MIMO systems.

- **Linear Precoding for Energy-Efficient Massive MIMO** The deployment of massive MIMO systems is attractive if the RF chains consist of inexpensive hardware components. Moreover, it is important to study the realistic massive MIMO systems with non-ideal hardware components, which may induce hardware impairment. Therefore, in the framework of the H2020 MSCA ADAM5 project, I am paying particular attention to this aspect of SE and EE in massive MIMO as well as hardware impairment mitigation to meet future WCS's requirements. Especially, the main focus was in the RF PAs which represent the dominating energy-consumption $(50 - 80\%)$ in the RF chains. Indeed, signals generated by massive MU-MIMO precoders suffer from the high PAPR, independently of whether single-carrier or multi-carrier transmission is adopted. Accordingly, the nonlinearity of the RF PA, which is the main hardware impairment and is expected to be low-cost and energy-efficient component to enable cost- and energy-efficient massive MU-MIMO BS deployments, yields harmful in-band distortion and OOB radiation.

  First, I have developed a PAPR-aware downlink transmission scheme in an OFDM-based massive MU-MIMO. Linear precoding of data and peak-cancelling signals (PCSs) were employed to reduce the PAPRs of the transmitted signals by exploiting the excess degrees-of-freedom (DoFs) provided by equipping the base station (BS) by a large number of transmit antennas. Specifically, we designed PCSs to be added to the frequency-domain precoded data signals, with the goal of reducing the

PAPRs of their time-domain counterpart signals. Most importantly, the added PCSs have to lie in the null-spaces of their associated MIMO channel matrices such that they do not cause any multi-user interference (MUI). In this regard, an efficient algorithm was developed, which was based on different data and PCSs precoders, and the corresponding achievable PAPR reduction and bit-error-rate (BER) performance are analyzed. Moreover, to optimize a tradeoff between performance and complexity, linear precoders based on matrix polynomials (M-POLY) and gradient-iterative approaches (**published in [J15]**) are studied for both data and PCSs precoding. Simulation results reveal that these latter provide similar performance as the regularized zero-forcing (RZF) and orthogonal projection null-space (OPNS) based data and PCSs precoders, while they need much lower computational complexity. The substantial PAPR reduction provided by the proposed algorithm offers interesting insights for the design of energy-efficient massive MU-MIMO-OFDM systems. **This work has been submitted to the peer-reviewed IEEE Open Journal of the Communications Society (OJ-COMS) [SJ2]**.

Second, I have investigated the compensation of the PA nonlinear distortion (NLD) in massive MIMO downlink systems. I have introduced a PA-aware precoding approach that exploits the high-dimensional DoFs, allowed by equipping the base station (BS) by a high number of antennas, and performs the precoded signals that when amplified and passed through the channel, guarantee excellent transmission quality. Specifically, we formulate the proposed PA-aware precoding approach as a simple convex optimization problem which enables efficient, low-complexity, and reliable algorithm implementations. The simulation results demonstrate the strong potential of the proposed approach in terms of improving the link quality and reducing the required computational complexity. **This work has been published in [J16]**.

- **Meta-Learning model for PA NLD mitigation in Massive MIMO systems** Despite the better performance, in terms of BER and computational complexity, provided by the aforementioned algorithm compared to the ones proposed in literature, its computational complexity is still needed to be effectively reduced. Therefore, via the MSc internship of Miss Samar Chebbi, we are investigating approaches to complement traditional machine learning (ML) methods, like the meta-learning (learning to learn) approach, with the aim to obtain lower complexity. It consists in developing a meta-learning model capable of being generalized with a new channel configuration that has never been learned during learning, avoiding the adaptation of the model.

- **Inter-Numerology Interference Analysis and Cancellation for Massive MIMO-OFDM** The extremely diverse service requirements is an important challenge for the upcoming 5G wireless communication technologies. OFDM-based massive MIMO and mixed numerologies transmission are proposed as solutions. In the framework of the ADAM5 project, I have investigated with Xinying Cheng, a PhD student I co-supervise with Prof. Daniel Roviras, the use of spatial multiplexing of users, sharing the same bandwidth, whose associated numerologies are different. We first introduced a precoding design that aims to manage the mixed numerologies spectrum sharing (SS) transmission. Then, we analysed the inter-numerology interference (INI) and derive the theoretical expressions of its radiation pattern in massive MIMO-OFDM downlink systems. We demonstrate that by using the proposed precoding scheme and considering two groups of users using two different numerologies, INI appears only in frequency selective channels. Besides, the transmission of users using numerology with large subcarrier spacing (SCS) is always with the best quality, only users using the numerology with small SCS suffer from INI. In that case, INI increases due to the difference in SCS, channel

selectivity and power allocation. Based on the derived INI closed-form expressions, the precoding scheme was improved and a new INI cancellation scheme was introduced. Our analysis has shown that the INI theoretical model matches the simulation results, and the introduced INI cancellation efficiently mitigates the INI and enhances the performance of massive MIMO-OFDM systems. This study was applied to downlink and uplink scenarios **that have been published in two peer-reviewed journals [J17] and [J18], respectively**.

3.3.4 Indoor Localization: From Matrix Completion to Deep learning

I started this theme by the co-supervision of the Raida Zouari's PhD with Prof. Ridha Bouallegue at ENIT school. I pursued my investigation in this field with my collaboration with Prof. Michel Terre via the supervision of the Wafa Njima's PhD. These studies aim at developing some advanced signal processing solutions for indoor localization. Moreover, we have been interested in developing some deep learning approaches to offer good localization accuracy with low complexity. My contributions on this theme are summarized below:

- **Matrix Completion Based Indoor Localization** Here, we consider the case where few number of sensors (anchor nodes) whose coordinates are known by installing them at known positions, and the rest unkown nodes, have to determine their own coordinates using measured inter-sensor distances and anchor nodes coordinates. Since, in IoT, sensors are not capable of high-power transmission which would be unable to make measurements with all nodes, the trilateration would not be able to offer good performance. Then, as a first contribution, we have proposed an approach based on matrix completion theory to enhance the trilateration based indoor localization. Specifically, the proposed indoor localization scheme is formulated as a simple optimization problem which enables efficient and reliable algorithm implementations. Many approaches, like Nesterov accelerated gradient (Nesterov), Adaptative Moment Estimation (Adam), Adadelta, Root Mean Square Propagation (RMSProp) and Adaptative gradient (Adagrad), have been implemented and compared in terms of localization accuracy and complexity. **This work has been published in a peer-reviewed journal [J13]** where we demonstrated that the Adam optimizer outperforms all other methods in terms of localization accuracy and computational complexity.

- **Deep Convolutional Neural Network (CNN) for Indoor Localization in IoT-Sensor Systems** In order to reduce the complexity of the fingerprinting approach, we have been interested in developing a localization framework that shifts the online prediction complexity to an offline preprocessing step, based on Convolutional Neural Networks (CNN). Motivated by the outstanding performance of such networks in the image classification field, the indoor localization problem is formulated as 3D radio image-based region recognition. It aims to localize a sensor node accurately by determining its location region. 3D radio images are constructed based on Received Signal Strength Indicator (RSSI) fingerprints. **This work has been published in a peer-reviewed journal [J12]** where we have shown that, when considering the trade-off between localization accuracy and computational complexity, our proposed method outperforms other popular approaches.

Part II

Scientific contributions

Chapter 4

Multicarrier Waveform Design for 5G and Beyond

4.1 Introduction

The future/fifth generation (5G and beyond) mobile communications are expected to enhance, significantly, major key performance indicators (KPIs), such as spectral efficiency, power consumption, latency, connection density, low cost terminals and mobility. Moreover, the future standard should support various new service regimes with different and often diverging requirements, presenting serious challenges on 5G commercial deployments [25]. The IMT-2020[1] vision defines the usage scenarios into three broad groups of use cases as enhanced mobile broadband (eMBB) where applications require ultra large bandwidth and spectral efficiency, massive machine type communications (mMTC) (also known as Internet of Things (IoT)) where a tight requirement for device battery life and complexity, and ultra-reliable and low latency communications (URLLC). These versatile services require critical capability objectives such as $20 Gbits/s$ peak data rate, 10^6 devices/km^2 connection density, ultra high energy efficiency, low cost terminals, $1ms$ latency and mobility up to $500 km/h$ [30]. Nevertheless, these challenges are difficult to be addressed by the traditional cyclically prefixed orthogonal frequency division multiplexing (CP-OFDM) and its low peak-to-average power ratio (PAPR) variant discrete Fourier transform spread OFDM (DFT-s-OFDM), which have consequently shaped the success of the today's 4G LTE[2].

Thus, the CEDRIC/LAETITIA team of the CNAM University, where I am associate researcher, has been interested in studying advanced multi-carrier waveforms (MWFs) to overcome the major limitations of the CP-OFDM in challenging new spectrum use scenarios, like asynchronous multiple access, mixed numerology, which allows the service to choose between a set of supported subcarrier spacing (SCS) and symbol duration, while improving their power consumption, significantly. Indeed, within the research projects PHYDYAS [31] and EMPHATIC, spurred on by the work of Prof. Maurice Bellanger, the CEDRIC/LAETITIA team developed recognized expertise in new MWF design, initially on filter-bank based multi-carrier modulations (FBMC) [32], then other waveforms like the fast Fourier Transform FBMC (FFT-FBMC) [24], studied within the framework of the ANR WONG5 project.

[1] International Mobile Telecommunication for 2020 and beyond
[2] Long-Term Evolution

In this context, I have been involved in many research projects and have supervised some PhD/Master students with the CEDRIC/LAETITIA team. I was in charge of 1) the energy-efficiency enhancement of the studied waveforms, 2) the study and proposition of new MWF design adapted to 5G critical MTC systems and 3) the development of an experimental testbed to evaluate the capability of the notable MWFs to accommodate 5G requirements.

This chapter aims to provide a complete picture of the ongoing 5G MWFs I studied and overviews the main researches I developed in work on MWF design. It is organized as follows: Section 6.3 presents preliminary concepts and reveals the 5G waveform design requirements. Section 6.4 provides a brief description of major MWF candidates for 5G and beyond. Author's contribution related to MWF design is presented in Section 5.5. A summary comparison of the MWFs key features is given. Section 5.6 summarizes author's contribution related to equalization for FBMC-OQAM. Finally, the outputs of these contributions are resumed in Section 6.5.

4.2 Fundamentals of the 5G MWF design

4.2.1 Preliminary concepts

In a typical communication system, the transmitter maps every modulated information point from the message space into the signal space whereas the receiver does the reverse operation [33]. The signal space is the time-frequency plane where time and frequency constitute its coordinates [34]. The waveform defines the physical shape of the signal that carries the modulated information. When considering a multicarrier scheme, the structure in signal space relies on N simultaneously-transmitted subcarriers, regularly spaced by ν_0 in frequency. The transmitted signal is given by

$$x(t) = \sum_{m=-\infty}^{+\infty} \sum_{n=0}^{N-1} X_{mn} f_{mn}(t), \tag{4.1}$$

and the received symbol $\hat{X}_{m_0 n_0}$, located in time index m_0 and subcarrier index n_0 can be found by the projection of the received signal $y(t)$ onto the corresponding receive function $g_{m_0 n_0}(t)$ as

$$\hat{X}_{m_0 n_0} =< y(t), g_{m_0 n_0}(t) >= \int_t y(t) g^*_{m_0 n_0}(t) dt, \tag{4.2}$$

where

- X_{mn} denotes the m-th transmitted symbol of the n-th subcarrier, which represents the random part of the waveform. One may choose X_{mn} from a set of a modulation symbols or a part of it, e.g., its real or imaginary part [35].
- $f_{mn}(t)$ and $g_{m_0 n_0}(t)$ denotes, respectively, the synthesis function, which maps X_{mn} into the signal space, and the analysis function. They are obtained by a prototype filter, respectively p_{tx} and p_{rx}, translated in both time and frequency, constructing two Gabor systems [35] [36] [37] [38] when they are given by equations (4.3) and (4.4), respectively.

$$f_{mn}(t) = p_{tx}(t - m\tau_0) e^{j2\pi n \nu_0 t}, \tag{4.3}$$

and

$$g_{m_0 n_0}(t) = p_{rx}(t - m_0\tau_0) e^{j2\pi n_0 \nu_0 t}, \tag{4.4}$$

where τ_0 denotes the symbol spacing in time.

Note that pulse shaping filters (known as prototype filters) have an important effect on the signal characteristics since they define how the energy is spread over the time and frequency domains. Thus, the amount of energy transferred from the transmitter to the receiver is determined by both transmit and receive filters [33]. The coordinates of the filters form a two-dimensional structure in the time-frequency plane are known as lattice [39] [40]. In addition, they identify the structure of the multicarrier scheme, i.e., orthogonal, bi-orthogonal, or non-orthogonal [41] [39] by finding out the correlation between the points in the lattice. Different shapes can be associated to the lattice geometry, either regular or hexagonal [42]. Moreover, additional dimensions, like space domain, can be included in the lattice.

4.2.2 The Baseline for 5G MWF Discussion: CP-OFDM and MWF design requirements

CP-OFDM is the dominant multicarrier modulation scheme that is currently being deployed in many standards such as the downlink of 4G LTE and the IEEE 802.11 family [43]. In OFDM systems, the spectrum is used in a very efficient manner due to the orthogonally overlapped subcarriers, allowing flexible frequency assigning.

The new radio for 5G and beyond is expected to support a variety of new services beyond the user centric communications to more machine type communications, as discussed in Section 7.1. Looking at the 5G requirements and asking the question if OFDM still suitable? Let us talk about strengths and weaknesses of OFDM. First of all, the best strength is its simplicity. It is FFT based which is very efficient and its single tap equalization for frequency selective channel that is really awesome. Second, it is fast, it supports wide bandwidth and MIMO. OFDM naturally supports MIMO in a way it is almost designed with MIMO. It is also very resilient, handling the interference in a multipath environment by ensuring circularity of the channel (thanks to the CP) and by enabling easy frequency-domain equalization (FDE). However, a major weaknesses of OFDM is related to the fact that it is power-hungry. It has high PAPR and it needs a linear or linearized power amplifier; with new methods like digital predistortion (DPD) [7] and envelope tracking (ET) [44], we can make it much better but this could be the strongest drawback for multicarrier schemes. Another critical issue is related to the fact that it is noisy, which is very important for a lot of 5G use cases. It has very large side lobes (i.e., high out-of-band (OOB) emissions), called low spectrum agility. Actually, with the FFT we got basically about at most 30 dB attenuation in the side lobes and we really need at least 60 or 70 dB or more, if we want to intersperse traffic within 5G mMTC. We need those side lobes to be really low to avoid adjacent channel interference (ACI). Typically, OOB emissions are reduced by various windowing/filtering approaches along with the guard band allocation [45] to meet the spectral mask requirements of the various standards. 3GPP LTE standard uses 10% of total bandwidth as guard bands to handle this problem, decreasing unfortunately the spectral efficiency. Finally, it is also very sensitive to carrier frequency offset (CFO). Furthermore, a big downfall of OFDM is the uplink interference [26]. In fact, with the OFDMA, we need all the signals coming up to the base station are lined-up. Although the use of the CP, it cannot be too big for spectral efficiency purpose. It cannot be able to support asynchronous communications in a connected network with millions, if not billions, of devices in 5G mMTC. Moreover, it seriously suffers from its limited flexibility and the unfriendly coexistence with different numerologies for various channel conditions and use cases.

In the diagram depicted in Figure 4.1, we can rearrange these strengths and weaknesses and want to group them as can be better shared between all 5G use cases. For eMBB, we see the ability to retain and

really improve upon the needs to support MIMO and to be a wide bandwidth even wider bandwidth like 100MHz. Furthermore, it needs to solve the sensitivity to CFO, UL access and its power-hungriness. For mMTC, there is a lot of issues: we need to make sure that it is still simple and even make it simpler. It also needs to solve the large side lobes, asynchronous UL access and the power-hungry problems. Finally, for URLLC, we definitely need to solve sensitivity and the large side lobes.

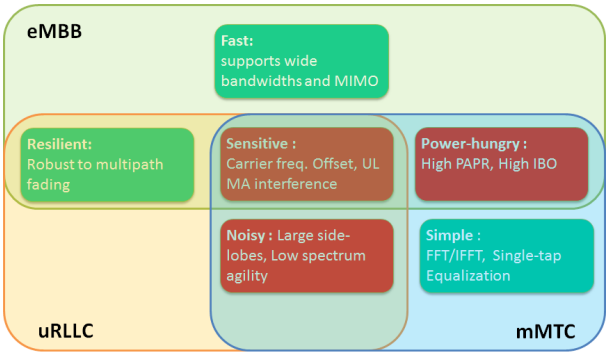

Figure 4.1: 5G MWF design Requirements.

Therefore, numerous MWFs are proposed taking into account all these considerations for the upcoming 5G and beyond standards. The major waveform candidates are classified and discussed thoroughly in the following sections.

4.3 Major MWF candidates for 5G and beyond

Filtering approach is used to enhance the capability of multi-carrier techniques to support asynchronous access to fragmented spectrum. The filtering-based MWF can either be subcarrier-wise or subband-wise. In the following, I give a brief description of the major studied filtered MWFs.

4.3.1 Subcarrier-Wise Filtering

FBMC-OQAM

FBMC has been proposed as an alternative to CP-OFDM offering better frequency localization and flexible access to the available resources. Indeed, contrary to OFDM's rectangular filter, FBMC uses well-frequency localized filters (like PHYDYAS [31] or IOTA [46]) to offer excellent spectral containment (i.e., better adjacent channel leakage performance). The duration of the prototype filters is usually a multiple of the FFT size ($L = KN$), where K is called the overlapping factor. Here, we exploit polyphase filter-banks [47] for pulse shaping, reducing side lobes effectively and having better spectrum agility. Furthermore, Nyquist constraints on the prototype filter combined with offset-quadrature amplitude modulation (OQAM) have to be used in order to ensure orthogonality between adjacent symbols and adjacent subcarriers while keeping maximum spectral efficiency. OQAM is used wherein it is actually not orthogonal in complex domain but it is orthogonal in real domain so it provides staggering of "in-phase" and "quadrature-phase" components in both time and frequency domains, and imaginary intrinsic interference is occurred which is orthogonal to the real transmitted symbols. Moreover, no more than one

subcarrier is required as guard band to support effectively asynchronous (i.e., non-orthogonal) transmissions [45]. Nevertheless, the equalization is more difficult without the use of CP. Furthermore, the biggest challenges is that the MIMO integration and pilot design with FBMC-OQAM are not straightforward as in CP-OFDM due to the non-orthogonality in the complex domain [48].

In this dissertation, we consider FBMC-OQAM with PHYDYAS prototype filter with $K = 4$, the most commonly used. Note that new form of FBMC, which is called Lapped-OFDM, uses the sine prototype filter with $K = 2$. Interested readers are referred to [49] for more details.

GFDM

Similar to FBMC, generalized frequency division multiplexing (GFDM) [21] [19] applies subcarrier-wise filtering. However, GFDM performs a time-frequency filtering over data blocks. A data block contains a set of symbols transmitted over a group of N_A consecutive sub-carriers over N_B time-slots and thus is composed of $N_T = N_A \times N_B$ symbols. From this implementation perspective, it is equivalent to a DFT-s-OFDM[3] signal [50], which also explains lower PAPR compared to CP-OFDM. Since the filters for pulse shaping are circularly convoluted over a data block, GFDM is a nonorthogonal transmission scheme because of symbols overlap in both time and frequency, generating inter and intra data blocks interference. Note that a CP is appended in each block in order to avoid inter block interference. Furthermore, GFDM requires successive interference cancellation (SIC) algorithms at the receiver, making its complexity quite high. Similar to FBMC-OQAM, MIMO integration and pilot design is not straightforward. Moreover, the block-wise transmission causes latency making it not suitable for short burst transmission.

It is worth to mention that a new transceiver design is needed for subcarrier-wise filtering based MWFs (FBMC and GFDM), and there is no backward compatibility with 4G LTE.

4.3.2 Subband-Wise Filtered MWF

UFMC

Alcatel-Lucent Bell Laboratories [51] is the major proponent of the universal filtered multicarrier (UFMC) [52], which is also referred to UF-OFDM in the literature. UFMC can be seen as a compromise between filtred-OFDM (detailed in next subsection) and FBMC, where a filtering operation is applied to a group of successive subcarriers instead of the subcarrier-wise filtering of FBMC. The key-idea of UFMC is that each resource block (RB) has its corresponding transmit filter with a passband larger than the FBMC prototype filter one, leading thus to a shorter impulse response. In typical UFMC systems, each symbol at the output of the IFFT is filtered and zero padding (ZP) [53] is then used to absorb the filter transient response. Here, no CP is used and the transitions regions (i.e., ramp-ups and ramp-downs) provide a soft ISI protection. Then, the symbols are not circularly convoluted with the channel leading to a more complicated receiver [54]. This latter uses a FFT of twice the size of IFFT used at the transmitter. It is worth to point out that the circular convolution can be obtained by collecting additional samples corresponding to the length of the ZP and using an overlap-and-add process [53]. Then, the FFT size becomes identical to the IFFT used at the transmission side.

UFMC has shorter filter lengths compared to subcarrier-wise filtering making it more suitable for short packet and low-latency transmissions. Furthermore, UFMC is suitable for all existing OFDM-related techniques like MIMO, channel estimation/equalization, pilot design, synchronization, PAPR

[3] Discrete Fourier transform spread orthogonal

reduction [45].

f-OFDM

In filtered-OFDM (f-OFDM) [55], the filtering granularity is more flexible than UFMC. Further details on several filters are given in [17]. The partition in the time-frequency grid is adjusted based on the different channel conditions and use cases. Then, f-OFDM is more suitable for the use of different numerologies (such as bandwidth, sub-carrier spacing, CP duration, and transmission time interval) [56] compared to UFMC with the cost of increased complexity. Contrary to UFMC, f-OFDM maintains the CP leading to a better immunity against the ISI and lower complexity at the receiver. Furthermore, f-OFDM differs to UFMC by adopting identically IFFT/FFT sizes and matched filtering at the receiver. f-OFDM has the advantage of having well frequency-localization, providing low OOB emissions, allowing asynchronous transmission, supporting different numerologies and offering high SE (i.e., requiring less number of guard tones). Although f-OFDM cannot offer excellent spectral containment as per-subcarrier filtered MWFs due to the shorter filter length utilization, it has the advantage to be compatible to MIMO and does not require any SIC algorithm. Nevertheless, its main drawback, compared to the classical CP-OFDM, is the complexity.

FFT-FBMC

FFT-FBMC scheme has been proposed within the WONG5 project [24], which aims at overcoming the FBMC intrinsic interference [57] [58]. FFT-FBMC utilizes a data precoding process in a subcarrier-wise manner using an IFFT [24]. Then, with the aid of the subcarrier-wise IFFT/FFT precoding/decoding and the CP insertion, the interference coming from the same subcarrier can be removed using a simple equalization. Furthermore, a new transmission strategy is adopted, together with a well-frequency localized prototype filter, in order to avoid the interference coming from adjacent subcarriers [24].

In FFT-FBMC proposal, a data stream of $MN/2$ is divided into M blocks of $N/2$ data complex samples. Then, each block of $N/2$, corresponding to each subcarrier $k \in \{0, 1, ..., M-1\}$, is fed to a N-IFFT operation. The $N/2$ data samples are alternately fed to the first and last $N/2$ bins of the N-IFFT. When the subcarrier index k is odd (resp. even), the symbols are fed to the first (resp. last) $N/2$ bins. After that, a CP is appended to the N-IFFT output that feds to a FBMC modulator of M carriers in the given subcarrier k.

Most importantly, the complex orthogonality is guaranteed in FFT-FBMC and single-tap equalization can be performed, as shown in [59]. Indeed, $MN/2$ channel frequency response coefficients, weighted by coefficients depending on the used prototype filter, represent the equivalent equalizer coefficients.

BF-OFDM

Block-Filtered OFDM (BF-OFDM) is a precoded filter-bank multi-carrier modulation that has been studied in [60] [61] [62]. As in FFT-FBMC, the precoding stage is performed by means of IFFT and the filtering operation is applied with a polyphase network (PPN). Nevertheless, this precoding strategy results in a complex receiver scheme. In order to tackle this issue, BF-OFDM slightly increases the transmitter complexity in order to rely on a low-complex CP-OFDM like receiver through the insertion of a filter pre-distortion stage at the transmitter side [25]. Here, each data block of $N/2$ samples is pre-equalized before going to the IFFT precoding operation. The pre-equalizer coefficients depend on

the frequency response of the used prototype filter. Note that the BF-OFDM receiver is just a simple OFDM one (i.e., only a FFT is used).

4.4 Contributions to related MWF design

Despite the effectiveness of the previously mentioned MWF class to handle most of the 5G challenges, they are not suitable for low-latency communications and short packet transmission due to the long prototype filters (i.e., long ramp-up/down of MWF signal leads to a loss in spectral efficiency). In addition, the complexity of these filtered MWFs makes them not very attractive to 5G and beyond. Besides, time-domain windowing based CP-OFDM processing, can also be a useful tool to advance the 5G waveform development.

Therefore, we have been interested in investigating new MWFs based on advanced windowing techniques. In the framework of the WONG5 project, we first investigated a MWF based on new windowing approach, introduced recently and called Weighted Overlap and Add (WOLA) processing [63]. The studied low-complexity waveform WOLA-OFDM, which is presented in [C24], allows transparent design where transmitter (Tx) and receiver (Rx) units use independent waveform processing techniques, complying with the 3GPP agreement [27]. Then, a new MWF approach based on the WOLA processing and a circular convolution approach has been introduced via the supervision of the Post-doc of Dr. Yahia Medjahdi I co-supervised with Prof. Daniel Roviras. The proposed MWF called WOLA based circular offset quadrature amplitude modulation (WOLA-COQAM) [C26] has shown better performance than the classical windowed based MWFs confirming the capability of WOLA processing in supporting asynchronous multi-user access.

Through the collaboration with the WONG5's partners, THALES, CEA-Leti and CentraleSupelec, we have carried out, in [J09], an exhaustive analysis and objective comparison of these studied MWFs with several other 5G MWFs in order to identify the most suitable waveform configuration to any 5G use case according to its critical requirements. Our WOLA approach has been shown to be very effective in MWF design enabling flexible multiple access to fragmented spectrum with relaxed synchronicity.

In the following, I give an overview of the studied MWFs based on WOLA processing and a summary of its performance assessment and comparison.

4.4.1 WOLA-OFDM

Since a large part of OOB emission of CP-OFDM is caused by the discontinuity between adjacent OFDM symbols in time-domain, a natural and straightforward way to reduce these indiserable OOB emissions is to avoid the traditional usage of rectangular pulse shape. Then, windowing schemes to smooth the time-domain signal transitions seem promising approaches. Therefore, the WOLA-OFDM has gained a great interest along this line of study due to its low computational complexity. At the transmitter side, the time-domain WOLA-OFDM symbol is cyclically extended with cyclic prefix and cyclic suffix. Then, the smooth transition of the last samples of a given symbol and the first samples of the next symbol is provided by a time-domain windowing. Here, the Meyer root raised-cosine (RRC) [64] has been considered, which combines the RRC time-domain pulse with the Meyer auxiliary function. In order to have similar overhead as in CP-OFDM, to comply within standards, adjacent symbols are overlapped in the edge transition regions (see Figure 2 in [26]). Furthermore, WOLA-OFDM presents a spectral efficiency (SE) loss of W_{TX} samples, cyclic suffix length, per packet compared to CP-OFDM.

The WOLA-OFDM SE expressed in bit per second per Hertz is given by equation (4.5).

$$\begin{aligned}\eta_{\text{WOLA}} &= \frac{SN}{S(N+N_{\text{CP}})+W_{TX}}\eta \\ &\xrightarrow{S\to\infty} \frac{S}{N+N_{\text{CP}}},\end{aligned} \tag{4.5}$$

where S is the total number of transmitted symbols, η is the modulation efficiency (including both modulation order and coding rate) and N the number of active subcarriers. When S is large, the WOLA-OFDM SE tends to the one of CP-OFDM.

In addition to the transmit windowing, the WOLA processing, initially introduced by Qualcomm Incorporated [63], is applied to aid the suppression of asynchronous inter-user interference (i.e. adjacent non-orthogonal signals). It is performed through two steps: First, the receiver takes $N+2W_{RX}$ samples (W_{RX} denotes the window edge size), which correspond to the samples of one WOLA-OFDM symbol. Then, these samples are windowed. In the second step, the overlap and add processing (see Figure 3 in [26]) is applied to minimizes the windowing effects on the useful data, creating the useful N samples from the $N+2W_{Rx}$ ones.

It is worth emphasizing that the applied receive window is independent of the one applied at the transmitter, complying with the 3GPP agreement [25].

4.4.2 WOLA-COQAM

We have been interested in investigating the combination of the WOLA processing with a filtering approach. Such combination can be very promising to handle most of the 5G challenges previously mentioned. Here, we consider a subcarrier-wise filtering, due to its good frequency localization, together with a burst truncation in order to reduce the SE loss caused by long prototype filter, making the transmission suitable to low-latency communications. In addition, a circular convolution [20] [65] is adopted to maintain smooth transition at the burst edges while removing the overhead signal. Then, the circular-OQAM (COQAM) signal, defined in a block interval $m \in [0, KN-1]$, is expressed as,

$$\mathbf{x}_{\text{COQAM}}[m] = \sum_{n=0}^{N-1}\sum_{k=0}^{2K-1} \mathbf{a}_k[n]\,\tilde{g}(m-kN/2)\,e^{j\frac{2\pi}{N}n\left(m-\frac{D}{2}\right)}e^{j\phi_{n,k}}, \tag{4.6}$$

where, the filter $\tilde{g}$ stands for circular convolution (see Figure 1 in [15]) with the prototype filter g of length $KN = D+1$. More precisely, $\tilde{g}$ is obtained by the periodic repetition of duration KN of g [65], so that,

$$\tilde{g}(m) = g(mod[m, KN]) \tag{4.7}$$

Note that the prototype filter g is originally designed for FBMC-OQAM systems. This means that the input data symbols $\mathbf{a}_k[n]$ are real-valued, since the orthogonality only applies to the real field. The phase term $\phi_{n,k}$ at subcarrier n and symbol index k can be expressed as $\frac{\pi}{2}(n+k)$. It is introduced on both transmitter and receiver side, in order to make the intrinsic interference purely imaginary-valued thus orthogonal to the useful data which is real-valued. A CP is then added in order to avoid multi-path channel interference. Thanks to circular convolution, the continuity of CP-COQAM signal is maintained inside a given CP-COQAM block. Then, a windowing is needed to enhance the spectral containment by

smoothing the inter-block discontinuities. Finally, the WOLA processing, previously explained, is also applied to suppress inter-user interference resulting from the mismatched FFT capture window. It is worth to mention that the first window part $[0, 2W_{RX}]$ applied at the receiver must be symmetrical w.r.t the point $\left(W_{RX}, \frac{1}{2}\right)$, correctly recover the weighted data samples.

4.4.3 Summary of MWFs performance assessment and comparison

In this section, I provide a summary of the comparative performance study of the major MWF candidates for 5G and beyond. In addition to the MWFs described above (FBMC-OQAM, GFDM, UFMC, f-OFDM, FFT-FBMC, BF-OFDM, WOLA-OFDM and WOLA-COQAM), other promising MWFs, studied in literature, have been considered in this comparative study in order to give a complete and clear picture of the ongoing MWF discussions and put in perspectives the main advantages and drawbacks of these solutions. These MWFs are : filtered multi-tone (FMT) [18] and windowed cyclic prefix based circular-OQAM (WCP-COQAM) [65]. Note that CP-OFDM is kept as a MWF reference basis. I classify and compare all of these MWFs regarding a given system model and several KPIs, such as OOB emissions, robustness to time and frequency synchronization errors, transceiver complexity and end-to-end PHY latency.

The tradeoff between frequency localization and time localization should be well optimized in order to address different challenges future mobile access networks will have to face. Indeed, frequency localization is important to allow relaxed synchronization transmissions across adjacent subbands with better adjacent channel leakage performance. On the other hand, the time localization is critical for low latency applications where longer filter/window durations are not suitable for URLLC.

All filtered and windowed MWFs granted lower OOB emissions compared to CP-OFDM (see Figure 4.2). The subcarrier-wise filtering based MWFs, like FBMC-OQAM and FMT, provide the best frequency localization, especially in the far-end PSD, compared to the other MWF candidates. They provide the fastest spectrum decaying and only one subcarrier guard is necessary to achieve very low PSD levels, as depicted in Figure 4.3. Note that Lapped-OFDM has lower PSD performance than the aforementioned MWFs due to the shorter prototype filter ($K = 2$ instead of $K = 4$ in FBMC-OQAM). Although GFDM is based on subcarrier-wise filtering approach, it does not have excellent frequency localization due to the abrupt transition between GFDM blocks caused by the rectangular window shape in the time domain. WCP-COAM and WOLA-COQAM, despite the time-domain transition between signal blocks, provides better OOB emissions performance compared to GFDM thanks to the performed time-domain windowing. Furthermore, subband-wise filtered MWFs lead to a better time localization with the cost of increasing the OOB emissions compared to the subcarrier-wise filtered MWFs. BF-OFDM and FFT-FBMC provide very good spectral confinement thanks to the adopted filter-bank approach. The performance of UFMC and f-OFDM, where a filter is applied to a group of subcarriers, are very similar. We move now to low-complexity MWF based on time-domain windowing, the WOLA-OFDM, offers satisfactory OOB emissions performance (about 20dB compared to CP-OFDM), but its far-end PSD performance remains moderate.

Spectral efficiency[4], which is highly affected by the window/filter duration, the shape of the filter, and extra overheads, depends on wether short or long packet sizes. Indeed, well frequency-localized MWFs (FBMC-OQAM and FMT) provide the worst SE performance, in case of very short packet transmissions, due to the long prototype filters. However, this class of MWFs reduces the need for guard bands and

[4]SE analysis corresponding to the major 5G MWFs is given in [J09]

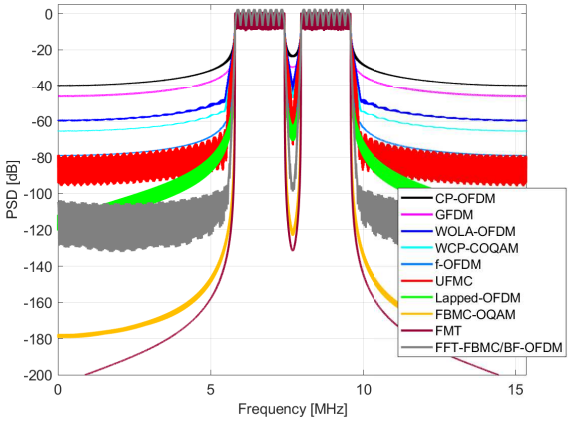

Figure 4.2: PSD comparison.

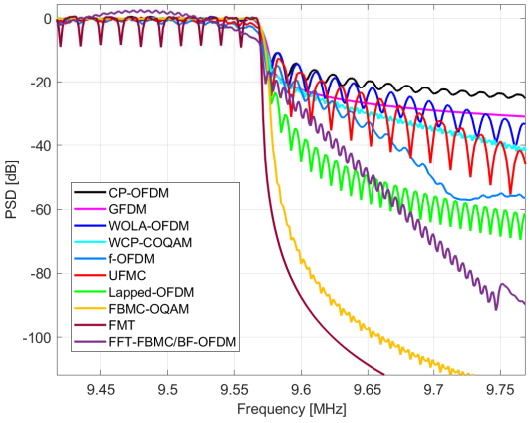

Figure 4.3: PSD edge comparison.

hence leading to a good occupation of the frequency band. Although the long prototype filters adopted by GFDM and WCP-COQAM, they offer better SE performance thanks to the circular convolution. It is worth empathizing that, in case of long packet transmissions (i.e., the filter impulse response length becomes negligible), all the studied MWFs provide almost the same SE performance.

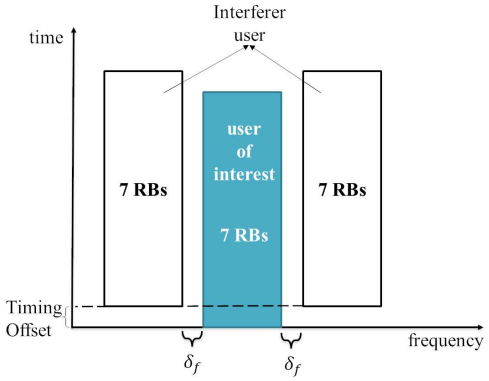

Figure 4.4: Asynchronous scenario.

MWFs using a GI/CP have higher latencies compared to other MWFs that do not consider adding a GI/CP, such as FBMC-OQAM, GFDM and FMT, when for long packet sizes. However, when packet sizes are very short, OFDM based MWFs (CP-OFDM, WOLA-OFDM, UFMC, f-OFDM) have the lowest latencies compared to the other MWFs that are affected by the filtering related ramp-up and ramp-down. On another hand, GI-less MWFs provide bad BER performance in multipath fading channel and complex receivers are required since the traditional FDE is not straightforward. Moreover, the MIMO deployment, which is a key technology for high throughput, is not feasible in MWFs like FBCM-OQAM and GFDM because of the non-orthogonality in complex domain.

In order to evaluate the capability of the studied MWFs to support asynchronous transmissions, we consider a scenario with two co-existing users sharing the available frequency as shown in Figure 4.4. The colored area and the non colored area correspond to time/frequency resources allocated to, respectively,

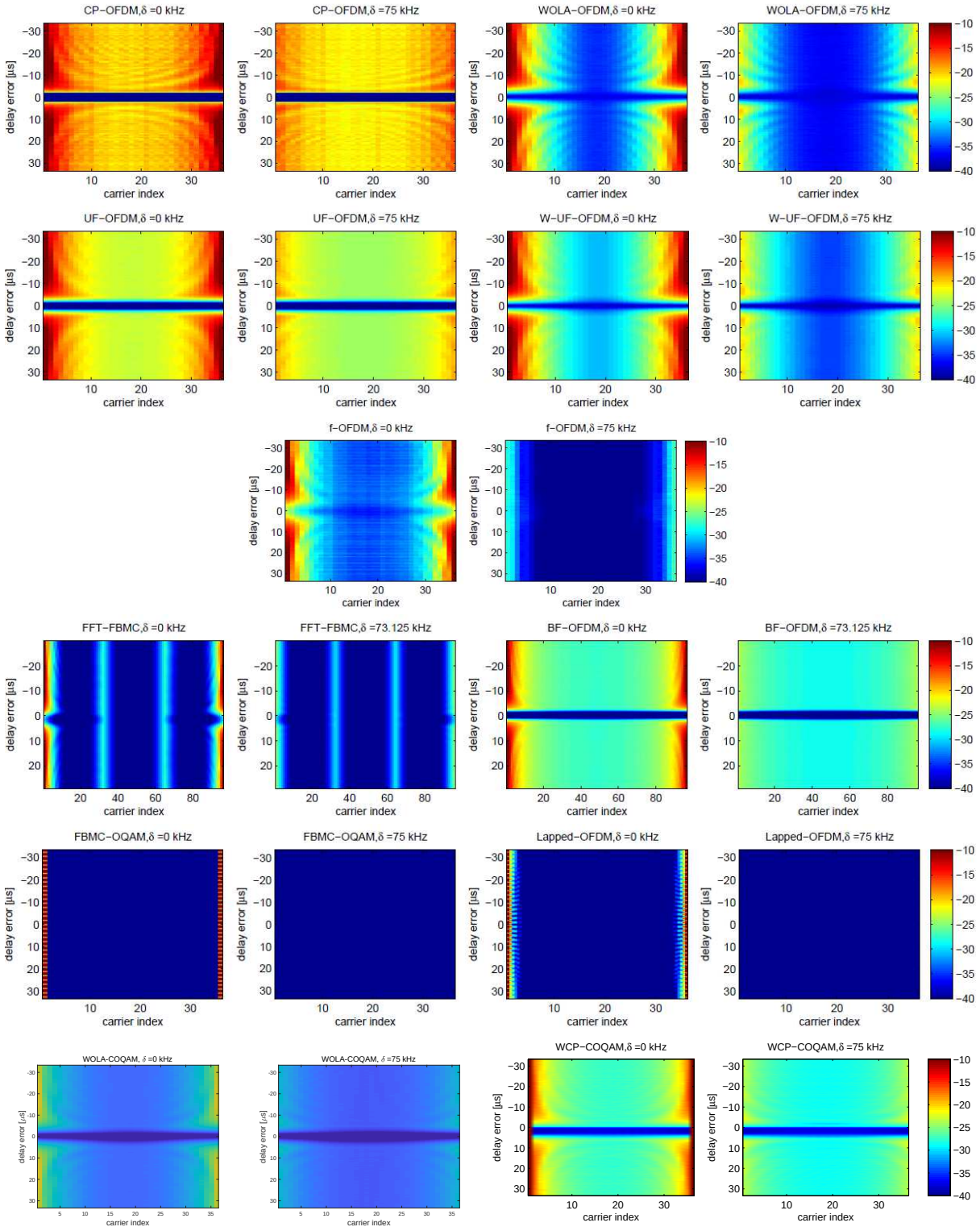

Figure 4.5: Per-subcarrier NMSE against TO.

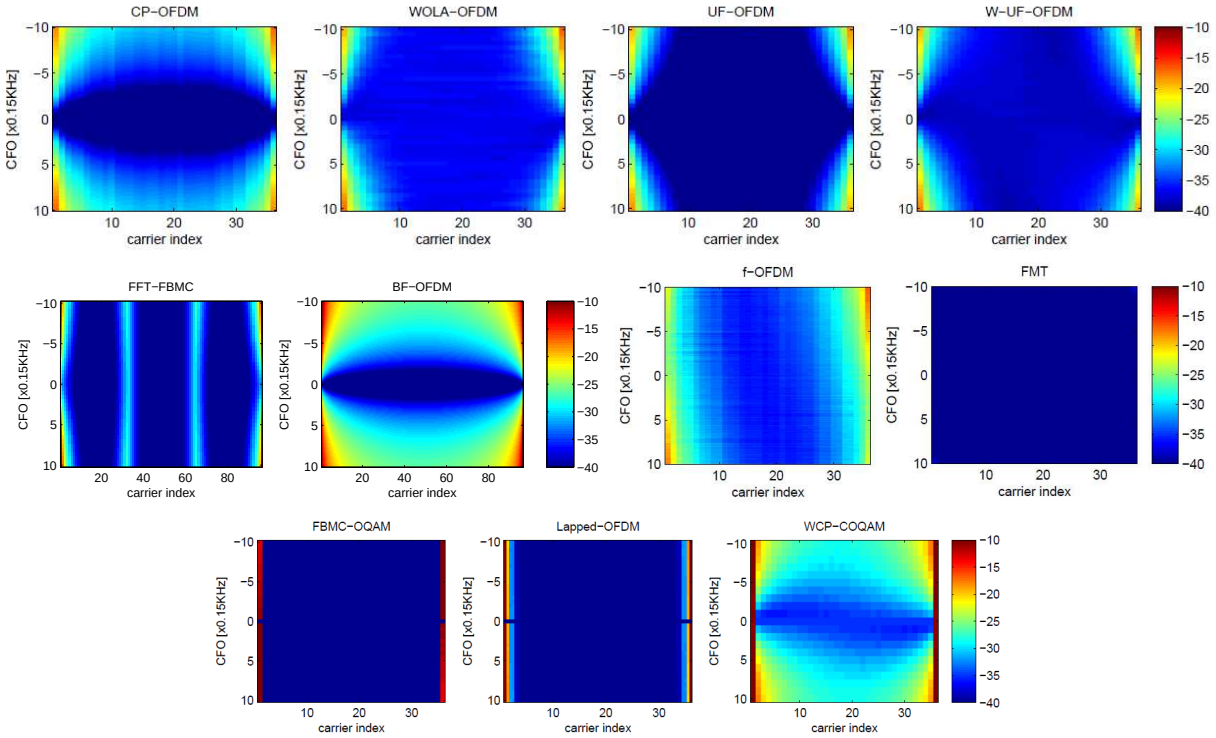

Figure 4.6: Per-subcarrier NMSE against CFO.

the user of interest (UOI) and interfering user. The UOI occupies 7 resource blocks (RBs) and there are 7 RBs for the interfering user on each side of the UOI. A guard-band, δ_f, between two users is separating the frequency bands of both users and a timing offset (delay error [μs]) is given to create asynchronism.

According to the results illustrated in Figures 4.5 and 4.6, one can note that well frequency-localized MWFs are robust against carrier frequency offset (CFO) and timing offset (TO) that reduce ICI and adjacent channel interference (ACI) in a multiple access environment. FBMC-OQAM and FMT, which have the best spectral localized transmit/receive filters, provide the best performance. Moreover, FFT-FBMC, f-OFDM and WOLA-OFDM can provide satisfactory performance compared to the classical CP-OFDM. Finally, BF-OFDM performs worse due to the fact that it uses a basic OFDM receiver. Note that adding the WOLA processing at the receiver side with the BF-OFDM transmitter would provide excellent performance making them very attractive for 5G and beyond.

Finally, when coming to the complexity[5], WOLA-OFDM provides the lowest level, it is almost the same as CP-OFDM. However, the computational complexity required by UFMC is excessively high about 200 times the CP-OFDM/WOLA-OFDM complexity. The other MWFs have tolerable computational complexity, compared to the CP-OFDM/WOLA-OFDM, it is approximately 2 times for BF-OFDM and FFT-FBMC, 3 times for FBMC-OQAM and 9 times for GFDM. A summary of the main advantages/disadvantages of these major MWF candidates is provided in Table 4.1.

[5]Complexity analysis corresponding to the major 5G MWFs is given in [J09]

Table 4.1: The major 5G MWF candidates

MWF	Design features	Advantages	Disadvantages
CP-OFDM	no filtering/windowing, orthogonality in complex domain	Simple FDE, Easy MIMO integration, Flexible frequency assignment, Low implementation complexity	High OOB emission, Sensitive to asynchronous transmissions, high power consumption
WOLA-OFDM	Tx/Rx windowing, orthogonality in complex domain	All advantages of CP-OFDM, Lower OOB emissions compared to CP-OFDM, Good robustness against TO and CFO	High power consumption
UFMC	RB Tx filtering, orthogonality in complex domain	Good frequency localization, Shorter filter length compared to subcarrier-wise operations (i.e., FBMC-OQAM and GFDM), Feasible MIMO integration	No immunity to ISI due to lack of CP, Higher receiver complexity due to increased FFT size
f-OFDM	SB Tx/Rx filtering, orthogonality in complex domain	Flexible filtering granularity, Better frequency localization, Shorter filter length compared to subcarrier-wise operations (i.e., FBMC-OQAM and GFDM), Compatible with MIMO	Very high implementation complexity, High latency for long bursts
FFT-FBMC	RB Tx/Rx filtering, orthogonality in complex domain	Very good frequency localization, Good robustness against TO and CFO, Lower implementation complexity (compared to FBMC-OQAM, GFDM and f-OFDM), Compatible with MIMO	Higher complexity implementation than CP-OFDM/WOLA-OFDM
BF-OFDM	RB Tx filtering, orthogonality in complex domain	Very good frequency localization, Good robustness against TO and CFO, Lower implementation complexity (compared to FBMC-OQAM, GFDM and f-OFDM), Receiver-like OFDM, Compatible with MIMO	Lower robustness against TO and CFO than FFT-FBMC and WOLA-OFDM
WCP-COQAM	SC Tx/Rx filtering, orthogonality in real domain	Flexible design, Low latency for long bursts, Good immunity to ISI due to circular convolution	Higher latency for short bursts, Challenging MIMO integration and pilot design, Higher implementation complexity than CP-OFDM
WOLA-COQAM	SC Tx/Rx filtering, Rx windowing, orthogonality in real domain	All advantages of WCP-COQAM, Good robustness against TO and CFO	Higher latency for short bursts, Challenging MIMO integration and pilot design, High implementation complexity
FBMC-OQAM	SC Tx/Rx filtering, orthogonality in real domain	Best frequency localization (i.e., lowest OOB emissions), Good spectral efficiency (no guard band or CP), Robust against Doppler effect, Suitable for asynchronous transmission	MIMO integration and pilot design are not straightforward, No immunity to ISI due to lack of CP, High implementation complexity
GFDM	SC Tx/Rx filtering, no orthogonality	Flexible design, Low latency for long bursts, Reduced PAPR (depending on the block size)	Higher latency for short bursts, MIMO integration and pilot design are not straightforward,High implementation complexity

4.5 Contributions to related equalization for FBMC-OQAM

As explained above, FBMC-OQAM is shown to offer the best spectral localization among all the post-OFDM MWFs, thanks to the adopted filter-bank approach, providing then the best performance in supporting asynchronous and mixed numerologies transmissions. Besides, it offers high spectrum efficiency since it avoids the use of CP and large guard bands. Furthermore, the orthogonality in real domain is guaranteed thanks to the use of the OQAM modulation. Consequently, it is sensitive to ISI and then it does not fulfil the robustness requirements when a frequency selective channel is considered. To overcome this problem, via the Hayfa Fhima's PhD, I co-supervised with Prof. Daniel Roviras, we had been interested in studying advanced equalization schemes to handle this FBMC-OQAM's issue.

One can remark that FBMC-OQAM is based on a non second order circular (NSOC) modulation [66]

and its signal is a cyclo-stationary one [67, 68]. Then, an application of widely linear (WL) [69] and FREquency SHift (FRESH) [70–72] processing makes a lot of sense. Indeed, these latter have been shown to enhance the performance of the traditional linear equalizers. In this regard, we have studied three different MMSE equalizer schemes, referred to as linear (LE), widely linear (WLE) and widely linear FRESH (WL FRESH) equalizers. For the developed equalizers, both symbol spaced (SSE) and fractionally spaced (FSE) processing have been evaluated, in synchronous DL/UL and asynchronous UL scenarios, with mixed numerologies transmissions.

In the following, I give a brief description of the studied equalizers as well as their expressions followed by their performance comparison. In order to assess their performance, we consider a system with two users using the same kind of modulation, either rectilinear (R) or quasi-rectilinear (QR) while using different numerologies. Let us recall that R modulations correspond to mono-dimensional modulations such as M-pulse amplitude modulation (M-PAM), whereas QR modulations are complex modulations corresponding, after a simple de-rotation operation, to a complex filtering of a R modulation [67].

4.5.1 Basics of LE, WLE and WL FRESH equalizers

Since the LE [73], [74], [75], uses only the information carried by the autocorrelation matrix of the received signal $y_p(l)$, it results in a vector $\mathbf{w}_{LE} \in \mathbb{C}^{1\times L_e}$ (L_e is the equalizer length) which is given by

$$\mathbf{w}_{LE} = \mathbf{r}_{x_e\mathbf{y}_p}\mathbf{R}^{-\mathbf{1}}_{\mathbf{y_p}}, \tag{4.8}$$

where $\mathbf{r}_{x_e\mathbf{y}_p} = \mathbb{E}[x_e(n)\mathbf{y}_p^H(l)]$, which has a dimension of $1 \times L_e$, is the inter-correlation vector between the transmit sample $x_e(n)$ and the equalizer input; and $\mathbf{R}_{\mathbf{y_p}} = \mathbb{E}[\mathbf{y_p}(l)\mathbf{y}_p^H(l)] \in \mathbb{C}^{L_e\times L_e}$ denotes the auto-correlation matrix.

In WLE [76], [74], [77], we exploit the information carried by both the auto-correlation and pseudo-autocorrelation matrices. Indeed, in the case of an improper modulation, it has been shown that the pseudo-autocorrelation matrix contains energy. Therefore, taking into consideration the pseudo-autocorrelation matrix in the design of the equalizer would result in better performance [66] than the classical LE. Then, the WLE vector, $\tilde{\mathbf{w}}_{WL} \in \mathbb{C}^{1\times 2L_e}$, can be given by

$$\tilde{\mathbf{w}}_{WL} = \mathbf{r}_{x_e\tilde{\mathbf{y}}_p}\mathbf{R}^{-\mathbf{1}}_{\tilde{\mathbf{y}}_\mathbf{p}}, \tag{4.9}$$

where the inter-correlation vector $\mathbf{r}_{x_e\tilde{\mathbf{y}}_p} \in \mathbb{C}^{1\times 2L_e}$ uses the equalizer input in its widely linear version (i,e, $\tilde{\mathbf{y}}_p(l) = [\mathbf{y}_p^T(l), \mathbf{y}_p^*(l)]^T$). Besides, $\mathbf{R}_{\tilde{\mathbf{y}}_\mathbf{p}} \in \mathbb{C}^{2L_e\times 2L_e}$ is the new auto-correlation matrix considering the WL signal $\tilde{\mathbf{y}}_p(l)$. This matrix can be represented by

$$\mathbf{R}_{\tilde{\mathbf{y}}_\mathbf{p}} = \mathbb{E}[\tilde{\mathbf{y}}_p(l)\tilde{\mathbf{y}}_p^H(l)] = \begin{bmatrix} \mathbf{R}_{\mathbf{y_p}} & \mathbf{C}_{\mathbf{y_p}} \\ \mathbf{C}^*_{\mathbf{y_p}} & \mathbf{R}^*_{\mathbf{y_p}} \end{bmatrix}, \tag{4.10}$$

where $\mathbf{C}_{\mathbf{y_p}} = \mathbb{E}[\mathbf{y_p}(l)\mathbf{y_p^T}(l)]$ represents the pseudo-autocorrelation matrix ($\in \mathbb{C}^{L_e\times L_e}$) of the signal $\mathbf{y}_p$.

When coming to WL FRESH equalizer, it exploits the cyclo-stationarity properties of rectilinear and quasi-rectilinear signals (i.e., the correlation between the spectral components of the signal) [67, 68, 70, 71]. It means that the auto-correlation and the pseudo-autocorrelation matrices of the received signal, called $\mathbf{R}_I(t,\tau)$ and $\mathbf{C}_I(t,\tau)$, are periodic in time [71]. Hence, they can be represented as Fourier series

expansions, given as follows [78]

$$\mathbf{R}_I(t,\tau) = \sum_{\alpha_i} \mathbf{R}_I^{\alpha_i}(\tau) e^{j2\pi\alpha_i t} \tag{4.11}$$

$$\mathbf{C}_I(t,\tau) = \sum_{\beta_i} \mathbf{C}_I^{\beta_i}(\tau) e^{j2\pi\beta_i t}. \tag{4.12}$$

Here, $\mathbf{R}_I^{\alpha_i}(\tau)$ and $\mathbf{C}_I^{\beta_i}(\tau)$ are defined, respectively, as the non-conjugate and conjugate cyclic correlation functions. Likewise, α_i and β_i are called the Second Order (SO) non conjugate and conjugate cyclic frequencies of the signal, which are given by

$$\begin{cases} \alpha_i = \dfrac{i}{T_1} & \text{for } i \in \mathbb{Z} \\ \beta_i = \pm 2\delta_f + \dfrac{i}{T_1} & \text{for } i \in \mathbb{Z}, \end{cases}$$

where δ_f stands for the guard band between the user of non interest (UNOI) and the user of interest (UOI) and T_1 is the symbol duration corresponding to UNOI.

For the sake of simplicity and without loss of generality, we consider only one set of couple of cyclic frequencies $(\pm\alpha_1, \pm\beta_1)$, where the greater amount of energy is located. Therefore, the corresponding WL FRESH equalizer is depicted by Figure 4.8 where observation vector is $\tilde{\mathbf{z}}_p(l) = [\mathbf{z}_1^T(l), \mathbf{z}_2^T(l), \mathbf{z}_3^T(l), \mathbf{z}_4^T(l), \mathbf{z}_5^T(l), \mathbf{z}_6^T(l)]^T$, where $\mathbf{z}_i(l) = [z_i(lT_0), z_i(lT_0 - T_e), ..., z_i(lT_0 - (L_e - 1)T_e)]^T$, for $i = 1, .., 6$.
$z_i(l), i \in \{1, 3\}$ are the frequency shifted versions of the received signal $y_p(l)$; this shift is done via the use of the cyclic frequencies $+\alpha_1, 0$ and $-\alpha_1$, respectively. Likewise, $z_i(l), i \in \{4, 6\}$ represents the frequency shifted version of the received signal complex conjugate $\mathbf{y}_p^*(l)$ and that is done by the use of the following conjugate cyclic frequencies $+\beta_1, 0$ and $-\beta_1$. Therefore, the studied WL FRESH equalizer is given by

$$\tilde{\mathbf{w}}_{\mathbf{WLFresh}} = \mathbf{r}_{x_e \tilde{\mathbf{z}}_\mathbf{p}} \mathbf{R}_{\tilde{\mathbf{z}}_\mathbf{p}}^{-1}, \tag{4.13}$$

where $\mathbf{r}_{x_e \tilde{\mathbf{z}}_\mathbf{p}} \in \mathbb{C}^{1 \times 6L_e}$ is the inter-correlation vector corresponding to the Fresh version of the equalizer input (i.e., $\tilde{\mathbf{z}}_\mathbf{p}(l)$). Besides, $\mathbf{R}_{\tilde{\mathbf{z}}_\mathbf{p}} = \mathbb{E}[\tilde{\mathbf{z}}_\mathbf{p}(l) \tilde{\mathbf{z}}_\mathbf{p}^\mathbf{H}(l)]$ is a matrix $\in \mathbb{C}^{6L_e \times 6L_e}$, and it is defined as the auto-correlation matrix of the signal $\tilde{\mathbf{z}}_\mathbf{p}(l)$.

4.5.2 Application to rectilinear signal case

In order to clearly show the performance of the studied equalization schemes, we started first by using M-PAM modulation, representing a class of rectilinear modulations. Here, we consider two users, UOI and an interferer user (UNOI) sharing the same frequency band with a guard band of δ_f. The UNOI's symbol duration is twice the UOI one (i.e., $T_1 = 2T_0$). Also, the pulse shaping filters of the two users (UOI and UNOI) are chosen to be rectangular ones.

Figure 4.7 shows the performance of the different equalizers, i.e., LE, WLE and WL FRESH, in terms of guard-band values. Results are obtained for frequency selective channel whose coefficients are chosen randomly and kept constant during the transmission of 10^4 symbols and $\frac{E_b}{N_0} = 20$ dB. For the Fresh equalizer the SO non conjugate and conjugate cyclic frequencies are chosen to be $\alpha_1 = \frac{1}{T_1}$ and $\beta_1 = 2\delta_f + \frac{1}{T_1}$. As expected [69] [73], we note, from results depicted in Figure 4.7, that the LE has the worst performance compared to WLE and WL FRESH. Furthermore, the WL FRESH equalizer outperforms the WLE because of the cyclo-stationarity characteristic of the transmitted signals. In addition, interesting

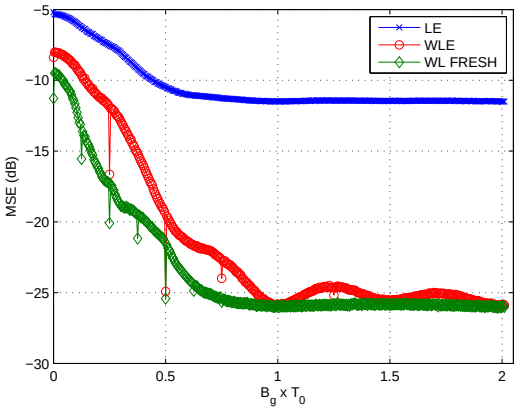

Figure 4.7: MSE Performance system with respect to GB (δ_f) in SSE mode: the UNOI symbol duration is twice the UOI one ($T_1 = 2T_0$).

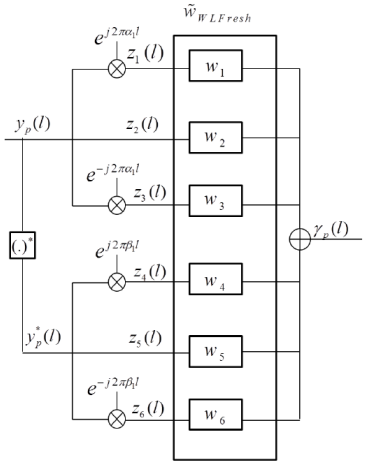

Figure 4.8: Widely linear Fresh equalization scheme.

and new finding compared to the existing literature can be highlighted. There are notches in the WLE curve when $\delta_f = \dfrac{i}{4T_0}$ in which the WLE performance increases. This can be explained by the fact that rectilinear SO cyclic frequencies are $\alpha_i = \dfrac{i}{T_1}$ and $\beta_i = \pm 2\delta_f + \dfrac{i}{T_1}$ and since the WLE exploits the energy contained at the null conjugate frequency; i.e., $\beta_i = 2\delta_f + \dfrac{i}{T_1} = 0 \Leftrightarrow \delta_f = \dfrac{i}{2\,T_1}$. As $T_1 = 2T_0$, then it performs better when $\delta_f = \dfrac{i}{4\,T_0}$.

We move now to the WL Fresh equalizer where another interesting and new remark can be added. The WL FRESH equalizer has also notches when $\delta_f = \frac{i}{8T_0} = \frac{i}{4T_1}$. This can be explained in the same manner as previously. Indeed, as the most energetic conjugate SO cyclic frequencies are equal to $\beta_i = \pm 2\,\delta_f + \frac{i}{T_1}$, after frequency shifting equal to $\pm\beta_1$, the most energetic conjugate cyclic frequencies become located at frequencies $\beta_i \pm \beta_1 = \pm 4\delta_f + \frac{i}{T_1}$ which are null for $\delta_f = \dfrac{i}{4\,T_1} = \dfrac{i}{8\,T_0}$.

4.5.3 Application to FBMC-OQAM

We consider a FBMC system having two users (UOI and UNOI) with quasi-rectilinear (QR) modulation of type OQAM, with two different numerologies. The system with Numerology 1 is considered as the UOI and it has $M_1 = 64$ sub-carriers, whereas the second system (UNOI) with the second numerology has twice the number of UOI's sub-carriers, meaning $M_2 = 2 \times M_1 = 128$. Δt is the time shift between the two user signals, describing the asynchronism between the UNOI and UOI. δ_f denotes the guard band between the two users. The modulation is chosen to be 64−OQAM.

Down-Link "DL" case

In this case, we consider that the BS serves simultaneously the two users (i.e., $\Delta t = 0$). We activate only 5 SCs for the UOI (using numerology 1) and 8 SCs for the UNOI (using numerology 2). The δ_f is chosen to be equal to the one UOI sub-carrier spacing ($\delta_f = \dfrac{F_e}{M_1}$). Since only the UOI subcarriers in the edge of the band are affected, we study the performance of the different equalizers in rejecting the interference caused by the UNOI. The BER performance of the studied equalizers in symbol spaced mode (SSE) mode

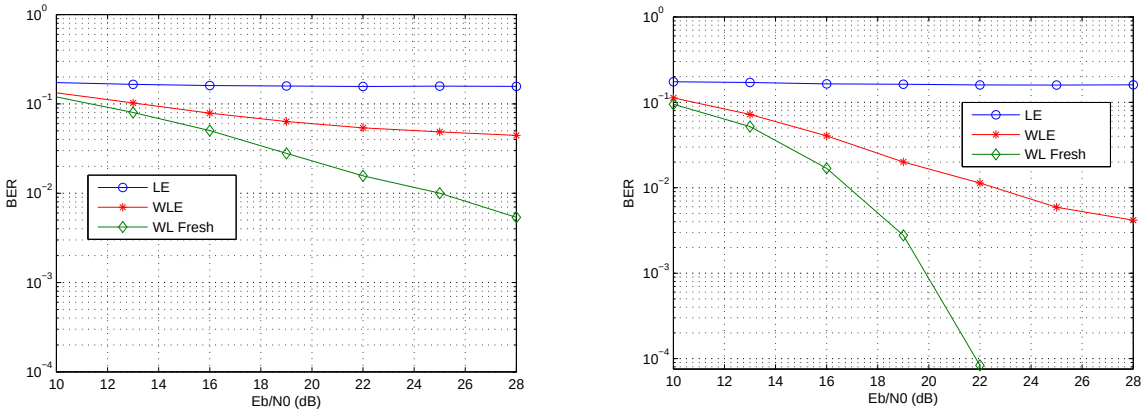

(a) $P = 1$ (b) $P = 8$

Figure 4.9: BER performance over a frequency selective channel with 8 taps.

as well as in fractionally spaced (FSE) mode are presented in Figures. 4.9.a and 4.9.b, respectively. We note from these results that the WL FRESH equalizer outperforms both the LE and WLE whereas the worst behavior is provided by the LE. This is true for both SSE and FSE cases. When the number of samples per symbol, P, increases, the WLE and WL Fresh equalizer performances increase, and the WL Fresh gives always the best performance.

Up-Link "UL" case

In this case, users (UOI and UNOI) can communicate asynchronously with the BS (i.e., Δt can be different from 0). Figures 4.10.(a) and 4.11.(a) show the performance of the classical LE for each active UOI's sub-carrier in the synchronous ($\Delta t = 0$) and asynchronous ($\Delta t = \frac{T_1}{2}$) cases, respectively. In the same way, Figures 4.10.(b) and 4.11.(b) represent the behavior of the WLE while the behavior of the WL FRESH equalizer is given in Figures 4.10.(c) and 4.11.(c).

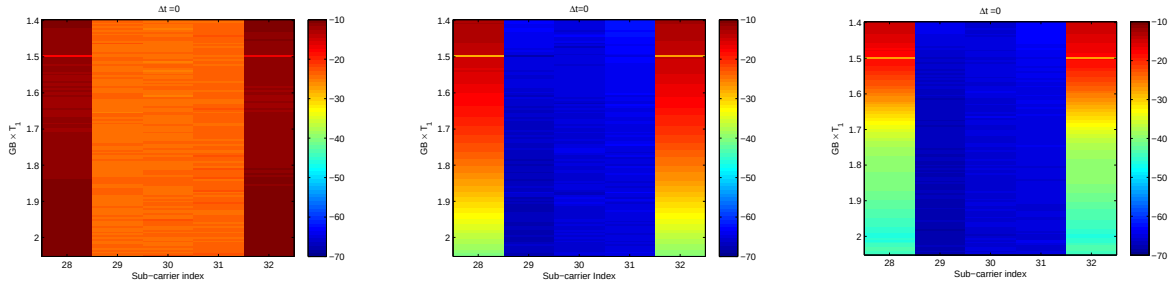

(a) LE (b) WLE (c) WL Fresh

Figure 4.10: Equalizers performances in term of MSE when UOI and UNOI are synchronous.

From these results, we can deduce that for all equalizer cases, only the SCs in the edge are affected by the interferer, in contrast to the SCs in the middle of the band. This remark remains true independently to the δ_f and asynchronism time range. Moreover, one can note that 1) LE has the worst performance either in synchronous or asynchronous case, even for SCs in the middle of the UOI's band, 2) WLE and WL-FRESH provide excellent performance for SCs in the middle of the UOI's band regardless of the δ_f and asynchronicity, 3) WLE and WL-FRESH offer better performance for the SCs at the edge

of the UOI's band, where a slight gain for WL-Fresh, 4) With WLE and WL-FRESH, the performance corresponding to SCs at the edge are not sensitive to asynchronicity, thanks to the excellent frequency localisation of FBMC-OQAM.

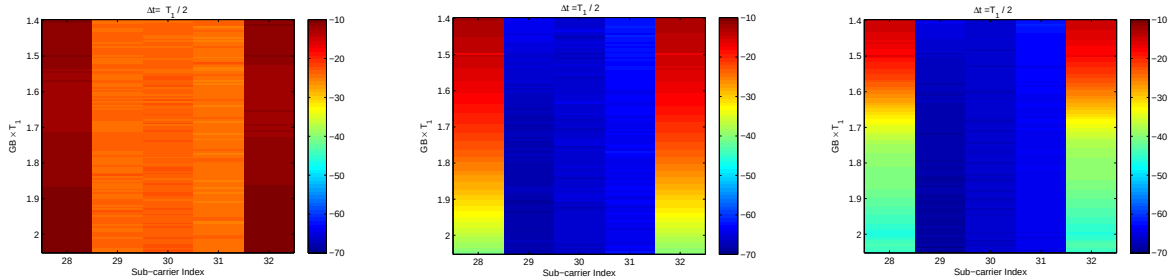

(a) LE (b) WLE (c) WL Fresh

Figure 4.11: Equalizers performances in term of MSE when UNOI is asynchronous with half an UNOI symbol period

4.6 Outputs

The combined outputs of the work on 5G MWFs described in Section 5.5 (MWF design based on the WOLA processing) and in Section 5.6 (channel equalization related to FBMC-OQAM) are resumed bellow.

Supervision and collaborations related to 5G MWFs

- 33% co-supervised postdoc (**Dr. Yahia Medjahdi**)
- 40% co-supervised PhD (**Dr. Hayfa Fhima**)
- Visiting researcher CEDRIC/CNAM, May-Sep. 2016 and Feb.-Apr. 2016
- Supported by ANR WONG5 project
- Collaboration with Prof. Yves Louet (CentraleSupelec, France), Dr. Jean-Baptiste Doré (CEA-Leti, France), Dr. Sylvain Traverso (THALES, France), Bruno Sens Chang (LabSC, FUT, Brazil)

Publications related to 5G MWFs

- 2 peer-reviewed journals **[J19, J09]**
- 9 peer-reviewed international conferences **[C40, C37, C36, C34, C30, C26, C25, C24]**

We also mention the joint work with Prof. Siala and Prof. Abdelkafi (Mediatron, Sup'Com, Tunisia) published in [C35], which is not detailed here. Even though this work falls into the design of MWFs, we addressed the problem of the optimization and adaption of waveforms, it will discussed in the perspectives.

Chapter 5

NLD characterization and mitigation techniques for energy-efficient 5G MWFs

5.1 Introduction

As explained in the previous chapter, all the MWFs suffer from the high PAPR making them very sensitive to power amplifier (PA) nonlinear distortion (NLD). Indeed, the PA, which has to be low-cost, low-size and energy-efficient, causes in-band and out-of-band distortions, damaging the good qualities of the advanced MWFs, in particular frequency localization. It is then primordial to study the performance of the aforementioned MWFs in presence of nonlinear PA. Therefore, as a first contribution, we have introduced theoretical study of the impact of nonlinear PA on the performance of the MWFs. Specifically, we have introduced analytical expressions of the MWF BER/SER via a theoretical characterization of the PA NLD. Furthermore, we have shown that OQAM signaling based MWFs, like FBMC-OQAM, are more sensitive to phase error than the ones that adopt QAM signaling. A summary of this contribution is given in Sections 6.2 and 6.3. These contributions are performed in part in the framework of the FP7 EMPHATIC project and in another part via the supervision of Mrs Hanen Bouhadda's PhD, in the framework the PHC-Utique C3 project.

In order to tackle the PA NLD's issues and enhance the energy-efficiency of the studied MWFs, we have been interested in investigating new digital signal processing solutions based on PAPR reduction and DPD techniques, which are more adequate to new MWFs than the classical ones studied for OFDM. Since filtered MWFs have different signal structure (i.e., overlapping signal structure), a direct application of traditional techniques cannot be effective and new schemes are desirable. Section 6.4 and 5.5 synthesis the developed works related to DPD and PAPR reduction, respectively. These contributions are performed via the supervision of the PhDs of Mrs Hanen Bouhadda ans Mrs Mounira Laabidi.

Moreover, a new joint optimization approach of PAPR reduction and DPD is presented in Section 5.6, showing better performance than the classical combination scheme. Section 6.5 details an experimental testbed conceived for studying the capability of the most promising MWFs to accommodate 5G requirements. A great emphasis is put on the MWF energy-efficiency enhancement using the studied PAPR reduction and DPD techniques. These two latter contributions were performed in the framework of the ANR WONG5 project and via the supervision of three Master students (Miss Yasmine Ben Afia, Miss

Xinying Cheng and Miss Xtina Fu). Finally, the outputs of these contributions are resumed in Section 7.4.

5.2 Sensitivity of (OQAM or QAM)-based OFDM systems to phase estimation error

In OQAM based OFDM systems, like FBMC-OQAM, the subcarrier orthogonality is satisfied only in the real domain. Specifically, each subcarrier is modulated in OQAM where the real and imaginary values are time staggered by half a symbol duration [17]. In such system, emitted data is real (real or imaginary part of the complex symbols) and an imaginary intrinsic-interference occurs in the transmission process. This interference, which is caused by the data symbols transmitted in the neighborhood area in the time-frequency domain, is imaginary and orthogonal to the useful real emitted data. Then, the detection process is easily performed when the channel is flat fading or slowly selective [79]. Contrary to classical OFDM systems, the performance of FBMC-OQAM is more sensitive to phase error which can be occurred by the amplification of the transmitted signal using nonlinear PA or by channel estimation error. Thus, we have been interested in providing an universal theoretical analysis for the impact of phase error on the BER performance of MWFs based on either QAM or OQAM processing. In particular, we have derived the exact BER of M-OQAM/QAM by considering the Gaussian intrinsic-interference approximation. These BER expressions can be evaluated without any numerical integration method.

The received data at subcarrier n_0 and instant m_0, is expressed, in OFDM case, by

$$r_{m_0,n_0} = h_{m_0,n_0}(a^I_{m_0,n_0} + ja^Q_{m_0,n_0}) + w_{m_0,n_0}, \tag{5.1}$$

where $a^I_{m_0,n_0}$ and $a^Q_{m_0,n_0}$ denote, respectively, the in-phase and the quadrature components of the transmitted complex symbol, w_{m_0,n_0} is the Gaussian noise term with variance σ^2_w and $h_{m_0,n_0} = \alpha e^{j\theta}$ is the complex channel coefficient, which is assumed to be slow-varying Rayleigh flat-fading, where the amplitude α follows the Rayleigh probability density function with an average fading power $\nu = \mathbb{E}[\alpha]$.

While in FBMC-OQAM case, it is expressed by

$$r_{m_0,n_0} = h_{m_0,n_0}(a_{m_0,n_0} + ju_{m_0,n_0}) + w_{m_0,n_0}, \tag{5.2}$$

where a_{m_0,n_0} and u_{m_0,n_0} denote, respectively, the real-valued transmitted data and the intrinsic-interference.

Given a channel estimate $\widehat{h} = \widehat{\alpha}e^{j\widehat{\theta}}$, where the phase estimate error $\psi = \theta - \widehat{\theta}$ and assuming a perfect amplitude estimation $\widehat{\alpha} = \alpha$, because this latter represents the same contribution as in the classical OFDM. Then, the in-phase ($a^I_{m_0,n_0}$) and quadrature ($a^Q_{m_0,n_0}$) components or real-valued (a_{m_0,n_0}) data and intrinsic-interference (u_{m_0,n_0}) could interfere when, respectively, OFDM or FBMC-OQAM are considered. The input of the decision device, in OFDM case, is given by

$$r = (a^I cos(\psi) - a^Q sin(\psi)) + \frac{w}{\widehat{h}}. \tag{5.3}$$

While in FBMC-OQAM case, it is given by

$$r = (acos(\psi) - usin(\psi)) + \mathfrak{Re}\left\{\frac{w}{\widehat{h}}\right\}. \tag{5.4}$$

For concise expressions and without loss of generality, the subscript of subcarrier and time index are removed.

Lemma 1: the BER conditioned on α, u and ψ for M-QAM/OQAM (OFDM/FBMC) is given by

$$BER_{M-QAM}(\alpha,u,\psi)=\sum_{i=1}^{\xi}w_iQ\left(\frac{[a_icos(\psi)-\ddot{a}_iusin(\psi)+b_i]\,\alpha}{\sigma_w}\right) \tag{5.5}$$

where $\xi=\sum_{l=1}^{\frac{1}{2}\log_2(M)}2^{l-1}\frac{\sqrt{M}}{2}$, $\ddot{a}_i$ denotes the sign of a_i and the coefficients w_i, a_i and b_i are listed in [J08].

Proof: is given in paper [J08]

Note that, in OFDM case, $u\in\{-\sqrt{M}+1,-\sqrt{M}+2,...,-1,1,...,\sqrt{M}-2,\sqrt{M}-1\}$ while in FBMC-OQAM case, u denotes the intrinsic-interference issued from the transmultiplexer impulse response coefficients given by $\int_{-\infty}^{+\infty}f_{m,n}(t)g^*_{m_0,n_0}(t)$. Here, the synthesis function is given by $f_{mn}(t)=p_{tx}[t-nT/2]e^{j\frac{2\pi}{T}m(t-\frac{D}{2})}e^{j\varphi_{m,n}}$ where $\varphi_{m,n}=\pi/2(m+n)-\pi mn$ and the delay term $D=L-1$ depends on the length of the prototype filter $p_{tx}[t]$. According to [80], the prototype filter is designed such that the intrinsic-interference term is orthogonal to the useful data, i.e., ju_{m_0,n_0} is pure imaginary-valued. Let us call $\int_{-\infty}^{+\infty}f_{m,n}(t)f^*_{m_0,n_0}(t)$ as $\chi_{\Delta m,\Delta n}$ (where $\Delta m=m_0-m$ and $\Delta n=n_0-n$), which can be calculated assuming null data except the considered symbol (m_0,n_0) where a unit impulse is applied [79]. Then $\chi_{\Delta m,\Delta n}$ can be derived as

$$\chi_{\Delta m,\Delta n}=\int_{-\infty}^{+\infty}p_{tx}(t)p_{tx}(t-\Delta nT/2)\times e^{j\frac{2\pi}{T}\Delta p(\frac{D}{2}-m)}e^{j\pi(\Delta m+m_0)\Delta n}e^{-j\frac{\pi}{2}(\Delta m+\Delta n)}, \tag{5.6}$$

where $p_{tx}(t)$ is the prototype filter impulse response.

Since the most part of the energy of the impulse response is localized in a restricted set around the considered symbol (denoted by Ω_{m_0,n_0}), the intrinsic-interference ju_{m_0,n_0} can be expressed as

$$ju_{m_0,n_0}=\sum_{(m,n)\in\Omega_{m_0,n_0}}a_{m,n}\chi_{\Delta m,\Delta n} \tag{5.7}$$

The coefficients ju_{m_0,n_0} represent the sum of many independent and identically distributed random variables. They are depicted by Table I in [81] where the PHYDYAS prototype filter with overlapping factor set to $K=4$ is considered. Here, we note that the resulting interference term is a sum of at least twenty independent random variables where the distribution of each of these variables depends on the modulation order. Based on the central limit theorem, the probability distribution of the intrinsic-interference can be approximated by a zero-mean Gaussian random variable with a variance $\sigma_u^2=(\log_2(M)^2-1)/3$.

Theorem 1: The closed-form BER expression for an uncoded M-(QAM or OQAM) over Rayleigh fading channel is given by

$$BER^{rayleigh}_{M-OQAM}(\psi)=\frac{1}{8}\sum_{i=1}^{\xi}w_i\left[1-\frac{1}{\sqrt{\pi}}\sum_{j=1}^{\kappa}\beta_j\frac{a_i\cos\psi-\ddot{a}_i\sqrt{2\sigma_u^2}x_j\sin\psi+b_i}{\sqrt{(a_i\cos\psi-\ddot{a}_i\sqrt{2\sigma_u^2}x_j\sin\psi+b_i)^2+2\sigma_w^2}}\right] \tag{5.8}$$

where $\beta_j=(2^{\kappa-1}\kappa!\sqrt{\pi})/(\kappa^2\left[H_{\kappa-1}(x_j)\right]^2)$ and x_j are, respectively, the weights and zeros of the κ-order Gauss-Hermite polynomial ($H_\kappa(x)=(-1)^\kappa e^{x^2}\frac{d^\kappa}{dx^\kappa}e^{-x^2}$). The tables containing the values of β_j and x_j

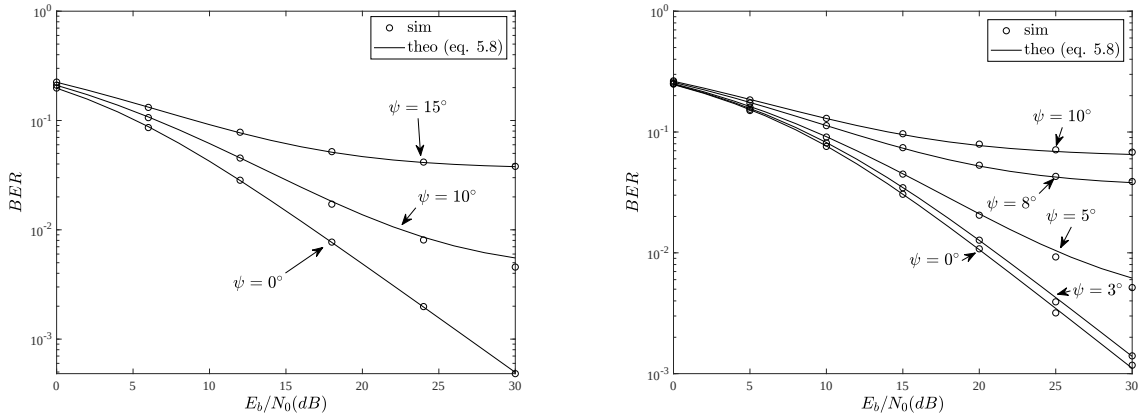

(a) 16-OQAM (b) 64-OQAM

Figure 5.1: BER performance of FBMC-OQAM in presence of phase offset, Rayleigh flat fading channel

can easily be found in literature ([82], Table (25.10), p. 924), or can be obtained numerically using numerical computation softwares, such as MATLAB.

Proof: See details of mathematical development in paper [J08].

Figures 5.1.a and 5.1.b provide the FBMC-OQAM BER performance with 16-OQAM and 64-QAM, respectively. We clearly observe a degradation of the BER performance when a phase rotation error occurs, showing that the effect of the intrinsic-interference is harmful even at low SNR. The analytical curves are obtained by using equation (5.8) and compared to the ones obtained by simulations. We observe from these figures a good agreement between both simulated and theoretical performance curves which are very close. It is worth to mention that the quadrature order of the Gauss-Hermite approximation in equations (5.8) was $\kappa = 20$. According to these results, one can note the effectiveness of the Gaussian intrinsic-interference approximation in the evaluation of FBMC-OQAM performance in presence of phase error and when a Rayleigh fading channel is considered.

5.3 PA NLD characterization and theoretical performance analysis for 5G MWFs

In order to derive a statistical characterization of the decision variables at the input of decision devices, we first describe the input and output signals of the nonlinear power amplifier. The MWF modulated symbol stream (given in equation (4.1)) has a complex envelop $x(t) = x^I(t) + jx^Q(t)$ that can be written, using the polar coordinates, as

$$x(t) = \rho(t)e^{j\phi(t)}, \tag{5.9}$$

where $\rho(t)$ and $\phi(t)$ are the modulus and phase of $x(t)$, respectively. As a general formulation, the amplified signal at the output of a memoryless nonlinear PA can be expressed as

$$\begin{aligned} z(t) &= \left[F_a(\rho(t))e^{jF_p(\rho(t))}\right] e^{j\phi(t)} \\ &= S(\rho(t))e^{j\phi(t)}, \end{aligned} \tag{5.10}$$

where $F_a(.)$ and $F_p(.)$ denote the AM/AM and AM/PM conversions, respectively, and

$$S(\rho(t)) = F_a(\rho(t)) \exp(jF_p(\rho(t))) \tag{5.11}$$

is the complex soft envelop of the amplified signal $z(t)$.

For any MWF signal, when the number of subcarriers, N, is sufficiently large, the input signal $x(t)$ is assumed to be a zero mean complex Gaussian random process. According to the Bussgang theorem [83], $z(t)$ can be written as

$$z(t) = K_0 x(t) + d(t), \tag{5.12}$$

where $d(t)$ is an additive zero-mean (non-Gaussian) noise having variance σ_d^2 and uncorrelated with $x(t)$ and K_0 is a constant complex gain.
According to [84], the NLD parameters K_0 and σ_d^2 can be computed theoretically as

$$K_0 = \frac{1}{2}\mathbb{E}\left[\frac{\partial S(\rho)}{\partial \rho} + \frac{S(\rho)}{\rho}\right] \tag{5.13}$$

and

$$\sigma_d^2 = \mathbb{E}(|d(t)|^2) = \mathbb{E}\left(|S(\rho)|^2\right) - |K|^2\,\mathbb{E}(\rho^2) \tag{5.14}$$

Note that the analytical computation of the NLD parameters, K_0 and σ_d^2, depends on the $S(\rho)$. In [84], only closed-form expressions for SEL model have been introduced, which are expressed as

$$K_0 = \left(1 - e^{-\frac{A_{sat}^2}{\sigma^2}}\right) + \frac{1}{2}\sqrt{\pi \frac{A_{sat}^2}{\sigma^2}} erfc\left(\sqrt{\frac{A_{sat}^2}{\sigma^2}}\right), \tag{5.15}$$

and

$$\sigma_d^2 = \sigma^2\left(1 - e^{-\frac{A_{sat}^2}{\sigma^2}} - K_0^2\right), \tag{5.16}$$

where σ^2 denotes the input signal power and A_{sat} is the saturation amplitude at the output of the SEL model. Nevertheless, for more complicated expressions of $S(\rho)$ (e.g., SSPA and TWTA models) or measured PA, the derivation of closed-form expressions for the NLD parameters is not straightforward and no such expressions have been introduced in literature. Therefore, via the supervision of Mrs Hanen's PhD, we investigated a new approach, based on polynomial approximation of the PA characteristics, that allows an universal derivation of K_0 and σ_d^2 for any modeled or measured PA. This work was supported by the PHC-Utique C3 project.

The proposed approach aims at approximating the complex soft envelop $S(\rho)$ of the amplified signal by using a polynomial model with odd and even coefficients, which can be written as

$$\begin{aligned} z(t) &= \sum_{l=1}^{L} a_l x(t)|x(t)|^{l-1} \\ &= e^{j\phi}\sum_{l=1}^{L} a_l \rho^l, \end{aligned} \tag{5.17}$$

where the new expression of $S(\rho)$ can be given by $\sum_{l=1}^{L} a_l \rho^l$.

The above theoretical expressions of K_0 and σ_d^2 (equations (5.15) and (5.16)) involve the computation of the expectation of ρ^l (l is a positive integer). This expectation is equivalent to calculate the l-th

derivation of the moment-generating function (MGF) [85].

Lemma 2: The NLD parameters K_0 and σ_d^2 can be given by

$$K_0 = a_1 + \sqrt{\frac{\pi}{8}} \sum_{l=2,leven}^{L} (l+1)a_l \sigma^{l-1} \prod_{i=0}^{\frac{l-2}{2}} (2i+1) + \frac{1}{2} \sum_{l=3,lodd}^{L} (l+1)a_l \left(\sqrt{2}\sigma\right)^{l-1} \left(\frac{l-1}{2}\right)! \tag{5.18}$$

and

$$\sigma_d^2 = \sum_{l=1}^{L} |a_l|^2 2^l \sigma^{2l} l! - 2|K_0|^2\sigma^2 + \sqrt{\frac{4\pi}{2}} \sum_{l,n=1,l\neq n,(l+n)odd}^{L} \mathrm{Re}[a_l a_n^*] \sigma^{l+n} \prod_{i=0}^{\frac{l+n-1}{2}} (2i+1)$$
$$+ 2 \sum_{l,n=1,l\neq n,(l+n)even}^{L} \mathrm{Re}[a_l a_n^*] \left(\sqrt{2}\sigma\right)^{l+n} (\frac{l+n}{2})! \tag{5.19}$$

Proof: is given in paper [J05]

It is worth to mention that K_0 and σ_d^2 are function of the standard deviation of the PA input signal σ that depends on the PA operating point (input back-off (IBO)) and can be written as $\sigma = \frac{A_{sat}}{\sqrt{10^{IBO/10}}}$. Considering that the nonlinearly amplified signal passes through a radio channel, the demodulated data at time instant m_0 and subcarrier n_0 is given by

$$r_{m_0,n_0} = K_0 h_{m_0,n_0}(a_{m_0,n_0} + ju_{m_0,n_0}) + h_{m_0,n_0} d_{m_0,n_0} + w_{m_0,n_0}, \tag{5.20}$$

where h_{m_0,n_0} indicates the channel coefficient corresponding to the subcarrier m_0 and instant n_0.

Remark 1: the instantaneous signal-to-noise ratio (SNR) after equalization remains the same for OFDM and FBMC-OQAM, as explained in [J07]. It can be expressed as

$$\gamma = \frac{|K_0|^2|h|^2\sigma^2}{|h|^2\sigma_d^2 + \sigma_w^2} \tag{5.21}$$

Note that, in case of FBMC-OQAM, $\sigma^2 = 2P_a$, P_a is the average power of the information-bearing real symbol a.

Lemma 3: With nonlinear PA, the closed-form BER expression of an uncoded M-(QAM or OQAM) based OFDM over AWGN channel ($h_{m_0,n_0} = 1$) is given by

$$BER_{AWGN} = \frac{2(\sqrt{M}-1)}{\sqrt{M}\log_2(M)} erfc\left(\sqrt{\frac{3\log_2(M)|K_0|^2\sigma^2}{(M-1)(\sigma_w^2+\sigma_d^2)}}\right) \tag{5.22}$$

Proof: is given in paper [J05].

Theorem 2: With nonlinear PA, the closed-form BER expression of an uncoded (QAM or OQAM based) OFDM over quasi-static frequency-flat Rayleigh channel is given by

$$BER_{Rayleigh} = a(1 - \frac{2}{\sqrt{\pi}} \sum_{n=0}^{+\infty} \sum_{k=0}^{+\infty} \frac{(-1)^{k+n}(\sqrt{b})^{2n+1}}{k!n!(2n+1)} (\frac{\sigma_w^2}{\nu})^{k+1} \frac{(\gamma_c)^{n+k+3/2}}{n+k+3/2}$$
$$ {}_2F_1(k+2, n+k+3/2; n+k+5/2; 1), \tag{5.23}$$

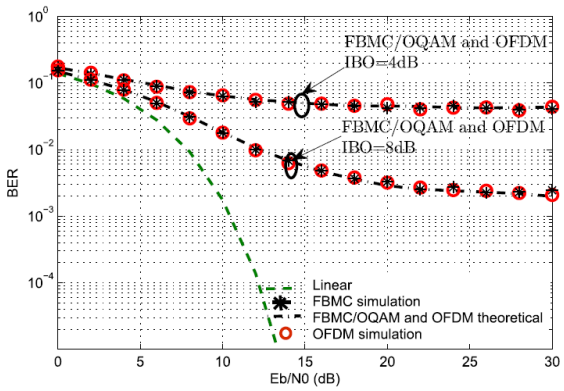

(a) AWGN channel,$M = 16$, $\phi_0 = \pi/6$.

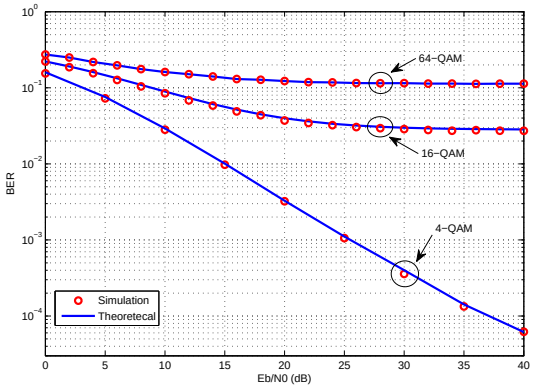

(b) Rayleigh channel, $IBO = 6$dB, $\phi_0 = \pi/3$.

Figure 5.2: BER vs E_b/N_0 for M-ary (QAM or OQAM) based OFDM, $N = 64$, PA: Saleh's TWTA model.

where ${}_2F_1(.,.;.;.)$ denotes the Hypergeometric function, (a,b) are modulation-specific constants, e.g., $(a = \frac{2(\sqrt{M}-1)}{\sqrt{M}log_2(M)}$ and $b = \frac{3log_2(M)}{(M-1)})$ for M-QAM, $\gamma_c = |K_0|^2\sigma^2$ and ν is the channel average fading power.

Proof: is given in paper [J07].

Figure 5.2.a and 5.2.b show the BER performance of a non-linearly amplified FBMC-OQAM and OFDM signals transmitted over, respectively, AWGN channel and flat-fading Rayleigh one. We can clearly note a very good agreement between the Monte-Carlo simulation results and those obtained analytically (equations (5.22) and (5.23)) for both FBMC-OQAM and OFDM systems. It is worth to mention that the infinite series, in equation (5.23), can be truncated to $n = 10$ and $k = 50$ terms with negligible loss in precision.

5.4 Adaptive Digital Predistortion for PA linearization

Baseband adaptive digital predistortion (DPD) is the most promising solution to compensate of the nolinearities and memory effects of the PA. The DPD consists in adding a processing unit before the PA such that the resulting system DPD plus PA is linear (up to the PA saturation). The DPD's characteristics are the inverse of the ones of the PA. Specifically, the DPD applies an expansion, in the PA compression zone, on the input signal in order to compensate the loss of gain and it must also apply a phase shift of opposite quantity of the one introduced by the PA. Typically, the DPD is adaptive, i.e., capable to update the coefficients of the DPD following the time-varying PA characteristics.

The common adopted hardware implementation combines a digital signal processor (DSP) and a field programmable gate array (FPGA) to realize the adaptive DPD architecture (see Figure 5.3). The DPD function is performed by the FPGA that provides implementation structure highly parallelized while the adaptation process is realized by the DSP which is more adequate for complex algorithm derived in sequential form. In Figure 5.3, the DPD architecture requires a feedback loop to take a part of the amplified signal and to demodulate it. After a synchronization and a power normalization processes, the new input and output signals permit to update the DPD function. The feedback loop contains a coupler,

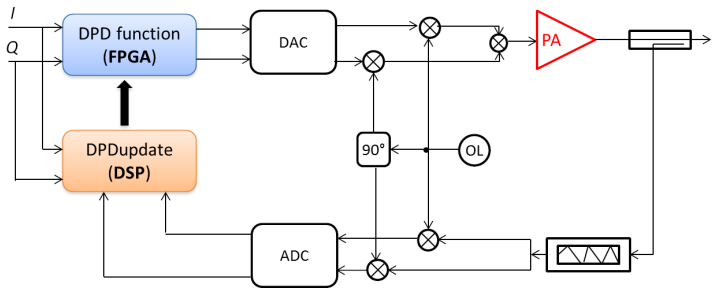

Figure 5.3: DPD architecture.

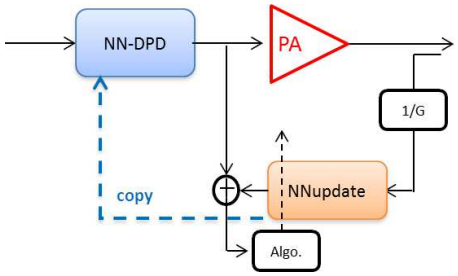

Figure 5.4: Simplified DPD architecture.

an attenuator, a mixer and analog to digital converters (ADC). Here, we consider the indirect learning architecture (ILA) which has been shown to be the most promising one.

The DPD is expected to provide good linearization performance and low cost. The DPD complexity cost represents both the computational complexity of the DPD function and the identification processing, which depends on the updating algorithm and the number of coefficients of the DPD function. For the sake of simplicity and without loss of generality, we consider, in the following, the simplified DPD architecture given in Figure 5.4.

Several mathematical models have been proposed for DPD modeling, which serve for PA modeling. These mathematical models, which are derived from the Volterra Series model, are Memory polynomial (MP) [86], generalized memory polynomial (GMP) [87], Laguerre-Volterra model [88], Kautz-Volterra model [89] and dynamic-deviation-reduction (DDR) Volterra model [90]. The review of the different methods for predistortion is not the main object of this dissertation and the interested reader is referred to [91].

Volterra based models are able to compensate both nonlinearity and memory effects of NL PA. Nevertheless, other techniques exist for synthesizing NL systems. Among them we have chosen a Neural Network (NN) implementation of the DPD, which has great capability to learn any arbitrary nonlinear input-output relationships from corresponding data [7]. Indeed, we have widely investigated DPD based on real-valued multi-layer perceptron (MLP) whose input signal consists of Cartesian in-phase and quadrature phase (I/Q) components. This NN structure is capable to compensate effectively both nonlinearity and memory effects [92]. Most importantly, this NN structure is able to compensate, together with the memory PA nonlinearity, other hardware imperfection like I/Q imbalance, DC offset [93]. In the following, I give enhanced DPD architectures that, in one hand, are able to take into consideration crosstalk between antennas in MIMO systems (Subsection 5.4.1) and, in another hand, are more adequate to OQAM based MWFs (Subsection 5.4.2), like FBMC-OQAM, which are more sensitive to phase error than classical OFDM.

5.4.1 Crossover Neural Network Predistorter for the compensation of memory crosstalk and PA nonlinearity in MIMO-OFDM systems

Via the supervision of Hanen Bouhadda's master internship, we have proposed a new crossover NN predistorter with memory (MCO-NNDPD) architecture capable to compensate both PA nonlinearity and memory crosstalk effects in MIMO-OFDM transmitters.

In order to assess the performance of the proposed architecture (Figure 5.5), the MIMO multiplexer

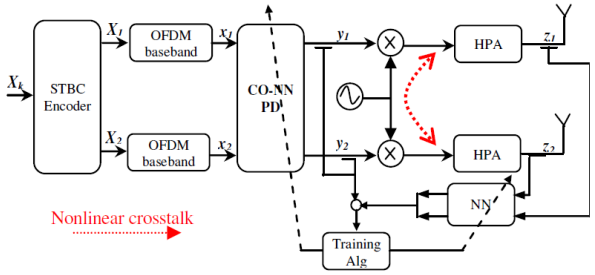

Figure 5.5: CO-NNPD and nonlinear crosstalk in MIMO-OFDM transmitter.

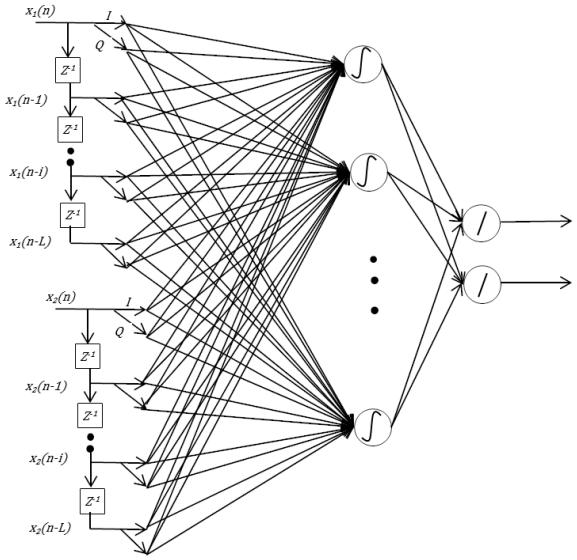

Figure 5.6: MCO-NNPD based on a MLP neural network.

adopted is the space time block coded (STBC) $2*2$ proposed by Alamouti [94]. Note that the crosstalk is the result of interferences occurring between the different paths in the same low-size integrated circuit. This crosstalk can be linear or nonlinear, in the first case, it will be tackled by the receiver equalizer. But in the second case the crosstalk, which is generated before the PAs (i.e., amplified in nonlinear manner), is much more harmful and it cannot be eliminated by the receiver. Then, the PA output affected by the memory crosstalk can be modeled as

$$\begin{aligned} z_1 &= f_1\left(y_1 + F(y_2)\right) \\ z_2 &= f_2\left(y_2 + F(y_1)\right) \end{aligned} \tag{5.24}$$

where f_1 and f_2 are the PA transfer functions corresponding, respectively, to antenna 1 and antenna 2, F denotes the memory crosstalk which represents the filtered part of the signal from the other branch. Here a low-pass filter with four poles is considered as $\{0.3162, 0.153, 0.1, 0.07\}$. The proposed NN structure is illustrated in Figure 5.6. It has two inputs (x_1 and x_2) where each one is scattered to I and Q components and then connected to a tap delay line on each branch. All the outputs of the two tap delay lines are fully connected to all neurones of the first NN hidden layer. Then, we have four outputs representing the I and Q components of the output signals (y_1 and y_2). The training algorithm adopted was the Levenberg-Marquardt (LM) one (see equation (5.26)).

Figure 5.7 shows the performance of several NN predistorter configurations on the considered STBC-MIMO-OFDM system with a Saleh's TWT amplifier [4] operated at an IBO of 7dB, in presence of memory crosstalk. We present the BER performance of the conventional/memoryless CO-NNPD (studied in [C08]) compared to the proposed MCO-NNPD (TD5,n_1-n_2,4), where TD5 denotes the tap delay line of length 5 while n_1 and n_2 represent the number of neurones in, respectively, the first and second hidden layers. The BER performance of linear PA case serves as a benchmark.

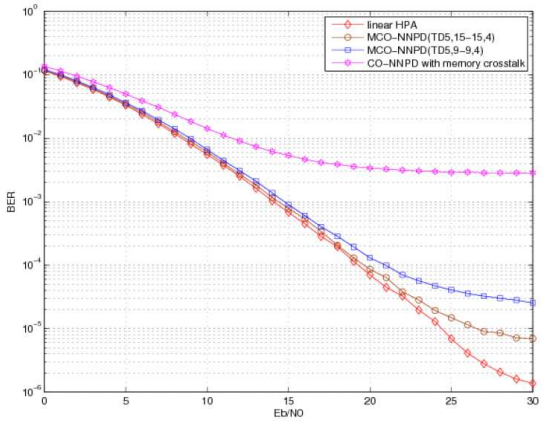

Figure 5.7: BER vs E_b/N_0, STBC MIMO OFDM system, BPSK modulation, 512 subcarriers, IBO of 7dB, Rayleigh channel.

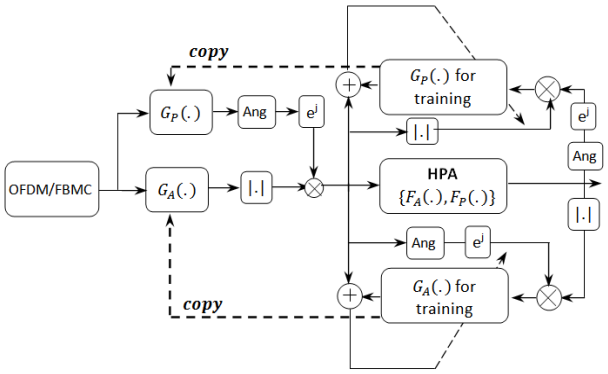

Figure 5.8: Second DPD scheme

5.4.2 Adaptive Predistortion adapted to FBMC-OQAM Systems

Due to the similarity between OFDM and FBMC-OQAM systems, it is natural to consider employing DPD to compensate amplitude and phase nonlinear distortions of FBMC-OQAM signals. However, FBMC-OQAM systems have a different signal structure compared with OFDM, for example, it is more sensitive to the phase distortion than OFDM signal. Therefore, I have been interested in investigating a new predistortion scheme based on the concept of separating the compensation of the phase and amplitude distortions.

Classical/First DPD scheme

The first technique is the one studied in [7] for OFDM systems (see Figure 5.4). It consists in two neural network (NN) units. The first one, NNDPD, realizes directly the predistortion function by applying deformations on the transmitted signal such that the resulting system is linear. The second, NNupdate, is updated regularly, using a training algorithm, according to the variation of the PA. Then, the coefficients of the NNupdate are transferred to the NNDPD using a simple copy. The NNDPD response can approximate simultaneously the inverse transfer functions of the nonlinear PA (AM/AM and AM/PM). The NN structure considered was a feedforward multilayer perceptron (MLP) neural network, which has two inputs, namely the I and Q components of the input signal, two linear output neurons that are the predistorted signals (I and Q) and one hidden layer with ten nonlinear neurons. The activation function, $f_a(.)$ used for the hidden layer is an hyperbolic tangent, while the output layer is linear. It is well known that each neuron in the network is composed of a linear combiner and an activation function which gives the neuron output as

$$x_{l,j}^{out} = f_a\left(\sum_{i=0}^{N_l-1} w_{l,j,i} x_{l-1,i}^{in} + b_{l,j}\right), \tag{5.25}$$

where $w_{l,j,i}$ is the weight which connects the i-th neuron in layer $l-1$ to the j-th neuron in layer l, $b_{l,j}$ is the bias term, and $x_{l-1,i}^{in}$ denotes the i-th component of the input signal to the neuron.

The weights of the NNupdate are adjusted using Levenberg-Marquardt (LM) algorithm, which has shown, in [7], to exhibit a very good performance with both a lower computational complexity and a

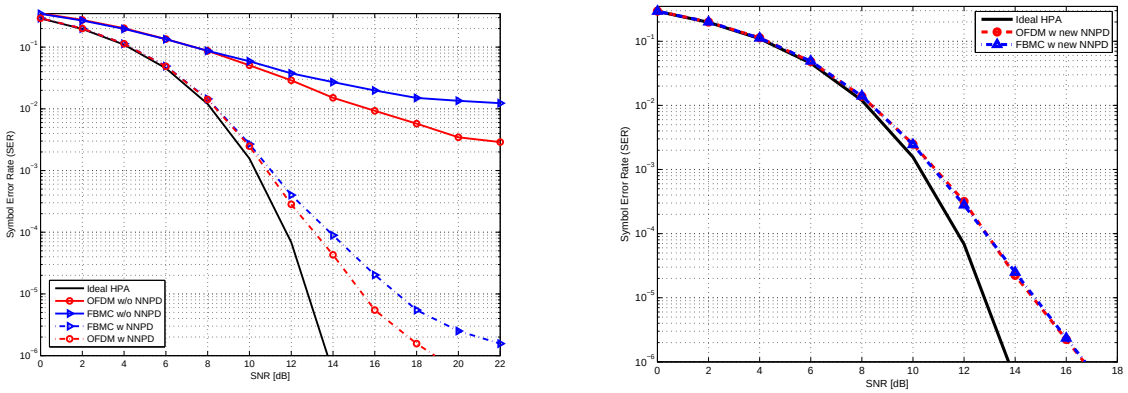

(a) first DPD scheme

(b) second DPD architecture

Figure 5.9: SER vs SNR for OFDM/FBMC system, IBO=6dB, 64 subcarriers, AWGN channel

faster convergence speed than other algorithms studied in literature. The LM algorithm was designed to approach second order training speed and the update of weights is as follows

$$w_{l,j,i}^{(t+1)} = w_{l,j,i}^{(t)} - \left[\mathbf{J}^T\mathbf{J} + \mu\mathbf{I}\right]\mathbf{J}^T\mathbf{e}, \tag{5.26}$$

where $\mathbf{e}$ is the error vector, $\mathbf{J}$ is the Jacobian matrix which contains the first derivatives of $\mathbf{e}$ w.r.t. the weights and biases, and μ is the training rate.

The symbol error rate (SER) performance of the classical DPD scheme over OFDM and FBMC-OQAM systems in presence of amplitude and phase distortions with a Saleh's TWTA operated at an IBO of $6dB$ are depicted in Figure 5.9.a. One can also note that this DPD scheme can reduce considerably the SER compared to the performance without any DPD correction. Nevertheless, it performs worse with FBMC-OQAM modulation when compared to the OFDM one. Such degradation can be explained by the fact that this DPD, which aims to compensate simultaneously the amplitude and phase nonlinearities, is not able to compensate perfectly the phase error. Indeed, the predistorted amplifier exhibits a residual AM/AM distortion, which can only be perfectly compensated as far as the input power is lower than the saturation power, affects the correction of the AM/PM distortion.

Proposed/Second DPD scheme

With that technique (Figure 5.8) the predistortion aims to compensate separately amplitude distortion and phase distortion by using two NNs. The first one (NN1) identifies the inverse AM/AM conversion and the second one (NN2) identifies the inverse AM/PM conversion. The two NNs have the same structure as the ones used in the first scheme, where each one has five neurons in the hidden layer in order to keep the same computational complexity. The transfer functions and training algorithm are also the same as described above.

The SER performance of the proposed DPD scheme for OFDM and FBMC-OQAM are given in Figure 5.9.b. Comparing the different curves, we clearly note an excellent match between the performance provided by the second predistortion scheme for both OFDM and FBMC-OQAM systems. We can note from these results that this DPD scheme is able to compensate perfectly the phase error due to the nonlinear PA.

5.5 PAPR reduction techniques for 5G MWFs

In MWF based communication systems, the PAPR reduction remains one of the most challenges that need to be tackled effectively. Numerous PAPR reduction techniques have been proposed for the classical OFDM, such as clipping [95], Tone Reservation (TR) [96], Selective Mapping (SLM) [97], Active Constellation Extension (ACE) [98], Partial Transmit Sequence (PTS) [99], Tone Injection (TI) [100], and block coding [101]. Review of these techniques is out of the scope of this dissertation and interested readers are referred to [102] and [103].

However, a direct application of the aforementioned PAPR reduction techniques proposed for OFDM to filtered MWFs is not effective due to their overlapping structure. Therefore, we have been interested in investigating improvements of these classical methods to be able to take into account the overlapping structure of the filtered MWFs. Indeed, contrary to the classical symbol-wise optimization methods, the proposed schemes optimize the PAPR with taking into account the whole interval upon which the filtered MWF symbol got spread. In this regard, two methods have been considered in our study, TR and SLM, which are the most promising ones. The performance of the proposed improved TR/SLM schemes are assessed through FBMC-OQAM since it has the most pronounced overlapping symbol structure.

5.5.1 Dispersive SLM based PAPR reduction in FBMC-OQAM systems

The dispersive SLM (DSLM) algorithm is summarized bellow,

Step 1-Initialization: Given M complex input symbol vectors $\{\mathbf{X}_m\}_{m=0}^{M-1}$ and U uniformly distributed phase rotation vectors $\{\Phi^{(u)}\}_{u=0}^{U-1} \in \{-1, 1\}$ of length N. We initialize $m = 0$
Step 2-Phase rotation: Compute U phase rotated version of the m-th symbol $\mathbf{X}_m$, obtaining $\{\mathbf{X}_m^{(u)} = \mathbf{X}_m \odot \Phi^{(u)}\}_{u=0}^{U-1}$.
Step 3-FBMC-OQAM modulation: Apply FBMC-OQAM modulation for all pattern of the m-th symbol vector with taking into account $K-1$ previous symbols, where K is being the adopted prototype filter length, to obtain ${x_m(t)^{(u)}}_{u=0}^{U-1}$
Step 4-PAPR calculation: Compute the PAPR of the modulated signals ${x_m(t)^{(u)}}_{u=0}^{U-1}$ on $[mT, mT + KT]$ interval time, giving U PAPRs.
Step 5-Selection: Select the vector which gives the lowest PAPR to this symbol,$\Phi^{(u_m)}$, and send $\mathbf{X}_m^{(u_m)} = \mathbf{X}_m \odot \Phi^{(u_m)}$.
Step 5-Increment: Increment m by 1 and go to **Step 2**.

The performance of the above algorithm is depicted in Figure 5.10. One can note that the provided PAPR reduction is quite similar to that of the OFDM with the classical SLM. Nevertheless, for high values of U there is a performance gap between OFDM and FBMC-OQAM. Without taking into account the memory effect of FBMC-OQAM (step 3 of the proposed algorithm), this gap should be significantly larger.

5.5.2 Dispersive TR based PAPR reduction in FBMC-OQAM systems

In the TR scheme, iterative clipping and filtering approach is considered. The total N subcarriers are partitioned into R peak reduction tones (PRTs) and $N-R$ data subcarriers. Symbols in PRTs are chosen such that time-domain FBMC-OQAM signal has a low PAPR. These PRTs do not carry any useful

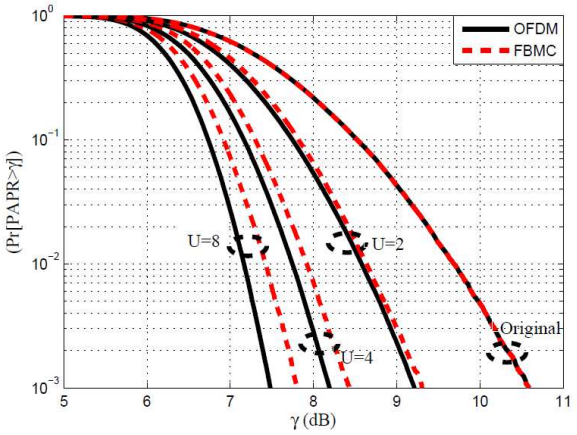

Figure 5.10: CCDF of PAPR comparison of DSLM and classical SLM schemes in FBMC-OQAM with $N = 64$ and $U = [2, 4, 8]$.

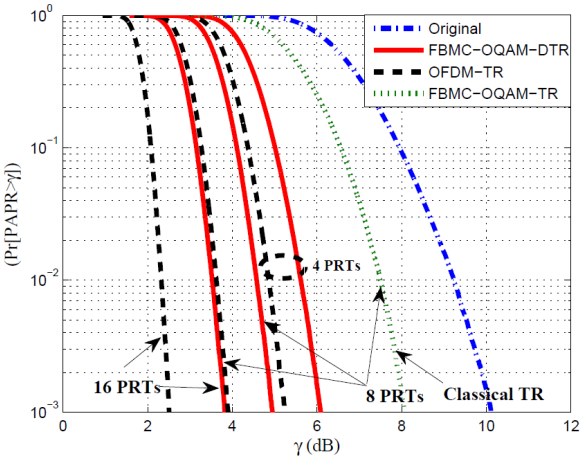

Figure 5.11: CCDF of PAPR comparison of DTR and classical TR schemes in FBMC-OQAM with $N = 64$ and PRT set $R = [4, 8, 16]$.

information and are orthogonal to the data subcarriers, making the data recovery trivial.

Unlike to the traditional TR, which adopts symbol-wise optimization, the proposed dispersive TR (DTR) takes into account the overlap of the past symbols, when optimizing the PRTs entries for the m-th symbol. Again, the considered prototype filter is the PHYDYAS one with an overlapping factor $K = 4$.

The DTR algorithm is as follows

Step 1-Initialization: Given a PRT location set $\mathcal{B}$, generate M complex input symbol vectors $\{\mathbf{D}_m\}_{m=0}^{M-1}$ and put zeros in the PRT locations (i.e., $\mathbf{C}_m$ is initially set to zero). We initialize $m = 0$. The input symbols in frequency domain can be expressed as

$$\mathbf{X}_m[n] = \mathbf{D}_m[n] + \mathbf{C}_m[n] \quad = \begin{cases} \mathbf{C}_m, & if\ n \in \mathcal{B} \\ \mathbf{D}_m, & if\ n \in \mathcal{B}^c \end{cases}, \tag{5.27}$$

Step 2-FBMC-OQAM modulation: Apply FBMC-OQAM modulation for all pattern of the m-th symbol vector with taking into account $K - 1$ previous symbols, obtaining $x_m(t)$.

Step 3-Peak-cancelling signal optimization: Compute the optimal values of of PRTs subject to

$$\underset{\mathbf{C}_m}{argmin} \left[\|x_m(t) + \varrho(\mathbf{C}_m)\| \right], \qquad m \in [mT, mT + KT], \tag{5.28}$$

where ϱ denotes FBMC-OQAM modulation. Note that the optimal $\mathbf{C}_m$) can be obtained by solving equation (5.28) using convex optimization algorithms such as Quadratically constrained quadratic programs (QCQP), gradient search [104], projection onto convex sets (POCS) [105], etc.

Then, the input symbol vector is updated as

$$\mathbf{X}_m = \mathbf{D}_m + \mathbf{C}_m \tag{5.29}$$

Step 4-Increment: Increment m by 1 and go to **Step 2**.

From results in Figure 5.11, one can observe the strong capability of the proposed DTR method in reducing the PAPR of FBMC-OQAM. Its performance are quite close to those obtained by classical TR for OFDM.

5.6 Ping-Pong Joint Optimization (P2JO) for PAPR reduction and PA linearization

As explained above, the two complementary techniques of PAPR reduction and PA linearization have to be deployed in order to improve both PA linearity and efficiency. In conventional systems, these solutions are optimized separately and applied independently. Indeed, designers start focusing on their association aiming at avoiding mutual effects in order to enhance interoperability, achieving an optimal performance. In literature, different schemes have been studied where PAPR reduction is followed by predistortion [106] [107] [108], These schemes showed attractive improvements in efficiency and linearity when both digital pre-processing techniques are combined. Furthermore, in [108], authors proposed a method to control the DPD-avalanche [109] by limiting the peaks generated from the digital predistorter. Another approach has been widely studied in [109] [110] [111] [112] [113], it consists in including PAPR control as a constraint in the estimation of the predistortion parameters.

In the framework of the ANR WONG5 project, we have been interested in investigating new solution to tackle this issue. In this regard, we have introduced a new and promising concept to optimize jointly PAPR reduction and PA linearization that aims at creating a good synergy between the two techniques in order to provide optimal performance. The proposed approach synthesises, in a Ping-Pong manner, only one correction signal that takes into account the PAPR reduction and PA linearization allowing then better trade-off between PA efficiency and linearity, compared to classical combinations studied in literature. In this work, the clipping control based tone reservation (CC-TR) method, which is commonly used and is adopted in DVB-T2 systems [114], is considered for PAPR reduction. It can obtain a moderate PAPR reduction with little degradation of bit-error-rate (BER) performance [115]. While for PA linearization, the neural network based DPD is an excellent for the PA linearization [7]. The proposed Ping-Pong Joint Optimization (P2JO) approach takes benefit from the fact that a common vision of PAPR reduction and PA linearization techniques is possible since they can be formulated as adding signal techniques, thanks to Bussgang theorem [83].

5.6.1 Classical combination of PAPR reduction and DPD by adding signal

Let us consider $\mathbf{x}$ as the signal issued from a MWF modulation (Figure 5.12). After scaling the signal to the desired PA back-off, using γ_0, we can generate a PAPR reduction signal $\mathbf{c}^{papr}$ using CC-TR technique [116] [117]. Then, the low-PAPR signal, expressed as

$$\mathbf{y}^{papr} = \mathbf{y}^0 + \mathbf{c}^{papr}, \tag{5.30}$$

will serve to generate a predistortion signal $\mathbf{c}^{dpd}$. Then, the signal at the input of the PA can be given by

$$\mathbf{y} = \mathbf{y}^{papr} + \mathbf{c}^{dpd} \tag{5.31}$$

We recall that we consider the CC-TR to generate the PAPR reduction signal where many iterations are needed for a given OFDM symbol. While, we execute only one time the considered neural network to obtain the predistortion signal. This combination scheme, considered in [106] [110] as a dynamic joint approach for PAPR reduction and predistortion, will be considered, in this work, as the classical combination and will serve as a reference to show how our proposed approach will achieve better trade-off between PA linearity and efficiency.

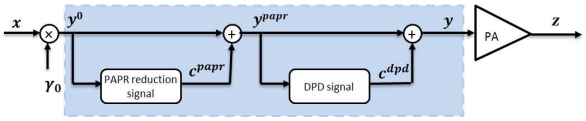

Figure 5.12: Principle of classical combination of PAPR reduction and predistortion by adding signal.

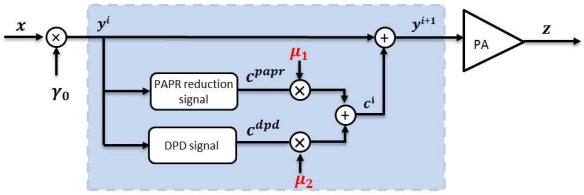

Figure 5.13: Ping-Pong Joint Optimization by adding signal.

Table 5.1: P2JO Parameters

i	Current iteration index
$maxIter$	Maximum number of iteration
A	Clipping level
$\mathbf{S}^d$	Identity matrix of order N with zeros at positions in $\mathcal{R}$
$\mathbf{S}^r$	Identity matrix of order N with zeros at positions in $\mathcal{R}^c$
γ_0	Scaling factor to control the PA Back-off

5.6.2 Proposed P2JO algorithm

The key idea is to synthesize the additional signal **c** for PAPR reduction and predistortion in a Ping-Pong manner and iteratively (Figure 5.13). In this technique, we:
1) add the PAPR reduction signal scaled by a factor $\mu_1 \leq 1$,
2) add the predistortion signal scaled by a factor $\mu_2 \leq 1$,
3) repeat steps 1) and 2) until we reach the desired performance.

Using this approach, we create a good synergy between the two operations in order to avoid mutual effects leading to a better trade-off between PA efficiency and linearity. Table **P2JO** describes the proposed P2JO algorithm and Table 5.1 contains a list of parameter definitions to be used in the algorithm. It is worth to mention that the proposed algorithm has been published in patent [P01].

5.6.3 P2JO performance assessment

In order to study the capability of the proposed approach, an uncoded OFDM system with N=256 subcarriers and using 16-QAM modulation with Gray mapping. The number of reserved tones is set to be 32, randomly selected over the bandwidth of the OFDM signal. The oversampling factor is set to 4 that guarantees a good PAPR approximation [118]. The considered PA is the Saleh's TWTA. The optimal clipping threshold A_{sat} is defined according to [115]. For the P2JO algorithm, we recall that, for PAPR reduction, we consider the CC-TR method, where its peak-cancelling signal, during each iteration, is extremely smaller than that of the original clipping noise. In order to keep a maximal performance of power efficiency and push the predistortion to offer its best performance, μ_1 should be adaptive when considering optimized TR PAPR reduction methods with adaptive peak-cancelling signal level, like in [115] [119]. Three values of μ_2 have been considered, 10^{-2}, 3×10^{-2} and 5×10^{-2}, to clearly show how we can take into consideration the mutual effect between TR PAPR reduction and DPD by the proposed iterative Ping-Pong approach. In the following, μ%P2JO refers to the use of the P2JO

P2JO: The P2JO approach

1: Set the minimum EVM_{min}, the reserved tone set R, the initial clipping level A_{sat}
and the maximal iteration number $maxIter$.
2: Set $i = 0$, the time-domain signal of the 0^{th} iteration $\mathbf{y}^0 = \mathbf{x}$,
where $\mathbf{x}$ is the original OFDM symbol.
3: TR : calculate the clipping noise, using the OFDM signal at iteration i and its clipped version ($mathbf{\bar{y}}^i$), as $\mathbf{w}^i =$
calculate the peak-cancelling signal $\mathbf{c}^{papr,i} = IFFT(\mathbf{S}^r \times FFT(\mathbf{w}^i))$
4: DPD : calculate the predistortion signal $\mathbf{c}^{dpd,i} = \mathbf{y}^{dpd,i} - \mathbf{y}^i$
where $\mathbf{y}^{dpd,i}$ is the predistorted version of $\mathbf{y}^i$ signal.
5: Update the signal $\mathbf{y}^{i+1} = \mathbf{y}^i + \mu_1\mathbf{c}^{papr,i} + \mu_2\mathbf{c}^{dpd,i}$
6: Calculate the amplified signal $\mathbf{z}^{i+1} = S(|\mathbf{y}^{i+1}|)exp(\angle\mathbf{y}^{i+1})$
7: Calculate $X^{i+1} = \mathbf{S}^d \times FFT(\mathbf{y}^{i+1})$
8: Calculate the error vector magnitude $EVM^{i+1} = \sqrt{\frac{E[X^{i+1}-X^0]}{E[X^0]}}$,
if $\left(EVM_{min} < EVM^{i+1} < EVM^i \ \ \& \ \ i < maxIter\right)$, set $i = i + 1$
and go to step 3).
otherwise, choose $\mathbf{y}^{i+1}$ as the transmitted signal and terminate the loop.
9: **End**.

algorithm where $\mu_2 = \mu \times 10^{-2}$. It is worth to note that, when $\mu_2 = 1$,the P2JO converges to the same performance obtained by the classical approach.

Figure 5.14 shows the BER performance of the μ%P2JO in presence of nonlinear Saleh's TWTA operated at outpout back-off (OBO) of 2.5dB, 3dB and 3.5dB and an AWGN channel. 'classical TR+DPD' and 'w/o corr' denotes, respectively, the classical approach and the OFDM system without any correction. One can note that the μ%P2JO outperforms the classical scheme in all cases, we note for a BER of 4×10^{-3}, a SNR gain of 1dB, 2.5dB and 11dB at, respectively, OBOs of 3.5dB, 3dB and 2.5dB. In order to show the impact of μ_2 on the P2JO performance, Figure 5.15 shows BER performance of 1%P2JO, 3%P2JO and 5%P2JO. We can clearly see that the more μ_2 is decreased, the more the performance is improved. This can be explained by the fact that the mutual effect between TR PAPR reduction and DPD is better considered when μ_2 is lower. To have a clear comprehension of the P2JO algorithm convergence speed, Figure 5.16 shows EVM performance versus iteration number for different values of OBOs. It can be observed that, when lower value of μ_2 is considered, the EVM decreases slowly and ensures a better convergence towards a lower EVM. At OBO of 2.5dB, 1%P2JO converges to an EVM of 9% in 100 iterations, while 5%P2JO converges to an EVM of 11.3% in only 20 iterations.

To study the effect of the proposed approach on the OOB emission, the PSD and the adjacent channel power ratio (ACPR) are considered. As depicted in Figure 5.17, the OOB emission reduction in the neighboring channels based on μ%P2JO outperforms those of the classical approach. Furthermore, Table 5.2 gives the ACPR performance of the P2JO approach compared to the classical one with Saleh's TWTA operating at OBOs of 2.5, 3, 3.5 and 4 dB. As can be observed, the schemes based on 1%P2JO provide an ACPR gain of 2dB compared to the classical approach.

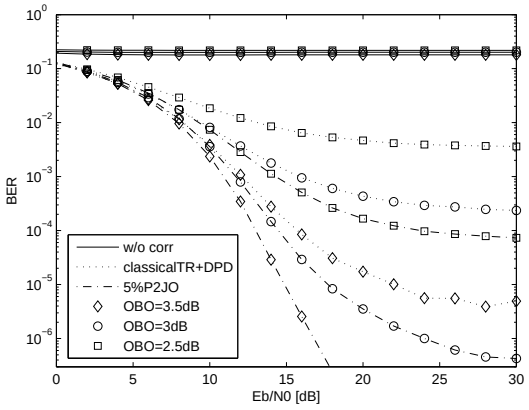

Figure 5.14: BER performance of an OFDM system with $R = 32$ for 16-QAM, Saleh's TWTA.

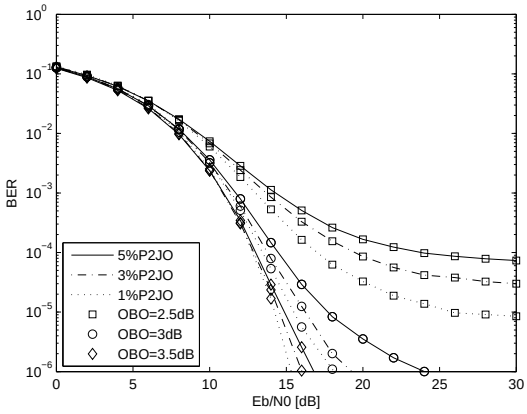

Figure 5.15: BER performance of an OFDM system with $R = 32$ for 16-QAM, Saleh's TWTA.

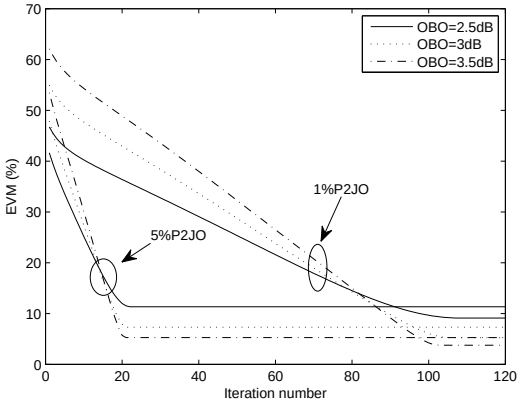

Figure 5.16: EVM vs iteration number of an OFDM system with $R = 32$ for 16-QAM, Saleh's TWTA.

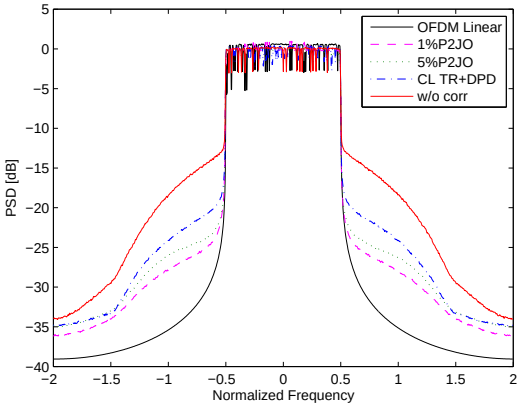

Figure 5.17: PSD of an OFDM system with $R = 32$ for 16-QAM at OBO=3dB, Saleh's TWTA.

Table 5.2: ACPR [dB] performances of an OFDM system with $R = 32$

OBO [dB]	**4**	**3.5**	**3**	**2.5**
1%P2JO	-30.13	-28.78	-26.98	-24.88
5%P2JO	-29.08	-27.83	-26.12	-24.20
CL TR+DPD	-28.37	-26.91	-24.82	-22.84
w/o corr.	-21.13	-20.53	-19.28	-18.24

5.7 Experimental testbed of Multi-carrier Waveforms for Heterogenous Networks

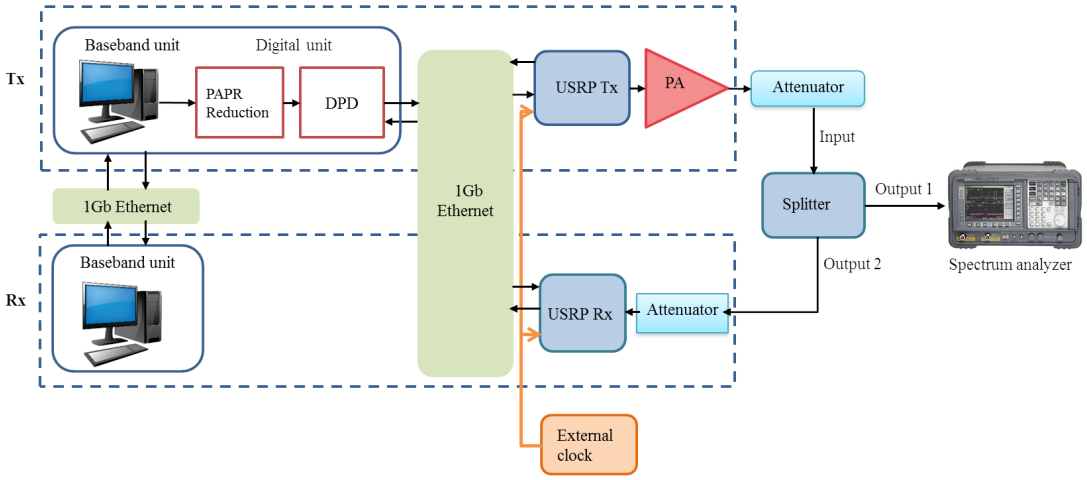

Figure 5.18: Overall architecture.

In the framework of the ANR WONG5 project, I have been in charge of the development of an experimental testbed to study the capability of new multi-carrier waveforms to accommodate 5G requirements. Experiments, which were done in a realistic laboratory-like environment, were performed with an implementation of the classical CP-OFDM and the most promising psot-OFDM MWFs, i.e., WOLA-OFDM and BF-OFDM, with configurable universal software radio peripherals (USRPs)-based software defined radio (SDR) prototype. These experiments have been crucial to convince evidences of advanced MWF technology feasibility using real-world environment imposing some RF imperfections, like RF PA nonlinearities, IQ imbalance and mirror-frequency interference, phase noise and A/D converter nonlinearities.

The testbed overall architecture, which is realized with Transmitter (Tx) and Receiver (Rx), is illustrated in Figure 5.18. The baseband components are software-based and implemented using MATLAB/C++ and they realize the digital algorithms, e.g., waveform generation, QAM modulation, channel equalization, demodulation, etc. Concerning SDR-hardware, two separate USRP devices, NI-USRP-2942R, are used as transmitter and receiver, integrating digital/IF/RF units [120]. The synchronization of USRP modules is ensured using an external clock from Marconi Instruments 2051 Digital and Vector Signal Generator. This external clock provides 10 MHz clock signal which is transmitted to the two USRPs, which is crucial for proper operation of MWFs. The RF PA is a SSPA PE15A4017 from Pasternack with a bandwidth of 20 MHz to 3 GHz and 27dB Gain [121].

Most importantly, a real-time SDR implementation is ensured by considering a specific computer configuration, interested readers are referred to [122]. The link performance results were provided for two scenarios : DL and UL following the experimentation cases.

Scenario 1 corresponds to interference free DL with nonlinear amplification. We provided details and deign guidance to improve EE-related power amplification and robustness of the studied MWFs through PAPR reduction and DPD techniques. Since BF-OFDM has overlapping signal structure, we introduced

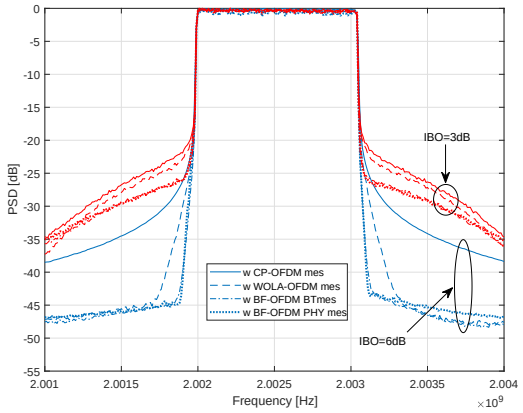

Figure 5.19: PSD performance of different WFs using SLM (V=8) and DPD.

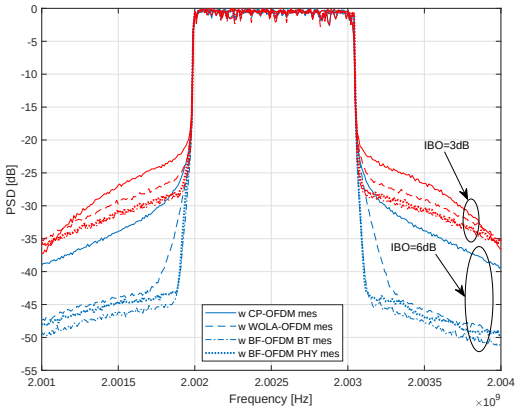

Figure 5.20: PSD performance of different WFs using TR (R=16) and DPD.

modified TR and SLM techniques that are more adequate to BF-OFDM than the classical ones. The key idea is, when reducing the PAPR of the current symbol $\mathbf{x}(i)$, we take into consideration the tail of the previous optimized symbol $\mathbf{x}(i-1)$. We move to DPD, it is based on the well-known polynomial model based inverse learning architecture (ILA) [7].

Figures 5.19 and 5.20 depict measured PSD performance comparison of the studied MWFs when SLM and TR are, respectively, performed with DPD. One can clearly see the significant gain provided by WOLA-OFDM and BF-OFDM compared to CP-OFDM, especially for IBO of 6dB. We can also note that BF-OFDM outperforms WOLA-OFDM due to the better spectrum containment provided by the subband filtering used by BF-OFDM. Further, BT-Gaussian based BF-OFDM [60] provides slightly better performance than PHYDYAS based BF-OFDM. For an IBO of 6dB, the CP-OFDM PSD performance is almost as the one in linear case. As explained in chapter 4, its PSD localization is worse compared to WOLA-OFDM and BF-OFDM.

Figure 5.21 compares measured BER of different MWFs when the RF PA is operated at an IBO of 3 and 6dB. Again, we can note that WOLA-OFDM and BF-OFDM provide almost the same performance as the classical CP-OFDM when PAPR reduction is performed by SLM/TR. At an IBO of 6dB, BER performance provided by all waveforms is very close to the one performed in linear case. It is worth mentioning that BER floor related to the demonstrator noise floor is not observable for BER $> 10^{-}5$, which represents a significant BER range for wireless communications standards.

Scenario 2 defines an asynchronous UL transmission case. We addressed the impact of the lack of synchronism between transmitters on the performance of the selected MWFs, which is of special relevance for future 5G mMTC applications. We provided further discussions and comparisons of the selected waveforms CP-OFDM,WOLA-OFDM and BF-OFDM, with corresponding parameter selections. Here, we consider a scenario with two co-existing users sharing the available frequency band as illustrated in Figure 4.4. The user of interest (UoI) occupies 7 resource blocks (RBs), about 1.1 MHz bandwidth from 2.0020 to 2.0031 GHz. The interferer user occupies, on each side of the user of interest, 7 RBs of 1.1 MHz bandwidth. A guard-band δ_f between the two users is separating the frequency bands of both users and a timing offset is given to create asynchronism. In order to well assess the performance of these

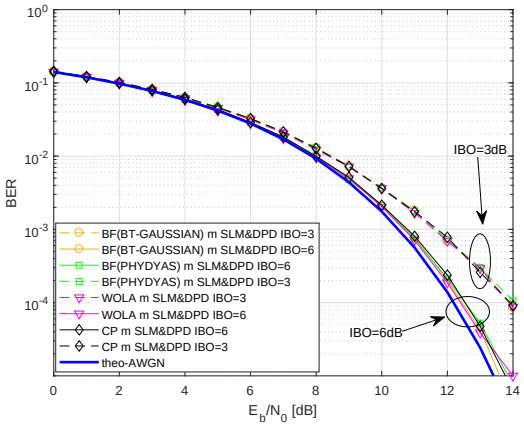

Figure 5.21: BER performance of different WFs using SLM and DPD, 16-QAM.

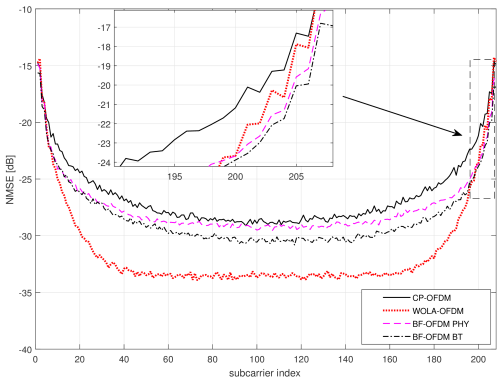

Figure 5.22: scenario 2: NMSE performance of different WFs when $\Delta t = 106\mu s$ and $\delta_f = 4.883$KHz.

waveforms, we measure the NMSE on the decoded symbols of the UOI. Per-subcarrier NMSE (Figure 5.22) is assessed versus guard band for $\Delta t = 106\mu s$ for 1/2 symbol duration.

From results illustrated in Figure 5.22, we clearly show that the inter-user interference level depends on the chosen MWF. CP-OFDM exhibits the worst performance due to its bad frequency response localization. Furthermore, we note that the interference level decreases slowly as the spectral distance between the victim subcarrier and the interferer ones increases.

We move to WOLA-OFDM, we can observe better performance compared to CP-OFDM. Its achieved interference level, in the middle of the bandwidth, is lower (approximately -34dB) compared to CP-OFDM scheme. These good results are related to the WOLA processing applied at the receiver that is able to suppress inter-user interference resulting from the mismatched FFT capture window.

Concerning BF-OFDM, it provides better protection to the edge subcarriers (in the vicinity of interferer subcarriers) compared to both CP-OFDM and WOLA-OFDM. In such region, the NMSE varies from -16dB when $\delta_f = 4.883$KHz to -24dB when $\delta_f = 39.06$KHz for BF-OFDM scheme while it varies from -14.2dB to -23dB for WOLA-OFDM scheme when the same band is considered. However, the gain of BF-OFDM for the inner subcarriers is marginal compared to CP-OFDM. This is a direct consequence of the BF-OFDM receiver which is no more than the classical CP-OFDM receiver (i.e., a simple FFT). Thus, BF-OFDM could be more interesting than WOLA-OFDM when few number of RBs will be considered for the UOI.

5.8 Outputs

The outputs related to work on NLD characterization and mitigation techniques to enhance the energy-efficiency of 5G MWFs are summarized bellow.

Supervision and collaborations related to the analysis of the EE related to power consumption in 5G MWFs

- 05 PhD co-supervision: (**Dr. H. Bouhadda** (40%), **Dr. M. Laabidi** (60%), **Dr. O. B. Belkacem** (45%), **Dr. M. Dakhli** (60%) and **Miss M. Benosman** (ongoing))
- Supported by FP7 EMPHATIC, PHC-Utique C3, PHC-TASSILI ATOME5+, ANR WONG5 projects
- Visiting researcher CEDRIC/CNAM, Mar.-June 2014 and Sep..-Nov. 2013

Publications related to the analysis of the EE related to power consumption in 5G MWFs

- 9 peer-reviewed journals **[J14, J11, J10, J08, J07, J06, J05, J04, J03]**
- 19 peer-reviewed international conferences **[C41, C38, C23, C22, C21, C21b, C21c, C19 -> C07]**
- 1 European patent **[P01]**
- 1 Book chapter **[B01]**

Chapter 6

Massive MIMO: Energy Efficiency and Hardware Efficiency

6.1 Introduction

To support the exponential growth in data traffic demand and simultaneously offer ubiquitous connectivity, researchers have been interested in designing new revolutionary wireless communication technologies. One of the most promising solutions to increase spectral, energy and hardware efficiencies by orders-of-magnitude is massive MU-MIMO [123], which is also known as large-scale MU-MIMO. However, massive MU-MIMO precoders exhibit signals with high PAPR, independently of whether single-carrier or multi-carrier transmission are adopted [124]. Accordingly, the nonlinearity of the radio frequency (RF) PA, which is the main hardware impairment and is expected to be low-cost and energy-efficient component to enable cost- and energy-efficient massive MU-MIMO BS deployments, yields harmful in-band distortion and out-of-band emissions. Furthermore, massive MU-MIMO should support mixed numerologies spectrum sharing (SS) transmissions, expected for 5G and beyond. Therefore, I have been interested in investigating: 1) the PAPR reduction problem as well as the compensation of PA nonlinearities in massive MU-MIMO based systems, leading then to highly energy-efficient systems and 2) the introduction of new precoding schemes to make massive MU-MIMO much more flexible, satisfying the extremely diverse service requirements.

This chapter exposes the main researches I conducted, within the H2020 MSCA ADAM5 project, to tackle the aforementioned massive MU-MIMO issues. Section 6.2 summarizes the technical contributions related to PAPR reduction problem. Several new methods, which have been developed, will be presented and compared in terms of performance and complexity. In Section 6.3, I move toward PA nonlinearity compensation in massive MU-MIMO. A new approach will be presented and compared to the most studied ones in literature. Section 6.4 is devoted to the work developed via the supervision of Xinying Cheng's PhD on the analysis and cancellation of inter-numerology interference (INI) in massive MIMO systems. Finally, Section 6.5 summarizes the outputs of these contributions.

6.2 Low-Complexity Linear Precoding for PAPR reduction in Massive MU-MIMO-OFDM Downlink Systems

In order to improve the PA efficiency, which leads to the global system energy-efficiency improvement, MU precoders that generate signals with low-PAPR would be of great interest. This will enable low-cost, low-size and power-efficient hardware implementations in massive MU-MIMO-OFDM systems. Indeed, some previous works have studied low-PAPR precoders for massive MU-MIMO-OFDM [125] [126] [127]. All of these methods exploit the excess DoFs and the large null-space offered by the massive MIMO downlink channel to perform low-PAPR precoding. These methods can achieve substantial PAPR reduction but with scarifying high computational complexity. In [J15], we present an approach to perform jointly MU Precoding and PAPR reduction, which was formulated as a simple convex optimization problem and solved online via gradient descent (GD) approach. Specifically, we design peak-canceling signals (PCSs) to be added to the frequency-domain precoded data signals, with the goal of reducing the PAPRs of their time-domain counterpart signals. Most importantly, the added PCSs have to lie in the null-spaces of their associated MIMO channel matrices such that they do not cause any MU interference (MUI) and OOB radiation. Furthermore, we introduced the MU-PP-GDm [J15] algorithm that aims to minimize alternately the objective functions with respect, respectively, to the MU precoding and PAPR reduction. This process is repeated over many iterations to achieve the desired MUI and PAPR performance. The MU-PP-GDm, which can be seen as an alternate approach using gradient-iterative method based linear precoding, has been shown to achieve satisfactory PAPR performance with lower computational complexity than the other previous works [125] [126] [127], especially when the number of users is sufficiently high. In addition, to optimize the tradeoff between performance and complexity, we have studied linear precoders based on matrix polynomials (M-POLY) approaches for both data and PCSs precoding [SJ1]. The key idea is to approximate the matrix inverse by a matrix polynomial decomposition with J terms, where the approximation accuracy can be guaranteed with very few terms. This approach was first studied for large-scale MIMO in [128] and then widely studied, for massive MIMO downlink related- power/spectral efficiency [129] [130] [131] and security [132] [133], where the polynomial coefficients are optimized using tools from random matrix theory [134].

In order to assess the performance of the different proposed precoding schemes, we assume the downlink of a typical single-cell massive MIMO-OFDM where the BS is equipped with M_t transmit antennas and serves M_r single-antenna user terminals (UTs) over a frequency-selective channel, where $M_t \gg M_r$. Let N denotes the total number of OFDM tones and $\mathbf{s}_n \in \mathbb{C}^{M_r \times 1}$, which is chosen from a complex-valued constellations $\mathcal{A}$, denotes the signal vector containing the information symbols associated with the n-th subcarrier for M_r users, where $n = 1, ..., N$ indexes the OFDM tones. The PAPRs of the generated time-domain signals are high, hence a performance degradation in presence of power-efficient RF PAs. To overcome this problem, the BS generates frequency-domain peak cancelling signals (PCSs) to reduce the PAPRs of the time-domain transmitted signals and to prevent severe PA distortions. These PCSs should be constrained to lie in the null-spaces of the MIMO channel matrices such that they do not damage neither the transmission quality of the M_r users through the N subcarriers (i.e., guaranteeing excellent MUI and capacity) nor the spectrum purity. In typical OFDM systems, a guard-band is considered in order not to disturb the transmission in adjacent bands. Then, we specify some unused subcarriers at both sides of the used band. These latter will serve to ensure that the proposed low-PAPR precoder does not generate any spectrum regrowth and to obtain a good approximation of the PAPR of the oversampled time-domain OFDM sysmbols. Therefore, the set of tones available are divided into two sets χ and χ^c,

where the subcarriers in set χ are used for data transmission and the subcarriers in its complementary set χ^c are used for guard-band. Moreover, we set $\mathbf{s}_n = \mathbf{0}_{M_r \times 1}$ for $n \in \chi^c$ such that no signal is transmitted on the guard-band. The frequency-domain signal vector, $\mathbf{x}_n \in \mathbb{C}^{M_t \times 1}$, $\forall n$, transmitted by the BS over the n-th subcarrier through the M_t antennas, is given by

$$\mathbf{x}_n = \sqrt{\alpha}\mathbf{W}_n\mathbf{s}_n + \sqrt{\beta}\mathbf{V}_n\mathbf{r}_n, \tag{6.1}$$

where $\mathbf{r}_n \in \mathbb{C}^{M_t \times 1}$ denotes the PCS vector for the n-th subcarrier. $\mathbf{W}_n \in \mathbb{C}^{M_t \times M_r}$ and $\mathbf{V}_n \in \mathbb{C}^{M_t \times M_t}$ are, respectively, the data and PCS precoding matrices for the n-th OFDM subcarrier. It is worth pointing out that the design of the precoded signals $\{\mathbf{x}_n, \forall n\}$, which collects the precoded data $\mathbf{d}_n = \mathbf{W}_n\mathbf{s}_n$ and PCS $\mathbf{c}_n = \mathbf{V}_n\mathbf{r}_n$ vectors, is the main scope of this section.

The PCS precoding matrix $\mathbf{V}_n$ has rank $M_t - M_r$, i.e., $M_t - M_r$ dimensions of the M_t-dimensional space spanned by the M_t BS antennas are exploited for PAPR reduction, which represent the projection onto the null-spaces of the MIMO channel matrices. The data and PCS precoding matrices are normalized as $tr\{\mathbf{W}_n\mathbf{W}_n^H\} = M_r$ and $tr\{\mathbf{V}_n\mathbf{V}_n^H\} = M_t - M_r$, $\forall n$. Note that α is a normalization factor designed to obtain an average transmit power, allocated to the information-carrying signal for each user, equal to P_u (i.e., it can be written as $\alpha = \frac{P_u}{M_r}$). β is dedicated to control the power allocated to all PCS signals, which can be optimized to perform an optimal trade-off between PAPR reduction and signal-to-noise ratio (SNR) gap.

After precoding, the M_t-dimensional vectors $\{\mathbf{x}_n, \forall n\}$ are reordered to M_t transmit antennas for OFDM modulation, according to the following one-to-one mapping

$$\left[\mathbf{x}_1^t, ..., \mathbf{x}_{M_t}^t\right]^T = \left[\mathbf{x}_1, ..., \mathbf{x}_N\right]. \tag{6.2}$$

Here, the $\mathbf{x}_{m_t}^t \in \mathbb{C}^{1 \times N}$ denotes the frequency-domain vector to be transmitted though the m_t-th antenna. The time-domain signals $\{\mathbf{a}_{m_t}^t, \forall m_t\}$ are obtained by applying an inverse discret Fourier transform (IDFT) to $\{\mathbf{x}_{m_t}^t\}$. Then, a cyclic prefix (CP) is added to the time-domain samples of each antenna in order to avoid inter-symbol interference (ISI).

For the sake of clarity and without loss of generality, we specify the wireless channel's input-output relation in frequency-domain only. Therefore, the vectors collecting the signals received by the M_r users at the n-th subcarrier can be expressed as

$$\mathbf{y}_n = \mathbf{G}_n\mathbf{x}_n + \mathbf{b}_n, \qquad n \in \chi \tag{6.3}$$

where $\mathbf{b}_n \in \mathbb{C}\mathcal{N}\left(\mathbf{0}_{M_r}, \sigma_b^2\mathbf{I}_{M_r}\right)$ denotes the Gaussian noise vectors with σ_b^2 represents the noise variance at one user. Note that $\mathbf{G}_n = \mathbf{K}^{1/2}\mathbf{H}_n \in \mathbb{C}^{M_r \times M_t}$ is the MIMO channel matrix associated with the n-th OFDM subcarrier. Thereby, $\mathbf{K} = diag\{\kappa_1, ..., \kappa_{M_r}\}$ denotes the path-losses from the BS to the M_r users. Furthermore, the wireless channel is assumed to be frequency-selective and modeled as a tap delay line with L_c taps. The time-domain channel response matrices $\mathbf{H}_l^t, l = 1, ..., L_c$, have i.i.d. circularly symmetric Gaussian distributed entries with zero mean and unit variance. The frequency-domain MIMO channel associated to the n-th OFDM subcarrier, $\mathbf{H}_n \in \mathbb{C}^{M_r \times M_t}$, is obtained as

$$\mathbf{H}_n = \sum_{l=1}^{L_c} \mathbf{H}_l^t e^{\frac{-j2\pi ln}{N}}. \tag{6.4}$$

6.2.1 Computing peak-canceling signals (PCSs)

In this subsection, we discuss how to design the optimal frequency-domain PCSs $\{\mathbf{r}_n\}$, in equation (6.1), to perform the best PAPR reduction performance. The key idea consists in fitting, iteratively, these

PCSs to their associated time-domain clipping-noise signals. These latter are computed by clipping the time-domain signals $\{\mathbf{a}_{m_t}^t\}$, at each antenna. Thereby, we compute first the precoded data $\{\mathbf{W}_n\mathbf{s}_n, \forall n\}$ that satisfy $\mathbf{G}_n\mathbf{W}_n\mathbf{s}_n = \mathbf{s}_n, \forall n \in \chi$. Then, we compute the clipped signals $\{\mathbf{a}_{m_t}^t\}$ as follows

$$\bar{a}_{m_t}(k) \quad = \begin{cases} a_{m_t}(k), & if\ |a_{m_t}(k)| < \lambda \\ \lambda e^{j\phi(k)}, & if\ |a_{m_t}(k)| > \lambda \end{cases}, \tag{6.5}$$

where $a_{m_t}(k) = |a_{m_t}(k)|e^{j\phi(k)}$, $\phi(k)$ is the phase of $a_{m_t}(k)$ and λ denotes the clipping threshold. In order to have the best PAPR reduction, λ has to be defiend as follows [119]

$$\lambda = \sqrt{\sigma_a^2 ln\left(\frac{N}{|\chi|}\right)} \tag{6.6}$$

where σ_a^2 denotes the variance of the modulated signal at each antenna.

Finally, the original frequency-domain clipping-noise associated to the m_t-th transmit antenna is $\mathbf{e}_{m_t}^t = DFT\left(\bar{\mathbf{a}}_{m_t} - \mathbf{a}_{m_t}\right)$. Here, the vector $\mathbf{e}_n$, associated to the n-th subcarrier, is collected from the M_t vectors $\left(\mathbf{e}_1^t, \mathbf{e}_2^t, ..., \mathbf{e}_{M_t}^t\right)$.

In order not to damage the transmission quality (i.e., perfect MUI), the added PCSs $\{\mathbf{r}_n\}$ are constrained to lie in the null-spaces of their associated MIMO channel matrices such that they do not disturb the signals received by M_r users through the $|\chi|$ active subcarriers. In addition, $\mathbf{r}_n$ has to respect the out-of-band constraint such that it has to be set to zero on the guard-band, as shown by the following equation

$$\begin{cases} \mathbf{r}_n = \mathbf{e}_n, & n \in \chi \\ \mathbf{r}_n = \mathbf{0}_{M_t \times 1}, & n \in \chi^c. \end{cases} \tag{6.7}$$

Thereby, the precoded version $\mathbf{c}_n = \mathbf{V}_n\mathbf{r}_n$ is added to the precoded data instead of $\mathbf{e}_n$, as shown in equation (6.1), where $\mathbf{V}_n$ represents the n-th MIMO channel null-space.

Due to the reconstruction of the precoded PCSs from their projections onto the MIMO channel null-spaces and the active data subcarriers in χ, it is obvious that the considered PCSs, at each iteration, can be smaller than their associated clipping noises when the traditional clipping and control (CC) method is employed in massive MIMO-OFDM systems. Hence, a regularization factor is needed in order to generate the optimal PCSs, leading then to a fast convergence toward the optimal solution. The regularization factor can be calculated using least-square approximation (LSA), as explained in [135]. It is defined as

$$p_n = \frac{\sum_{m_t} |\mathbf{c}_n||\mathbf{e}_n|}{\sum_{m_t} |\mathbf{c}_n|^2}, \qquad n \in \chi \tag{6.8}$$

Using such regularization factor, the amplitudes of PCSs, $\mathbf{c}_n$, generated by LSA, almost equal to those of the original clipping noise $\mathbf{e}_n$. Then, we transmit $p_n\mathbf{V}_n\mathbf{r}_n$ instead of $\mathbf{V}_n\mathbf{r}_n$. Obviously, it may reduce the number of iterations to achieve the optimal PAPR reduction.

6.2.2 Linear Data and PCS Precoders for low-PAPR massive MIMO-OFDM

In this section, I describe two developed algorithms that consist of iterative CC method with the peak-canceling signals constrained in the null-spaces of the associated MIMO channel matrices. The goal is to design signals $\{\mathbf{x}_n\}$ which satisfy the MU precoding (i.e., in-band and out-of-band constraints) and

meanwhile their time-domain signals have low PAPR. It is worth noticing that the proposed formulation can perform the PAPR reduction problem and the MU precoding, jointly (1st algorithm) or separately (2sd algorithm). Note that MU precoding and PAPR reduction are using two orthogonal spaces (beamforming space for data transmission and null-space for PAPR reduction). Therefore, we developed two algorithms that are summarized in subsection 6.2.3 and 6.2.4 ,respectively.

6.2.3 1st Algorithm: Gradient-iterative method based MU-PP-GDm algorithm

In order to reduce the computational complexity required for data and PCS precoders, the algorithm MU-PP-GDm, which is introduced in [J15], adopts gradient-iterative method for data and PCS precoding. Here, the null-spaces of channel matrices $\{\mathbf{V}_n\}$ are computed using the singular value decomposition (SVD) as explained in [J15], where the $\{\mathbf{V}_n\}$ are of dimension $M_t \times (M_t - M_r)$ instead of $M_t \times M_t$. Furthermore, MU-PP-GDm aims at computing $\mathbf{r}_n$ such that $\mathbf{V}_n\mathbf{r}_n$ is very close to $\mathbf{e}_n$. thereby, it is equivalent to find the solution $\tilde{\mathbf{r}}_n$ according to the following simple convex optimization problem, in equation (6.9), with taking into consideration in-band and out-of-band constraints.

$$\underset{\{\tilde{\mathbf{r}}_n\}}{minimize} \quad G(\mathbf{r}_n) = \|\mathbf{V}_n\mathbf{r}_n - \mathbf{e}_n\|_2^2, \qquad n \in \chi$$

$$subject\ \ to \begin{cases} \mathbf{s}_n = \mathbf{H}_n\mathbf{d}_n, & n \in \chi \\ \mathbf{e}_n = \mathbf{0}_{(M_t - M_r)\times 1}, & n \in \chi^c \end{cases} \tag{6.9}$$

In this algorithm [J15], the joint MU precoding and PAPR reduction is achieved by alternately repeating the PAPR reduction process using the CC method, restoring the restrictions on the PAPR reduction signal components using null-spaces of MIMO channels and performing MU precoding. To make the problem tractable, the equality constraint $\mathbf{s}_n = \mathbf{H}_n\mathbf{d}_n$, is relaxed as

$$\underset{\{\tilde{\mathbf{r}}_n, \tilde{\mathbf{d}}_n\}}{minimize} \quad J(\mathbf{d}_n, \mathbf{r}_n) = F(\mathbf{d}_n) + G(\mathbf{r}_n), \quad n \in \chi$$

$$subject\ \ to \begin{cases} \tilde{\mathbf{d}}_n = \mathbf{0}_{M_t\times 1}, & n \in \chi^c \\ \tilde{\mathbf{r}}_n = \mathbf{0}_{(M_t - M_r)\times 1}, & n \in \chi^c \end{cases} \tag{6.10}$$

The search directions of the steepest descent method at the iterate $\mathbf{d}_n^{(l)}$ and $\mathbf{r}_n^{(l)}$ are determined by the negative gradient of J at, respectively, $\mathbf{d}_n^{(l)}$ (denoted by $-\nabla_d^l J(\mathbf{d}_n^{(l)}, \mathbf{r}_n^{(l)})$) and $\mathbf{r}_n^{(l)}$ (denoted by $-\nabla_r^l J(\mathbf{d}_n^{(l+1)}, \mathbf{r}_n^{(l)})$), where

$$\nabla_d^l J(\mathbf{d}_n^{(l)}, \mathbf{r}_n^{(l)}) = \frac{2}{\mathcal{L}_{d_n}} \mathbf{H}_n^H \left(\mathbf{H}_n\mathbf{d}_n^{(l)} - \mathbf{s}_n\right), \quad n \in \chi \tag{6.11}$$

and

$$\nabla_r^l J(\mathbf{d}_n^{(l+1)}, \mathbf{r}_n^{(l)}) = \frac{2}{\mathcal{L}_{r_n}} {\mathbf{V}_n}^H \left(\mathbf{V}_n\mathbf{r}_n^{(l)} - \mathbf{e}_n^{(l+1)}\right), \quad n \in \chi \tag{6.12}$$

where $\mathcal{L}_{d_n} = 2\sigma_{max}^2(\mathbf{H}_n)$ and $\mathcal{L}_{r_n} = 2\sigma_{max}^2(\mathbf{V}_n)$ are the Lipschitz constants [136] for, respectively, $\|\mathbf{H}_n\mathbf{d}_n - \mathbf{s}_n\|_2^2$ and $\|\mathbf{V}_n\mathbf{r}_n - \mathbf{e}_n\|_2^2$.

The details of the proposed MU-PP-GDm is summarized in Table **Algorithm1**. It is followed by a computational complexity analysis of that algorithm. The complexity is expressed in terms of the number of floating point operations (FLOPs). Here, we consider one FLOP as one scalar complex multiplication [137] and neglect the computational complexity of matrix and vector additions. Specifically, we consider the number of complex multiplications required at the BS for generating τ precoded data and PCS vectors, where τ is the number of transmit symbols generated in one channel coherence interval.

Algorithm1: The MU-PP-GDm algorithm

Given a set of N modulated complex symbols $\{\mathbf{s}_n\}$.

1: **Initialize** $\mathbf{x}_n^{(1)} = \mathbf{0}_{M_t \times 1}$,
$\mathbf{e}_n^{(1)} = \mathbf{0}_{(M_t - M_r)\times 1}$,
$\mathbf{dx}_n^{(0)} = \mathbf{0}_{M_t \times 1}$,
$Lx_n = 2\sigma^2_{max}(\mathbf{H}_n)$, $Le_n = 2\sigma^2_{max}(\mathbf{V}_n^0)$,
and set the maximal iteration number N_{iter}
and the momentum term μ

2: **for** l=1,...,$maxIter$ **do**

3: $\mathbf{dx}_n^{(l)} = \frac{2}{\mathcal{L}_{x_n}} \mathbf{H}_n^H \left(\mathbf{H}_n \mathbf{x}_n^{(l)} - \mathbf{s}_n\right) + \mu \mathbf{dx}_n^{(l-1)}, \quad \forall n \in \chi$

4: $\mathbf{x}_n^{(l+1)} = \mathbf{x}_n^{(l)} - \mathbf{dx}_n^{(l)}, \quad \forall n \in \chi$

5: $\mathbf{a}_{m_t}^{t(l+1)} = IFFT\left(\mathbf{x}_{m_t}^{t(l+1)}\right), \quad \forall m_t = 1...M_t$

6: $\mathbf{e}_{m_t}^{t(l+1)} = FFT\left(\bar{\mathbf{a}}_{m_t}^{t(l+1)} - \mathbf{a}_{m_t}^{t(l+1)}\right)$

7: $\mathbf{r}_n^{t(l+1)} = \mathbf{r}_n^{t(l)} - \frac{2}{\mathcal{L}_{\tau_n}} {\mathbf{V}_n}^H \left(\mathbf{V}_n \mathbf{r}_n^{(l)} - \mathbf{e}_n^{(l+1)}\right), \quad \forall n \in \chi$

8: $\mathbf{p}_n = \frac{\sum_k |\mathbf{V}_n \mathbf{r}_n^{(l+1)}||\mathbf{e}_n^{(l+1)}|}{\sum_k |\mathbf{V}_n \mathbf{e}_n^{(l+1)}|^2}, \quad \forall n \in \chi$

9: $\mathbf{x}_n^{(l+1)} = \mathbf{x}_n^{(l+1)} + \mathbf{p}_n \mathbf{V}_n \mathbf{r}_n^{(l+1)}, \quad \forall n \in \chi$

10: **end for**

11: **return** $\{\tilde{\mathbf{x}}_n = \mathbf{x}_n^{(N_{iter}+1)}\}$

Hence, using the MU-PP-GDm algorithm only matrix-vector multiplications are performed and no matrix inversion or matrix-matrix multiplication is required. One can observe that the precoded data vector $\mathbf{d_n}$ can be expressed as

$$\mathbf{d}_n^{(l)} = \begin{cases} \mathbf{H}_n^H \mathbf{s}_n, & l = 1 \\ \mathbf{H}_n^H (\mathbf{H}_n \mathbf{d}_n^{(l-1)}), & 2 \le l \le N_{iter}, \end{cases} \tag{6.13}$$

where l denotes the iteration index.

Hence, it requires $\tau|\chi| M_t M_r (2N_{iter} - 1)$ FLOPS to compute the precoded data vectors for $\tau|\chi|$ data symbols. Concerning PCS precoding, $\tau \left[|\chi| \left(M_t(M_t - Mr) + M_t^2\right) + 2M_t N log(N)\right]$ complex multiplications are required at each iteration. Thereby, the overall complexity required by MU-PP-GDm to compute both data and PCS precoded vectors is given by equation (6.14).

$$C_{MU-PP-GDm} = \tau N_{iter} \left[2M_t N log(N) + 2|\chi| M_t^2 - 2|\chi| M_t M_r\right] \tag{6.14}$$

6.2.4 2sd algorithm: disjoint MU precoding and PAPR reduction

Contrary to the 1st algorithm, which performs jointly MU precoding and PAPR reduction, this algorithm aims at performing, first, MU precoding and then PAPR reduction over the iterative CC method. The algorithm is summarized in Table **Algorithm2**.

Algorithm2: disjoint MU precoding and PAPR reduction

Given a set of N modulated complex symbols $\{\mathbf{s}_n \in \mathbb{C}^{M_r \times 1}\}$.

1: **Set** $\mathbf{d}_n = \mathbf{0}_{M_t \times 1}$, $n = 1, ..., N$, the maximal iteration number N_{iter}

2: **Compute** the precoded data vector $\mathbf{d}_n = \mathbf{W_n s_n}$, $\forall n \in \chi$

3: **Initialize** $\mathbf{x}_n^{(1)} = \mathbf{d}_n$, $\forall n$

4: **for** l=1,...,$maxIter$ **do**

5: $\mathbf{a}_{m_t}^{t(l)} = IFFT\left(\mathbf{x}_{m_t}^{t(l)}\right)$, $\forall m_t = 1...M_t$

6: $\mathbf{e}_{m_t}^{t(l)} = FFT\left(\bar{\mathbf{a}}_{m_t}^{t(l)} - \mathbf{a}_{m_t}^{t(l)}\right)$

7: $\mathbf{r}_n^{(l)} = \mathbf{e}_n^{(l)}$, for $n \in \chi$ and $\mathbf{r}_n^{(l)} = \mathbf{0}_{M_t \times 1}$, for $n \in \chi^c$

8: $\mathbf{p}_n = \frac{\sum_{m_t} |\mathbf{V}_n \mathbf{r}_n^{(l)}||\mathbf{e}_n^{(l)}|}{\sum_{m_t} |\mathbf{V}_n \mathbf{r}_n^{(l)}|^2}$, $\forall n \in \chi$

9: $\mathbf{x}_n^{(l+1)} = \mathbf{x}_n^{(l)} + \mathbf{p}_n \mathbf{V}_n \mathbf{r}_n^{(l)}$, $\forall n \in \chi$

10: **end for**

11: **return** $\{\mathbf{x}_n^{(Niter+1)}\}$

Looking at the proposed algorithm, it computes the precoded data vectors in Step 2, the clipping-noises in Steps 5 and 6 and its constrained version in Step 7. Finally, it updates, in Step 9, the transmitted frequency-domain precoded vectors $\{\mathbf{x}_n\}$ by adding the scaled precoded PCS vectors $\{p_n \mathbf{V}_n \mathbf{r}_n\}$. One can note that its computational complexity is dominated by Steps 2, 5, 6 and 9. In the following three subsections, we analyze the computational complexity of the proposed algorithm using different data and PCS precoder designs, to compute $\{\mathbf{W}_n \mathbf{s}_n\}$ (Step 2) and $\{p_n \mathbf{V}_n \mathbf{r}_n\}$ (Step 9).

Table 6.1 summarizes the three studied methods in, respectively, subsections 6.2.4.A, 6.2.4.B and 6.2.4.C.

Table 6.1: Summary of the three studied methods for data and PCS precoders.

	Data precoding	PCS precoding	Total complexity
RZF-OPNS	Computation of $\mathbf{W}_n$ using matrix inversion as in (6.15) Complexity is given in (6.16)	Computation of $\mathbf{V}_n$ using matrix inversion as in (6.17) Complexity is given in (6.18)	is given in (6.19)
POLY-POLY-Horner	Computation of $\mathbf{W}_n$ using M-POLY as in (6.20) $\mathbf{d}_n$ is computed using Horner's implementation as in (6.28)	Computation of $\mathbf{V}_n$ using M-POLY as in (6.25) $\mathbf{c}_n$ is computed using Horner's implementation as in (6.29)	is given in (6.30)
POLY-OPNS	Computation of $\mathbf{W}_n$ using M-POLY as in (6.20) $\mathbf{d}_n$ is computed using Horner's implementation as in (6.28)	Computation of $\mathbf{V}_n$ using matrix inversion as in (6.17) Complexity is given in (6.18)	is given in (6.31)

A. RZF data and OPNS PCS precoders (RZF-OPNS)

For data precoding, the regularized zero-forcing (RZF) precoder is the most widely used solution for the optimization problem in (6.35), which is given by

$$\mathbf{W}_n = \mathbf{H}_n^H \left(\mathbf{H}_n \mathbf{H}_n^H + \xi_1 \mathbf{I}_{M_r}\right)^{-1}, \qquad \forall n \tag{6.15}$$

where ξ_1 is a regularization constant.

It can be seen that the computational complexity required, in one channel coherence interval, for data precoding using RZF is comprised of the complexity required for computing one precoding matrix and τ precoded data vectors, for each active subcarrier. Generating such precoding matrix requires, for $|\chi|$ active subcarriers, $\left(2M_t M_r^2 + M_r^3\right)|\chi|$ FLOPs. Then, $\tau|\chi|M_t M_r$ FLOPs are required to perform the vector-matrix multiplications and to generate $\tau|\chi|$ precoded data vectors. Finally, the total computational complexity required by RZF data precoder is

$$C_{RZF} = \left(2M_t M_r^2 + M_r^3 + \tau M_t M_r\right)|\chi| \tag{6.16}$$

Concerning PCS precoder at the n-th subcarrier, the PCS is designed to lie into the null-spaces of the estimated channels between all M_r users and the BS. Then, the OPNS $\mathbf{V}_n$ is given by

$$\mathbf{V}_n = \mathbf{I}_{M_t} - \mathbf{H}_n^H \left(\mathbf{H}_n \mathbf{H}_n^H\right)^{-1} \mathbf{H}_n, \qquad \forall n \tag{6.17}$$

which has rank $M_t - M_r$ and exists only if $M_r < M_t$.

To compute the precoding matrices $\{\mathbf{V}_n\}$ for all activated subcarriers in χ, which are computed one time in one coherence interval, we require $\left(3M_t M_r^2 + M_r^3\right)|\chi|$ FLOPs. In the loop of the proposed algorithm, the computing of τ PCS precoded vectors entails 1) the computing of the clipping noises $\{e_n\}$ by the operation clipping and control and the N-point IDFT, which has a complexity of $2M_t N log(N)$ FLOPs and 2) the projection of $\{\mathbf{e_n}\}$ onto the channel null-space matrices $\{\mathbf{V_n}\}$ that requires $|\chi|$ matrix-vector multiplications with a complexity of $M_t^2|\chi|$ FLOPs. Hence, the total complexity is

$$C_{OPNS} = N_{iter}\left(|\chi|M_t^2 + 2M_t N log(N)\right), \tag{6.18}$$

where N_{iter} denotes the maximal iteration number.

The overall complexity of the algorithm when using RZF and OPNS for, respectively, data and PCS precoding is given by equation (6.19).

$$C_{RZF-OPNS} = |\chi|\left(5M_t M_r^2 + 2M_r^3\right) + \tau\left[M_t M_r|\chi| + N_{iter}\left(M_t^2|\chi| + 2M_t N log(N)\right)\right] \tag{6.19}$$

B. M-POLY based data and PCS precoders (POLY-POLY-Horner)

In order to mitigate the high computational complexity imposed by the previous methods, while achieving good performance, we propose to replace the matrix inversion and matrix-matrix multiplication by matrix polynomial decompositions (M-POLY) to compute the precoded data and PCS vectors.

The proposed M-POLY data precoder, $\mathbf{W}_n$, for the n-th subcarrier has the form

$$\mathbf{W_n} = \frac{1}{\sqrt{M_t}} \bar{\mathbf{H}}_n^H \sum_{i=0}^{J} w_i \left(\bar{\mathbf{H}}_n \bar{\mathbf{H}}_n^H\right)^i, \tag{6.20}$$

where $\bar{\mathbf{H}}_n = \frac{1}{\sqrt{M_t}}\mathbf{H}_n$ and $\mathbf{w} = [w_0, ..., w_J]^T$ contains the real-valued coefficients of the M-POLY data precoder, which have to be optimized. It has been shown in [128] [133] that, for $M_r, M_t \to \infty$, the optimum coefficients $\mathbf{w}$ do not depend on the fast channel fluctuations and can be computed using results from random matrix theory and free probability theory [138] [139]. The optimal coefficient vector $\mathbf{w}$ minimizes the average mean square error (MSE) between transmitted and received data corresponding to all users. Using the solution provided in [128], a closed-form expression for the optimum coefficients is defined as

$$\mathbf{w}_{opt} = \gamma \boldsymbol{\Xi}^{-1} \boldsymbol{\Phi}, \tag{6.21}$$

where the elements of matrix $\boldsymbol{\Xi}$ and vector $\boldsymbol{\Phi}$ are, respectively, given by

$$[\boldsymbol{\Xi}]_{m,n} = B_1 B_2 \xi^{(m+n)} + (1 - B_1 B_2)\xi^{(m)}\xi^{(n)} + B_2 \sigma_b^2 \xi^{m+n-1}, \tag{6.22}$$

and

$$[\boldsymbol{\Phi}]_m = \xi^{(m)}, \tag{6.23}$$

where B_1 and B_2 are defined as $B_1 = Tr(\mathbf{KP})$ and $B_2 = Tr((\mathbf{KP})^{-1})$. Here, $\mathbf{P}$ denotes the diagonal power allocation matrix and $\xi^{(m)}$ represents the m-th order moment of the sum of the eigenvalue of matrix $\bar{\mathbf{H}}_n \bar{\mathbf{H}}_n^H$, which is defined in closed-form by [[128], Theorem 2]

$$\xi^{(m)} = \sum_{i=0}^{m-1} \binom{m}{i} \binom{m}{i+1} \frac{\delta^i}{m}, \tag{6.24}$$

when $M_r, M_t \to \infty$ with their ratio $\delta = M_r/M_t$ being constant. Finally, γ is a normalization factor such that $Tr(\mathbf{W}_n \mathbf{W}_n^H) = 1$ holds.

For the PCS precoding, the proposed M-POLY precoder is given by

$$\mathbf{V}_n = \mathbf{I}_{M_t} - \bar{\mathbf{H}}_n^H \left(\sum_{i=0}^{Q} v_i \left(\bar{\mathbf{H}}_n \bar{\mathbf{H}}_n^H \right)^i \right) \bar{\mathbf{H}}_n, \tag{6.25}$$

where $\mathbf{v} = [v_0, ..., v_Q]$ are the real-valued coefficients of the M-POLY PCS precoder, which have to be optimized. The optimization goal is the minimization of asymptotic average PCS (PAPR reduction process) leakage caused to all users. The corresponding optimization problem is formulated as [133]

$$\begin{aligned} &\underset{\{\mathbf{v}\}}{minimize} \quad \beta \mathbb{E}\left[Tr(\mathbf{G}_n \mathbf{V}_n \mathbf{V}_n^H \mathbf{G}_n^H) \right] \\ &subject\ to\ \ Tr(\mathbf{V}_n \mathbf{V}_n^H) = 1/\delta - 1. \end{aligned} \tag{6.26}$$

The solution of the formulation in (6.26) is provided in [[133] Theorem 2] and the optimal coefficient vector $\mathbf{v}_{opt}$ is given by

$$\mathbf{v}_{opt} = \boldsymbol{\Sigma}^{-1} \boldsymbol{\Theta}, \tag{6.27}$$

where $[\boldsymbol{\Sigma}]_{m,n} = \xi^{m+n+1} + \epsilon \xi^{m+n}$ and $\boldsymbol{\Theta} = [\xi^2 + \epsilon\xi, ..., \xi^{Q+2} + \epsilon\xi^{Q+1}]$, where ϵ is chosen such that $Tr(\mathbf{V}_n \mathbf{V}_n^H) = 1/\delta - 1$

One can note that coefficient vector $\mathbf{w}_{opt}$ and $\mathbf{v}_{opt}$ does not depend on channel estimates, and hence, can be calculated off-line using equations (6.21) and (6.27).

One efficient way to calculate the precoded data and precoded PCS vectors, via the M-POLY precoding scheme, is when using Horner's rule [140]. First, the precoded data vectors, $\{\mathbf{d}_n\}$, can be obtained as

$$\mathbf{d}_n = \frac{\bar{\mathbf{H}}_n^H}{\sqrt{M_t}} \left(w_0 \mathbf{s}_n + w_1 \bar{\mathbf{H}}_n \bar{\mathbf{H}}_n^H \left(\mathbf{s}_n + \frac{w_2}{w_1} \bar{\mathbf{H}}_n \bar{\mathbf{H}}_n^H \left(\mathbf{s}_n + \frac{w_3}{w_2} \bar{\mathbf{H}}_n \bar{\mathbf{H}}_n^H \mathbf{s}_n ... \right) \right) \right), \tag{6.28}$$

where, we first multiply $\mathbf{s}_n$ with matrix $\bar{\mathbf{H}}_n^H$, then we multiply the result with the channel matrix $\bar{\mathbf{H}}_n$ and finally add $\mathbf{s}_n$ to the resulting vector. This operation is performed J times and the resulting vector is multiplied by $\bar{\mathbf{H}}_n^H$. It can be shown that in order to compute all the precoded data vectors associated to all activated subcarriers, it results in a total complexity of $\tau(2J+1)M_t M_r|\chi|$.

Using the same way as in (6.28), we can compute $\{\mathbf{c}_n\}$ using equation (6.29).

$$\mathbf{c}_n = \mathbf{r}_n - \left(v_0 \bar{\mathbf{H}}_n^H \bar{\mathbf{H}}_n \left(\mathbf{r}_n + \frac{v_1}{v_0} \bar{\mathbf{H}}_n^H \bar{\mathbf{H}}_n \left(\mathbf{r}_n + ... \right) \right) \right), \tag{6.29}$$

where, $\mathbf{c}_n$ is efficiently calculated by first multiplying $\mathbf{r}_n$ with the channel matrix $\bar{\mathbf{H}}_n$, then the resulting vector is multiplied with $\bar{\mathbf{H}}_n^H$. After adding $\mathbf{r}_n$ to the latter resulting vector, we repeat these operations Q times. This leads to a complexity of $2(Q+1)M_t M_r|\chi|$. Therefore, with taking into consideration of computing the clipping noises by the clipping and control approach and the N-point IDFT, the computational complexity to compute τ precoded PCS vectors, over N_{iter} iterations, is $\tau N_{iter}(2M_t N log(N) + 2(Q+1)M_t M_r|\chi|)$.

Hence, the overall complexity needed by the proposed algorithm when using the M-POLY approach to compute both the precoded data and PCS vectors is given by equation (6.30).

$$C_{POLY-POLY} = \tau \left[(2J+1)M_t M_r|\chi| + N_{iter}(2M_t N log(N) + 2(Q+1)M_t M_r|\chi|) \right] \tag{6.30}$$

C. M-POLY data and OPNS PCS precoders (POLY-OPNS)

An alternative to the above mentioned methods is to compute the precoded data vectors using M-POLY as given by equation (6.28) and compute the precoded PCS vectors using the OPNS precoder as explained in subsection (6.2.4). Thereby, the overall computational complexity required by this POLY-OPNS precoding scheme is given by equation (6.31).

$$C_{POLY-OPNS} = |\chi|(3M_t M_r^2 + M_r^3) + \tau \left[(2J+1)M_t M_r|\chi| + N_{iter}(2M_t N log(N) + |\chi| M_t^2) \right] \tag{6.31}$$

6.2.5 Performance Evaluation

In this section, we carry out simulations to illustrate the performance of the considered low-PAPR massive MU-MIMO-OFDM system. We consider an uncoded OFDM with $N = 512$ subcarriers (i.e., the number of DFT/IDFT points) and use a spectral map χ, in which $|\chi| = 128$ subcarriers are used for data transmission. We recall that we specify some unused subcarriers at both ends of the used band. These latter serve, in one hand, to ensure that the proposed low-PAPR precoder does not generate any spectrum regrowth. In another hand, it corresponds to $L = 4$-oversampling in the time-domain in order to measure the PAPR levels accurately. A 16-QAM with Gray mapping is considered. Note that we adopt the suboptimal power allocation $\mathbf{P} = \mathbf{K}^{-1/2}$ and instead of transmitting $\{\mathbf{s}_n\}$, we transmit $\{\mathbf{P}\mathbf{s}_n\}$. Moreover, the wireless channel is assumed to be frequency-selective as modeled in (6.4) with $L_c = 8$ taps. All presented results are averaged over 1000 channel realizations.

Complexity-Performance Tradeoff of M-POLY Data and PCS Precoders

We start by evaluating the performance of the studied M-POLY data and PCS precoders in order to identify the values of J and Q (see equations (6.20) and (6.25)) that ensures a good complexity-performance tradeoff. To this end, we consider a massive MU-MIMO-OFDM system with $M_t = 500$ antennas at the BS and serving $M_r = 100$ single-antenna users to be in a case where the precoding complexity is an issue. In Figure 6.1, we depict the normalized mean square error (NMSE) for the studied M-POLY data and PCS precoders for different values of J and Q. One can note that the performance of the M-POLY precoders quickly improves as the number of terms of the two polynomials J and Q increase. Moreover, they can achieve a NMSE of -35dB when $J = 5$ and $Q = 3$, which can be a sufficient performance needed in practical systems. It is worth to point out that choosing larger values for J and Q gives better performance, however doing so requires more computational complexity. Furthermore, This latter is more sensitive to Q than to J because of the computing of the precoded PCSs depends on the number of iterations as shown by equation (6.30). That is why we vary J from 0 to 10 while Q from 0 to only 3.

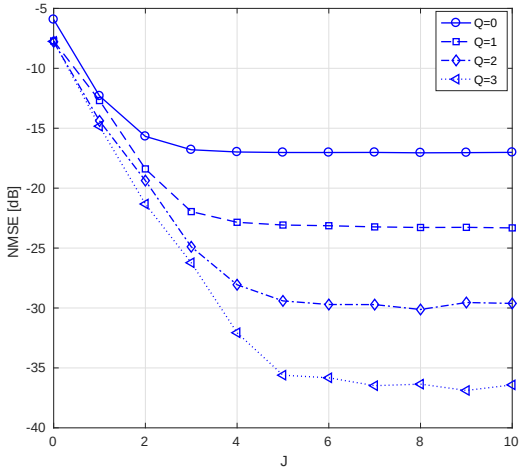

Figure 6.1: NMSE of M-POLY precoding (with different J and Q) for $M_t = 500$, $M_r = 100$, $N_{iter} = 5$ and 16-QAM.

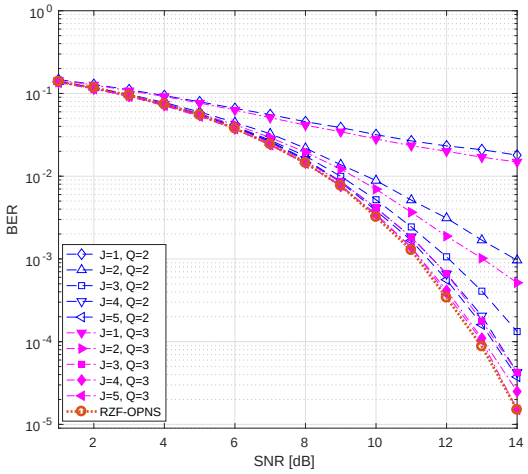

Figure 6.2: BER of RZF-OPNS precoding and M-POLY precoding (with different J and Q) for $M_t = 500$, $M_r = 100$, $N_{iter} = 5$ and 16-QAM.

Figure 6.2 shows more directly the relationship between the user performance and M-POLY orders J and Q. Hence, we show the bit error rate (BER) versus the signal-to-noise ratio (SNR) for the studied M-POLY data and PCS precoders for different values of J and Q and compare them to those of RZF-OPNS precoders. Indeed, we assume that the channel is perfectly known, in order to be in a regime where the RZF-OPNS based data and PCS precoders are perfect (i.e., the RZF achieves excellent transmission quality and the OPNS does not leak any interference) and it serves as a reference. Again, we can see that the M-POLY precoders quickly approaches the performance of the RZF-OPNS precoders as the polynomial orders J and Q increase, and they achieve similar performance to the RZF-OPNS precoders when $J = 5$ and $Q = 3$. The proposed M-POLY precoders never outperform the RZF-OPNS ones, which is natural since M-POLY precoding is an approximation of RZF-OPNS.

In the following, we will use these polynomial orders ($J = 5$ and $Q = 3$) to, first, compare the computational complexity of the M-POLY data and PCS precoders with the other studied precoders.

Then, we evaluate its performance in terms of PAPR reduction and hence its capability to make us able to operate the power amplifiers with lower IBO. This will enhance the amplifier efficiency and then the global energy efficiency of the studied massive MU-MIMO-OFDM system.

Computational complexities comparison

We start by comparing the computational complexities of the four studied data and PCS precoders, the 'RZF-OPNS', 'MU-PP-GDm' and 'POLY-OPNS' precoders with that the proposed 'POLY-POLY-Horner' precoder based on the Horner's implementation rule.

According the aforementioned closed-form expressions (see section 6.2.2) and the configuration given in section 6.2.5, it is possible to numerically assess the complexities of the studied data and PCS precoders. In particular, Figs. 6.3 and 6.4 show the computational complexity (in GigaFLOPs) versus the number of users in the cell. Here, the number of BS antennas was assumed to be constant $M_t = 500$, the number of iterations is fixed to $N_{iter} = 5$ and the channel coherence interval is fixed to $\tau = 1$ and $\tau = 10$ in Figs. 6.3 and 6.4, respectively. For the given setting, the performance gains in terms of PAPR reduction of the studied precoders are substantial and almost similar. Regarding these results, one can note that the M-POLY data and PCS precoders have a substantial lower computational complexity than the other precoders for $M_r < M_t/5$. However, even for larger M_r the POLY-POLY-Horner based precoders still have lower computational complexity than the precoders based on matrix inversion like 'RZF-OPNS' and 'POLY-OPNS'. Furthermore, they are preferable as they do not incur the stability issues that may arise in the implementation of the large-scale matrix inversions required for RZF and/or OPNS. It is worth to mention that the 'MU-PP-GDm' algorithm that adopts an alternate data and PCS precoding becomes more interesting (i.e., it has lower computational complexity) than the POLY-POLY-Horner based precoders when the number of users is very large. The break-even point, where 'MU-PP-GDm' outperforms the M-POLY based precoders, is at $M_r < M_t/5$.

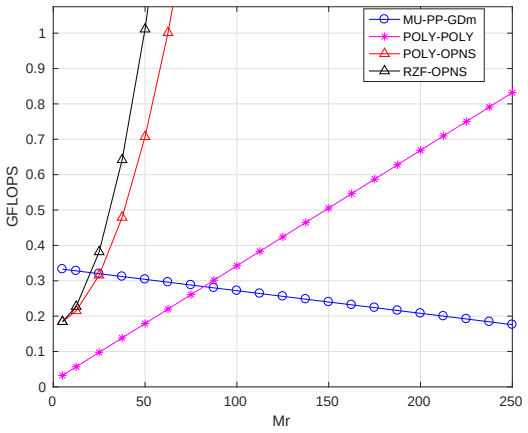

Figure 6.3: Computational complexity of different linear precoders for a system with $M_t = 500$, $N_{iter} = 5$ and $\tau = 1$.

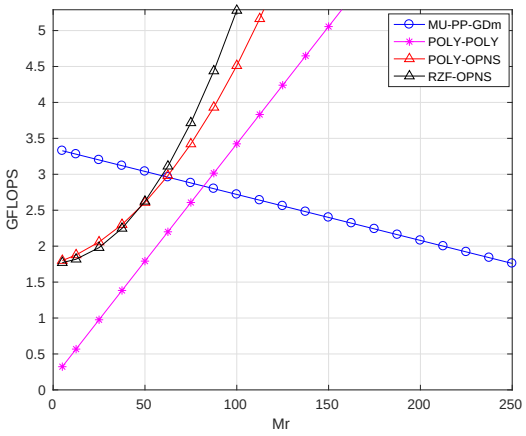

Figure 6.4: Computational complexity of different linear precoders for a system with $M_t = 500$, $N_{iter} = 5$ and $\tau = 10$.

Performance Evaluation : PAPR reduction

In this subsection, we discuss the convergence rate of the two proposed algorithms based on a sequential design, where the RZF-OPNS, POLY-OPNS and POLY-POLY-Horner are considered, and an alternate design spanned by the MU-PP-GDm approach. Figure 6.5 shows the average PAPR versus the number of iterations for different numbers of users. In order to simplify the presentation of results, we plot only the performance of the 'POLY-POLY-Horner' which are similar to the ones given by RZF-OPNS and POLY-OPNS. From these results, we can first note that POLY-POLY-Horner based precoding yields a larger PAPR reduction gain than the MU-PP-GDm. It can achieve, with only 5 iterations, an average PAPR of 2.8dB, 3dB and 4.5dB when the number of user is, respectively, $M_r = 25$, $M_r = 100$ and $M_r = 250$. Moreover, The PAPR reduction gain is reduced when the number of users is increased and this result is expected because of the null-space, onto which the PCSs are projected, is reduced.

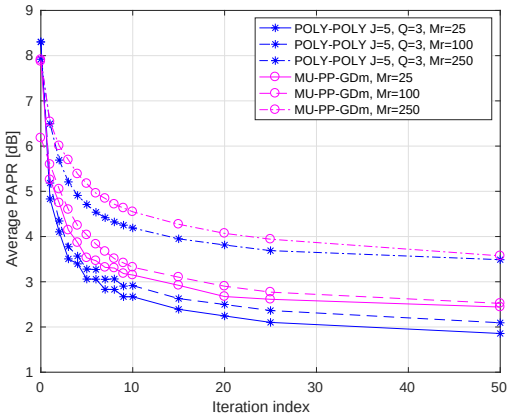

Figure 6.5: Convergence rate of PAPR of selfish and collaborative approaches (with different Mr) for $M_t = 500$.

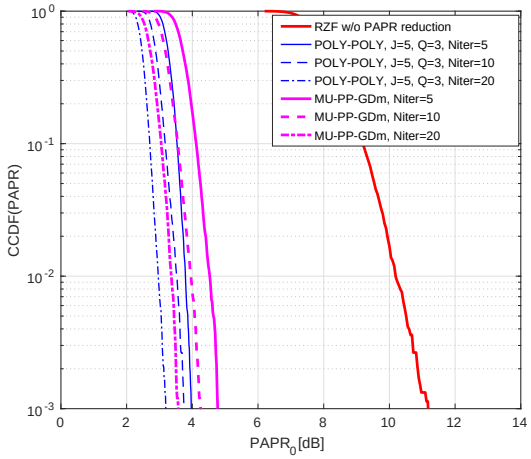

Figure 6.6: PAPR CCDF of selfish and collaborative approaches (with different N_{iter}) for $M_t = 500$ and $M_r = 100$.

Again to evaluate the efficiency of the proposed M-POLY precoding based algorithm in terms of PAPR reduction, Figure 6.6 depicts the complementary cumulative distribution function (CCDF) of the PAPR with different iteration numbers. One can note that the two proposed algorithm offer substantial PAPR reduction compared with the conventional RZF without any PAPR reduction. Indeed, at CCDF of 1%, it achieves a gain of 6.2dB, 6.6dB and 7.1dB when 5, 10 and 20 iterations are, respectively, performed. This is a substantial PAPR reduction gain with low computational complexity spanned by few number of iterations, motivating then the use of low-cost and low-size radio frequency (RF) components in future wireless massive MU-MIMO-OFDM systems. In the following, we address how this translates to multiuser radio link performance under nonlinear PA units.

Performance Evaluation : multiuser radio link bit error rate (BER)

Here, we evaluate and analyze the multiuser radio link bit error rate (BER) of the proposed POLY-POLY-Horner based precoding and the conventional RZF precoders without PAPR reduction, in the case where both exhibit the same antenna transmit power. Figure 6.7 shows the uncoded BER performance

versus the SNR. The RZF precoder with ideal PA units (denoted by RZF ideal PA) is regarded as a benchmark. In order to clearly show the gain achieved by reducing the PAPR of the transmitted signals, we assume that the PAs are ideally linearized, they behave as soft envelope limiter (SEL), such that only the distortions caused by the saturation exist. It can be clearly seen that the performance of the involved low-PAPR precoder surpasses that of the classical RZF, in all cases. The benefit of using the low-PAPR precoder is especially clear from moderate to relatively high SNR. With an IBO of 1dB, the proposed low-PAPR precoder achieves a SNR gain of 4.5dB, compared to the RZF, at BER of 2×10^{-2} with only 5 iterations. When increasing the IBO, e.g. 3dB, the proposed low-PAPR precoder has significantly better performance, very close to those of ideal massive MIMO-OFDM, from moderate to high SNR. Accordingly, the loss of performance due to in-band distortions cannot be compensated by increasing the number of transmit antennas but it needs advanced signal processing techniques (e.g., low-PAPR precoders).

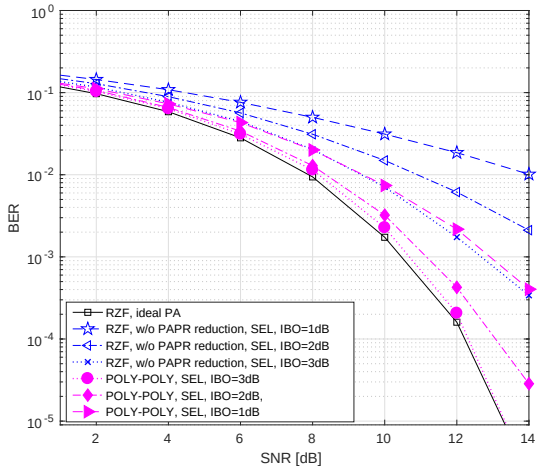

Figure 6.7: BER of M-POLY precoders (with different IBO) for $M_t = 500$, $M_r = 100$ and 16-QAM, in presence of ideally linearized PA.

6.3 PA-aware Massive MIMO DL systems

In addition to PAPR reduction, a digital predistortion (DPD) technique based PA linearization is primordial. In this regard, some approaches have been introduced, in recent literature, which aim at compensating for PA nonlinear behaviour in massive MIMO systems [141] [142] [1]. Nevertheless, the implementation of high-precise DPDs is not suitable for massive MIMO systems due to the large number of DPD modules, which are computationally impractical. In [1], a low-complexity architecture based DPDs have been proposed, which updates the precoder to compensate the gap in performance due to the low-precision related DPDs. In [142], authors proposed a DPD based solution that requires only one DPD component per user to linearize an arbitrary number of PAs enabling then the reduction of the complexity associated to the linearization of the different used PAs. Nevertheless, the associated computational complexity is still unsatisfying, limiting its practical application in massive MU-MIMO.

In this regard, I have been interested in investigating an extremely low-complexity solution, that

does not require any DPD, in order to enable ultra-low latency and highly energy-efficient massive MU-MIMO communications. Moreover, the proposed solution should take into consideration both PAPR reduction and DPD. Then, we have introduced, in [J16], a PA-aware precoding approach that exploits the high dimensional DoFs and designs the precoded signals that, when amplified and passed through the channel, guarantee excellent transmission quality. Furthermore, a new formulation have been proposed for the PA-aware precoding approach. It consists in a simple convex optimization problem which enables efficient, low-complexity and reliable algorithm implementation. The developed algorithm is referred to as MU-PNL-GDm.

In order to evaluate the performance of the proposed approach, we adopted a single carrier massive MU-MIMO system where the BS has M_t RF PAs and serves M_r users. The resulting amplified signals are given by

$$\mathbf{y} = [f_1(x_1), f_2(x_2), ..., f_{M_t}(x_{M_t})]^T = F(\mathbf{x}) \tag{6.32}$$

where $f_{m_t}(.)$ denotes the nonlinear amplification operation of the m_t-th PA. Finally, the input-output relationship of the MU-MIMO dwnlink system with nonlinear PAs can be denoted as

$$\mathbf{r} = \mathbf{H}\mathbf{y} + \mathbf{b} \tag{6.33}$$

The AM/AM and AM/PM conversions are modelled by the modified Rapp model [143] proposed by the 3GPP for the New Radio (NR) evaluation.

6.3.1 Existing PA linearization techniques: DPD Concept and Solutions

Two indirect learning architectures (ILAs) based on DPD, that were studied in [1], are considered for the used massive MU-MIMO system (see Figure 6.8). The first ILA, referred to as ILA1, the DPD-PA

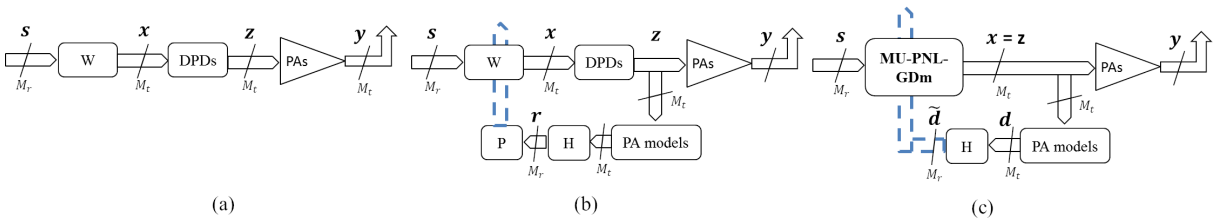

Figure 6.8: (a) Conventional DPD for massive MU-MIMO downlink ILA 1. (b) Precoding-aware DPD solution ILA2 [1]. (c) The proposed MU-PNL-GDm, combines MU precoding and PA nonlinearities compensation [2].

structure is duplicated for each RF chain in the massive MU-MIMO transmitters and associated algorithm is deployed to update independently each DPD. Here, the conventional zero-forcing (ZF) precoding scheme is considered, where the corresponding precoder is $\mathbf{W} = \mathbf{H}^H \left(\mathbf{H}\mathbf{H}^H\right)^{-1}$. Using this classical ILA1, a high-precise, i.e. high complexity, DPD structure is required to extend the operation of the PA into weakly nonlinear region, but its practical application for massive MIMO is limited due to the associated computational complexity. In order to enable the use of low-complexity DPD, an improved ILA is proposed [1], which referred to as ILA2. The key idea consists in finding the appropriate MU precoder for the adopted DPD. Therefore, the classical ILA1 is modified by incorporating the channel matrix and adaptive ZF precoder ($\mathbf{R}$) in the feedback path as shown in Figure 6.8.(b) and we update the precoder

parameter (i.e., $\mathbf{W}$ coefficients) by copying the new estimate parameter of $\mathbf{R}$. Here, the model parameter $\mathbf{R}$ is estimated using an iterative algorithm, where the search direction of the steepest descent method at the iterate $\mathbf{R}_k$ is determined by the negative gradient of the cost function $\|\mathbf{Rr}-\mathbf{x}\|^2$. Then, the precoder matrix is adjusted as

$$\mathbf{R}_{k+1} = \mathbf{R}_k - \lambda \times 2\left(\mathbf{R}_k\mathbf{r}_k - \mathbf{x}_k\right)\mathbf{r}_k^H \tag{6.34}$$

where λ is the updating rate.

6.3.2 Proposed Joint MU Precoding and Energy-Efficiency enhancement Algorithm

The key idea is to compute the precoded symbols $\mathbf{x}$ that satisfy $\mathbf{Hy} = \mathbf{s}$. Here, we formulate a simple convex optimization problem by minimizing the mean square error (MSE) between the intended signal $\mathbf{s}$ and the amplified precoded signal $\mathbf{y}$ through the channel $\mathbf{H}$ as follows

$$\begin{aligned} \underset{\mathbf{x}}{minimize} \quad & \mathbb{E}\left[\|\mathbf{s}-\mathbf{H}F(\mathbf{x})\|^2\right] \\ subject\ \ to \quad & \mathbb{E}\left[\|\mathbf{x}\|^2\right] \leq P_t \end{aligned} \tag{6.35}$$

The problem in (6.35) is not straightforward to address directly because of the nonlinear operation induced by PAs. Since PA input signals are complex Gaussian, one can decompose the nonlinear signal at the PA output into a linear function of the PA input and an uncorrelated distortion term, by using the well-known Bussgang theorem [144]. Then, we can write the amplified signal in (6.32) as

$$\mathbf{y} = \mathbf{Qx} + \mathbf{d} \tag{6.36}$$

where $\mathbf{Q} = diag\left([q_1, q_2, ..., q_{M_t}]\right)$ is the $M_t \times M_t$ square diagonal matrix with elements of $\{q_{m_t}\}$ on the diagonal. Note that q_{m_t} is the m_t-th PA complex gain and d_{m_t} stands for the added zero-mean distortion noise with variance σ_d^2. As we explained in [J05], these NLD parameters (q_{m_t} and σ_d^2) can be analytically computed for any measured or modelled PA.

Substituting (6.36) in (6.33), we have

$$\mathbf{r} = \mathbf{HQx} + \mathbf{Hd} + \mathbf{z} \tag{6.37}$$

Then, the optimization method in (6.35) can be rewritten as

$$\begin{aligned} \underset{\mathbf{x}}{minimize} \quad & J(\mathbf{x}) = \|\mathbf{HQx} + \mathbf{Hd} - \mathbf{s}\|_2^2 \\ subject\ \ to \quad & \|\mathbf{x}\|_2^2 \leq P_t \end{aligned} \tag{6.38}$$

The considered optimization problem leads to efficient, yet flexible implementation for massive MU-MIMO based systems by avoiding the use of DPDs and enabling low-complexity first order algorithm that only requires matrix-vector multiplications [J16]. The search directions of the steepest gradient descent (GD) method at the iterate $\mathbf{x}^{(l+1)}$ is determined by the negative gradient of the cost function J at $\mathbf{x}^{(l)}$, which is given by

$$\nabla_x J(\mathbf{x}^{(l)}) = 2\mathbf{Q}^H\mathbf{H}^H\left(\mathbf{HQx}^{(l)} + \mathbf{Hd}^{(l)} - \mathbf{s}\right) \tag{6.39}$$

The precoded vector is adjusted as given by (6.40). Here, the gradient descent with momentum (GDm) is considered.

$$\mathbf{x}^{(l+1)} = \mathbf{x}^{(l)} - \Delta\mathbf{x}^{(l)} \tag{6.40}$$

where $\Delta\mathbf{x}^{(l)} = \lambda\nabla_x J(\mathbf{x}^{(l)}, \mathbf{d}^{(l)}) + \mu\Delta\mathbf{x}^{(l-1)}$. The proposed algorithm, referred to as MU-PNL-GDm, is summarized as follows

Algorithm: The MU-PNL-GDm algorithm

Given a set of M_r modulated complex symbols $\mathbf{s}$.

1: **Initialize** $\mathbf{x}^{(1)} = \mathbf{0}_{M_t\times 1}$, $\mathbf{d}_n^{(1)} = \mathbf{0}_{(M_r)\times 1}$, $\Delta\mathbf{x}^{(0)} = \mathbf{0}_{M_t\times 1}$, and set the maximal number of iterations $maxIter$, the learning rate λ and the momentum coefficient μ

2: **for** l=1,...,$maxIter$ **do**

3: $\Delta\mathbf{x}^{(l)} = 2\lambda\mathbf{Q}^H\mathbf{H}^H\left(\mathbf{HQx}^{(l)} + \mathbf{Hd}^{(l)} - \mathbf{s}\right) + \mu\Delta\mathbf{x}^{(l-1)}$

4: $\mathbf{x}^{(l+1)} = \mathbf{x}^{(l)} - \Delta\mathbf{x}^{(l)}$

5: Adjustment of the power of $\mathbf{x}^{(l+1)}$ to the desired IBO.

6: $\mathbf{d}^{(l+1)} = F(\mathbf{x}^{(l+1)}) - \mathbf{Qx}^{(l+1)}$

7: **end for**

8: **return** $\mathbf{x}^{(maxIter+1)}$

6.3.3 Performance assessment and comparison

Table 6.2 shows the MUI and complexity comparison for three different values of IBO (0dB and 3dB). According to these results, one can note that ILA1 can only outperform the EZF (see paper [J16]) in the case when we operate the PA quite far from its saturation region (i.e, IBO=3dB). Otherwise, for low values of IBO, it has the worst MUI performance. The PA input and output are assumed to obey the memoryless modified Rapp model [143] with parameters $G = 16$, $V_{sat} = 1.9$, $p = 1.1$, $A = -345$, $B = 0.17$ and $q = 4$ [143]. One can note that by using DPD in the classical way does not have a great interest when the IBO is low. Note that ILA2 and the proposed MU-PNL-GDm, which exploits the excessive DoFs in massive MU-MIMO, provide very good and satisfying performance achieving gains of about 15 and 10dB over the classical ILA1 and EZF, for IBO=0 and 3dB. It is worth to mention that the achieved gain is more pronounced when IBO goes lower. Most importantly, we note that the proposed MU-PNL-GDm scheme requires about 55% of the computational complexity needed by ILA2, when achieving the same MUI performance.

6.4 Analysis and Cancellation of Inter-Numerology Interference in Massive MIMO-OFDM Downlink Systems

An essential step, which brings more flexibility in the communication system, is the mixed numerologies proposed in 5G New Radio (NR) [145]. Mixed numerologies structures are also included in the 3GPP NR standardization and are widely studied in literature [146] [147] [148] [149] [150]. Although, the usage of mixed numerologies significantly improves the system flexibility, there is a lot of interference between users using different numerologies and the occurred inter-numerology interference (INI) affects the system

Table 6.2: Complexity and MUI [dB] performance comparison: 16-QAM, $M_t = 100$, $M_r = 10$,

	IBO=0dB			**IBO=3dB**		
Scheme	Niter	MUI	Complexity	Niter	MUI	Complexity
EZF	-	-25.41	127800	-	-29.87	127800
ILA1	-	-23.39	137200	-	-35.03	137200
ILA2	3	-43.11	206100	2	-44.65	179400
MU-PNL-GDm	6	-40.11	118800	5	-42.15	99000

performance. In [151], authors investigated the INI problem in SISO-OFDM system and underlined its causes related system parameters, such as subcarrier spacing (SCS), number of activated subcarriers, power, etc. Furthermore, a theoretical model was developed in [152] as a function of frequency spacing between numerologies, overlapping windows and channel frequency response, in SISO Windowed-OFDM system. Recently, authors in [153] [154] dealt with mixed numerologies spectrum sharing (SS), where users are sharing the same time/frequency resources. Unlike in non-overlapping mixed numerologies system, it is impossible to avoid interference using windowed/filtered waveforms. In this regard, a new transceiver design considering a mixed numerologies SS system for classical MIMO-OFDM was introduced in [154].

To the best of our knowledge, no previous work has studied the INI issue in massive MU-MIMO-OFDM system in the open literature. Furthermore, it is still not yet clear how massive MU-MIMO-OFDM systems behave when mixed numerologies SS transmission is considered. Again within the framework of the H2020 ADAM5 project and via the supervision of Cheng's PhD, I co-supervise with Prof. Daniel Roviras, we have been interested in investigating this INI issue for massive MU-MIMO-OFDM in downlink and uplink scenarios. Through this investigation, new and interesting findings have been highlighted, having great difference to the ever proposed SISO-OFDM and classical MIMO-OFDM systems. Indeed, a new transmission/reception strategy has been proposed for DL/UL scenario enabling flexible management of MN SS transmission. Moreover, a theoretical INI model has been built for each scenario, which could be a valuable tool to guide 5G system design and parameter selection. Besides, efficient INI cancellation schemes have been developed making massive MU-MIMO-OFDM very attractive to future WCSs [J17][J18].

6.4.1 Proposed transmission strategy

We assume a DL scenario, where the M_r users can be divided into NUM groups using NUM numerologies, represented by index num, where $num = 1, ..., NUM$. N_{num} and CP_{num} represent, respectively, the IFFT/FFT size and CP size of group num. For the sake of simplicity and without loss of generality, we present, in this section, results corresponding to two users ($M_r = 2$) belonging to two different numerologies ($num \in \{1, 2\}$). Consequently, we have two channel frequency responses corresponding to the two numerologies, denoted by $\bar{\mathbf{H}}^{(num)} \in \mathbb{C}^{M_r \times M_t \times N_{num}}$. Besides, synchronization is achieved over the least common multiplier (LCM) methods [154] [148] [152], where $N_1 = N \times N_2, CP_1 = N \times CP_2$, where $N = 2^i$ and i is an integer. $\mathbf{x}_{m_t}^{(1)}$ and $\mathbf{x}_{m_t}^{(2,n)}$ are OFDM-modulated symbols on the m_t-th transmit corresponding, respectively, to user 1 and user 2. The length of $\mathbf{x}^{(1)}$ is N times the length of $\mathbf{x}^{(2,n)}$ and all symbols are aligned.

To enable flexible management of INI, a new transmission strategy is considered, where we consider

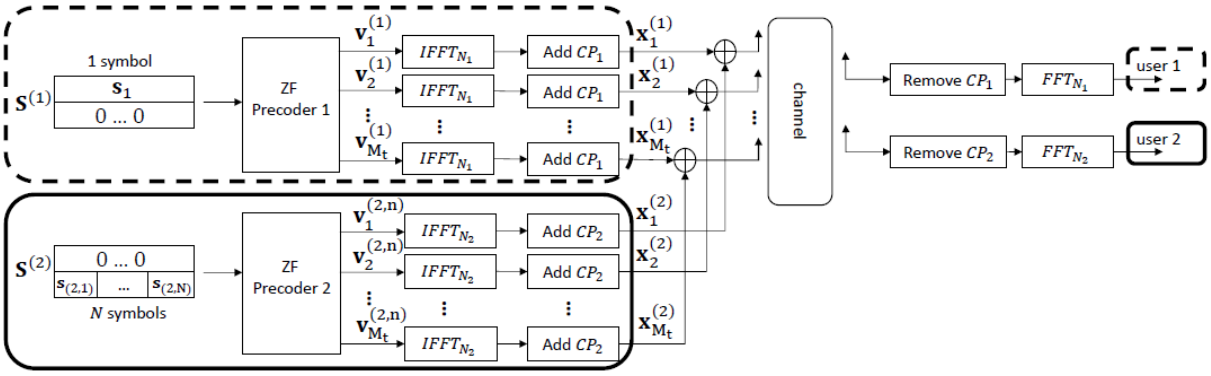

Figure 6.9: System model of the massive MIMO OFDM downlink with two different numerologies: M_t transmit antennas at the BS, two single-antenna terminals, two blocks illustrate two different numerologies with OFDM of N_1 and N_2 subcarriers.

two ZF based linear precoding branches [155], one for each numerology. Looking at branch one (dash-line block) in Figure 6.9, the first line of matrix $\mathbf{S}^{(1)}$ is the data information vector $\mathbf{s}^{(1)}$ for user 1 in numerology 1, while the second line is set to zero aiming to protect user 2. Also, in the second branch (solid-line block), matrix $\mathbf{S}^{(2)}$ contains data vector $\mathbf{s}^{(2)}$ for user 2 and null-vector is prepared for user 1. Then, each data stream is precoded using ZF, which is designed to cancel completely the Intra-NI between users using the same numerology. Nevertheless, INI between users using different numerologies can be occurred and the received signal of user 1 ($\mathbf{y}_1$) and the n-th received signal of user 2 ($\mathbf{y}_{2,n}$) can be, respectively, given by

$$\mathbf{y}_1[n_1] = \mathbf{s}_1[n_1] + \mathbf{ini}^{(2,1)}[n_1] + \mathbf{b}_1[n_1], n_1 = 1, ..., N_1, \tag{6.41}$$

and

$$\mathbf{y}_{2,n}[n_2] = \mathbf{s}_{2,n}[n_2] + \mathbf{ini}_n^{(1,2)}[n_2] + \mathbf{b}_{2,n}[n_2], n_2 = 1, ..., N_2, \tag{6.42}$$

where $\mathbf{ini}^{(2,1)}$ is INI from numerology 2 to numerology 1 while $\mathbf{ini}_n^{(1,2)}$ represents INI from numerology 1 to n-th numerology 2 symbol. $\mathbf{b}_1$ and $\mathbf{b}_{2,n}$ are receiver noises whose entries are i.i.d circularly-symmetric complex Gaussian distribution with zero-mean and ${\sigma_b}^2$ variance. Thus, the goal is to derive theoretical expressions for these INIs, which will be given in the following.

6.4.2 INI Analysis

Corollary 1: No INI is occurred by large numerology to small one in MN SS massive MU-MIMO-OFDM. An immunity is given to small numerology whether the IFFT/FFT sizes, SCS, channel selectivity, power allocation are, thanks to the ZF based proposed transmission strategy. Thus, we have

$$\mathbf{ini}_n^{(1,2)} = 0 \qquad n = 1, ..., N. \tag{6.43}$$

Proof: see [J17].

Corollary 2: By using the proposed transmission strategy in MN SS massive MIMO-OFDM, users using large numerology (i.e. larger IFFT/FFT size) are not totally protected. Where the total INI is the

summation of INI caused by N modulated symbols in numerology 2 and is expressed as

$$\mathbf{ini}^{(2,1)} = \sum_{n=1}^{N} \mathbf{ini}_n^{(2,1)}, \tag{6.44}$$

where $\mathbf{ini}_n^{(2,1)}$ denoted the INI caused by the n-th symbol in numerology 2. Its expression, at the n_1-th subcarrier in numerology 1 is expressed as

$$\mathbf{ini}_n^{(2,1)}[n_1] = \sum_{n_1'=1}^{N_1} \sum_{n_2=1}^{N_2} \mathbf{E}_n(n_1, n_1')\mathbf{Z}(n_1', n_2) \sum_{m_t=1}^{M_t} \mathbf{hf}_{1,m_t}^{(1)}[n_1']\mathbf{v}_{m_t}^{(2,n)}[n_2], \tag{6.45}$$

where:
$\mathbf{v}_{m_t}^{(2,n)}$ is the frequency-domain precoded vector corresponding to antenna m_t, as shown in Figure 6.9,
$\mathbf{hf}_{m_r,m_t}$ is the channel frequency response between transmitting antenna m_t and user m_r,

$$\mathbf{E}_n \in \mathbb{C}^{N_1 \times N_1} = \begin{cases} \mathbf{G}_1^{(2)}\mathbf{W}_1^{(2)} & for \quad n = 1, \\ \mathbf{G}_2^{(2)}\mathbf{ID}_n^{(2)}\mathbf{W}_3^{(2)} & for \quad n = 2, ..., N. \end{cases} \tag{6.46}$$

$\mathbf{Z} = \mathbf{G}_2^{(2)}\mathbf{W}_2^{(2)} \in \mathbb{C}^{N_1 \times N_2}$,
$\mathbf{G}_1^{(2)} = \begin{bmatrix} \mathbf{0}_{N_1 \times CP_1} & \mathbf{DFT}_{N_1} \end{bmatrix} \in \mathbb{C}^{N_1 \times (N_1 + CP_1)}$,

$\mathbf{G}_2^{(2)} = \mathbf{DFT}_{N_1} \in \mathbb{C}^{N_1 \times N_1}$,

$\mathbf{W}_1^{(2)} = \begin{bmatrix} \mathbf{IDFT}_{N_1} \\ \mathbf{0}_{CP_1 \times N_1} \end{bmatrix} \in \mathbb{C}^{(N_1 + CP_1) \times N_1}$,

$\mathbf{W}_3^{(2)} = \mathbf{IDFT}_{N_1} \in \mathbb{C}^{N_1 \times N_1}$,

$$\mathbf{ID}_n^{(2)} = \begin{bmatrix} \mathbf{0}_{T_1 \times (N_1/2)} & \mathbf{0}_{T_1 \times (N_1/2)} \\ \mathbf{I}_{T_2} & \mathbf{0}_{T_2 \times (N_1 - T_2)} \\ \mathbf{0}_{T_3 \times (N_1/2)} & \mathbf{0}_{T_3 \times (N_1/2)} \end{bmatrix} \in \mathbb{C}^{N_1 \times N_1},$$

for matrix $\mathbf{ID}_n^{(2)}$, we have

$$\begin{cases} T_1 = N_1 - (N - n + 1)(N_2 + CP_2), \\ T_2 = \begin{cases} N_2 + CP_2 + D & for \quad n = 2, ..., N - 1 \\ N_2 + CP_2 & for \quad n = N, \end{cases} \\ T_3 = \begin{cases} (N - n)(N_2 + CP_2) - D & for \quad n = 2, ..., N - 1 \\ (N - n)(N_2 + CP_2) & for \quad n = N. \end{cases} \end{cases} \tag{6.47}$$

Interested readers are referred to [J17].
Remark 1: In a constant channel (i.e., $\mathbf{hf}_{1,m_t}^{(1)}[n_1] = \mathbf{hf}_{1,m_t}^{(2)}[n_2]$)), transmission of user 1's data is performed with excellent performance. Then, we have

$$\mathbf{ini}_n^{(2,1)}[n_1] = 0 \tag{6.48}$$

Proof: see [J17].
In contrast to SISO and classical MIMO systems, massive MIMO is able to support mixed numerologies and no INI is generated when the channel is flat-fading. This finding is valid only for massive MIMO when the proposed transmission strategy is employed.
Remark 2: Channel selectivity and difference between N_1 and N_2 increase the $\mathbf{ini}^{(2,1)}$.
In frequency-selective channel case, vector $\mathbf{hf}_{1,m_t}^{(1)}$ can be obtained through the interpolation of vector $\mathbf{hf}_{1,m_t}^{(2)}$, where $N-1$ values are added between every two points. Accordingly, we have

$$\mathbf{hf}_{1,m_t}^{(1)}[(n_2-1)N+1] = \mathbf{hf}_{1,m_t}^{(2)}[n_2], \tag{6.49}$$

where $n_2 = 1, ...N_2$.
Therefore, the difference between $\mathbf{hf}_{1,m_r}^{(1)}[n_1]$ and $\mathbf{hf}_{1,m_r}^{(2)}[n_2]$ is closely related to the channel selectivity and the difference between N_1 and N_2. The higher selectivity and difference between N_1 and N_2 are, the higher difference between the two channel frequency responses, leading to greater interference.
Remark 3: Power allocation for different users has a direct influence on the power of interference $\mathbf{ini}^{(2,1)}$.
Here, a simple power allocation scheme is adopted. The power allocated to the m_r-th user (p_{m_r}) is proportional to the inverse of its path-loss $\sqrt{\kappa_{m_r}}$. Then, the greater large-scale fading in user m_r leads to greater transmitting power for that user. This means, if user 2 is farther away from the BS, i.e. $\kappa_2 < \kappa_1$, user 1 receive more INI because of the increased transmitting power for user 2.

Table 6.3: NMSE (dB) of user of interest with interfering numerology and different channels

User of Interest	user1 ($N_1 = 1024$)		user2 ($N_2 = 512$)	user2 ($N_2 = 256$)
Interfering User	user2($N_2 = 512$)	user2($N_2 = 256$)	user1($N_1 = 1024$)	
$L_c = 1$	-300	-300	-300	-300
$L_c = 2$	-52	-48	-300	-300
$L_c = 8$	-42	-37	-300	-300
$L_c = 18$	-38	-33	-300	-300

In order to check the accuracy of the derived theoretical INI expressions, we depict in Tables 6.3 and 6.4 NMSE performance for two different scenarios, when ($p_1 = p_2$) or not. Looking at Table 6.3, we can verify that 1) transmission for user 2 which uses small IFFT/FFT size is always with the best quality (NMSE value of around -300 dB), no matter what IFFT/FFT size or channel selectivity. 2) numerology 2 with small IFFT/FFT size does not suffer from the INI from numerology 1 in case of constant channel. Contrary, in frequency-selective channel case, user 1 suffers more INI from numerology 2 when the difference between IFFT/FFT size increases. Meanwhile, we can note that the more selective the channel is, the worse is the user1's performance. 3) If we consider a more realistic scenario with the long time evolution (LTE) path-loss model given in [156], user 1 suffers greater INI with the growth of path-loss on user 2, as shown in Table 6.4. When $N_1 = 1024, N_2 = 512$ and $L_c = 8$, there is degradation of 20 dB when $\kappa_1/\kappa_2 = 20$ dB compared to $\kappa_1/\kappa_2 = 0$ dB. This degradation increase to 23 dB and 26 dB when $\kappa_1/\kappa_2 = 23$ dB and $\kappa_1/\kappa_2 = 26$ dB. Moreover, It can be seen also that, after the INI cancellation implemented at the BS, transmission of user 1 performs as well as user 2, reaching -300 dB for all values of path-losses.

Table 6.4: NMSE values before and after INI cancellation

User of Interest	user1 ($N_1 = 1024$)			
Interfering User	user2($N_2 = 512$)		user2($N_2 = 256$)	
κ_1/κ_2 (dB)	original (dB)	corrected (dB)	original (dB)	corrected (dB)
20	-22	-300	-18	-300
23	-19	-300	-14	-300
26	-16	-300	-11	-300

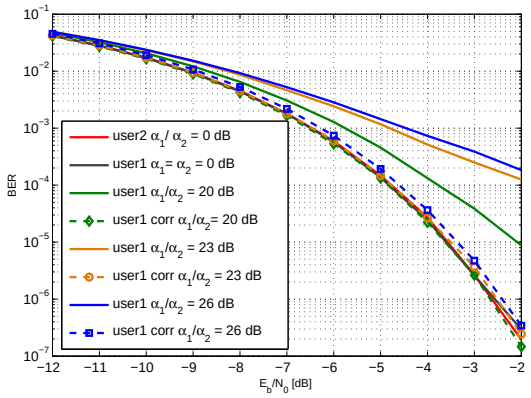

Figure 6.10: BER performance with and without INI cancellation on user 1: $N_1 = 1024, N_2 = 256$, $\kappa_1/\kappa_2 = 0, 20, 23$ and 26 dB.

6.4.3 INI cancellation

As explained above, the transmission corresponding to any numerology is affected only by INI coming from smaller numerology (i.e., users using smaller IFFT/FFT size). Therefore, the proposed INI cancellation scheme aims at adding correcting signal to each numerology's data such that, after precoding and propagating through the channel, the reception is with the best quality. With the aid of the derived INI expressions, it is straightforward to calculate in advance the total INI coming from all other users using smaller numerology and calibrate the transmitted data (i.e., pre-cancel the INI). Specifically, the computation of INI always starts from numerology with the smallest IFFT/FFT size. Numerology with the largest IFFT/FFT size can be corrected by suppressing INIs from all the other numerologies.
For example, when considering two users, instead of transmitting $\mathbf{s}_1$, we transmit $\widetilde{\mathbf{s}}_1 = \mathbf{s}_1 - \mathbf{ini}^{(2,1)}$. This change permits to improve the transmission of user 1 while it does not damage the transmission of user 2. Note that In the cancellation process, the estimated $\mathbf{ini}^{(2,1)}$ of equation (6.45) can be computed over only several subcarriers on numerology 2 (over a window of length L subcarriers), having the most amount of energy.

Figure 6.10 shows the BER performance of user 1 with and without INI cancellation. One can note that the performance of user 1 is significantly declined when the path-loss of user 2 increases. For example, we can compare $\kappa_1/\kappa_2 = 0$ dB and $\kappa_1/\kappa_2 = 26$ dB. When $E_b/N_0 = -3$ dB, user 1 can achieve

$BER \leq 10^{-6}$ when $\kappa_1/\kappa_2 = 0$ dB while the BER of user 1 is larger than 10^{-4} when $\kappa_1/\kappa_2 = 26$ dB.

Also, in Figure 6.10, the BER performance with INI cancellation is presented for user 1 and user 2 with different path-loss on user 2. $N_1 = 1024$, $N_2 = 512$. All the dash lines represent the BER after the implementation of the cancellation algorithm introduced in section IV. It can be observed that the algorithm improves the performance of user 1 under different path-loss cases. After the cancellation, user 1 and user 2 have a negligible BER loss, even when $\kappa_1/\kappa_2 = 26$ dB. We can also observe a slight BER mismatch when the path-loss of user 2 becomes great (the dash-blue curve), which is mainly caused by the introduced INI cancellation power p_{ini}. However, as we explained above, this effect is negligible.

6.5 Outputs

The combined outputs of the work on Massive MIMO described in Section 6.2 (PAPR reduction), in Section 6.3 (PA NLD mitigation) and in Section 6.4 (INI analysis and cancellation) are summarized bellow.

Supervision and collaborations related to work on Massive MIMO

- 01 PhD co-supervision: (**Miss Xinying Cheng** (ongoing))
- Supported by H2020 MCSA IF ADAM5 project
- Visiting researcher CEDRIC/CNAM, Nov. 2018 to Oct. 2020

Publications related to work on Massive MIMO

- 04 peer-reviewed journals **[J18, J17, J16, J15]**

Chapter 7

Indoor Localization: From Matrix Completion to Deep Learning

7.1 Introduction

In addition to our contributions related to communication technology toward 5G and its emerged applications, I have been interested in researches concerning localization, which is among the most challenging issues related to IoT/mMTC. The position information can be used for target tracking, surveillance applications, guiding autonomous vehicles, etc. The outdoor localization is performed by global positioning system (GPS) which is not adequate for indoor environment. Therefore, several indoor localization methods have been developed where the receive signal strength indicator (RSSI) from wireless access point (anchor node) has attracted lots of attention due to its easy acquisition. These methods are mainly based on **Trilateration** [157] and **Fingerprinting** [158].

Using trilateration, a node (object) determines its coordinates via a geometric method that exploits inter-sensor distances and the coordinates of anchor nodes (installed at known positions). However, it does not achieve good localization precision when it is applied to a few number of available measurement distances to neighboring nodes. This is related to the fact that IoT sensors are not capable of high-power transmission which would not allow measurements with all anchor nodes. As a first contribution, we investigated the matrix-completion approach to enhance the performance of the trilateration by completing the matrix containing the inter-nodes distances. The developed work is synthesized in Section 7.2.

Fingerprint based localization can achieve high accuracy but needs to pay heavy computational complexity for similarity evaluation of the measured fingerprint to a fingerprints' database constructed offline, making it not adequate for a real-time localization. As a second contribution, we developed a localization framework based on a deep convolutional neural network (CNN) where the localization problem is formulated as radio image-related region classification. In Section 7.3, I give an overview of classical similarity evaluation methods and their performance and then I emphasise the development of the CNN framework. Finally, the outputs of these contributions are resumed in Section 7.4.

7.2 Matrix Completion based Trilateration for indoor localization

In order to enhance the trilateration method, a high number of pairwise distances between sensors is required. However, obtaining the complete matrix of distances, called Euclidean distance matrix (EDM), is not straightforward, leading to an incomplete pair-wise distance information. Then, a matrix completion approach is of paramount importance to recover the real EDM from the incomplete one, making the trilateration more interesting and precise. The proposed scheme employs mathematical concepts based on sparse representation and matrix completion theories. Specifically, the proposed indoor localization scheme is formulated as a simple optimization problem which enables efficient and reliable algorithm implementations.

7.2.1 System model

In order to assess the performance of our approach, we considered a system (Figure 7.1) where each sensor node uses two steps to compute its position: 1) Refine and complete the Euclidean distance matrix and 2) Compute the coordinates by using the classical trilateration process.

The Euclidean Distance Matrix, referred to as $\mathbf{X}$, contains the distance information between each pair of sensor nodes, which can be built through RSSI measurements.

The value of RSSI can be calculated in dBs as

$$R_{ml} = p_e - \kappa_{ml} + x_{\sigma_c}, \tag{7.1}$$

where p_e denotes the transmission power, x_{σ_c} is a Gaussian random variable with zero mean and variance σ_c^2, which describes the random shadowing effects, and κ_{ml} represents the path-loss in dBs which can be obtained using the the log normal shadowing propagation model [159], given by

$$\kappa_{ml} = \kappa_0 + 20log_{10}(f) + 10\varrho log_{10}(\frac{d}{d_0}), \tag{7.2}$$

where κ_0 is the path-loss value at a reference distance d_0, ϱ is the path-loss exponent, f is the used frequency in MHz, and d is the distance between the m-th and l-th nodes.

Due to the limitation of radio communication range, some RSSI measurements corresponding to different sensor nodes are missing. Thus, the matrix $\mathbf{X}$ is incomplete (only a small number of $\mathbf{X}$ entries are available) and can be affected by noise, leading then to an ineffective localization precision. This incomplete EDM can not effectively serve for localization and it should be completed.

7.2.2 Problem formulation

Let us define the matrix $\mathbf{X}_{true}$ as the complete real EDM. Our goal is to reconstruct the complete distance matrix from incomplete and noisy data. The problem of recovering a low rank matrix from a small number of known entries is known as minimizing the matrix rank. Due to the non convexity and non linearity of the matrix rank [160], its minimization cannot be solved numerically. Inspired from the theory of Compressed Sensing (CS), Candes and Recht proposed to replace the rank function by the nuclear norm [161]. The optimization problem can be formulated as

$$\begin{cases} \min\limits_{\hat{\mathbf{X}}} ||\hat{\mathbf{X}}||_* \\ s.t.\ \hat{x}_{ij} = x_{ij} \text{ where } i,j \in \omega \end{cases}, \tag{7.3}$$

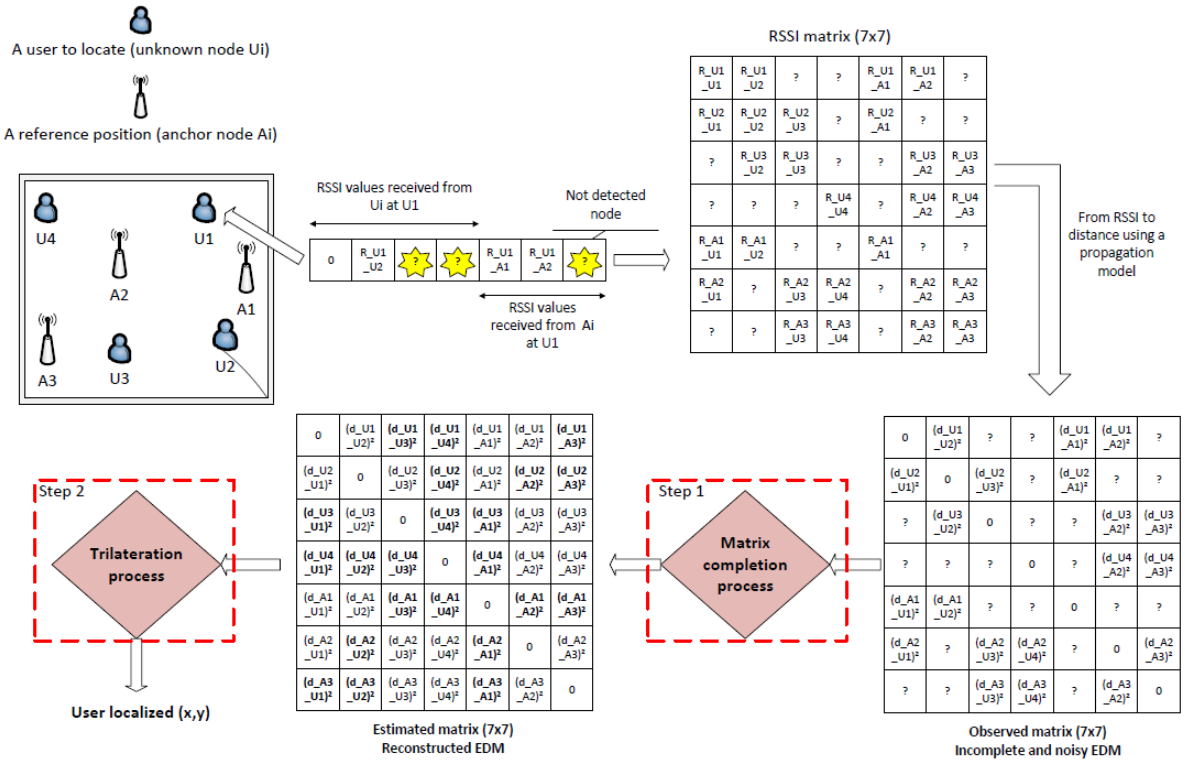

Figure 7.1: Algorithm details considering the sensor network consisting of 7 sensor nodes from which 3 are anchors [J13]

where ω is the set of known entries.

Let us define n is the total number of sensor nodes (anchor and unknown nodes) placed in the indoor environment with m nodes with known positions named 'Anchor nodes' and $(n-m)$ sensors with unknown positions. We denote by U_i the i-th unknown node, where $i = 1, 2, ..., (n-m)$ and A_j the j-th anchor node, where $j = 1, 2, ..., m$. $\mathbf{X}$, which is the $(n \times n)$ Euclidean distance matrix, can be partitioned as given by equation (7.4).

$$\mathbf{X} = \begin{bmatrix} \mathbf{X}_{11} & \mathbf{X}_{12} \\ \mathbf{X}_{21} & \mathbf{X}_{22} \end{bmatrix}, \tag{7.4}$$

where: $\mathbf{X}_{22}$ contains the exact distances between each pair of anchors. Its entries are $\{d_{A_j A'_j} = ||C_{A_i} - C_{A_j}||_2\}$, which are the pairwise distance between anchor node (A_j) and anchor node (A'_j). Note that $C_{A_j} \in \mathbb{R}^3$ denotes the location coordinates of anchor node j.

$\mathbf{X}_{11}$ is the $(n-m) \times (n-m)$ distance sub matrix between each pair of unknown nodes.

$\mathbf{X}_{12}$ and $\mathbf{X}_{21}$, where $\mathbf{X}_{12} = {\mathbf{X}_{21}}^T$, are the distance sub matrices between each pair of anchors and unknown nodes.

It is worth to mention that $\mathbf{X}_{11}$, $\mathbf{X}_{12}$ and $\mathbf{X}_{21}$ are obtained from RSSI measurements using the log normal shadowing propagation model given by equation(7.2).

Given the real Euclidean distance matrix is of low rank ($r << n$) and taking into account that observations can be affected by noise, the constraint in (7.3) can be relaxed and the optimization problem can be given by

$$\min_{\hat{\mathbf{X}}} \lambda \times ||\hat{\mathbf{X}}||_* + ||\mathbf{H} \odot (\hat{\mathbf{X}} - \mathbf{X})||_F^2, \tag{7.5}$$

where λ is a tunable parameter, $||.||_F$ is the Frobenius norm, $||\hat{\mathbf{X}}||_F = \sqrt{\sum_{i=1}^{n}\sum_{j=1}^{n}|\hat{x}_{ij}|^2}$, and $\mathbf{H}$ is $n \times n$ a matrix whose entries are

$$h_{ij} = h_{ji} = \begin{cases} 1 & \text{if } (i,j) \in \omega \\ 0 & otherwise \end{cases}, \tag{7.6}$$

Let us denote the objective function as

$$J(\hat{\mathbf{X}}) = f(\hat{\mathbf{X}}) + \lambda \times l(\hat{\mathbf{X}}), \tag{7.7}$$

where $f(\hat{\mathbf{X}}) = ||\mathbf{H} \odot (\hat{\mathbf{X}} - \mathbf{X})||_F^2$ and $l(\hat{\mathbf{X}}) = ||(1 - \mathbf{H}) \odot \hat{\mathbf{X}}||_*$.

It is worth to point out that the formulated optimization problem can be effectively solved via iterative gradient descent (GD) method and its variants. Then, we developed a simple and efficient algorithm based on many optimization approaches, which are described in the next Subsection. The developed algorithm is summarized in Table 7.1, where $\mathbf{V}^{(t)}$ is the update matrix and index t refers to the number of update iteration.

Table 7.1: The proposed algorithm for matrix completion

1. Input: $\mathbf{X}$, $\mathbf{H}$, number max of iterations
2. Initialization: $\hat{\mathbf{X}}^{(0)}$, t
3. while $t <$number max of iterations
   Update $\hat{\mathbf{X}}$:
   $$\hat{\mathbf{X}}^{(t+1)} = \hat{\mathbf{X}}^{(t)} - \mathbf{V}^{(t)}, \tag{7.8}$$
   $t = t + 1$
   end
4. Return $\hat{\mathbf{X}}$

7.2.3 Optimization through GD and its variants for Matrix Completion

In this work several optimization methods were deployed and tested to solve the given optimization problem (i.e., find the update matrix $\mathbf{V}^{(t)}$ at each iteration), Gradient descent (GD), Nesterov accelerated gradient (NAG), Adaptive Gradient (Adagrad), Root Mean Square Propagation (RMSProp), Adadelta and Adaptive Moment Estimation (Adam). Interested readers to these algorithms are referred to [162].

Here, we discard the class of algorithms that are computationally very expensive for high dimensional data sets, e.g. the second-order Newton's method [7]. In the following, I give the expression of $\mathbf{V}^{(t)}$ related to each method.

Gradient descent (GD)

Gradient descent is an iterative method that aims to find local minimum of differentiable cost functions [162]. It is the most common first-order optimization algorithm in machine learning and deep learning. GD is based on updating each element of matrix $\hat{\mathbf{X}}^{(t)}$ in the direction to optimize the objective function $J(\hat{\mathbf{X}}^{(t)})$. The new parameter $\mathbf{V}^{(t)}$ can be adjusted as

$$\mathbf{V}^{(t)} = \alpha \nabla(J(\hat{\mathbf{X}}^{(t)})), \tag{7.9}$$

where α denotes the learning rate from range $(0, 1)$ and $\nabla(J(\hat{\mathbf{X}}^{(t)}))$ refers to the gradient of the cost function with respect to the matrix entries. Its computation is detailed in [163] and the update matrix is given by

$$\mathbf{V}^{(t)} = \alpha \times (2 \times \mathbf{H} \odot (\hat{\mathbf{X}}^{(t)} - \mathbf{X}^{(t)}) + \lambda \times (1 - \mathbf{H}) \odot (\hat{\mathbf{X}}^{(t)} \cdot ((\hat{\mathbf{X}}^{(t)})^T \cdot \hat{\mathbf{X}}^{(t)} + \epsilon \times \mathbf{I})^{-0.5})), \tag{7.10}$$

where ϵ is a regularization parameter.

Note that this update matrix contains two components, referred to as $\mathbf{U}^{(t)} = \alpha \times (2 \times \mathbf{H} \odot (\hat{\mathbf{X}}^{(t)} - \mathbf{X}^{(t)})$ and $\mathbf{W}^{(t)} = \lambda \times (1 - \mathbf{H}) \odot (\hat{\mathbf{X}}^{(t)} \cdot ((\hat{\mathbf{X}}^{(t)})^T \cdot \hat{\mathbf{X}}^{(t)} + \epsilon \times \mathbf{I})^{-0.5}))$. In the following, the update of $\mathbf{U}^{(t)}$ will be done using GD while the update of $\mathbf{W}^{(t)}$ will be performed using some advanced methods.

Nesterov accelerated gradient (NAG)

To update $\mathbf{W}^{(t)}$ with NAG [162], we use the following rule

$$\mathbf{W}^{(t)} = \mu \times \mathbf{W}^{(t-1)} + \lambda \times \nabla(l(\hat{\mathbf{X}}^{(t)} - \mu \times \mathbf{W}^{(t-1)})), \tag{7.11}$$

where μ is an updating rate factor. The mathematical derivation are detailed in [163], obtaining

$$\begin{aligned} \mathbf{W}^{(t)} = \mu \times (1 - \mathbf{H}) \odot (\hat{\mathbf{X}}^{(t-1)} \cdot ((\hat{\mathbf{X}}^{(t-1)})^T \cdot \hat{\mathbf{X}}^{(t-1)} + \epsilon \times \mathbf{I})^{-0.5}) \\ + \lambda \times (1 - \mathbf{H}) \odot (\hat{\mathbf{Y}}^{(t)} \cdot ((\hat{\mathbf{Y}}^{(t-1)})^T \cdot \hat{\mathbf{Y}}^{(t-1)} + \epsilon \times \mathbf{I})^{-0.5}), \end{aligned} \tag{7.12}$$

Adaptive Gradient (Adagrad)

Adagrad [162] update rule is as

$$\mathbf{W}^{(t)} = \frac{1}{\sqrt{\mathbf{G}^{(t)} + \epsilon \times \mathbf{I}}} \odot \mathbf{E}^{(t)}, \tag{7.13}$$

where

$$\begin{aligned} \mathbf{E}^{(t)} &= \frac{\delta l(\hat{\mathbf{X}}^{(t)})}{\delta \hat{\mathbf{X}}^{(t)}} \\ &= (1 - \mathbf{H}) \odot (\hat{\mathbf{X}}^{(t)} \cdot ((\hat{\mathbf{X}}^{(t)})^T \cdot \hat{\mathbf{X}}^{(t)} + \epsilon \times \mathbf{I})^{-0.5}), \end{aligned} \tag{7.14}$$

and the memory of squared gradients over time

$$\mathbf{G}^{(t)} = \sum_{i=1}^{t} (\mathbf{E}^{(i)})^2, \tag{7.15}$$

It is worth to point out that no learning rate is needed.

Root Mean Square Propagation (RMSProp)

RMSProp [164] uses only recent past gradients computed in a restricted time. Here, we compute the local average of previous $(\mathbf{E}^{(t)})^2$ as

$$\tilde{\mathbf{G}}^{(t)} = \rho \times \mathbf{G}^{(t-1)} + (1-\rho) \times (\mathbf{E}^{(t)})^2, \tag{7.16}$$

Then, we apply the update

$$\mathbf{W}^{(t)} = \frac{1}{\sqrt{\tilde{\mathbf{G}}^{(t)} + \epsilon \times \mathbf{I}}} \odot \mathbf{E}^{(t)}, \tag{7.17}$$

Adadelta

Adadelta [164] update rule is as follow:

- we compute gradient $\mathbf{E}^{(t)}$ as in equation (7.14).
- we compute the local average $\tilde{\mathbf{G}}^{(t)}$ of previous $(\mathbf{E}^{(t)})^2$
- we compute new term accumulating prior updates (Momentum : acceleration term)

$$\mathbf{Z}^{(t)} = \rho \times \mathbf{Z}^{(t-1)} + (1-\rho) \times (\mathbf{W}^{(t-1)})^2, \tag{7.18}$$

- Then, we apply the update

$$\mathbf{W}^{(t)} = \frac{\sqrt{\mathbf{Z}^{(t)} + \epsilon \times \mathbf{I}}}{\alpha\sqrt{\tilde{\mathbf{G}}^{(t)} + \epsilon \times \mathbf{I}}} \odot \mathbf{E}^{(t)}. \tag{7.19}$$

Adaptive Moment Estimation (Adam)

The Adam [165] update rule consists of the following steps.

- Compute second gradient moment with local accumulation (Adadelta/RMSProp)

$$\mathbf{N}^{(t)} = \beta_1 \times \mathbf{N}^{(t-1)} + (1-\beta_1) \times (\mathbf{E}^{(t)})^2, \tag{7.20}$$

- Compute the first gradient moment

$$\mathbf{M}^{(t)} = \beta_2 \times \mathbf{M}^{(t-1)} + (1-\beta_2) \times \mathbf{E}^{(t)}, \tag{7.21}$$

- Compute bias-corrected first moment and second moment estimate

$$\hat{\mathbf{N}}^{(t)} = \frac{\mathbf{N}^{(t)}}{1-\beta_1}, \tag{7.22}$$

$$\hat{\mathbf{M}}^{(t)} = \frac{\mathbf{M}^{(t)}}{1-\beta_2}, \tag{7.23}$$

- Update parameters

$$\mathbf{W}^{(t)} = \frac{\hat{\mathbf{M}}^{(t)}}{\sqrt{\hat{\mathbf{N}}^{(t)} + \epsilon \times \mathbf{I}}}. \tag{7.24}$$

7.2.4 Simulation results and Discussion

We consider a wireless sensor network of $n = 45$ sensor nodes with $m = 10$ of them are anchors and 35 are unknown nodes, placed in an area of 400 m^2 (i.e. 20 m $\times$ 20 m). The sensor nodes (anchors and unknown nodes) are randomly placed in the studied area. The shadowing propagation model parameters are $\varrho = 3.23$, $p_e = 20$ dBm, $d_0 = 1$ m, and $f = 2.4$ GHz.

For evaluating the studied solutions based on GD and its variants combined with the trilateration process, we define the following Localization error metric

$$error_{loc} = \frac{||\hat{\mathbf{C}} - \mathbf{C}||_2}{n - m}, \tag{7.25}$$

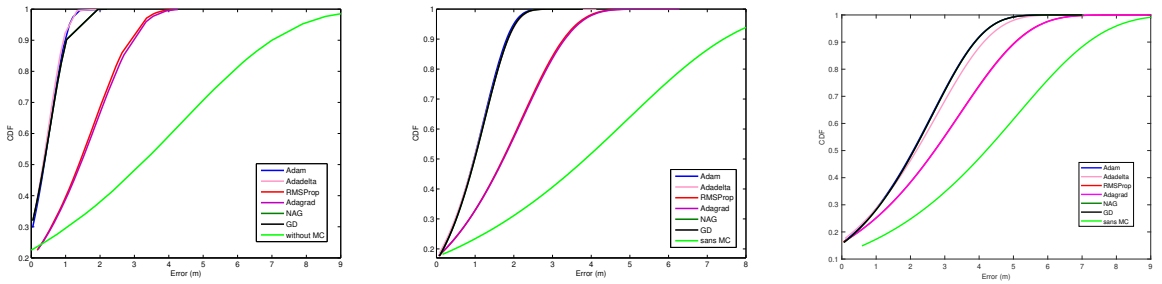

(a) sigma shadowing = 0 (b) sigma shadowing = 2 (c) sigma shadowing = 5

Figure 7.2: Algorithms' performances

To verify that trilateration guarantees better localization accuracy when more distance information is provided, we firstly, apply the trilateration with observed distances only. We can easily notice that it introduces the worst localization accuracy compared to tested combinations in both noisy and noiseless environments (Figure 7.2). The localization accuracy is much better when we use a complete EDM than using only the observed distances. Moreover, to apply the trilateration process, at least 3 detected anchors are needed. If this is not the case, the sensor node cannot be localized. This problem can be solved when using a compete EDM containing all pairwise distances. Therefore, the combination of matrix completion technique and trilateration is highly recommended.

The performances of GD and NAG in terms of localization accuracy are very close. So that, their CDF are superimposed for each sigma shadowing value. Adagrad exhibits worse performance than the other optimization methods. This is due to the fact that, it accumulates the squared gradients in the denominator. So, the sum of positive terms keeps growing and the learning rate becomes very small, thus making the algorithm no longer able to ensure updates in order to reach a lower minimum.

Instead of accumulating all past squared gradients, RMSProp and Adadelta use a window of size (ρ) of accumulated past gradients. RMSProp improves a little bit the localization error compared to those introduced by Adagrad in a noiseless environment. But, the result is still worse than those obtained by GD and NAG. The performances of RMSProp and Adagrad are quite close in a noisy environment. They exhibits almost the same CDF performance (Figure 7.2).

Adadelta performs slightly better than GD and NAG for sigma shadowing = 0 and 2. We notice that Adadelta is more affected by noise than other algorithms. Indeed, it provides the best localization accuracy when $\sigma_c = 0$ and its performance decreases when σ_c is higher. In this latter case, Adam, GD and NAG are better than Adadelta in terms of EDM reconstruction error, localization accuracy and

convergence speed. Adam is better compared to other algorithms considering the tradeoff between the localization accuracy and convergence speed. Indeed, it has the fastest convergence speed toward the lowest EDM reconstruction error, performing the best localization accuracy. Its localization mean error is 1.2 m and 2.6 m when, respectively, $\sigma_c = 2$ and $\sigma_c = 5$. As mentioned before, these results have been done on 10 simulations and the variance is about 0.1 m for each value of sigma shadowing. Therefore, we recommend Adam for such indoor localization schemes.

7.3 RSSI Fingerprinting based Indoor Localization

RSSI fingerprinting technique is based on two phases: offline and online. During the offline phase, a radio map is constructed. For known positions named 'reference positions', RSSI measurements received from all access points (APs) are associatred to real coordinates of the location, constructing the 'training database' or the 'radio map'. In the online phase, the test fingerprint is used to estimate the user's location. This technique can be of great interest, especially when used with advanced approaches like similarity evaluation and Neural Networks (NN).

7.3.1 Similarity Evaluation based Indoor Localization

This method consists in comparing the test fingerprint to the whole training base, in order to associate it to the average position of the K-Nearest Neighbors (KNN) [166]. Therefore, different similarity evaluation metrics together with different methods of combining the locations of neighbors are possible. In this subsection, we give a comparative study of several combinations of these similarity evaluation and position estimation methods in performing good localization accuracy.

Similarity Evaluation

Numerous similarity evaluation metrics have been tested, which can be divided into to categories: (1) deterministic methods including the Euclidean distance and the Manhattan distance, (2) probabilistic methods including the Gauss distance and the Kernel method. Let us note by $\mathbf{o} = (o_1, o_2, ..., o_D)$ the test fingerprint containing received RSSI from D APs and $\mathbf{o_l} = (o_{l1}, o_{l2}, ..., o_{lD})$ the training fingerprint corresponding to D APs at position l.

The Euclidean distance: It is based on the Minkowski distance of order p [167] and the similarity metric is defined as

$$S(o, o_l) = \sqrt{\sum_{d=1}^{D} (o_d - o_{ld})^2}, \tag{7.26}$$

where o_j denotes the received RSSI from the d-th AP at a test location and o_{lj} is the he received RSSI from the d-th AP at the l-th training location.

The Manhattan distance: The similarity metric is defined as [168]

$$S(o, o_l) = \sum_{d=1}^{D} |o_d - o_{ld}|, \tag{7.27}$$

The Gauss method: The similarity metric depends on the detected APs [169]. To compare a test fingerprint $\mathbf{o}$ to a training fingerprint $\mathbf{o_l}$, we can consider three cases: 1) the AP is detected in the

training and test phases, 2) the AP is not detected in the test phase and 3) the AP is not detected in the training phase. In case 1, the probability of the training fingerprint to match the test fingerprint is given by

$$P_{exp} = \sqrt[M]{\prod_{m=1}^{M} e^{-\left(\frac{o_m - o_{lm}}{\sigma_0}\right)^2}}, \tag{7.28}$$

where M is the number of detected APs in the training and test phases and σ_0 is an adjustable parameter. In case 2 and 3, coefficients of penalty are considered for, respectively, T APs not detected in test phase and N APs not detected in training phase. These coefficients are, respectively, given by

$$P_{penT} = \prod_{t=1}^{T} e^{-\left(\frac{o_t - min(\mathbf{o_l})}{\sigma_0}\right)^2}, \tag{7.29}$$

and

$$P_{penN} = \prod_{n=1}^{N} e^{-\left(\frac{o_{ln} - min(\mathbf{o})}{\sigma_0}\right)^2}. \tag{7.30}$$

The two coefficients of penalty are combined to a single penalty, given by

$$P_{pen} = \sqrt[T+N]{P_{penT} \times P_{penN}}. \tag{7.31}$$

Then, the probability of similarity, P, computed for each training fingerprint is defined as

$$P(o, o_l) = \sqrt{P_{pen} \times P_{exp}} \tag{7.32}$$

Note that $D = M + T + N$.

The Kernel method: A probability of similarity is assigned to each training fingerprint using the Kernel Gaussian. The probability of similarity is given by [170]

$$P(o, o_l) = \frac{1}{2\pi\sigma_0^2} \prod_{d=1}^{D} e^{-\frac{(o_d - o_{ld})^2}{2\sigma_0^2}} \tag{7.33}$$

Position Estimation

Concerning the estimation of the position, which is expressed using latitude and longitude as $c_t = (lat_t, long_t)$, corresponding to the t-th test fingerprint. This position is computed by combining the positions corresponding of training fingerprints corresponding to the K-nearest neighbors. Three combination methods are used: 1) simple average which consists in averaging the coordinates of the neighbors' locations. 2) weighted average, where we assign a weight to each neighbor's location as given by

$$latitude = \frac{\sum_{k=1}^{K} latitue_k.w(k)}{\sum_k w(k)} \tag{7.34}$$

and

$$longitude = \frac{\sum_{k=1}^{K} longitude_k.w(k)}{\sum_k w(k)}, \tag{7.35}$$

where the weight can be assimilated to the distance between test and training fingerprints $w(k) = 1/S(o, o_l)$ or their probability of similarity $w(k) = P(o, o_l)$. And 3) using Nadaraya Watson Kernel

Table 7.2: Mean error corresponding to the different combinations.

	Simple average	**Weighted average**	**Nadaraya estimator**
Euclidean distance	5.51m	5.5m	5.59m
Manhattan distance	5.38m	5.25m	5.4m
Gauss method	7.63m	7.7m	7.81m
Kernel method	5.51m	5.9m	5.59m

estimator [171] that calculates the coordinate c_t (latitude or longitude)of the test fingerprint o using coordinates of K training fingerprints, given by

$$E(c_t/o) = \frac{\sum_{k=1}^{K} c_k G(o - o_k)}{\sum_{k=1}^{K} G(o - o_k)}, \tag{7.36}$$

where $G(o - o_k)$ is the Kernel function given by

$$G(o - o_k) = \frac{1}{(2\pi)^{D/2}} e^{(-\frac{1}{2}(o-o_k)^D.(o-o_k))} \tag{7.37}$$

Performance assessment

Different combinations of the aforementioned similarity evaluation and position estimation metrics are tested. The location error loc_{error} corresponding to all the combinations are given in Table 7.2. The location error is given by

$$loc_{error} = \sqrt{(lat_{est} - lat_r)^2 + (lon_{est} - lon_r)^2}, \tag{7.38}$$

where lat_{est} and lon_{est} are the estimated coordinates, and lat_r and lon_r are the real coordinates of the test fingerprint.

Looking to these results, one can note that the Nadaraya estimator has almost the worst performance in estimating the real coordinates. Furthermore, the weighted average is the best position estimation metric with deterministic similarity evaluation metrics (Euclidean and Manhattan distances) and the simple average is the best with the probabilistic metrics (Gauss and Kernel methods). Most importantly, the best results in terms of mean location error is obtained when using the Manhattan distance for similarity evaluation and the weighted average of K-nearest neighbors for the position estimation. It is worth to mention that these results were obtained for $K = 5$-Nearest Neighbors, which is identified to be the most suitable for the tested configuration.

7.3.2 Deep CNN for Indoor Localization

We deal with the issue of indoor localization in the context of IoT networks as a 3D radio image-fingerprint-based location recognition problem. Motivated by the outstanding performance of CNN in image classification problems, it is used with taking into account the correlation between different RSSI measurements to predict the position of a given node. We propose to split the studied environment into regions, "classes", limited in space, and we construct radio images from measured RSSI fingerprints, which are used as the CNN input data to predict the region index to which belongs the desired node.

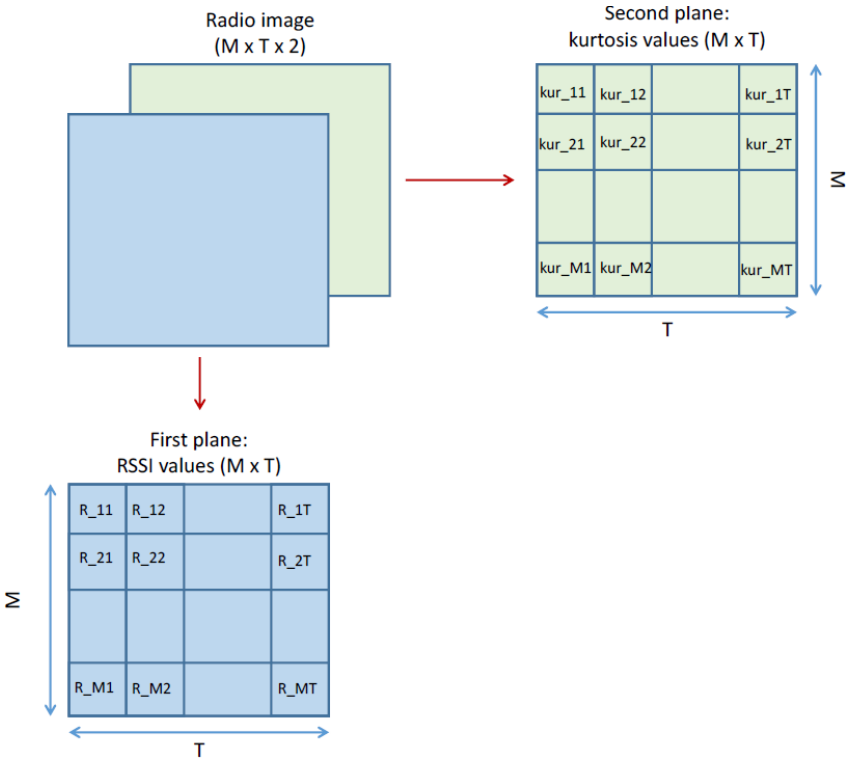

Figure 7.3: The structure of the radio images [J12].

Radio Image Construction

After collecting RSSI values from M APs during a time interval T, forming a 2D radio image. Then, a kurtosis is computed, which serves as the third dimension of the 3D radio image. Specifically, we put T measured RSSI values from M APs in the two first dimensions, and we put the computed kurtosis values in the third dimension. The kurtosis is defined by Karl Pearson as the fourth moment [172]. R_{mt} is the t-th RSSI value received from the m-th AP, where $m = 1, 2, ..., M$ and $t = 1, 2, ..., T$. For a given sensor node, the kurtosis is calculated as follows

$$kur_{mk} = \frac{1}{T} \times \sum_{t=1}^{T} (\frac{R_{mt} - \mu_k}{\sigma_k})^4, \tag{7.39}$$

where

$$\mu_k = \frac{\sum_{m=1}^{M} R_{mk}}{M}, \tag{7.40}$$

and

$$\sigma_k = \frac{\sum_{m=1}^{M} R_{mk}^2}{M}, \tag{7.41}$$

Then, the size of each realization is of $(M \times T \times 2)$ (Figure 7.3). Constructed radio images needed to be classified and organized, so each image is labeled q, $q = 1, 2, ..., Q$. Then, N realizations of each sensor node should belong to the associated class. Images are organized into Q folders labeled $class1, class2, ..., classQ$, each contains the appropriate 3D radio images.

To find a sensor's position, after acquiring RSSI values and doing the preprocessing of the data, a radio image is constructed having the same dimension and structure of those used for training. This image

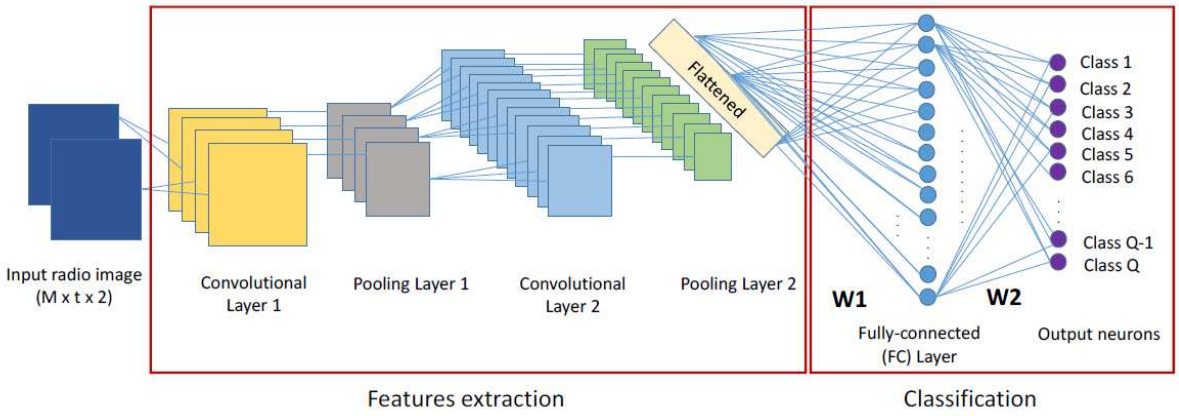

Figure 7.4: An example of a CNN architecture with two convolution layers, one pooling layer and one fully-connected layer [J12].

is fed to the trained model in order to predict the region to which the sensor node belongs. For this, probabilities are assigned to each class, and the predicted class is the one that corresponds to the highest probability.

Deep CNN Architecture Overview

The deep CNN includes specialized NN layers, where each layer ensures a specific function. Here, the structure of the CNN designed for region recognition consists of convolutional layers and pooling layers followed by one or more fully-connected layers. The CNN takes radio images as input and the classes' labels as outputs. The architecture of a CNN is given in Figure 7.4.

In the training phase, the backpropagation algorithm is used. The weights w are updated iteratively in order to reduce the cross-entropy loss function, between the initial prediction (estimated class) and the label (real class). The aforementioned optimisation methods have been adopted, such as the classical SGD [162], RMSProp [164] and Adam [165]. SGD is the most common first order optimization algorithm in machine learning and deep learning. RMSProp and Adam are first order gradient-based optimization of stochastic objective function algorithms. They are advanced methods used to optimize the learning process registered by SGD employing an adaptive learning rate.

Comparison of the Indoor Localization Accuracy of Different Approaches

The proposed indoor localization method based on CNN using RSSI fingerprinting is evaluated and compared to standard methods, like trilateration and classical MLP neural networks. All methods use the RSSI information to localize a specific sensor node. For the trilateration technique, it is based on pairwise distances between APs and the node to be localized, requiring at least three known pairwise distances. Traditional MLP NN, referred to as "Classic NN", which is a neural network composed of F_c fully connected (FC) layers. Many architectures have been deployed and tested in order to identify the best one, providing the best localization accuracy. Using the "Classical NN", the best localization accuracy 84.75% is obtained with $F_c = 2$ hidden layers with, respectively, 100 and 200. The number of output neurones is 120 corresponding to the number of regions/classes. Then, a deep CNN is deployed

Table 7.3: Comparison of the accuracy associated with different algorithms using a grid of size 2 m × 2 m and 10 anchors.

Indoor Localization Technique	**Accuracy (%)**
Trilateration	30
Classic NN	84.75
CNNLocWoC	91.57
CNNLocWC	94.13

Table 7.4: The deep learning network architectures used.

Deep Learning Algorithm	**Network Architecture**
Classic NN	FC(100)
	FC(200)
	FC(120)
CNNLocWoC	Conv(200,2)
	Max-pooling(2,2)
	Conv(120,2)
	FC(120)
CNNLocWC	Conv(200,2)
	Max-pooling(2,2)
	Conv(300,2)
	FC(120)

either with kurtosis or not, referring to as CNNLocWC and CNNLocWoC, respectively. Again, many architectures have been deployed and tested in order to identify the best one for each case. The identified architectures are given in Table 7.4.

In order to show the capability of the CNN based solutions, we give in Table 7.3 the localization accuracy comparison of the studied methods.

We clearly note that the classical trilateration provides the worst localization accuracy compared to the other tested solutions based on neural networks. The "Classic NN" is associated with good localization accuracy, but it is less accurate than the localization methods based on CNN. This latter provides the best localization accuracy. When used with kurtosis, only 5.84% of classes were wrongly estimated, confirming the ability of deep CNNs in providing very good performance for indoor localization.

7.4 Outputs

The outputs related to work on indoor localization are summarized bellow.

Supervision and collaborations related to work on Indoor Localization

- 02 PhD co-supervision: **Dr. Wafa Njima** (40%) and **Dr. Raida Zouari** (60%)
- Collaboration with Prof. Michel Terre (CEDRIC/CNAM-Paris)
- Visiting researcher CEDRIC/CNAM, Feb.-Apr. 2016

Publications related to work on Indoor Localization

- 02 peer-reviewed journals **[J13, J12]**
- 06 peer-reviewed international conferences **[C42, C29, C28, C27, C20, C17]**

Chapter 8

Research perspectives

In this chapter, I give the research paths I intend to follow during the next 5 years. My future works will be strongly correlated with the studies conducted within the framework of the two research projects, the H2020 MSCA ADAM5 (2018-2020), in which I am the principal researcher, and the PHC-TASSILI ATOME5+ (2019-2022), in which I am in charge of supervising PhD students. Furthermore, I also plan to develop other activities in parallel, for which a preliminary analysis has already been carried out. At the end of this chapter, some longer-term perspectives are highlighted. Figure 8.1 gives an overview of the intended research perspectives with an expected time-line.

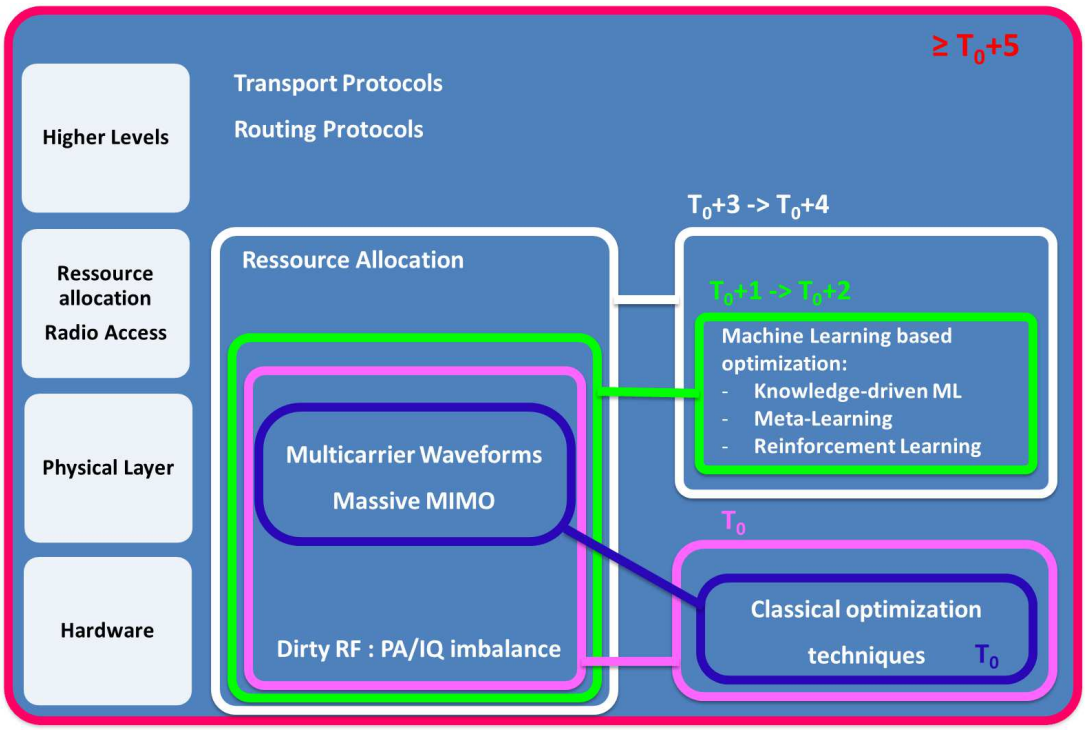

Figure 8.1: Research perspectives.

8.1 Optimization of Energy-Efficiency toward future wireless communications 6G

While the 5G is rolling out, academic and industrial researchers have started work on the sixth generation of the radio-mobile network. 100 times faster than 5G, with improved coverage and available everywhere including in space, 6G [173], whose emergence is expected in ten years, should also finalize the reliability of 5G services (eMBB, mMTC, URLLC) with taking into consideration very low latency and energy consumption. Furthermore, 6G should meet the requirements of future emerging applications (autonomous cars, connected devices also autonomous,...), which require high level of autonomy and have a great awareness of the environment and knowledge of the activities and needs of users. Autonomous and intelligent communication systems have the potential to improve overall system performance and reduce the workload associated with configuring and managing communication systems. 6G will offer new digital technology perspectives. Nevertheless, the complexity of the future 6G will exceed the current technology capabilities as well as conventional optimization approaches. Then, a fundamental evolution towards technologies like multi-carrier waveforms and massive MIMO is of paramount importance. In this regard, my research project is to reinforce the development of the composite of two timely concepts, Massive MIMO, flexible multi-carrier waveforms, the most promising direction in 6G wireless communications, where energy-efficiency, low latency, good reliability and high data rate are of crucial importance. The contribution of my previous work in this context is obvious, leading then to a fruitful contribution.

8.1.1 Study of Hardware Imperfection in Multi-carrier/Multi-antenna based 6G systems

The implementation of a multi-standard communication system with very wide spectral bands, all with low energy consumption, reduced size and low cost, is not without consequences for the terminal. Indeed, building compact and low-cost radio equipment implies non-ideal hardware (HW) quality. Then, various RF impairments could take place in the used radio transceiver, such as oscillator phase noise, mirror-frequency interference due to IQ mismatch, Tx Leakage due to an adjacent antenna and non-linear distortion due to power amplifier (PA). We are talking about radio imperfections generated by the radio frequency (RF) chain, known as "Dirty-RF" [174]. In addition, crosstalk between antennas may occur, affecting then the transmission quality. These imperfections, which are often neglected, have detrimental effects on massive MIMO communications with multi-carrier waveforms.

In my previous works [J16], the study was limited to the PA non-linearities. A first objective is to study the impact of Dirty-RF on massive MIMO performance with taking into account the optimization of the multi-carrier waveform as a function of the propagation channel (delay spread, time-varying,...) and, on the other hand, of the type of non-linear imperfections caused by the RF chain. The second objective is the development of reliable digital signal processing based solutions to mitigate RF impairments on both the transmitter and receiver sides of 6G communication systems. This will enable extensive use of low-cost and low-power components.

8.1.2 Optimization and adaptation of MWFs toward future wireless communications 6G

As explained in Chapter 4, all the MWF design-related research works are motivated by the fact that perfect orthogonality, recommended by all the pioneering works on OFDM, is not sufficient to guarantee excellent performance, in presence of time and frequency dispersions, commonly encountered in cellular radio-mobile systems. Taking this fact into account, a part of research works [175] have focused on optimizing the localization in time and frequency of the adopted waveforms, with however relaxing the perfect orthogonality of these waveforms. Nevertheless, satisfying both of antagonistic constraints of perfect orthogonality and good localization is not without impacts on the system performance which remains quite low and disappointing to fulfill the requirements of practical radio-mobile networks. Furthermore, the frequency localization metric remains a purely intuitive criterion and does not lead to increased robustness against channel dispersions. Another part of research works aim at reducing the inter-symbol interference and inter-carrier interference, often in a context of identical waveforms at emission and reception. However, doing that has a dramatically impact on the limitation of degrees of freedom in the optimization of practical communication systems. Few works deal with different waveforms in transmission and reception, with, however, a preservation of a strict orthogonality, referred to as biorthogonality [40, 175–177].

In 2018, I collaborated with a research team in Mediatron laboratory of Sup'Com school, which have proposed a new approach of waveform optimization [178–181]. The proposed approach, referred to as POPS (Ping-pong Optimized Pulse Shaping), permit an effective optimization of waveforms for any channel propagation statistics, with relaxing the constraints of identical waveforms in emission and reception. In my research project, the POPS approach will be judiciously used to perform the adaptive waveform communications (AWC).

In this regard, a first research activity will be about the modeling of artificial imperfections, in terms of time and frequency dispersions, caused by the new 5G+/6G applications. A second part consists in optimizing batteries (or dictionaries) for each service of interest, with taking into account the considered channel statistics. Then, I intend to study the real-time estimation of propagation statistics, during communication, with the application of the most suitable waveform pairs. In this context, I will study the reduction of pilot contamination in massive MIMO systems, in order to simplify the coherent detection of pilot symbols (referred to as Pilot Aided Channel estimation-PACE), known at the receiver side. If the pilots are sufficiently close in time and frequency (applied to OFDM), the impulse response of the transmission channel can be reconstructed in two-dimensions (2D) through interpolation. In the context of massive MIMO, the principle of channel estimation via interpolation can be extended to spatial domain, leading to a 3D implementation in the grid of PACE pilots.

On the other hand, the pilot contamination problem in massive MIMO, adopting time-division duplex (TDD), can limit their expected capacity performance. For channel reciprocity, in TDD mode, the channel state information (CSI) is obtained at the base station (BS) when transmitting in the uplink. The channel coherence interval is generally not very large to enable the use of orthogonal pilot sequences in different cells. The non-orthogonal pilots of adjacent cells contaminate the pilots of the cell of interest. Thus, the channel estimation at each BS contains the channel information of mobile terminals (MTs) in the other cells, together with the ones of its own users. Consequently, when the BS combines linearly the received signal in order to decode the transmitted symbols of its own MTs, it also combines linearly the symbols of users of adjacent cells, leading to an inter-cell interference. This latter does not vanish by increasing the number of BS antennas, even to infinity [182, 183]. One goal will be the implementation

of 3D PACE for the channel estimation in massive MIMO applied to MWFs. Then, we will investigate the pilot decontamination in massive MIMO, with different MWFs, by extending the blind equalization techniques studied in SISO to multi-cell massive MIMO [184] in order to reduce the effects of channel estimation error caused by the pilot contamination. Moreover, we will investigate the impact of the pilot distribution on the PAPR.

8.2 Meta-Learning for Energy-Efficiency enhancement in Massive MIMO systems

In the framework of the H2020 MSCA ADAM5 project, we have developed algorithms [J15, J16] to improve the energy-efficiency related to power amplification in massive MIMO systems. Several optimization methods have been deployed and compared in terms of performance and complexity. All these methods offer good performance but their complexities remains a major problem to be solved, especially when the channel is fast time-varying and the number of users is large enough.

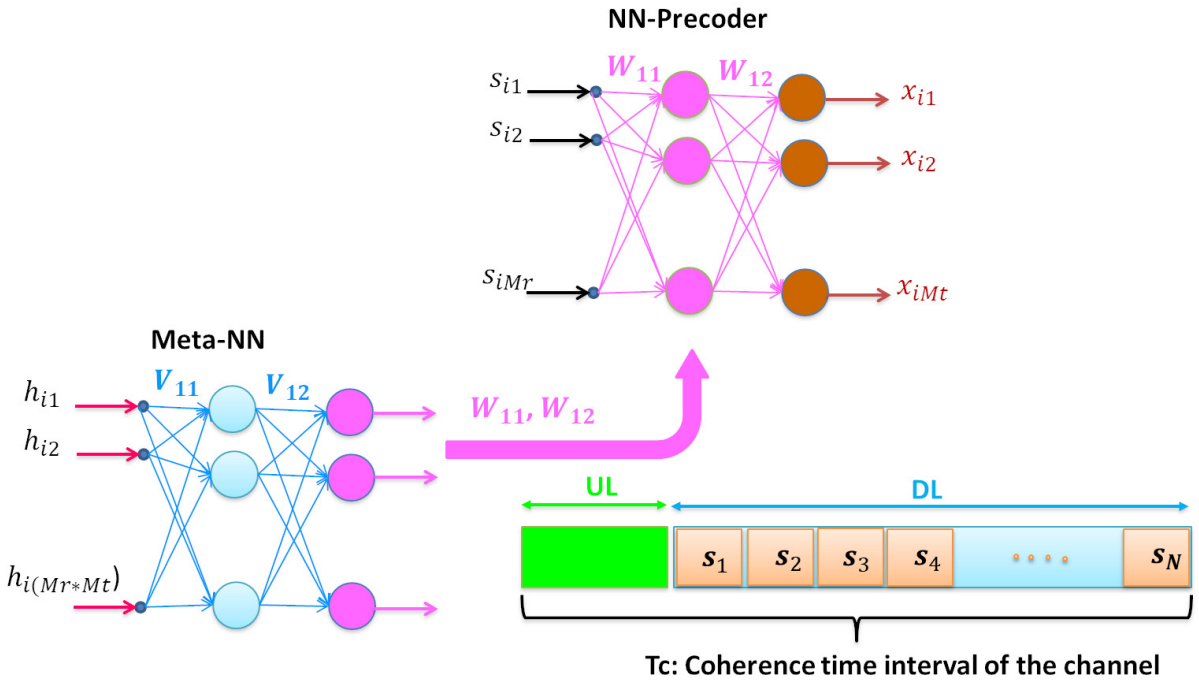

Figure 8.2: Meta-model for energy-efficiency enhancement in massive MIMO systems.

In order to overcome this problem, we are investigating a new advanced approach to complement traditional machine learning (ML) methods, the meta-learning [185] (learning to learn) approach, which allows lower complexity. The aim is to develop a meta-learning model capable of being generalized with a new configuration that has never been learned during learning (like a new channel matrix, for example). Specifically, we propose to use two neural networks (NN precoder and Meta-NN, as shown by Figure 8.2). The first one, the NN Precoder, which can be generalized for any data streams ($\mathbf{s}_i \in \mathbb{C}^{M_r} \times 1$) for

a given channel configuration, is used to generate the precoded data vector ($\mathbf{x}_i \in \mathbb{C}^{M_t} \times 1$) such that when nonlinearly amplified and then propagated through the channel, the received data symbols is very similar to the transmitted ones. Note that the NN-Precoder is executed N times per channel coherence time interval, T_c (see Figure 8.2). The second NN, the Meta-NN, is used to generate the weights of the NN-Precoder corresponding to a channel configuration. Meta-NN, which can be generalized for any channel configuration, is then executed only one time per channel coherence time. Doing that, we avoid the adaptation of the NN-Precoder and the corresponding computational complexity when the channel changes and we use instead a generalization of the Meta-NN. Preliminary results have been obtained showing that the proposed meta-model provides the same BER performance as the algorithm, proposed in [J16], but with a lower computational complexity of one order of magnitude.

In this regard, I initiated a collaboration with researchers from the CEDRIC/VERTIGO team, specialists in the field of machine learning. This collaboration was initiated by the supervision of the Samar Chebbi's master internship (ongoing) and should be pursued by the supervision of a PhD.

8.3 ML-aided Multi-carrier Waveform parameters selection for Future Heterogeneous Network towards 6G

The studied MWFs have shown to overcome the limitations of the today's OFDM technique in supporting asynchronous communications and enabling flexible accommodation of various applications/services with different requirements. From the flexibility perspective, ultra reliability, low latency, high security, high spectral efficiency, high energy efficiency, and low complexity are some example requirements of different service types. Therefore, different optimizations need to be done for meeting some of these requirements together while providing complete satisfaction for all users simultaneously. The aim is to develop machine learning approach to help base stations to decide on the waveform parameters of each user using channel information (random maximum excess delay, random maximum Doppler effect, and random service type (eMBB, uRLLC, or mMTC)). The MWF parameters can be the numerology parameters (the subcarrier spacing CP duration, slot duration, maximum allowed bandwidth,...), the number of numerologies, the waveform processing technique (windowing, filtering, ...). Three performance metrics (SINR, spectral efficiency, and flexibility) will be considered.

8.4 Knowledge-driven Machine Learning for radio access management optimization in Massive MIMO systems

In communication systems, mathematical models for performance's optimization are often available making then the adoption of deep learning more flexible than a purely data-driven approach. Indeed, the optimization of these theoretical models is sometimes incompatible with real-time wireless communications, i.e., the complexity and the time to do so might not be compatible with fast time-varying wireless communication scenarios (e.g., user joins/leaves the network, the channel realizations change, time-varying hardware impairments, and so on); In this regard, my project is to study new approaches of machine learning which capitalize on the availability of these theoretical models to reduce the amount of empirical data required and thus the learning complexity. The key idea is to complement purely data-driven machine learning, such as knowledge-driven machine learning [186].

The objective is to develop knowledge-driven machine learning approach, to complement purely data-driven ML, in order to solve radio access problems in networks with massive connectivity and different QoS requirements, which is essential in beyond 5G and the future 6G. The work will be dedicated to the field of radio resource management for real-time energy-efficiency maximization in multi-user massive MIMO networks. The goal is to allocate the transmit powers of the users to maximize the network's bit/Joule energy-efficiency, which is defined as the ratio between the system sum achievable rate and the total network power consumption. Here, power amplifier imperfection will be considered, where a model to formulate the energy-efficiency optimization problem is available, but the presence of interference-related PA distortion makes it too complex to be globally solved at an affordable computational complexity. This is especially problematic when the optimization is performed in fast time-varying channel because it causes a considerable complexity overhead that prevents the use of real-time implementations.

8.5 System-wide optimisation: Machine learning and distributed intelligence

As a long-term perspectives, I intend to investigate effective ML approaches to achieve global system optimization. A possible global optimization may include the resource allocation policy at the base stations. Routing strategy to be applied to the different flows crossing the network, scheduling policies in the switches, and transport protocol parameters can also be jointly optimized for the specific context. Nevertheless, such multi-dimensional optimization, which is an interesting task, is impossible to solve directly in real-time using traditional optimization methods. Therefore, I believe that ANN based knowledge-driven deep learning can indeed help the development of an innovative scalable approach to the above problem. This multi-level model is a very advanced topic.

8.6 Conclusion

All of the aforementioned research perspectives represent, in one hand, the evolution of some existing works and, on the other hand, investigating new directions, characterizing my future research activities. These six proposals include developments concerning signal processing for 6G multi-carrier and multi-antenna communications, optimization of energy efficiency, hardware imperfection problems, resource allocation and machine-learning.

Bibliography

[1] M. Yao, M. Sohul, R. Nealy, V. Marojevic, and J. Reed, "A digital predistortion scheme exploiting degrees-of-freedom for massive mimo systems," in *2018 IEEE International Conference on Communications (ICC)*, May 2018, pp. 1–5.

[2] R. Zayani, H. Shaiek, and D. Roviras, "Efficient precoding for massive mimo downlink under pa nonlinearities," *IEEE Communications Letters*, vol. 23, no. 9, pp. 1611–1615, 2019.

[3] Gerhard Fettweis and Ernesto Zimmermann, "Ict energy consumption ? trends and challenges," 2008.

[4] A. A. M. Saleh, "Frequency-independent and frequency-dependent nonlinear models of twt amplifiers," *IEEE Transactions on Communications*, vol. 29, no. 11, pp. 1715–1720, November 1981.

[5] T. Wang and J. Ilow, "Compensation of nonlinear distortions with memory effects in ofdm transmitters," in *IEEE Global Telecommunications Conference, 2004. GLOBECOM '04.*, 2004, vol. 4, pp. 2398–2403 Vol.4.

[6] Jian Li and J. Ilow, "Adaptive volterra predistorters for compensation of non-linear effects with memory in ofdm transmitters," in *4th Annual Communication Networks and Services Research Conference (CNSR'06)*, May 2006, pp. 4 pp.–103.

[7] Rafik Zayani, Ridha Bouallegue, and Daniel Roviras, "Adaptive predistortions based on neural networks associated with levenberg-marquardt algorithm for satellite down links," *EURASIP Journal on Wireless Communications and Networking*, vol. 2008, no. 1, pp. 132729, Jul 2008.

[8] Richard S. Sutton, "Two problems with backpropagation and other steepest-descent learning procedures for networks," in *Proceedings of the Eighth Annual Conference of the Cognitive Science Society*. 1986, Hillsdale, NJ: Erlbaum.

[9] Ning Qian, "On the momentum term in gradient descent learning algorithms," *Neural Netw.*, vol. 12, no. 1, pp. 145–151, Jan. 1999.

[10] R. Fletcher and C. M. Reeves, "Function minimization by conjugate gradients," *The Computer Journal*, vol. 7, no. 2, pp. 149–154, 01 1964.

[11] D. F. Shanno, "Conditioning of quasi-newton methods for function minimization," *Mathematics of Computation*, vol. 24, no. 111, pp. 647–656, 1970.

[12] Donald W. Marquardt, "An algorithm for least-squares estimation of nonlinear parameters," *Journal of the Society for Industrial and Applied Mathematics*, vol. 11, no. 2, pp. 431–441, 1963.

[13] H. Bogucka and A. Conti, "Degrees of freedom for energy savings in practical adaptive wireless systems," *IEEE Communications Magazine*, vol. 49, no. 6, pp. 38–45, June 2011.

[14] Mohammad Dastbaz, Colin Pattinson, and Babak Akhgar, *Green Information Technology: A Sustainable Approach*, Morgan Kaufmann Publishers Inc., San Francisco, CA, USA, 1st edition, 2015.

[15] Y. Medjahdi, R. Zayani, H. Shaiek, and D. Roviras, "Wola processing: A useful tool for windowed waveforms in 5g with relaxed synchronicity," in *2017 IEEE International Conference on Communications Workshops (ICC Workshops)*, May 2017, pp. 393–398.

[16] M. Bellanger, "Physical layer for future broadband radio systems," in *2010 IEEE Radio and Wireless Symposium (RWS)*, Jan 2010, pp. 436–439.

[17] B. Farhang-Boroujeny, "Ofdm versus filter bank multicarrier," *IEEE Signal Processing Magazine*, vol. 28, no. 3, pp. 92–112, May 2011.

[18] G. Cherubini, E. Eleftheriou, S. Oker, and J. M. Cioffi, "Filter bank modulation techniques for very high speed digital subscriber lines," *IEEE Communications Magazine*, vol. 38, no. 5, pp. 98–104, May 2000.

[19] N. Michailow, M. Matthé, I. S. Gaspar, A. N. Caldevilla, L. L. Mendes, A. Festag, and G. Fettweis, "Generalized frequency division multiplexing for 5th generation cellular networks," *IEEE Transactions on Communications*, vol. 62, no. 9, pp. 3045–3061, 2014.

[20] M. J. Abdoli, M. Jia, and J. Ma, "Weighted circularly convolved filtering in ofdm/oqam," in *2013 IEEE 24th Annual International Symposium on Personal, Indoor, and Mobile Radio Communications (PIMRC)*, Sep. 2013, pp. 657–661.

[21] G. Fettweis, M. Krondorf, and S. Bittner, "Gfdm - generalized frequency division multiplexing," in *VTC Spring 2009 - IEEE 69th Vehicular Technology Conference*, April 2009, pp. 1–4.

[22] H. Cho, Y. Yan, G. Chang, and X. Ma, "Asynchronous multi-user uplink transmissions for 5g with ufmc waveform," in *2017 IEEE Wireless Communications and Networking Conference (WCNC)*, March 2017, pp. 1–5.

[23] L. Zhang, A. Ijaz, P. Xiao, M. M. Molu, and R. Tafazolli, "Filtered ofdm systems, algorithms, and performance analysis for 5g and beyond," *IEEE Transactions on Communications*, vol. 66, no. 3, pp. 1205–1218, March 2018.

[24] R. Zakaria and D. Le Ruyet, "Theoretical analysis of the power spectral density for fft-fbmc signals," *IEEE Communications Letters*, vol. 20, no. 9, pp. 1748–1751, 2016.

[25] R. Gerzaguet, D. Demmer, J. Doré, and D. Ktiénas, "Block-filtered ofdm: A new promising waveform for multi-service scenarios," in *2017 IEEE International Conference on Communications (ICC)*, May 2017, pp. 1–6.

[26] R. Zayani, Y. Medjahdi, H. Shaiek, and D. Roviras, "Wola-ofdm: A potential candidate for asynchronous 5g," in *2016 IEEE Globecom Workshops (GC Wkshps)*, Dec 2016, pp. 1–5.

[27] "3rd Generation Partnership Project (3GPP), overall description stage 2, technical specification group access network 38.300, 12 2017, 2.0.0.," .

[28] H. Lin and P. Siohan, "Multi-carrier modulation analysis and wcp-coqam proposal," *EURASIP Journal Advanced Signal Processing*, vol. 79, no. 2014, 2014.

[29] J. Guerreiro, R. Dinis, and P. Montezuma, "On the optimum multicarrier performance with memoryless nonlinearities," *IEEE Transactions on Communications*, vol. 63, no. 2, pp. 498–509, Feb 2015.

[30] S. Lien, S. Shieh, Y. Huang, B. Su, Y. Hsu, and H. Wei, "5g new radio: Waveform, frame structure, multiple access, and initial access," *IEEE Communications Magazine*, vol. 55, no. 6, pp. 64–71, 2017.

[31] "Phydyas-physical layer for dynamic spectrum access and cognitive radio," in *Document 5.1 deliverable*, 2009, vol. www.ict-phydyas.org.

[32] M. G. Bellanger, "Specification and design of a prototype filter for filter bank based multicarrier transmission," in *2001 IEEE International Conference on Acoustics, Speech, and Signal Processing. Proceedings (Cat. No.01CH37221)*, 2001, vol. 4, pp. 2417–2420 vol.4.

[33] A. Sahin, I. Guvenc, and H. Arslan, "A survey on multicarrier communications: Prototype filters, lattice structures, and implementation aspects," *IEEE Communications Surveys Tutorials*, vol. 16, no. 3, pp. 1312–1338, 2014.

[34] D. Gabor, "Theory of communication. part 1: The analysis of information," *Journal of the Institution of Electrical Engineers - Part III: Radio and Communication Engineering*, vol. 93, no. 26, pp. 429–441, 1946.

[35] Jinfeng Du and Svante Signell, "Classic ofdm systems and pulse shaping ofdm/oqam systems," 2007.

[36] Peter L. Søndergaard, "Finite discrete gabor analysis," 2007.

[37] Peter Jung, "Weyl-heisenberg representations in communication theory," 2007.

[38] Du Jinfeng, "Pulse shape adaptation and channel estimation in generalised frequency division multiplexing," 2008.

[39] T. Strohmer and S. Beaver, "Optimal ofdm design for time-frequency dispersive channels," *IEEE Transactions on Communications*, vol. 51, no. 7, pp. 1111–1122, 2003.

[40] F. . Han and X. . Zhang, "Wireless multicarrier digital transmission via weyl-heisenberg frames over time-frequency dispersive channels," *IEEE Transactions on Communications*, vol. 57, no. 6, pp. 1721–1733, 2009.

[41] W. Kozek and A. F. Molisch, "Nonorthogonal pulseshapes for multicarrier communications in doubly dispersive channels," *IEEE Journal on Selected Areas in Communications*, vol. 16, no. 8, pp. 1579–1589, 1998.

[42] F. Han and X. Zhang, "Hexagonal multicarrier modulation: A robust transmission scheme for time-frequency dispersive channels," *IEEE Transactions on Signal Processing*, vol. 55, no. 5, pp. 1955–1961, 2007.

[43] T. Hwang, C. Yang, G. Wu, S. Li, and G. Ye Li, "Ofdm and its wireless applications: A survey," *IEEE Transactions on Vehicular Technology*, vol. 58, no. 4, pp. 1673–1694, 2009.

[44] J. J. Yan, D. E. Cowles, D. Kimball, and A. Mattsson, "Multi-carrier envelope tracking power amplifier," in *MILCOM 2018 - 2018 IEEE Military Communications Conference (MILCOM)*, 2018, pp. 313–316.

[45] Y. Medjahdi, S. Traverso, R. Gerzaguet, H. Shaiek, R. Zayani, D. Demmer, R. Zakaria, J. Doré, M. Ben Mabrouk, D. Le Ruyet, Y. LouÃ«t, and D. Roviras, "On the road to 5g: Comparative study of physical layer in mtc context," *IEEE Access*, vol. 5, pp. 26556–26581, 2017.

[46] Y. Medjahdi, D. Le Ruyet, D. Roviras, H. Shaiek, and R. Zakaria, "On the impact of the prototype filter on fbmc sensitivity to time asynchronism," in *2012 International Symposium on Wireless Communication Systems (ISWCS)*, 2012, pp. 939–943.

[47] D. Demmer, R. Zakaria, J. Doré, R. Gerzaguet, and D. L. Ruyet, "Filter-bank ofdm transceivers for 5g and beyond," in *2018 52nd Asilomar Conference on Signals, Systems, and Computers*, 2018, pp. 1057–1061.

[48] H. Lin, "Flexible configured ofdm for 5g air interface," *IEEE Access*, vol. 3, pp. 1861–1870, 2015.

[49] M. Bellanger, D. Mattera, and M. Tanda, "Lapped-ofdm as an alternative to cp-ofdm for 5g asynchronous access and cognitive radio," in *2015 IEEE 81st Vehicular Technology Conference (VTC Spring)*, 2015, pp. 1–5.

[50] A. Sahin, R. Yang, E. Bala, M. C. Beluri, and R. L. Olesen, "Flexible dft-s-ofdm: Solutions and challenges," *IEEE Communications Magazine*, vol. 54, no. 11, pp. 106–112, 2016.

[51] V. Vakilian, T. Wild, F. Schaich, S. ten Brink, and J. Frigon, "Universal-filtered multi-carrier technique for wireless systems beyond lte," in *2013 IEEE Globecom Workshops (GC Wkshps)*, 2013, pp. 223–228.

[52] T. Wild, F. Schaich, and Y. Chen, "5g air interface design based on universal filtered (uf-)ofdm," in *2014 19th International Conference on Digital Signal Processing*, 2014, pp. 699–704.

[53] B. Muquet, Zhengdao Wang, G. B. Giannakis, M. de Courville, and P. Duhamel, "Cyclic prefixing or zero padding for wireless multicarrier transmissions?," *IEEE Transactions on Communications*, vol. 50, no. 12, pp. 2136–2148, 2002.

[54] F. Schaich, T. Wild, and Y. Chen, "Waveform contenders for 5g - suitability for short packet and low latency transmissions," in *2014 IEEE 79th Vehicular Technology Conference (VTC Spring)*, 2014, pp. 1–5.

[55] X. Zhang, M. Jia, L. Chen, J. Ma, and J. Qiu, "Filtered-ofdm - enabler for flexible waveform in the 5th generation cellular networks," in *2015 IEEE Global Communications Conference (GLOBECOM)*, 2015, pp. 1–6.

[56] Xiaoying Zhang, Lei Zhang, Pei Xiao, Dongtang Ma, Jibo Wei, and Yu Xin, "Mixed numerologies interference analysis and inter-numerology interference cancellation for windowed ofdm systems," *IEEE Transactions on Vehicular Technology*, vol. 67, no. 8, pp. 7047–7061, 2018.

[57] R. Zakaria and D. Le Ruyet, "A novel filter-bank multicarrier scheme to mitigate the intrinsic interference: Application to mimo systems," *IEEE Transactions on Wireless Communications*, vol. 11, no. 3, pp. 1112–1123, 2012.

[58] R. Zakaria and D. Le Ruyet, "A novel fbmc scheme for spatial multiplexing with maximum likelihood detection," in *2010 7th International Symposium on Wireless Communication Systems*, 2010, pp. 461–465.

[59] R. Zakaria and D. Le Ruyet, "Analysis of the fft-fbmc equalization in selective channels," *IEEE Signal Processing Letters*, vol. 24, no. 6, pp. 897–901, 2017.

[60] D. Demmer, R. Gerzaguet, J. Doré, D. Le Ruyet, and D. Kténas, "Block-filtered ofdm: A novel waveform for future wireless technologies," in *2017 IEEE International Conference on Communications (ICC)*, 2017, pp. 1–6.

[61] D. Demmer, R. Gerzaguet, J. Doré, D. Le Ruyet, and D. Kténas, "Filter design for 5g bf-ofdm waveform," in *2017 European Conference on Networks and Communications (EuCNC)*, 2017, pp. 1–5.

[62] R. Gerzaguet, Y. Medjahdi, D. Demmer, R. Zayani, J. Doré, H. Shaiek, and D. Roviras, "Comparison of promising candidate waveforms for 5g: Wola-ofdm versus bf-ofdm," in *2017 International Symposium on Wireless Communication Systems (ISWCS)*, Aug 2017, pp. 355–359.

[63] Qualcomm, Incorporated, "R1-162199 - Waveform candidates," .

[64] I. Gaspar, M. Matthé, N. Michailow, L. Leonel Mendes, D. Zhang, and G. Fettweis, "Frequency-shift offset-qam for gfdm," *IEEE Communications Letters*, vol. 19, no. 8, pp. 1454–1457, 2015.

[65] P. Siohan H. Lin, "Multi-carrier modulation analysis and wcp-coqam proposal," *EURASIP J. Adv. Signal Process.*, vol. 2014, no. 79, 2014.

[66] B. Picinbono and P. Chevalier, "Widely linear estimation with complex data," *IEEE Transactions on Signal Processing*, vol. 43, no. 8, pp. 2030–2033, Aug 1995.

[67] R. Dayana and R. Kumar, "Co-operative cyclo-stationary feature detection with universal filtered multi-carrier spectrum sensing for cognitive radio network," in *2016 IEEE International Conference on Recent Trends in Electronics, Information Communication Technology (RTEICT)*, May 2016, pp. 1647–1650.

[68] V. Lazov and G. Vandersteen, "Cyclo-stationary process analysis within telecom applications," in *2016 IEEE International Instrumentation and Measurement Technology Conference Proceedings*, May 2016, pp. 1–6.

[69] H. Gerstacker, R. Schober, and A. Lampe, "Receivers with widely linear processing for frequency-selective channels," *IEEE Transactions on Communications*, vol. 51, no. 9, pp. 1512–1523, Sep. 2003.

[70] P. Chevalier, J. Delmas, and R. Chauvat, "Reception filter impact on widely linear fresh receiver performance for saic/maic with frequency offsets," in *2016 IEEE Sensor Array and Multichannel Signal Processing Workshop (SAM)*, July 2016, pp. 1–5.

[71] R. Chauvat, P. Chevalier, and J. Delmas, "Widely linear fresh receiver for saic/maic with frequency offsets," in *2015 International Symposium on Wireless Communication Systems (ISWCS)*, Aug 2015, pp. 536–540.

[72] M. Elgenedy, M. Sayed, N. Al-Dhahir, and R. C. Chabaan, "Cyclostationary noise mitigation for simo powerline communications," *IEEE Access*, vol. 6, pp. 5460–5484, 2018.

[73] H. Fhima, H. Shaiek, R. Zayani, D. Roviras, B. S. Chang, and R. Bouallegue, "Analysis of widely linear equalization over frequency selective channels with multiple interferences," in *2018 14th International Conference on Wireless and Mobile Computing, Networking and Communications (WiMob)*, Oct 2018, pp. 83–88.

[74] Pascal Chevalier and François Pipon, "New insights into optimal widely linear array receivers for the demodulation of bpsk, msk, and gmsk signals corrupted by noncircular interferences-application to saic," *IEEE Transactions on Signal Processing*, vol. 54, no. 3, pp. 870–883, 2006.

[75] A. Ikhlef and J. Louveaux, "An enhanced mmse per subchannel equalizer for highly frequency selective channels for fbmc/oqam systems," in *2009 IEEE 10th Workshop on Signal Processing Advances in Wireless Communications*, June 2009, pp. 186–190.

[76] H. Fhima, B. S. Chang, R. Zayani, H. Shaiek, D. Roviras, and R. Bouallegue, "Performance of linear and widely linear equalizers for fbmc/oqam modulation," in *2018 25th International Conference on Telecommunications (ICT)*, June 2018, pp. 605–609.

[77] H. Fhima, R. Zayani, H. Shaiek, D. Roviras, B. S. Chang, and R. Bouallegue, "Widely linear equalizer performance with multiple independent interferences," in *2017 IEEE Symposium on Computers and Communications (ISCC)*, July 2017, pp. 912–917.

[78] Hayfa Fhima, "Study and implementation of widely linear (wl) receiver for filter bank based multicarrier (fbmc-oqam) modulations over frequency selective channels," 2019.

[79] Z. Rostom and D. Le Ruyet, "Ser analysis by gaussian interference approximation for fbmc system in the presence of phase error," in *2015 IEEE International Conference on Communications (ICC)*, 2015, pp. 2662–2667.

[80] P. Siohan, C. Siclet, and N. Lacaille, "Analysis and design of ofdm/oqam systems based on filterbank theory," *IEEE Transactions on Signal Processing*, vol. 50, no. 5, pp. 1170–1183, 2002.

[81] R. Zayani, H. Shaiek, D. Roviras, and Y. Medjahdi, "Ber analysis of filter-bank multicarrier with offset quadrature amplitude modulation systems with phase estimation error," *IET Communications*, vol. 11, no. 15, pp. 2269–2273, 2017.

[82] M. Abramowitz and I. A. Stegun, "Handbook of mathematical functions with formulas, graphs, and mathematical tables," *Washington National Bureau of Standards*, 1984.

[83] JJ Bussgang, "Recrosscorrelation functions of amplitude-distorted gaussian," *Research Laboratory of Electronics, Massachusetts Institute of Technology, Cambridge. Technical Report*, vol. 216, 1952.

[84] D. Dardari, V. Tralli, and A. Vaccari, "A theoretical characterization of nonlinear distortion effects in ofdm systems," *IEEE Transactions on Communications*, vol. 48, no. 10, pp. 1755–1764, 2000.

[85] R. Raich, Hua Qian, and G. T. Zhou, "Orthogonal polynomials for power amplifier modeling and predistorter design," *IEEE Transactions on Vehicular Technology*, vol. 53, no. 5, pp. 1468–1479, 2004.

[86] Lei Ding, G. T. Zhou, D. R. Morgan, Zhengxiang Ma, J. S. Kenney, Jaehyeong Kim, and C. R. Giardina, "A robust digital baseband predistorter constructed using memory polynomials," *IEEE Transactions on Communications*, vol. 52, no. 1, pp. 159–165, 2004.

[87] D. R. Morgan, Z. Ma, J. Kim, M. G. Zierdt, and J. Pastalan, "A generalized memory polynomial model for digital predistortion of rf power amplifiers," *IEEE Transactions on Signal Processing*, vol. 54, no. 10, pp. 3852–3860, 2006.

[88] P. M. Lavrador, J. C. Pedro, and N. B. Carvalho, "A new volterra series based orthogonal behavioral model for power amplifiers," in *2005 Asia-Pacific Microwave Conference Proceedings*, 2005, vol. 1, pp. 4 pp.–.

[89] J. Dooley, B. O'Brien, and T. J. Brazil, "Behavioral modeling of rf power amplifiers using adaptive recursive polynomial functions," in *2006 IEEE MTT-S International Microwave Symposium Digest*, 2006, pp. 852–855.

[90] A. Zhu, J. C. Pedro, and T. J. Brazil, "Dynamic deviation reduction-based volterra behavioral modeling of rf power amplifiers," *IEEE Transactions on Microwave Theory and Techniques*, vol. 54, no. 12, pp. 4323–4332, 2006.

[91] Genevieve Baudoin; Olivier Venard; Dang-Kien Germain Pham, "Digital predistortion," *Digitally Enhanced Mixed Signal Systems*, May 2019.

[92] C. Tarver, A. Balatsoukas-Stimming, and J. R. Cavallaro, "Design and implementation of a neural network based predistorter for enhanced mobile broadband," in *2019 IEEE International Workshop on Signal Processing Systems (SiPS)*, 2019, pp. 296–301.

[93] D. Wang, M. Aziz, M. Helaoui, and F. M. Ghannouchi, "Augmented real-valued time-delay neural network for compensation of distortions and impairments in wireless transmitters," *IEEE Transactions on Neural Networks and Learning Systems*, vol. 30, no. 1, pp. 242–254, 2019.

[94] S. M. Alamouti, "A simple transmit diversity technique for wireless communications," *IEEE Journal on Selected Areas in Communications*, vol. 16, no. 8, pp. 1451–1458, 1998.

[95] Heung-Gyoon Ryu, Byoung-Ii Jin, and In-Bae Kim, "Papr reduction using soft clipping and aci rejection in ofdm system," *IEEE Transactions on Consumer Electronics*, vol. 48, no. 1, pp. 17–22, 2002.

[96] A. Behravan and T. Eriksson, "Tone reservation to reduce the envelope fluctuations of multicarrier signals," *IEEE Transactions on Wireless Communications*, vol. 8, no. 5, pp. 2417–2423, 2009.

[97] R. W. Bauml, R. F. H. Fischer, and J. B. Huber, "Reducing the peak-to-average power ratio of multicarrier modulation by selected mapping," *Electronics Letters*, vol. 32, no. 22, pp. 2056–2057, 1996.

[98] Zhixing Yang, Haidong Fang, and Changyong Pan, "Ace with frame interleaving scheme to reduce peak-to-average power ratio in ofdm systems," *IEEE Transactions on Broadcasting*, vol. 51, no. 4, pp. 571–575, 2005.

[99] S. H. Muller and J. B. Huber, "Ofdm with reduced peak-to-average power ratio by optimum combination of partial transmit sequences," *Electronics Letters*, vol. 33, no. 5, pp. 368–369, 1997.

[100] J. Chen and C. Wen, "Papr reduction of ofdm signals using cross-entropy-based tone injection schemes," *IEEE Signal Processing Letters*, vol. 17, no. 8, pp. 727–730, 2010.

[101] T. A. Wilkinson and A. E. Jones, "Minimisation of the peak to mean envelope power ratio of multicarrier transmission schemes by block coding," in *1995 IEEE 45th Vehicular Technology Conference. Countdown to the Wireless Twenty-First Century*, 1995, vol. 2, pp. 825–829 vol.2.

[102] Seung Hee Han and Jae Hong Lee, "An overview of peak-to-average power ratio reduction techniques for multicarrier transmission," *IEEE Wireless Communications*, vol. 12, no. 2, pp. 56–65, 2005.

[103] T. Jiang and Y. Wu, "An overview: Peak-to-average power ratio reduction techniques for ofdm signals," *IEEE Transactions on Broadcasting*, vol. 54, no. 2, pp. 257–268, 2008.

[104] Chan-Soo Hwang, "Peak power reduction method for multicarrier transmission," *Electronics Letters*, vol. 37, no. 17, pp. 1075–1077, 2001.

[105] A. Gatherer and M. Polley, "Controlling clipping probability in dmt transmission," in *Conference Record of the Thirty-First Asilomar Conference on Signals, Systems and Computers (Cat. No.97CB36136)*, 1997, vol. 1, pp. 578–584 vol.1.

[106] O Abel Gouba and Yves Louët, "A joint approach for papr reduction and predistortion by adding signal in cognitive radio," in *Cognitive Radio Oriented Wireless Networks (CROWNCOM), 2013 8th International Conference on*. IEEE, 2013, pp. 220–225.

[107] C. Nader, P. N. Landin, W. Van Moer, N. Bjorsell, and P. Handel, "Performance evaluation of peak-to-average power ratio reduction and digital pre-distortion for ofdm based systems," *IEEE Transactions on Microwave Theory and Techniques*, vol. 59, no. 12, pp. 3504–3511, Dec 2011.

[108] C. Nader, P. N. Landin, W. Van Moer, N. Bjorsell, P. Handel, and D. Ronnow, "Peak-power controlling technique for enhancing digital pre-distortion of rf power amplifiers," *IEEE Transactions on Microwave Theory and Techniques*, vol. 60, no. 11, pp. 3571–3581, Nov 2012.

[109] P. N. Landin, W. Van Moer, M. Isaksson, and P. Handel, "Peak-power controlled digital predistorters for rf power amplifiers," *IEEE Transactions on Microwave Theory and Techniques*, vol. 60, no. 11, pp. 3582–3590, Nov 2012.

[110] R. N. Braithwaite, "A combined approach to digital predistortion and crest factor reduction for the linearization of an rf power amplifier," *IEEE Transactions on Microwave Theory and Techniques*, vol. 61, no. 1, pp. 291–302, Jan 2013.

[111] R. N. Braithwaite, "Descent-based coefficient estimator for analog predistortion of a dual-band rf transmitter," vol. 1, no. 1, pp. 1995–1998, June 2017.

[112] A. Mbaye, G. Baudoin, A. Gouba, Y. Louet, and M. Villegas, "Combining crest factor reduction and digital predistortion with automatic determination of the necessary crest factor reduction gain," in *2014 44th European Microwave Conference*, Oct 2014, pp. 837–840.

[113] R. Piazza, B. S. M. R., and B. Ottersten, "Generalized direct predistortion with adaptive crest factor reduction control," in *2015 IEEE International Conference on Acoustics, Speech and Signal Processing (ICASSP)*, April 2015, pp. 3242–3246.

[114] Channel Coding Digital Video Broadcasting (DVB): Framing Structure and Modulation for Digital Terrestrial Television Broadcasting System(DVB-T2), ," October 2010.

[115] H. Li, T. Jiang, and Y. Zhou, "An improved tone reservation scheme with fast convergence for papr reduction in ofdm systems," *IEEE Transactions on Broadcasting*, vol. 57, no. 4, pp. 902–906, Dec 2011.

[116] J. Tellado, *Multicarrier Modulation With Low PAR: Applications to DSL and Wireless*, USA: Kluwer Academic, 2000.

[117] M. Hu, Y. Li, X. Lu, and H. Zhang, "Tone reservation to minimize nonlinearity impact on ofdm signals," *IEEE Transactions on Vehicular Technology*, vol. 64, no. 9, pp. 4310–4314, Sept 2015.

[118] H. Ochiai and H. Imai, "Performance analysis of deliberately clipped ofdm signals," *IEEE Transactions on Communications*, vol. 50, no. 1, pp. 89–101, Jan 2002.

[119] T. Jiang, C. Ni, C. Xu, and Q. Qi, "Curve fitting based tone reservation method with low complexity for papr reduction in ofdm systems," *IEEE Communications Letters*, vol. 18, no. 5, pp. 805–808, May 2014.

[120] "USRP-2942 Specifications, available at: https://www.ni.com/pdf/manuals/374410d.pdf," .

[121] "Pasternack PE15A4017, available at: https://www.pasternack.com/images/productpdf/pe15a4017.pdf," .

[122] R. Zayani, H. Shaiek, X. Cheng, X. Fu, C. Alexandre, and D. Roviras, "Experimental testbed of post-ofdm waveforms toward future wireless networks," *IEEE Access*, vol. 6, pp. 67665–67680, 2018.

[123] Emil Björnson, Jakob Hoydis, and Luca Sanguinetti, "Massive MIMO networks: Spectral, energy, and hardware efficiency," *Foundations and Trends® in Signal Processing*, vol. 11, no. 3-4, pp. 154–655, 2017.

[124] C. Mollen, E. G. Larsson, and T. Eriksson, "Waveforms for the massive mimo downlink: Amplifier efficiency, distortion, and performance," *IEEE Transactions on Communications*, vol. 64, no. 12, pp. 5050–5063, Dec 2016.

[125] C. Studer and E. G. Larsson, "Par-aware large-scale multi-user mimo-ofdm downlink," *IEEE Journal on Selected Areas in Communications*, vol. 31, no. 2, pp. 303–313, February 2013.

[126] H. Bao, J. Fang, Z. Chen, H. Li, and S. Li, "An efficient bayesian papr reduction method for ofdm-based massive mimo systems," *IEEE Transactions on Wireless Communications*, vol. 15, no. 6, pp. 4183–4195, June 2016.

[127] H. Bao, J. Fang, Q. Wan, Z. Chen, and T. Jiang, "An admm approach for papr reduction for large-scale mimo-ofdm systems," *IEEE Transactions on Vehicular Technology*, vol. 67, no. 8, pp. 7407–7418, Aug 2018.

[128] S. Zarei, W. Gerstacker, R. R. Muller, and R. Schober, "Low-complexity linear precoding for downlink large-scale mimo systems," in *2013 IEEE 24th Annual International Symposium on Personal, Indoor, and Mobile Radio Communications (PIMRC)*, Sep. 2013, pp. 1119–1124.

[129] H. Sifaou, A. Kammoun, L. Sanguinetti, M. Debbah, and M. Alouini, "Power efficient low complexity precoding for massive mimo systems," in *2014 IEEE Global Conference on Signal and Information Processing (GlobalSIP)*, Dec 2014, pp. 647–651.

[130] A. Kammoun, A. Muller, E. Bjornson, and M. Debbah, "Linear precoding based on polynomial expansion: Large-scale multi-cell mimo systems," *IEEE Journal of Selected Topics in Signal Processing*, vol. 8, no. 5, pp. 861–875, Oct 2014.

[131] A. Benzin, G. Caire, Y. Shadmi, and A. M. Tulino, "Low-complexity truncated polynomial expansion dl precoders and ul receivers for massive mimo in correlated channels," *IEEE Transactions on Wireless Communications*, vol. 18, no. 2, pp. 1069–1084, Feb 2019.

[132] H. Deng, H. Wang, C. Liu, and W. Wang, "Performance analysis of linear precoding for secure multiuser mimo systems with a multiple-antenna eavesdropper," in *2015 IEEE Global Communications Conference (GLOBECOM)*, Dec 2015, pp. 1–6.

[133] J. Zhu, R. Schober, and V. K. Bhargava, "Linear precoding of data and artificial noise in secure massive mimo systems," *IEEE Transactions on Wireless Communications*, vol. 15, no. 3, pp. 2245–2261, March 2016.

[134] Walid Hachem, Philippe Loubaton, and Jamal Najim, "Deterministic equivalents for certain functionals of large random matrices," *The Annals of Applied Probability*, vol. 17, no. 3, pp. 875–930, 2007.

[135] H. Li, T. Jiang, and Y. Zhou, "An improved tone reservation scheme with fast convergence for papr reduction in ofdm systems," *IEEE Transactions on Broadcasting*, vol. 57, no. 4, pp. 902–906, Dec 2011.

[136] G.H. Golub and C. F. van Loan, "Matrix Computations, 3rd edition, johns hopkins univ., sweden„" Press 1996.

[137] Raphael Hunger, "Floating point operations in matrix-vector calculus," in *Associate Institute for Signal Processing, Tech. Rep. TUM-LNS-TR-05-05*, 2005.

[138] F. Hiai and D. Petz, *The Semicircle Law, Free Random Variables and Entropy*, Mathematical Surveys and Monographs. American Mathematical Society, 2000.

[139] Antonia M. Tulino and Sergio VerdÃº, "Random matrix theory and wireless communications," *Foundations and TrendsÂ® in Communications and Information Theory*, vol. 1, no. 1, pp. 1–182, 2004.

[140] R. R. Muller and S. Verdu, "Design and analysis of low-complexity interference mitigation on vector channels," *IEEE Journal on Selected Areas in Communications*, vol. 19, no. 8, pp. 1429–1441, Aug 2001.

[141] M. Abdelaziz, L. Anttila, A. Brihuega, F. Tufvesson, and M. Valkama, "Digital predistortion for hybrid mimo transmitters," *IEEE Journal of Selected Topics in Signal Processing*, vol. 12, no. 3, pp. 445–454, June 2018.

[142] Alberto Brihuega, Lauri Anttila, Mahmoud Abdelaziz, and Mikko Valkama, "Digital Predistortion in Large-Array Digital Beamforming Transmitters," *arXiv e-prints*, p. arXiv:1812.01274, Dec 2018.

[143] Nokia, "R4-163314, realistic power amplifier model for the new radio evaluation," *3GPP TSG-RAN WG4 Meeting 79*, 2016.

[144] H. Shaiek, R. Zayani, Y. Medjahdi, and D. Roviras, "Analytical analysis of ser for beyond 5g post-ofdm waveforms in presence of high power amplifiers," *IEEE Access*, vol. 7, pp. 29441–29452, 2019.

[145] A. A. Zaidi, R. Baldemair, H. Tullberg, H. Bjorkegren, L. Sundstrom, J. Medbo, C. Kilinc, and I. Da Silva, "Waveform and numerology to support 5g services and requirements," *IEEE Communications Magazine*, vol. 54, no. 11, pp. 90–98, Nov. 2016.

[146] S. Lien, S. Shieh, Y. Huang, B. Su, Y. Hsu, and H. Wei, "5g new radio: Waveform, frame structure, multiple access, and initial access," *IEEE Communications Magazine*, vol. 55, no. 6, pp. 64–71, Jun. 2017.

[147] P. Guan, D. Wu, T. Tian, J. Zhou, X. Zhang, L. Gu, A. Benjebbour, M. Iwabuchi, and Y. Kishiyama, "5g field trials: Ofdm-based waveforms and mixed numerologies," *IEEE Journal on Selected Areas in Communications*, vol. 35, no. 6, pp. 1234–1243, Jun. 2017.

[148] L. Zhang, A. Ijaz, P. Xiao, A. Quddus, and R. Tafazolli, "Subband filtered multi-carrier systems for multi-service wireless communications," *IEEE Transactions on Wireless Communications*, vol. 16, no. 3, pp. 1893–1907, Mar. 2017.

[149] L. Zhang, A. Ijaz, P. Xiao, and R. Tafazolli, "Multi-service system: An enabler of flexible 5g air interface," *IEEE Communications Magazine*, vol. 55, no. 10, pp. 152–159, Oct. 2017.

[150] A. Yazar and H. Arslan, "Reliability enhancement in multi-numerology-based 5g new radio using ini-aware scheduling," *EURASIP Journal on Wireless Communications and Networking*, vol. 2019, no. 1, pp. 110, May 2019.

[151] A. B. Kihero, M. S. J. Solaija, A. Yazar, and H. Arslan, "Inter-numerology interference analysis for 5g and beyond," in *2018 IEEE Globecom Workshops (GC Wkshps)*, Dec. 2018, pp. 1–6.

[152] X. Zhang, L. Zhang, P. Xiao, D. Ma, J. Wei, and Y. Xin, "Mixed numerologies interference analysis and inter-numerology interference cancellation for windowed ofdm systems," *IEEE Transactions on Vehicular Technology*, vol. 67, no. 8, pp. 7047–7061, Aug. 2018.

[153] S.Rajagopal and Md. S. Rahman, "Multi-user MIMO with flexible numerology for 5g," *CoRR*, vol. abs/1610.03056, 2016.

[154] J. Choi, B. Kim, K. Lee, and D. Hong, "A transceiver design for spectrum sharing in mixed numerology environments," *IEEE Transactions on Wireless Communications*, vol. 18, no. 5, pp. 2707–2721, May 2019.

[155] Q. H. Spencer, A. L. Swindlehurst, and M. Haardt, "Zero-forcing methods for downlink spatial multiplexing in multiuser mimo channels," *IEEE Transactions on Signal Processing*, vol. 52, no. 2, pp. 461–471, Feb. 2004.

[156] Study on channel model for frequencies from 0.5 to 100 GHz (Release 14), "V14.3.0," *document*, vol. Tr, no. 38, pp. 901, 3GPP 2018.

[157] Z. Yang and Y. Liu, "Quality of trilateration: Confidence-based iterative localization," *IEEE Transactions on Parallel and Distributed Systems*, vol. 21, no. 5, pp. 631–640, 2010.

[158] Y. Shu, Y. Huang, J. Zhang, P. Coué, P. Cheng, J. Chen, and K. G. Shin, "Gradient-based fingerprinting for indoor localization and tracking," *IEEE Transactions on Industrial Electronics*, vol. 63, no. 4, pp. 2424–2433, 2016.

[159] Tsai Michael, "Path-loss and shadowing (large-scale fading)," *SIAM Review*, vol. 20, no. 2011, 2011.

[160] Maryam Fazel Benjamin Recht and Pablo A. Parrilo, "Guaranteed minimum-rank solutions of linear matrix equations via nuclear norm minimization," *SIAM Review*, vol. 52, no. 3, pp. 471–501, 2010.

[161] Candès Emmanuel J and Recht Benjamin, "Exact matrix completion via convex optimization," *SIAM Review*, vol. 9, no. 717, 2009.

[162] Sebastian Ruder, "An overview of gradient descent optimization algorithms," *CoRR*, vol. abs/1609.04747, 2016.

[163] W. Njima, R. Zayani, I. Ahriz, M. Terre, and R. Bouallegue, "Beyond stochastic gradient descent for matrix completion based indoor localization.," *Applied Sciences.*, vol. 9, no. 12, pp. 2414, 2019.

[164] G. Hinton, N. Srivastava, and K. Swersky, "Neural networks for machine learning lecture 6a overview of mini-batch gradient descent," *arXiv*, vol. 14, 2012.

[165] J. Adam Kingma, D.P.; Ba, "A method for stochastic optimization," *arXiv*, 2014.

[166] D. Li, B. Zhang, and C. Li, "A feature-scaling-based k-nearest neighbor algorithm for indoor positioning systems," *IEEE Internet of Things Journal*, vol. 3, no. 4, pp. 590–597, 2016.

[167] V. Honkavirta, T. Perala, S. Ali-Loytty, and R. Piche, "A comparative survey of wlan location fingerprinting methods," in *2009 6th Workshop on Positioning, Navigation and Communication*, 2009, pp. 243–251.

[168] A. Moreira, M. J. Nicolau, F. Meneses, and A. Costa, "Wi-fi fingerprinting in the real world - rtls@um at the evaal competition," in *2015 International Conference on Indoor Positioning and Indoor Navigation (IPIN)*, 2015, pp. 1–10.

[169] W. Njima, I. Ahriz, R. Zayani, M. Terre, and R. Bouallegue, "Comparison of similarity approaches for indoor localization," in *2017 IEEE 13th International Conference on Wireless and Mobile Computing, Networking and Communications (WiMob)*, 2017, pp. 349–354.

[170] T. Roos, P. Myllymaki, and H. Tirri et al., "A probabilistic approach to wlan user location estimation.," *International Journal of Wireless Information Networks*, vol. 9, pp. 155–164, 2002.

[171] Y. Jin, W. Soh, and W. Wong, "Indoor localization with channel impulse response based fingerprint and nonparametric regression," *IEEE Transactions on Wireless Communications*, vol. 9, no. 3, pp. 1120–1127, 2010.

[172] Westfall PH., "Kurtosis as peakedness.," *R.I.P. Am Stat.*, vol. 68, no. 3, pp. 191–195, 2014.

[173] INC. NTT DOCOMO, "5g evolution and 6g.," *white paper.*, 2020.

[174] S. Gunturi and J. Balakrishnan, "Mitigation of narrowband interference in differentially modulated communication systems," in *2009 IEEE International Conference on Acoustics, Speech and Signal Processing*, 2009, pp. 2549–2552.

[175] P. Jung, "Pulse shaping, localization and the approximate eigenstructure of ltv channels (special paper)," in *2008 IEEE Wireless Communications and Networking Conference*, 2008, pp. 1114–1119.

[176] D. Schafhuber, G. Matz, and F. Hlawatsch, "Pulse-shaping ofdm/bfdm systems for time-varying channels: Isi/ici analysis, optimal pulse design, and efficient implementation," in *The 13th IEEE International Symposium on Personal, Indoor and Mobile Radio Communications*, 2002, vol. 3, pp. 1012–1016 vol.3.

[177] G. Matz, D. Schafhuber, K. Grochenig, M. Hartmann, and F. Hlawatsch, "Analysis, optimization, and implementation of low-interference wireless multicarrier systems," *IEEE Transactions on Wireless Communications*, vol. 6, no. 5, pp. 1921–1931, 2007.

[178] M. Siala, F. Abdelkefi, and Z. Hraiech, "Novel algorithms for optimal waveforms design in multicarrier systems," in *2014 IEEE Wireless Communications and Networking Conference (WCNC)*, 2014, pp. 1270–1275.

[179] Z. Hraiech, M. Siala, and F. Abdelkefi, "Numerical characterization for optimal designed waveform to multicarrier systems in 5g," in *2014 22nd European Signal Processing Conference (EUSIPCO)*, 2014, pp. 156–160.

[180] Z. Hraiech, F. Abdelkefi, M. Siala, and W. Ben-Ameur, "Characterization of ping-pong optimized pulse shaping-ofdm (pops-ofdm) for 5g systems," in *2015 IEEE 81st Vehicular Technology Conference (VTC Spring)*, 2015, pp. 1–6.

[181] Z. Hraiech, F. Abdelkefi, and M. Siala, "Pops-ofdm: Ping-pong optimized pulse shaping-ofdm for 5g systems," in *2015 IEEE International Conference on Communications (ICC)*, 2015, pp. 4781–4786.

[182] A. Farhang, N. Marchetti, L. E. Doyle, and B. Farhang-Boroujeny, "Filter bank multicarrier for massive mimo," in *2014 IEEE 80th Vehicular Technology Conference (VTC2014-Fall)*, 2014, pp. 1–7.

[183] A. Farhang, A. Aminjavaheri, N. Marchetti, L. E. Doyle, and B. Farhang-Boroujeny, "Pilot decontamination in cmt-based massive mimo networks," in *2014 11th International Symposium on Wireless Communications Systems (ISWCS)*, 2014, pp. 589–593.

[184] V. Savaux, F. Bader, and J. Palicot, "Ofdm/oqam blind equalization using cna approach," *IEEE Transactions on Signal Processing*, vol. 64, no. 9, pp. 2324–2333, 2016.

[185] X. Cheng, R. Zayani, H. Shaiek, and D. Roviras, "Analysis and cancellation of mixed-numerologies interference for massive mimo-ofdm ul," *IEEE Wireless Communications Letters*, vol. 9, no. 4, pp. 470–474, 2020.

[186] A. Zappone, M. Di Renzo, M. Debbah, T. T. Lam, and X. Qian, "Model-aided wireless artificial intelligence: Embedding expert knowledge in deep neural networks for wireless system optimization," *IEEE Vehicular Technology Magazine*, vol. 14, no. 3, pp. 60–69, 2019.